ICAM

Institute for Computational and Applied Mechanics

RADIATIVE ENERGY TRANSFER IN MOLECULAR GASES

By

Surendra N. Tiwari, Principal Investigator
and ICAM Director

NASA Grant NAG-1-363
NASA Langley Research Center
Hampton, Virginia 23665-5225

ODU/ICAM Report 92-101
February 1992

Old Dominion University
Norfolk, Virginia 23529-0247

ICAM

Institute for Computational and Applied Mechanics

RADIATIVE ENERGY TRANSFER IN MOLECULAR GASES

By

Surendra N. Tiwari, Principal Investigator
and ICAM Director

NASA Grant NAG-1-363
NASA Langley Research Center
Hampton, Virginia 23665-5225

ODU/ICAM Report 92-101
February 1992

Old Dominion University
Norfolk, Virginia 23529-0247

FOREWORD

This represents a collection of the work completed in the past and in recent years in the field of infrared radiative energy transfer in molecular gases. The primary motivation of this compilation has been due to recent demand of the subject by graduate students working on research projects in the areas of high temperature gas dynamics, design of high pressure combustion chambers and high enthalpy nozzles, entry and reentry phenomena, supersonic and hypersonic propulsion, and in defense oriented research. The materials presented here should provide some essential information on spectral models, gray as well as nongray radiative formulations, computational procedures, and a few specific applications.

This work, in part, was conducted in cooperation with the NASA Langley Research Center (Fluid Mechanics Division-Theoretical Flow Physics Branch) and the Institute of Computational and Applied Mechanics (ICAM) of Old Dominion University. The work on this project was partially supported by the NASA Langley Research Center through grant NAG1-363. The grant was monitored by Mr. Robert L. Yang, Assistant University Affairs Officer.

RADIATIVE ENERGY TRANSFER IN MOLECULAR GASES

By
S. N. Tiwari*
Department of Mechanical Engineering and Mechanics
Old Dominion University, Norfolk, Virginia 23529

ABSTRACT

Basic formulations, analyses, and numerical procedures are presented to investigate radiative interactions in gray as well as nongray gases under different physical and flow conditions. After preliminary fluid-dynamical considerations, essential governing equations for radiative transport are presented that are applicable under local and nonlocal thermodynamic equilibrium conditions. Auxiliary relations for relaxation times and spectral absorption models are also provided.

For specific applications, several simple gaseous systems are analyzed. The first system considered consists of a gas bounded by two parallel plates having the same temperature. Within the gas there is a uniform heat source per unit volume. For this system, both vibrational nonequilibrium effects and radiation-conduction interactions are investigated. The second system consists of fully developed laminar flow and heat transfer in a parallel plate duct under the boundary condition of a uniform surface heat flux. For this system, effects of gray surface emittance are investigated. With the single exception of a circular geometry, the third system considered is identical to the second system. Here, the influence of nongray walls is also investigated, and a correlation between the parallel plates and circular tube results is presented. The particular gases selected for this investigation are, CO, CO_2, H_2O, CH_4, N_2O, NH_3, OH, and NO. The temperature and pressure range considered are 300-2000K, and 0.1-100 atmosphere, respectively. Illustrative results obtained for different cases are discussed and some specific conclusions are provided.

---

* Eminent Professor, Department of Mechanical Engineering and Mechanics, College of Engineering and Technology.

NOMENCLATURE

Latin Symbols

A, A_i	Total band absorptance, cm^{-1}
A_{oi}	Correlation quantity, cm^{-1}
$\bar{A}$, $\bar{A}_i$	Dimensionless band absorptance, A_i/A_{oi}
B^2, B_i^2	Correlation quantity
B_e, B_{ei}	Rotational Constant, cm^{-1}
B_ν	Black-body intensity of frequency ν and at local temperature
$B_\omega(T_1)$, $B_\omega(T_w)$	Spectral surface radiosity, $(watts/cm^2)cm^{-1}$
C	Speed of light
C_o^2, C_{oi}^2	Correlation quantity, $atm^{-1}\ cm^{-1}$
D	Diameter of a circular tube, cm
$E_n(t)$	Exponential integral
E_r	Rotational energy
E_v	Vibrational energy
E_v^*	Equilibrium vibrational energy
e	Total black body emissive power, $watts/cm^2$
e_ω	Planck's function, $(watts/cm^2)/cm^{-1}$
$e_{1\omega}$, $e_{1\omega i}$	Planck's function evaluated at temperature T_1
$e_{\omega c}$, $e_{\omega i}$	Planck's function evaluated at wave number ω_c
h	Planck's constant
$\bar{h}$	Heating function
H_i	Gas property for the large path length limit
$\bar{H}$	Nondimensional heating function
I_ν	Intensity of a beam of radiation of frequency ν
J_ν, $J_{\nu c}$	Radiative source function
k	Boltzmann constant; also thermal conductivity, $(watts/cm^2)/K$
L	Distance between plates, cm
M	Radiation-conduction parameter for the large path length limit
M_1	Gray gas initeraction parameter for parallel plates

M_2	Gray gas interaction parameter for circular tube
N	Rdiation-conduction parameter for optically thin limit
$\tilde{N}$	Definition on N for NLTE case
$\bar{N}$	Gray gas optically thin parameter
P	Gas pressure, atm
P_e, P_{ei}	Equivalent broadening pressure of ith band
q_w	Wall heat flux, watts/cm^2
q_R	Total radiative heat flux, watts/cm^2
q_{Ri}	Radiation heat flux for ith band, watts/cm^2
$q_{R\omega}$, $q_{R\omega i}$	Spectral radiative flux, (watts/cm^2)/cm^{-1}
Q	Heat source or sink, watts/cm^3
r	Physical coordinate for circular tube
r_o	Radius of the tube
S(T)	Total band intensity, atm^{-1} cm^{-2}
S_ν	Non-equilibrium source function
S_ν^*	Equilibrium source function
s	Distance along direction of radiative propagation
T	Temperature, kinetic temperature, K
T_o	Reference temperature (equilibrium)
T_1, T_2, T_w	Wall temperature
T_b	Bulk temperature, K
u, u_i	Dimensionless coordinate, C_o^2Py or C_o^2Pr
u_o, u_{oi}	Dimensionless path length, C_o^2PL or C_o^2Pr$_o$
v_x	Velocity, cm/sec
v_m	Mean velocity, cm/sec
y	Physical coordinate, cm
Greek Symbols	
α	Thermal diffusivity, cm^2/sec
β, β_i	Line structure parameter, B^{2}Pe
γ_1	Nondimensional quantity, 3 $\tau_o^2/\bar{N}$
γ_2	Nondimensional quantity, $3(\kappa_p r_o)^2/\bar{N}$
ε, ε_1, ε_i, ε_w	Surface emittance

η_c	Vibrational relaxation time, sec
η_r	Radiative lifetime of vibrational state, sec
θ	Dimensionless temperature, $(T - T_1)/(QL^2/k)$
θ_P	Dimensionless temperature, $(T - T_1)/(q_w L/k)$
θ_T	Dimensionless temperature, $(T - T_w)/(q_w r_o/k)$
θ_{bP}	Dimensionless bulk temperature, $(T_b - T_1)/(q_w L/k)$
θ_{bT}	Dimensionless bulk temperature, $(T_b - T_w)/(q_w r_o/k)$
Θ_{bT}	Dimensionless bulk temperature, $\theta_{bT}/2$
κ_ν	Absorption coefficient of frequency ν
κ_ν^*	Equilibrium absorption coefficient at frequency ν
κ_ω	Equilibrium spectral absorption coefficient, cm^{-1}
κ_m	Modified Planck mean coefficient, cm^{-1}
κ_p	Planck mean coefficient, cm^{-1}
λ	Thermal conductivity, watts/cm^2/K
ν	Frequency
ν_c, ν_o, ν_i	Frequency corresponding to band center
ξ	Dimensionless coordinate, y/L or r/r_o
ρ	Density
σ	Stefan-Boltzmann constant
τ	Optical coordinate, $\kappa_p y$ or $\kappa_p r$
τ_o	Optical thickness, $\kappa_p L$ or $\kappa_p r_o$, or $\kappa_p D$
τ_ω	Optical coordinate, $\kappa_\omega y$ or $\kappa_\omega r$
$\tau_{o\omega}$	Optical thickness, $\kappa_\omega L$ or $\kappa_\omega r_o$
ϕ	Dimensionless function, $(e_\omega - e_{1\omega})/(QL/A_o u_o)$
ϕ^*	Dimensionless function, $(T - T_1)/(QL/H)$
Ω	Solid angle
ω	Wave number, cm^{-1}
ω_c, ω_i	Band center, cm^{-1}

TABLE OF CONTENTS

LIST OF FIGURES

1. INTRODUCTION

In order to understand and investigate radiative interactions in gases, one should be quite familiar with basic transfer processes (mass, momentum, and energy) in gaseous systems. It is also essential to have fundamental knowledge of different numerical and computational procedures. For a basic understanding of these subject areas one should refer to [1-10].

In the past three decades, a tremendous progress has been made in the field of radiative energy transfer in nonhomogeneous nongray gaseous systems. As a result, several useful books [11-29] and review articles [30-40] have become available for engineering, meteorological, and astrophysical applications. In the sixties and early seventies, radiative transfer analyses were limited to one-dimensional cases. Multidimensional analyses and sophisticated numerical procedures emerged in the mid-to-late seventies. Today, the field of radiative energy transfer in gaseous systems is getting an ever increasing attention because of its application in the areas of the earth's radiation budget studies and climate modeling, fire and combustion research, entry and reentry phenomena, hypersonic propulsion and defense-oriented research.

The main objectives of this study is to explore the extent of radiative contributions of different molecular gases under varying physical and flow conditions. Attention has been directed specifically towards infrared active diatomic and polyatomic gases, wherein the absorption and emission of thermal radiation occurs as a result of vibration rotation bands. In order to present a systematic study, it is necessary to assume a suitable model for vibration-rotation bands, and to obtain relevant spectroscopic information for the gases under consideration. The assumption of local thermodynamic equilibrium (LTE) will have to be justified, and any influence of nonequilibrium (NLTE) should be investigated. Wherever applicable, radiative contributions from weaker combination and overtone bands should be included in the general nongray analysis.

In addition the effect of surface emittance (gray as well as nongray) upon gaseous radiation should be investigated.

Basic governing equations and essential information on molecular radiative interactions are provided in [11-29]. Radiative properties for important molecular species are available [33-37]. In this report, basic equations of fluid mechanics and heat transfer are presented and radiative transport models are provided for molecular radiative interactions. The extent of radiative interactions are investigated for several illustrative cases of absorbing-emitting species between parallel plates and circular geometries. The entire procedure can be extended to investigate radiative interactions in other geometries.

2. BASIC THEORETICAL FORMULATION

The governing equations for fluid mechanics and heat transfer are available in standard references [1-8]. These are presented here without providing detailed derivations. Specific conservation equations for a Newtonian fluid are derived in [1-3, 5].

The law of conservation of mass applied to a material volume yields the equation of continuity as

$$\partial\rho/\partial t + \nabla\cdot(\rho\underset{\sim}{u}) = 0 \tag{2.1a}$$

For an incompressible fluid, this reduces to

$$\nabla\cdot\underset{\sim}{u} = 0 \tag{2.1b}$$

The Newton's second law applied to a Newtonian fluid yields the Navier-Stokes equation as

$$\rho\frac{D\underset{\sim}{u}}{Dt} = \rho\underset{\sim}{f} - \nabla p + \frac{\partial}{\partial x_j}\left[u\left(\frac{\partial u_i}{\partial x_j} + \frac{\partial u_j}{\partial x_i}\right) - \frac{2}{3}\delta_{ij}\mu\frac{\partial u_k}{\partial x_k}\right] \tag{2.2a}$$

where δ_{ij} is the Kronecker delta function and $i,\ j,\ k = 1, 2, 3$. In the derivation of Eq. (2.2a), it has been assumed that the coefficient of bulk viscosity is zero. For an incompressible fluid and constant viscosity (μ), Eq. (2.2a) reduces to a simpler form as

$$D\underset{\sim}{u}/Dt = \underset{\sim}{f} - \nabla p/\rho + \nu\nabla^2\underset{\sim}{u} \tag{2.2b}$$

It should be noted that Eq. (2.2b) is not applicable to a fluid whose viscosity is a strong function the temperature.

The energy equation for a simple homogeneous system is expressed usually in three different forms as [1, 5, 6]

$$\rho(De/Dt) = \partial Q/\partial t - \nabla\cdot\underset{\sim}{q} - p\left(\nabla\cdot\underset{\sim}{u}\right) + \Phi \tag{2.3a}$$

$$\rho(Dh/Dt) = \partial Q/\partial t - \nabla\cdot\underset{\sim}{q} + DP/Dt + \Phi \tag{2.3b}$$

$$\rho c_p(DT/Dt) = \partial Q/\partial t + \nabla\cdot(k\nabla T) - \nabla\cdot q_R + \beta T(Dp/Dt) + \Phi \tag{2.3c}$$

where

$$\underset{\sim}{q} = q_c + q_r = -k\nabla T + q_R$$

$$\Phi = \mu\Big[2(\partial u/\partial x)^2 + 2(\partial v/\partial y)^2 + 2(\partial w/\partial z)^2 + (\partial v/\partial x + \partial u/\partial y)^2 + (\partial w/\partial y + \partial v/\partial z)^2 + (\partial u/\partial z + \partial w/\partial x)^2 - \frac{2}{3}(\partial u/\partial x + \partial v/\partial y + \partial w/\partial z)^2\Big]$$

and Q represents the heat generated (or lost) per unit volume by external agencies, and β is the coefficient of thermal expansion of the fluid. Simplified forms of Eqs. (2.3) can be obtained easily for specific applications.

In order to close the system of conservation equations (2.1)-(2.3), it is essential to establish relations between the thermodynamic variables p, ρ, T, e and h and relate these to transport properties μ and k. Since the local thermodynamic state is fixed by any two independent state variables, one may express the equations of state for a simple system as

$$p = p(e, \rho) \tag{2.4a}$$

$$T = T(e, \rho) \tag{2.4b}$$

For a perfect gas, the following thermodynamic relations are applicable:

$$p = \rho RT,\ e = c_v T,\ h = c_p T \tag{2.5a}$$

$$c_v = R/(\gamma - 1), c_p = \gamma R/(\gamma - 1), \gamma = c_p/c_v \tag{2.5b}$$

where R is the gas constant, c_v is the specific heat at constant volume, c_p is the specific heat at constant pressure, and γ is the ratio of specific heats. Thus, for a perfect gas, Eq. (2.4) may be expressed as

$$p = (\gamma - 1)\rho e \tag{2.6a}$$

$$T = (\gamma - 1)e/R \tag{2.6b}$$

The transport properties are related to the thermodynamic variables through use of the kinetic theory of gases. The variation in viscosity is given by Sutherland's formula

$$\mu = c_1 T^{3/2}/(T + c_2) \tag{2.7}$$

where c_1 and c_2 are specific constants for a given gas. The thermal conductivity k usually is determined through use of the Prandtl number defined by $Pr = c_p \mu / k$. This is possible because for most gases the ratio c_p/Pr is essentially constant.

Following the nomenclature of the kinetic theory of gases, Eqs. (2.1)-(2.3), in general, are referred to as the Navier-Stokes equations. For computational conveniences, it is quite often desirable to express these equations in a compact vector form. For the case of no external heat addition and in the absence of body forces, the Navier-Stokes equations are expressed in the vector form as [9]

$$\frac{\partial U}{\partial t} + \frac{\partial E}{\partial x} + \frac{\partial F}{\partial y} + \frac{\partial G}{\partial z} = 0 \tag{2.8}$$

where U, E, F, and G are vectors and are defined as

$$U = \begin{bmatrix} \rho \\ \rho u \\ \rho v \\ \rho w \\ Et \end{bmatrix}$$

$$E = \begin{bmatrix} \rho u \\ \rho u^2 + p - \tau_{xx} \\ \rho uv - \tau_{xy} \\ \rho uw - \tau_{xz} \\ (E_t + p)u - u\tau_{xx} - v\tau_{xy} - w\tau_{xz} + q_{cx} + q_{Rx} \end{bmatrix}$$

$$F = \begin{bmatrix} \rho v \\ \rho uv - \tau_{xy} \\ \rho v^2 + p - \tau_{yy} \\ \rho vw - \tau_{yz} \\ (E_t + p)v - u\tau_{xy} - v\tau_{yy} - w\tau_{yz} + q_{cy} + q_{Ry} \end{bmatrix}$$

$$G = \begin{bmatrix} \rho w \\ \rho uw - \tau_{xz} \\ \rho vw - \tau_{yz} \\ \rho w^2 + p - \tau_{zz} \\ (E_t + p)w - u\tau_{xz} - v\tau_{yz} - w\tau_{zz} + q_{cz} + q_{Rz} \end{bmatrix}$$

$$E_t = \rho(e + V^2/2); V^2 = u^2 + v^2 + w^2$$

$$\tau_{xx} = \frac{2}{3}\mu\left(2\frac{\partial u}{\partial x} - \frac{\partial v}{\partial y} - \frac{\partial w}{\partial z}\right)$$

$$\tau_{yy} = \frac{2}{3}\mu\left(2\frac{\partial v}{\partial y} - \frac{\partial u}{\partial x} - \frac{\partial w}{\partial z}\right)$$

$$\tau_{zz} = \frac{2}{3}\mu\left(2\frac{\partial w}{\partial z} - \frac{\partial u}{\partial x} - \frac{\partial v}{\partial y}\right)$$

$$\tau_{xy} = \mu\left(\frac{\partial u}{\partial y} + \frac{\partial v}{\partial x}\right) = \tau_{yx}$$

$$\tau_{xz} = \mu\left(\frac{\partial w}{\partial x} + \frac{\partial u}{\partial z}\right) = \tau_{zx}$$

$$\tau_{yz} = \mu\left(\frac{\partial v}{\partial z} + \frac{\partial w}{\partial y}\right) = \tau_{zy}$$

Note that the first row of the vector Eq. (2.8) corresponds to the continuity equation as given by Eq. (2.1a). Similarly, the second, third, and fourth rows represent the three momentum equations, and the fifth row represents one form of the energy equation.

It should by noted that derivations of the governing equations presented in this section assume the conditions of continuum and existence of a local thermodynamic equilibrium. For the case of two-dimensional laminar flow in channels, the energy equations given by Eqs. (2.3) and (2.8) reduce to [18]

$$\rho c_p\left(\frac{\partial T}{\partial t} + u\frac{\partial T}{\partial x} + v\frac{\partial T}{\partial y}\right) = \frac{\partial}{\partial y}\left(k\frac{\partial T}{\partial y}\right) + \beta T u\frac{dP}{dx} + \mu\left(\frac{\partial u}{\partial y}\right)^2 - div\ q_R \tag{2.9}$$

The energy equation given in this form can be applied to radiatively induced nonequilibrium situation by replacing the divergence of the radiative flux by its nonequilibrium counterpart. At the same time it must be assumed that the departure in population distribution over excited

states from the Boltzmann distribution will not significantly change the internal energy, and the transport properties from their equilibrium values [16]. As discussed in [19], this assumption is justified under the conditions where vibrational characteristic temperature $h\nu/k$ is greater than or is of the order of vibrational temperature. Consequently, the temperature appearing in Eq. (2.9) will be regarded as the kinetic temperature.

In obtaining Eq. (2.9), it has been assumed that the conduction heat transfer in the x direction is negligible compared with the net conduction in the y direction. This represents the physical condition of a large value of the Peclet number. By an analogous reasoning, the radiative heat transfer in the x direction can be neglected in comparison to that transferred in the y direction. If, in addition, it is assumed that the Eckert number of the flow is small, then Eq. (2.9) reduces to

$$\frac{\partial T}{\partial t} + u\frac{\partial T}{\partial x} + v\frac{\partial T}{\partial y} = \alpha\frac{\partial^2 T}{\partial y^2} - \frac{1}{\rho C_p}\frac{\partial q_R}{\partial y} \tag{2.10}$$

In the preceding equation $\alpha = k/\rho C_p$ represents the thermal diffusivity of the fluid and it has been assumed that the fluid properties are constant locally.

It should be evident that in order to apply the energy equation to any problem involving a radiation participating medium, it is essential to have an appropriate formulation for the radiative flux vector q_R. However, before going into the formulation of the radiative flux equations, it is desirable to present some heat transfer results already available in the literature for simplified geometries and conditions without the radiative interactions. These are discussed briefly in the next section.

3. SIMPLE FLUID-DYNAMICAL APPLICATIONS

Attention is directed here to present solutions of the viscous heat conducting equations for simple internal flows. These solutions are available in the literature and are presented here for the sake of comparison with the solutions of radiative interactions obtained in Sec. 6. Before presenting solutions for specific cases, it is desirable to provide some basic definitions associated with velocity and temperature variations in internal flows.

3.1 Basic Definitions for Internal Flows

The basic definitions needed for description of internal flow in channels are provided in this section.

1. Entrance (or Inlet) Region

It is the region in the flow up to which the velocity profile changes its shape due to presence of the boundary layer (Fig. 3.1). The flow in such regions are divided into the boundary-layer flow and the potential flow in the core. Because of the developing boundary layers, the velocity U in the core (outside the boundary layer) increases along the length. This is the region of potential flow (i.e., the region of negligible frictional effects). The change in core velocity is related to the pressure change in the core.

2. Fully-Developed Flow

The flow in the region where the shape of velocity profiles remains constant is called the fully-developed flow. For such a flow, the velocity components $v = 0$, $w = 0$ and $u = u(y)$.

3. Mean Velocity

The mean velocity (u_m or $\bar{u}$) is defined as the average (or mean) velocity at any particular location in the direction of flow. For the case of a fully-developed flow, this is defined as

$$\bar{u} = u_m = \frac{1}{A_c}\int_{A_c} u\, dA \tag{3.1}$$

where A_c is the cross-sectional area of the duct.

4. Hydraulic (or Equivalent) Diameter

The concept of hydraulic diameter is very useful in the study of turbulent flows and noncircular duct flows; however, it is extensively used also in the study of laminar flows. The hydraulic diameter D_h is defined by the following relation

$$D_h = 4A/P \tag{3.2}$$

where A represents the flow area (or the area of the duct) and P is the wetted perimeter. For circular ducts with actual diameter D, $D_h = \left[4\left(\pi D^2/4\right)\right]/(\pi D) = D$. For square ducts with sides a, $D_h = \left[4\left(a^2\right)\right]/(4a) = a$. For parallel plates a distance L apart, $D_h = [4(L \times 1)]/2 = 2L$, i.e., the hydraulic diameter is equal to twice the depth of the channel.

5. Friction Factor (or Darcy Friction Factor)

In duct flows, the pressure drop along the flow direction varies, in general, as follows

$$\Delta p/L = F(V, D, \rho, \mu, e) \tag{3.3}$$

where e represents the statistical measure of surface roughness. Dimensional analysis of Eq. (3.3) yields the nondimensional equation for the friction factor f as

$$f = \frac{(-dp/dx)D_h}{\rho u_m^2/2} = F(Re, e/D_h) \tag{3.4}$$

where $Re = \rho u_m D_h/\mu$. Thus, the pressure drop in ducts may be expressed by a simple relation between f and Re. Based on the concept of Eq. (3.4), the friction factor is defined in general as

$$f = 4\tau_w/(\rho u_m^2/2) \tag{3.5}$$

where τ_w represents the wall shear stress.

6. Skin-Friction Coefficient (or Fanning Friction Factor)

The concept of the fanning friction factor is used in the study of external flow fields. The skin-friction coefficient (or simply the friction coefficient) c_f is defined as

$$c_f = \tau_w/(\rho u_m^2/2) \tag{3.6}$$

For external flows, c_f varies with the location x along the flow. Thus, an average skin-friction coefficient for a characteristic length L is obtained by the relation

$$\bar{c}_f = \frac{1}{L}\int_o^L c_f(x)dx \tag{3.7}$$

7. Slug Flow

The slug flow is a case of an idealized fluid motion. It assumes that the flow in ducts is of uniform (constant) velocity in the direction of flow. The concept is useful is preliminary estimations of the pressure drop and drag.

8. Thermal Entrance Region

The thermal entrance region is the region of the thermal boundary layer (TBL) development (Fig. 3.2). In this region, the shape of the temperature profile changes because of the presence of the thermal boundary layer.

9. Thermally Fully-Developed Flow

The flow in the region where the shape of the temperature profile remains constant is called the thermally fully-developed flow (TFDF). Mathematically, for any set of boundary conditions, a fully developed temperature profile is said to exist when the nondimensional temperature is a unique function of y only (i.e., it is independent of the x coordinate).

10. Convection Heat Transfer Coefficient

The convective heat transfer coefficient h is defined by the Newtons law of cooling as

$$q_w = Q/A = h(T_w - T_f) \tag{3.8}$$

where T_f is the fluid temperature adjacent to the wall.

11. Bulk Temperature

The bulk temperature (or mixing-up temperature) is the mean temperature at any location x in the flow direction. It is the temperature which fluid would assume if it was instantaneously and adiabatically mixed after leaving the cross section under consideration. Mathematically, the bulk temperature T_b (or T_m) is defined as

$$T_b = \frac{1}{u_m A_c} \int_{A_c} u\, T\, dA \tag{3.9}$$

3.2 Steady Fully-Developed Duct Flows

Steady fully-developed duct flow solutions are available for different geometries and flow conditions. Results for flows between two parallel plates and within a circular tube are presented here.

Consider first a steady incompressible constant properties laminar flow between two parallel plates (Fig. 3.3). The governing equations for this case are simplified form of Eqs. (2.1b) and

(2.2b). If a conservative body force is assumed then $\nabla p - \rho \underline{f} = \nabla \hat{p}$. Since the plates are infinite in z-direction, the velocity w in z direction is negligible. Also for a fully-developed flow v = 0. Thus, for steady fully-developed flow between two parallel plates, Eqs. (2.1b) and (2.2b) combine to yield

$$d^2u/dy^2 = (1/\mu)d\hat{p}/\partial x = \text{const.} \tag{3.10}$$

With boundary conditions $u(\pm L/2) = 0$ and $(du/dy)_{y=0} = 0$, the solution of Eq. (3.10) is found to be

$$u(y) = -\frac{1}{2\mu}\frac{d\hat{p}}{dx}\left(\frac{L^2}{4} - y^2\right) \tag{3.11}$$

By using the definitions of u_m, Re, D_h and f, it can be shown that

$$fRe = 96 \tag{3.12}$$

where $D_h = 2L$, $Re = \rho u_m D_h/\mu$. It should be noted that , for fully-developed flow, fRe = constant for all ducts; the value of the constant depends on the shape of the duct. The result of Eq. (3.12) is obtained for a laminar flow but it applies quite accurately also to turbulent flows.

Next, consider the case of steady, incompressible, constant properties, and fully-developed laminar flow in a circular tube (Fig. 3.4). A combination of Eqs. (2.1b) and (2.2b) in this case results in

$$d^2u/dr^2 + (1/r)du/dr = (1/\mu)d\hat{p}/dx \tag{3.13}$$

With boundary conditions $u(r_o) = 0$ and $(du/dr)_{r=0} = 0$, the solution of Eq. (3.13) is found to be

$$u(r) = -(1/4\mu)(d\hat{p}/dx)(r_0^2 - r^2) \tag{3.14}$$

This is referred to as the Hagen-Poiseville profile.

The maximum velocity occurs in the center of the tube and is given by

$$u_{\max} = -(r_0^2/4\mu)d\hat{p}/dx \tag{3.15}$$

The mean velocity u_m is found to be $u_{\max}/2$. The volume flow rate Q_v is given by

$$Q_v = Au_m = (\pi r_0^2)u_m = -(\pi r_0^4/8\mu)d\hat{p}/dx \tag{3.16}$$

The friction factor in this case is found to be

$$fRe = 64 \tag{3.17}$$

where $Re = \rho D u_m/\mu$.

3.3 Heat Transfer in Laminar Duct Flows

The heat transfer in duct flows is influenced directly by the conditions at the bounding surfaces. The two typical conditions are that of the constant wall heat flux and constant wall temperature. However, a combination of these also occurs in some cases.

For a constant wall heat flux, $\partial T/\partial x$ is found to be constant, but this is not the case with the constant wall temperature condition. To demonstrate this, consider the case of a laminar fully-developed flow with constant properties between parallel plates (Fig. 3.5). For this case, let us define the nondimensional temperature as

$$\theta = (T_w - T)/(T_w - T_b) = f(\xi); \xi = y/L \tag{3.18}$$

Thus, for a thermally fully-developed flow, it follows that

$$\partial\theta/\partial x = \frac{\partial}{\partial x}[(T_w - T)/(T_w - T_b)] = 0 \tag{3.19a}$$

or

$$\frac{\partial}{\partial x}(T_w - T) - [(T_w - T)/(T_w - T_b)]\frac{\partial}{\partial x}(T_w - T_b) = 0 \tag{3.19b}$$

For constant properties, an energy balance on the differential distance dx results in

$$Q - W = \dot{m}\Delta H = (\rho u_m A_c)(c_p \Delta T) \tag{3.20a}$$

Since $W = 0$ and $Q = q_w A$, Eq. (3.20a) becomes

$$q_w A = (\rho u_m A_c) c_p (\partial T/\partial x) dx \tag{3.20b}$$

Note that we have assumed a colorically perfect gas in developing the relations in Eq. (3.20). Also, A is the area normal to the direction of q_w. Thus, for a parallel-plate geometry, $A = 2\ dx$, and for a circular duct, $A = P\ dx$, where P is the perimeter of the duct.

For the parallel-plate geometry, Eq. (3.20b) is expressed as

$$\partial T/\partial x = 2q_w/(\rho u_m A_c c_p) \tag{3.21}$$

Equation (3.21) demonstrates that for the case a constant wall heat flux (and fully-developed flow), the temperature gradient along x axis is constant.

The heat transfer to (or from) the wall can be written as

$$q_w = hA(T_w - T_b) \tag{3.22a}$$

and

$$q_w = -kA\frac{\partial}{\partial y}(T_w - T) \tag{3.22b}$$

Since T_b is constant along y and T_w is fixed for a given x, a comparison of the two relations for the heat flux in Eq. (3.22) provides the relation

$$h = -k\frac{\partial}{\partial y}[(T_w - T)/(T_w - T_b)] \tag{3.23}$$

For a thermally fully developed flow, a comparison of Eqs. (3.19) and (3.23) indicates that the derivate in Eq. (3.23) has a unique value at the wall that is independent of x. Thus, for a fully-developed flow, h must be uniform along the duct.

It is evident from Eq. (3.22a) that for a constant q_w, h, and A, $(T_w - T_b)$ is constant along the x axis. Consequently,

$$\frac{\partial}{\partial x}(T_w - T_b) = \frac{\partial T_w}{\partial x} - \frac{\partial T_b}{\partial x} = 0 \tag{3.24}$$

Thus, for the case of a fully-developed flow and heat transfer with constant surface heat flux, a combination of Eqs. (3.19b), (3.21), and (3.24) yields the result

$$\frac{\partial T}{\partial x} = \frac{\partial T_w}{\partial x} = \frac{\partial T_b}{\partial x} = \text{const.} \tag{3.25}$$

and the value of the constant is obtained from Eq. (3.21).

For the case of a constant wall temperature, $\partial T_w/\partial x = 0$ and from Eqs. (3.18) and (3.19) one obtains

$$\frac{\partial T}{\partial x} = \left(\frac{T_w - T}{T_w - T_b}\right)\frac{\partial T_b}{\partial x} = f(\xi)\frac{\partial T_b}{\partial x} \tag{3.26}$$

In this case, therefore, $\partial T/\partial x$ is a function of the normal (or radial) position in the duct.

Aside from the specification of the boundary conditions, the problem of heat transfer in laminar duct flows may also be classified according to the velocity distribution, i.e, heat transfer in slug flow, in fully-developed flow, and in entrance region flow. The cases of heat transfer in fully-developed laminar flows between two parallel plates and within a circular tube are considered in the following subsections.

3.3.1 Parallel Plates: Constant Wall Heat Flux

Consider the case of laminar fully-developed flow as shown in Fig. 3.5. For steady flow, the momentum equation for this case is Eq. (3.10) and with plate spacing of $2L$, the expression for the velocity distribution $u = u(y)$ is found to be

$$u = -(1/2\,\mu)(d\hat{p}/dx)\left(L^2 - y^2\right) = (3u_m/2)\left[1 - (y/L)^2\right] \tag{3.27}$$

The general form of the energy equation (Eq. (2.3c)) reduces, in this case, to

$$u\partial T/\partial x + v\partial T/\partial y = \alpha\left(\partial^2 T/\partial x^2 + \partial^2 T/\partial y^2\right) + (\nu/c_p)(\partial u/\partial y)^2 \tag{3.28}$$

For constant properties, Eq. (3.28) is a linear equation in T since velocities can be determined independent of temperature. Thus, Eq. (3.28) may be solved by superposition, first obtaining the solution neglecting the viscous term and then including it. For low and moderate subsonic velocities, the frictional term is negligible.

By noting that for fully-developed flow $v = 0$ and for thermally fully-developed flow with constant wall heat flux $\partial T/\partial x$ = const., Eq. (3.28) can be expressed (for the case with negligible frictional heating) as

$$u\partial T/\partial x = \alpha\partial^2 T/\partial y^2; (dT/dy)_{y=0} = 0,\ (T)_{y=L} = T_w(x) \tag{3.29}$$

By using Eq. (3.20b), the value of $\partial T/\partial x$ in the above equation is found to be

$$\partial T/\partial x = \text{const.} = \alpha q_w/(u_m L k);\ \alpha = k/\rho c_p \tag{3.30}$$

A combination of Eqs. (3.27), (3.29) and (3.30) gives

$$d^2T/dy^2 = c\left(L^2 - y^2\right); c = 3q_w/\left(2kL^3\right); (dT/dy)_{y=0} = 0;\ T(L) = T_w(x) \tag{3.31}$$

The solution of this readily follows as

$$T_w - T = (q_w L/8k)\left(5 - 6\xi^2 + \xi^4\right); \xi = y/L \tag{3.32}$$

By defining nondimensional temperature as

$$\theta = (T - T_w)/(q_w L/k);\ \ \theta_b = (T_b - T_w)/(q_w L/k) \tag{3.33}$$

the solution given by Eq. (3.32) is written as

$$\theta(\xi) = (1/8)\left(6\xi^2 - \xi^4 - 5\right) \tag{3.34}$$

Now, by using the definition of the bulk temperature, Eq. (3.9), and combining it with Eq. (3.27), there is obtained

$$\theta_b = \frac{3}{2}\int_0^1 \theta(\xi)(1-\xi^2)\,d\xi \tag{3.35}$$

By substituting Eq. (3.34) into Eq. (3.35) and integrating, one obtains

$$-\theta_b = 17/35 \tag{3.36}$$

If one defines the Nusselt number as $Nu = hL/k$ and uses the relation for heat transfer as $q_w = h(T_w - T_b)$, then

$$Nu = hL/k = [q_w/(T_w - T_b)](L/k) = -1/\theta_b \tag{3.37}$$

However, for duct flows, it is customary to express the Nusselt number in terms of the hydraulic diameter as $Nu = hD_h/k$. For the parallel-plate geometry, $D_h = 4L$ and the expression for the Nusselt number is found to be

$$Nu = hD_h/k = -4/\theta_b = 8.235 \tag{3.38}$$

This is the relation for nondimensional heat transfer between two parallel plates and is a constant only for the case of fully-developed flow.

Solutions for the parallel-plate geometry with constant wall temperature are available in the literature for different flow conditions [1, 5-8]. Some specific results for the case of a fully-developed flow are available in [6, 10].

3.3.2 Circular Tube: Constant Wall Heat Flux

Consider the case of a laminar fully-developed flow with negligible frictional heating in a circular tube with constant wall heat flux (Fig. 3.6). For this physical problem, the fully-developed velocity profile is given by Eq. (3.14) and this may be expressed alternately as

$$u = 2u_m\left[1-(r/r_0)^2\right] = \left(2u_m/r_0^2\right)\left(r_0^2 - r^2\right) \tag{3.39}$$

The energy equation in Cartesian coordinate is given by Eq. (3.28) which for fully-developed flow with no viscous dissipation is expressed in cylindrical coordinates (with appropriate boundary conditions) as

$$u\partial T/\partial x = \alpha\left[\frac{1}{r}\frac{\partial}{\partial r}\left(r\frac{\partial T}{\partial t}\right)\right] \tag{3.40a}$$

$$(\partial T/\partial r)_{r=0} = 0; \quad T(r_0) = T_w(x) \tag{3.40b}$$

It should be noted that for the constant wall heat flux case $\partial T/\partial x = \partial T_b/\partial x = \partial T_w/\partial x = \text{const.}$, and therefore, the term $(\partial^2 T/\partial x^2)$ in the energy equation becomes zero. The value of the constant $\partial T/\partial x$ is evaluated from an energy balance on a differential volume as in Fig. 3.5 (see Eq. 3.20b). For this case of circular geometry, one finds

$$\partial T/\partial x = \partial T_b \partial x = 2q_w/(\rho c_p u_m r_0) = 2\alpha q_w/(k u_m r_0) \tag{3.41}$$

A combination of Eqs. (3.40) and (3.41) results in the energy equation for this case as

$$\frac{1}{r}\frac{\partial}{\partial r}\left(r\frac{\partial T}{\partial r}\right) = A(r_0^2 - r^2); \quad A = 4q_w/kr_0^3 \tag{3.42}$$

An integration of Eq. (3.42) and application of the boundary conditions given by Eq. (3.40b) results in

$$T_w - T = (A/16)(3r_0^4 - 4r_0^2 r^2 + r^4) \tag{3.43}$$

From the definition of the bulk temperature, as given by Eq. (3.9), one obtains

$$\begin{aligned} T_w - T_b &= (1/u_m A_c)\int_{A_c} u(T_w - T)dA_c \\ &= (1/u_m \pi r_0^2)\int_0^{2\pi}\int_0^{r_0} u(T_w - T)(r d\theta)dr \end{aligned} \tag{3.44}$$

A combination of Eqs. (3.39), (3.43) and (3.44) results in the relation for the bulk temperature as

$$T_w - T_b = (11/24)(r_0 q_w/k) \tag{3.45}$$

consequently,

$$q_w = h(T_w - T_o) = h(11/24)(r_o q_w/k)$$

and

$$Nu = hD/k = (24/11\ r_0)(2r_0) = 4.364 \tag{3.46}$$

Equation (3.46) provides the result for nondimensional heat transfer for fully-developed laminar flow in a circular duct with uniform surface heat flux. There are several variations of this physical problem and extensive results for most cases are provided by Shah and London [10].

3.3.3 Circular Tube: Constant Wall Temperature

This is the same physical problem as discussed in the preceding section but the boundary condition is changed now to the uniform wall temperature. To make the problem a little more interesting, let us include the viscous heating term in the energy equation and neglect the axial temperature gradient (i.e., assume a fully-developed temperature profile). For this case, the energy equation and boundary conditions may be expressed as

$$\frac{d}{dr}\left(r\frac{dT}{dr}\right) = -(\mu/k)r(du/dr)^2 \tag{3.47a}$$

$$(dT/dr)_{r=0} = 0, \quad T(r_0) = T_w = \text{const.} \tag{3.47b}$$

The solution of Eq. (3.47) is obtained by utilizing Eq. (3.39) as

$$T - T_w = \left(\mu u_m^2/k\right)\left[1 - (r/r_0)^4\right] \tag{3.48}$$

If T_c represents the temperature at the center of the tube, then the expression for the maximum temperature rise in the duct is obtained from Eq. (3.48) as

$$T_c - T_w = \mu u_m^2 / k \tag{3.49}$$

The heat transfer from the wall, in this case, is found to be

$$q_w = -k(\partial T/\partial r)_{r=0} = 4\mu u_m^2 / r_0 = 4k(T_c - T_w)/r_0 \tag{3.50}$$

For the physical problem where the viscous heating is negligible but the axial temperature variation is given by Eq. (3.26), the expression for the nondimensional heat transfer is found to be [8, 10]

$$Nu = 3.658 \tag{3.51}$$

A comparison of results given by Eqs. (3.46) and (3.51) reveals that the extent of heat transfer is influenced significantly by the surface temperature variation.

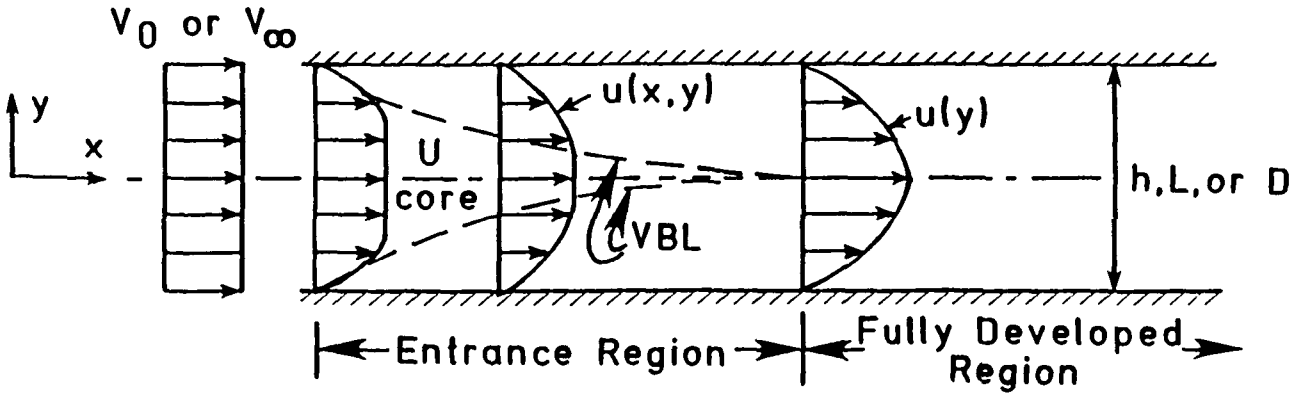

Figure 3.1 Entrance region flow between two parallel plates

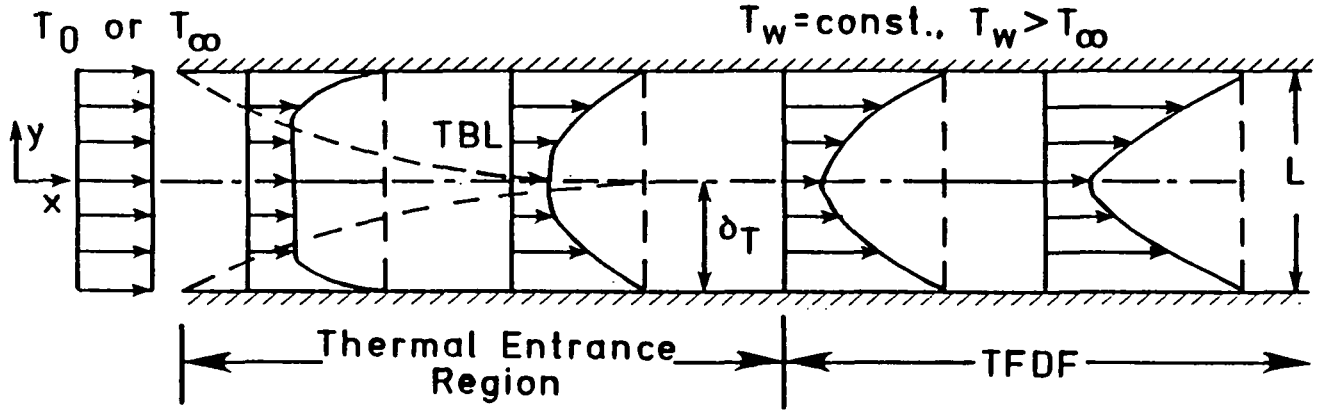

Figure 3.2 Thermal entrance region flow between two parallel plates

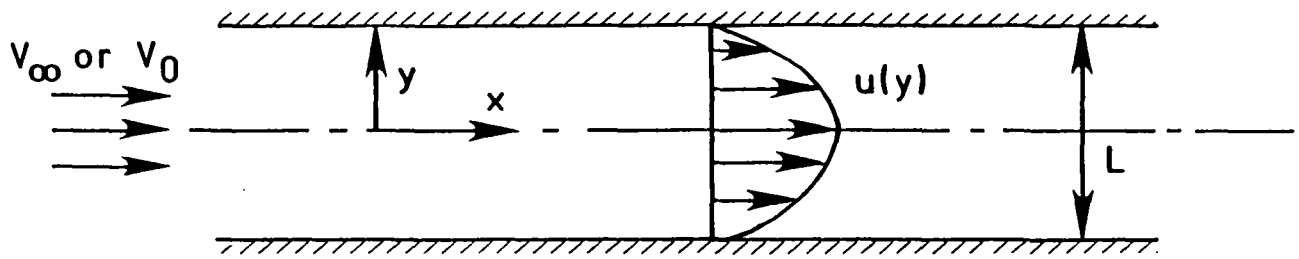

Figure 3.3 Incompressible laminar flow between two parallel plates

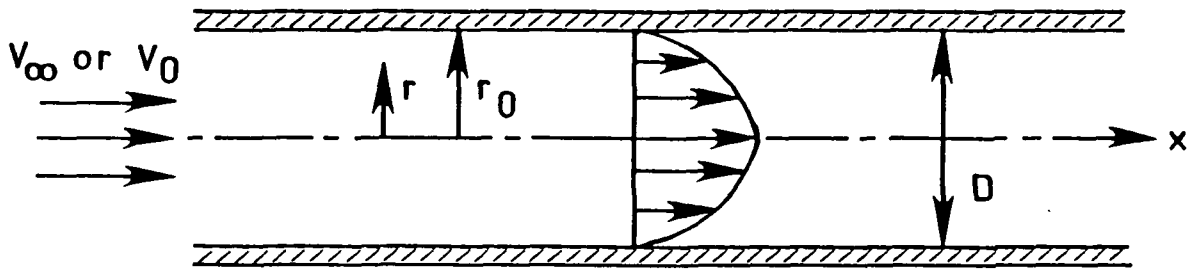

Figure 3.4 Incompressible laminar flow in a circular tube

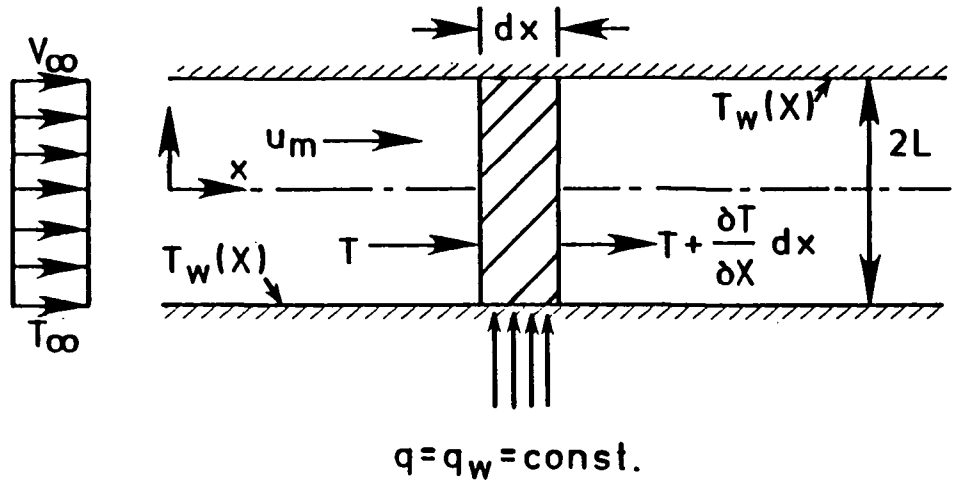

Figure 3.5 Laminar flow between two parallel plates with constant wall heat flux

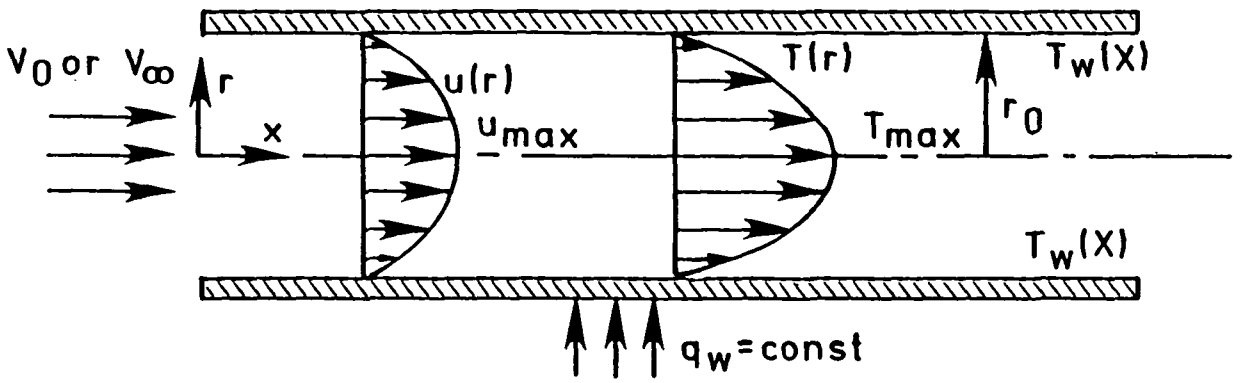

Figure 3.6 Laminar flow in circular tube with constant wall heat flux

4. RADIATIVE TRANSPORT MODELS

As mentioned in Sec. 2, an appropriate model for radiative transport is essential in applying the energy equation to any problem involving participating mediums. This section provides essential information on rate equations and equations for relaxation times, the equation of radiative transfer, band absorption and correlations, and radiative flux equations.

4.1 Physical Model and Coordinate System

For many engineering and astrophysical applications, the radiative transport equations are formulated for one-dimensional planar system. For this study, the physical model consists of an absorbing-emitting gas bounded by two infinite parallel plates (Fig. 4.1). The plate surfaces are assumed to emit and reflect in a diffuse manner.

Diatomic and polyatomic gases are considered at sufficiently low temperatures such that the electronic, ionization, and dissociation effects can be neglected. For nonequilibrium analyses, the gas model is considered to be that of a rigid rotator and harmonic oscillator. It is assumed that the translational energy is governed by the Boltzmann law and a local kinetic temperature, referred to simply as the temperature, is defined. Rotational modes requiring only a few collisions to attain equilibrium are assumed to be in equilibrium at the kinetic temperature. Consequently, the governing equations given by Eqs. (2.8)-(2.10) are applicable to the case of radiation participating mediums.

4.2 Rate Equations and Equations for Relaxation Times

The rate of change of vibrational energy of a system of oscillators can be expressed as

$$\frac{dE_v}{dt} = \left(\frac{dE_v}{dt}\right)_{coll} + \left(\frac{dE_v}{dt}\right)_{rad} \tag{4.1}$$

where terms on the right represent contributions due to collisional and radiative processes respectively. The radiation field exchanges energy with rotational as well as vibrational degree

of freedom, and one can write

$$-div q_R = \left(\frac{dE_v}{dt}\right)_{rad} + \left(\frac{dE_r}{dt}\right)_{rad} \qquad (4.2)$$

where E_r represents rotational energy per unit volume. Because of small separation of rotational levels, the change in rotational energy is small as compared to the change in vibrational energy and therefore its contribution in Eq. (4.2) is usually neglected.

The divergence of radiative flux q_R is related to the specific intensity I_ν, and for one-dimensional problem considered here it is given by the expression

$$div\, q_R = \frac{dq_R}{dy} = \int_0^\infty \frac{dq_{R_\nu}}{dy} d\nu = \int_0^\infty \int_0^{4\pi} \frac{dI_\nu}{ds} d\Omega d\nu \qquad (4.3)$$

A combination of Eqs. (4.1)-(4.3) results in

$$\frac{dE_v}{dt} = \left(\frac{dE_v}{dt}\right)_{coll} - \int_0^\infty \int_0^{4\pi} \frac{dI_\nu}{ds} d\Omega d\nu \qquad (4.4)$$

The vibrational energy of a system of oscillators undergoing a collisional relaxation process is given by the Bethe-Teller relation

$$\frac{dE_v}{dt} = \frac{E_v^* - E_v}{\eta_c} \qquad (4.5)$$

where E_v^* represents the equilibrium value of vibrational energy, and η_c having the dimensions of time is called the vibrational relaxation time. In general, the relaxation time is referred to as the average time required to transfer energy from one mode to another by collision. It is inversely proportional to the collisional frequency.

A simple derivation of Eq. (4.5) is given in [16, 19]. Since no assumption about the size of the difference $E_v^* - E_v$ was made in its derivation, Eq. (4.5) should be valid for large departure from the equilibrium. However, the assumption of simple harmonic oscillators restricts its

applicability to small departures. By employing the initial condition E_{vo}, an integration of Eq. (4.5) gives,

$$E_v - E_v^* = (E_{vo} - E_v^*) \exp(-t/\eta_c) \tag{4.6}$$

It is obvious from this equation that the relaxation time is the time required for the difference $E_v - E_v^*$ to come to l/e of its initial value.

Before making use of Eq. (4.5), certain limitations inherent in its derivation must be justified. The equation was derived on the assumption of dilute concentration of the system of oscillators in a heat bath of constant state. However, it was pointed out in [16] that for all practical purposes, Eq. (4.5) is valid irrespective of the number of excited molecules. Another assumption made in the derivation is of a single quantum transition between adjacent levels of harmonic oscillators. The effect of multiple quantum transitions was investigated by Northup and Hsu [41]. They conclude that results of multiple transitions follow the general pattern of the Bethe-Teller relationship up to a temperature of 7000K. The effect of anharmonicity was investigated by Bazley an Montroll [42.]. Their calculations show that the deviations of the fractional level population from the harmonic oscillator values are generally of the order of the anharmonicity. Consequently, the relaxation behavior of a system of anharmonic oscillators can be represented quite accurately by that of a system of harmonic oscillators. Goody [14] suggests that it would probably be wisest to accept Eq. (4.5) as an experimental rather than a theoretical result. Whatever reasoning one might adopt, for the physical model considered in this study, there should be no doubt now in accepting the relation given by Eq. (4.5).

In order to be able to use Eq. (4.5) an explicit relation for $\eta_c = \eta_c(T, P)$ is required. This is provided by the Landau-Teller relation

$$\eta_c = K_1 P^{-1} \exp\left(K_2 T^{-1/3}\right) , \tag{4.7}$$

where K_1 and K_2 are positive constants and depend on the physical properties of the molecule. It should be noted that the vibrational relaxation time increases with decreasing pressure and temperature. Generally, the product of pressure and relaxation time is plotted against the temperature on a logarithmic scale. Such a plot is known as Landau-Teller plot and for two level transitions it is a straight line for a wide range of temperatures.

Information on collisional relaxation times is available in the literature for some molecular gases [43–66]. For diatomic gases, an empirical relation is given by Millikan and White [50, 52, 66]

$$P\eta_c = \exp\left[A\left(T^{-1/3} - 0.015\mu^{1/4}\right) - 18.42\right] \tag{4.8}$$

where A is a constant and is related to the molecular constants of the colliding species and μ is the reduced mass of the colliding pairs. Values of A and μ are given in the references, and for CO colliding with CO these are A = 175, and μ = 14. The collisional relaxation time for CO_2 is given by the relation [53]

$$P\eta_c = \exp\left(AT^{-1/3} - B\right) \times 10^{-6} \tag{4.9}$$

where $A = 36.5$ and $B = -3.9$. The collisional relaxation time for methane is given by Richards and Sigafoos as [56]

$$P\eta_c = \exp\left(-5.4 + 40T^{-1/3}\right) \times 10^{-6} \tag{4.10}$$

In all expressions for η_c, P is the total pressure in atmosphere, η_c is in seconds, and T represents the temperature in degrees Kelvin. Although these relations show a strong dependency of η_c on pressure, in reality it has a larger temperature variation. This is because collisional frequencies are higher at higher temperatures and consequently it takes relatively less time to deactivate the excited states. Further discussions on collisional relaxation times for different colliding pairs are provided by Tiwari and Manian in [67].

4.3 The Equation of Radiative Transfer

The equation of radiative transfer is derived for a simple harmonic oscillator on the assumption that rotational and vibrational levels are populated according to the Boltzmann distribution. The rotational energy is characterized by the equilibrium temperature whereas the vibrational energy is described by the nonequilibrium temperature T_v. The derivation which follows is analogous to that of Goody [14] and Gilles [69].

Two level transitions between the vibrational states are considered such that there results a single independent vibration-rotation band corresponding to the fundamental frequency of vibration. Consequently, the nonequilibrium transfer equation, as presented here, is only applicable to fundamental bands of diatomic and polyatomic gases. At moderate temperatures, however, the combination and overtone bands do not contribute significantly to the radiative transfer processes except at very large path lengths. For the conditions where the assumption of local thermodynamic equilibrium is valid, the transfer equation given here will reduce directly to the traditional macroscopic equation for radiative transfer available in the literature [11, 12, 18].

For a two level system let $n(v-1)$ and $n(v)$ represent the number density of molecules in the lower and upper vibrational levels respectively. In each vibrational level, molecules are assumed to be distributed over rotational levels according to the Boltzmann distribution function $f(J)$ such that $\sum_J f(J) = 1$. Here v is the vibrational quantum number and J is a set of rotational quantum numbers corresponding to the lower vibrational level. Consequently, number density in the state $(v-1, J)$ will be given as $n(v-1)\, f(J)$. Number of molecules that actually make the transition from a state $(v-1, J)$ to (v, J') are governed by the Einstein coefficients, a $(J', J)A(v, v-1)$ for spontaneous emission, $b(J', J)B(v, v-1)$ for induced or stimulated emission, and $b(J, J')B(v-1, v)$ for absorption. Based on the assumption that rotational and vibrational wave functions are separable, the multiplication of J and v coefficients is possible.

Further, for J coefficients it can be assumed that

$$\sum_J a(J', J) = \sum_J b(J', J) = \sum_J b(J, J') = 1$$

Spontaneous emission is independent of radiation field, i.e., it is isotropic. However, absorption and induced emission depend upon the intensity of radiation I_ν. Following Goody [14], sharp energy levels are initially considered and the transition is assumed to take place with the loss of a quantum of energy $h\nu$. In a rigorous analysis, by considering the broadening of the energy levels and by defining a line shape function, Gilles [68] derives the same transfer equation as given by Goody after the latter relaxes the requirements of sharp levels. For details, reference should be made to these works.

For a two level transition of molecules contained in a volume of depth ds and unit cross section, the change in radiative intensity, within the solid angle $d\Omega$, may be written as

$$\begin{aligned}\frac{dI_\nu}{ds}d\Omega = {} & n(v)f(J')a(J', J)A(v, v-1)\left(\frac{d\Omega}{4\pi}\right) \\ & - [n(v-1)f(J)b(J, J')B(v-1, v) \\ & - n(v)f(J')b(J', J)B(v, v-1)]\frac{I_\nu}{c}d\Omega \end{aligned} \tag{4.11}$$

where the first term on the right hand side represents the contribution due to spontaneous emission, the second and third terms represent absorption and induced emission respectively, and c is the speed of light.

Application of the principle of detailed balance gives the following relationships between the Einstein coefficients

$$a(J', J)A(v, v-1) = \delta_\nu b(J', J)B(v, v-1) \tag{4.12a}$$

$$b(J', J)B(v, v-1) = \frac{g(J)}{g(J')}b(J, J')B(v-1, v) \tag{4.12b}$$

where $\delta_\nu = 8\pi\nu^2/c^3$, and $g(J)$ is the statistical weight of J rotational level. For a simple harmonic oscillator, the following expression is obtained from quantum mechanics

$$B(v, v-1) = vB(0, 1) \tag{4.13}$$

Introduction of Eqs. (4.12) and (4.13) into Eq. (4.11) enables one to write the transfer equation solely in terms of the coefficient $B(0,1)$. Since each pair of vibrational levels of a simple harmonic oscillation absorb and emit identical quanta, a summation over all vibrational levels must be taken. In doing so, following relationships are further employed

$$E_v = \sum_{v=1}^{\infty} v\, n(v) \tag{4.14}$$

where E_v is written in the normalized form, and

$$E_v^* = n[\exp(h\nu_o/kT) - 1]^{-1} \tag{4.15}$$

such that [16]

$$E_v/E_v^* = [\exp(h\nu_o/kT) - 1]/[\exp(h\nu_o/kT_v) - 1] \tag{4.16}$$

In writing Eq. (4.16) it has been assumed that the energy distribution over the vibrational levels is of the Boltzmann type with a corresponding nonequilibrium temperature T_v. Goody [14] does not explicitly make this assumption and derives the transfer equation directly in terms of the ratio E_v/E_v^*.

By making use of all above information, the transfer equation, Eq. (4.11), can now be written as

$$\frac{dI_\nu}{ds} = \frac{nB(0,1)b(J,J')f(J)}{c[1-\exp(-h_{\nu_o}/kT_v)]}\left\{\frac{2h\nu^3}{c^2}\exp\left[-\frac{h}{k}\left(\frac{\nu_o}{T_v}+\frac{\nu-\nu_o}{T}\right)\right]\right.$$
$$\left. - I_\nu + I_\nu \exp\left[-\frac{h}{k}\left(\frac{\nu_o}{T_v}+\frac{\nu-\nu_o}{T}\right)\right]\right\} \tag{4.17}$$

where n is the total number of molecules. The form of this equation is identical to that of Eq. (4.11), i.e., the terms on the right hand side represent contributions due to spontaneous emission, absorption, and induced emission, respectively. Equation (4.17) is analogous to the transfer equation obtained by Gilles [68].

Defining the net absorption coefficient κ_ν and a source function S_ν in the following manner, Eq. (4.17) is expressed as

$$\frac{dI_\nu}{ds} = \kappa_\nu(S_\nu - I_\nu) \tag{4.18a}$$

where

$$\kappa_\nu(n,T,T_v) = \frac{nB(0,1)b(J,J')f(J)}{c[1-\exp(-h\nu_o/kT_v)]}\left\{1-\exp\left[-\frac{h}{k}\left(\frac{\nu_o}{T_v}+\frac{\nu-\nu_o}{T}\right)\right]\right\} \tag{4.18b}$$

$$S_\nu(T,T_\nu) = (2h\nu^3/c^2)\left\{\exp\left[\frac{h}{k}\left(\frac{\nu_o}{T_v}+\frac{\nu-\nu_o}{T}\right)\right]-1\right\} \tag{4.18c}$$

For the physical model considered here, Eq. (4.18) is the most general form of the radiative transfer equation. Under the assumption of LTE, $T_v = T$, and there is obtained from Eqs. (4.18b) and (4.18c)

$$\kappa_\nu^*(n,T) = \frac{nB(0,1)}{c}\, b(J,J')f(J)\frac{1-\exp(-h\nu/kT)}{1-\exp(-h\nu_o/kT)} \tag{4.19a}$$

$$S_\nu^* = B_\nu(T) = (2h\nu^3/c^2)/[\exp(h\nu/kT)-1] \tag{4.19b}$$

where B_ν represents the blackbody intensity of frequency ν at local temperature.

A combination of Eqs. (4.16) through (4.19) gives an alternate form of the radiative transfer equation as

$$\frac{dI_\nu}{ds} = \kappa_\nu\left(\frac{\kappa_\nu^*}{\kappa_\nu}B_\nu\frac{E_v}{E_v^*}-I_\nu\right) = \kappa_\nu^*\left(B_\nu\frac{E_v}{E_v^*}-\frac{\kappa_\nu}{\kappa_\nu^*}I_\nu\right) \tag{4.20}$$

This is the form of nonequilibrium transfer equation obtained by Goody [14]. It is seen that the quantity $B_\nu(\kappa_\nu^*/\kappa_\nu)(E_\nu/E_v^*)$ is the source function $S(T,T_v)$. Another form of the nonequilibrium transfer equation is derived by Tiwari and Manian in [67].

Before proceeding further, it is necessary to clarify a few points pertaining to the preceding equations and then make some useful approximations. From Eqs. (4.18b) and (4.19a), it is

apparent that at the band center the nonequilibrium absorption coefficient κ_ν is equal to its equilibrium counterpart κ_ν^*. Away from the band center κ_ν has a very weak dependence on T_v. It was pointed out by Goody [14] that at atmospheric temperatures, the ratio κ_ν/κ_ν^* differs from unity by less than 1.5% in the wings of the 15μ CO_2 band (probably the worst case), as E_v/E_v^* varies over a wide range of 0 to 2. In reality, it is the equilibrium value of the absorption coefficient actually measured in the laboratory. Following such reasonings, the differences between κ_ν and κ_ν^* are usually ignored. With this in mind, an examination of Eqs. (4.17) and (4.20) would reveal that the effect of vibrational nonequilibrium is only important in the spontaneous emission. This fact has also been discussed and experimentally established by Millikan [47] and Hooker and Millikan [49]. However, according to Gilles [68] this corresponds to a low temperature approximation and is only valid when vibrational and kinetic temperatures are of the same order of magnitude. He argues that at high temperatures NLTE effects cannot be ignored from the induced emission and absorption terms, and introduces two other approximations.

Further, from Eq. (4.18), it should be noted that at $\nu = \nu_o$ the source function becomes the Planck function evaluated at the nonequilibrium temperature T_v, and away from the band center it has only a weak dependency on the kinetic temperature.

For the present study, the difference between κ_ν and κ_ν^* are ignored, and Eq. (4.20) is taken as the nonequilibrium radiative transfer equation. In essence, it is assumed here that the absorption coefficient is independent of the nonequilibrium effects and that the NLTE effects come only through the source function, which can now be written as $J_\nu(T, T_v) = B_\nu(E_v/E_v^*)$. This notation for the source function is introduced to distinguish it from the previous notation of $S_\nu(T, T_v)$.

Under steady-state conditions, for each fundamental band, a combination of Eqs. (4.4), (4.5)

and (4.20) yields

$$(E_v/E_v^*)\left[(E_v^*/\eta_c)+\int d\Omega\int \kappa_\nu B_\nu d\nu\right]=(E_v^*/\eta_c)+\int d\Omega\int \kappa_\nu I_\nu d\nu \tag{4.21}$$

where integration is taken over the frequency range of an individual band and over the solid angle from zero to 4π. Defining a time constant η_r as

$$\eta_r = E_v^*/\left[\int d\Omega\int \kappa_\nu B_\nu d\nu\right] \tag{4.22}$$

and combining Eqs. (4.20) and (4.21), there is obtained

$$\frac{dI_\nu}{ds}=\kappa_\nu(J_\nu - I_\nu) \tag{4.23a}$$

where

$$J_\nu = B_\nu[(\eta_r+\eta_c X)/(\eta_r+\eta_c)] \tag{4.23b}$$

$$X=\left(\int d\Omega\int \kappa_\nu I_\nu d\nu\right)/\left(\int d\Omega\int \kappa_\nu B_\nu d\nu\right) \tag{4.23c}$$

It can be shown [33] that $\eta_r = 1/A(1,0)$ is the radiative lifetime of the vibrational states, where $A(1,0)$ is the Einstein coefficient for spontaneous emission from the first vibration level.

By employing Eqs. (4.3) and (4.23), the source function J_ν can be expressed in an alternate form as

$$J_\nu=\frac{B_\nu}{\eta_r+\eta}\left\{\eta_r+\eta_c\left[\left(\bar{h}+\int d\Omega\int \kappa_\nu J_\nu d\nu\right)/\left(\int d\Omega\int \kappa_\nu B_\nu d\nu\right)\right]\right\} \tag{4.24a}$$

where

$$\bar{h}=-\int (dq_{R\nu}/dy)d\nu \tag{4.24b}$$

It should be noted here that J_ν like B_ν is a slowly varying function of ν and for narrow bands it can be assumed as being independent of ν. The value for B_ν and J_ν are, therefore, taken to

be the values evaluated at the band center. Further, by noting that both B_ν and J_ν are isotropic, Eq. (4.24) is expressed as

$$J_{\nu_c} = B_{\nu_c} + \frac{1}{2}(\eta_c/\eta_r)\bar{H} \tag{4.25a}$$

where

$$\bar{H} = \bar{h}/\left(2\pi \int \kappa_\nu d\nu\right) \tag{4.25b}$$

For isotropic radiation, the blackbody intensity of radiation B_ν is related to the Planck function $e_{b\nu}$ by $e_{b\nu} = \pi B_\nu$.

In the limit of very low pressure, the collisional relaxation time η_c is large and in Eq. (4.23b) η_r can be neglected by comparison. The source function then becomes $J_\nu = B_\nu X$. Further, from Eqs. (4.3), (4.23), and (4.24), it can be shown that the divergence of radiative flux is zero. The transfer equation for this case becomes as for incoherent scattering and a general integral formulation of this is given by Wang [69]. In the limit of high pressure, on the other hand, the collisional relaxation time approaches zero and the source function, Eq. (4.23b), becomes the Planck function. This is the situation of LTE usually assumed in most radiation transfer analyses.

The degree of nonequilibrium effects is characterized by the order of magnitude of the parameter (η_c/η_r) in the transfer equation. Significant deviations from the LTE results will start when this ratio is unity or higher.

By combining Eqs. (4.15), (4.19b), and (4.22) and by noting that within the band B_ν is assumed to be independent of frequency, an expression of η_r is obtained

$$\eta_r^{-1} = 8\pi(\nu_o/c)^2 \int (\kappa_\nu/n)d\nu = 8\pi c\omega_c^2(P/n) \int (\kappa_\omega/P)d\omega \tag{4.26}$$

where n is the number density of molecules, and $\omega_c = (\nu_o/c)$ is the wave number corresponding to ν_o. In order to be consistent with the definition of κ_ν as given in Eq. (4.19a), B_ν was first divided by $h\nu$ and then used to obtain the above relation. Applying the perfect gas law $P = nkT$,

and by using appropriate units for c and k, Eq. (4.26) is expressed in an alternate form as

$$\eta_r^{-1} = (8\pi\omega_c^2)(4.08 \times 10^{-12})T_o S(T_o) \tag{4.27}$$

where $S(T_o)$ having the units of cm^{-2} – atm^{-1} is the integrated band intensity and is defined in the next section, T_o is a reference temperature, and η_r has the units of seconds. For fundamental bands of some important molecules, values of η_r were calculated and these are provided in Appendix A.

4.4 Band Absorption and Correlations

The study of radiative transmission in nonhomgeneous gaseous systems requires a detailed knowledge of the absorption, emission, and scattering characteristics of the specific species under investigation. In absorbing and emitting mediums, an accurate model for the spectral absorption coefficient is of vital importance in the correct formulation of the radiative flux equations. A systematic representation of the absorption by a gas, in the infrared, requires the identification of the major infrared bands and evaluation of the line parameters (line intensity, line half-width, and spacing between the lines) of these bands. The line parameters depend upon the temperature, pressure and concentration of the absorbing molecules and, in general, these quantities vary continuously along a nonhomogeneous path in the medium. In recent years, considerable efforts have been expended in obtaining the line parameters and absorption coefficients of important atomic and molecular species [70-76].

A quantity that has application with respect to the band approximation is the integrated band absorption S, also known as integrated band intensity or simply band intensity, and is defined as

$$S(T) = \int_{\Delta\omega} \frac{\kappa_\omega}{P} d\omega \tag{4.28}$$

where κ_ω is the spectral absorption coefficient. This quantity is independent of pressure because the total area of he individual rotational lines is not dependent on pressure. The temperature

variation of the integrated band intensity is given by the relation [33-37]

$$TS(T) = T_o S(T_o) F(T) \tag{4.29}$$

where T_o denotes an arbitrary reference temperature. $F(T) = 1$ for fundamental and pure rotation bands, but it differs from unity for overtone and combination bands. For combination and overtone bands of important molecules, relations for $F(T)$ are available in the literature [35, 70-74]. Band intensities for some important gases are presented in Appendix A.

As discussed by Sparrow and Cess [18], optically thin radiation can often be formulated in terms of the Planck mean absorption coefficient κ_p, and the modified Planck mean absorption coefficient κ_m, which for a single band are defined as

$$\kappa_p(T) = \frac{\int_{\Delta\omega} \kappa_\omega(T) e_\omega(T) d\omega}{e(T)} \tag{4.30}$$

$$\kappa_m(T, T_1) = \frac{\int_{\Delta\omega} \kappa_\omega(T) e_\omega(T_1) d\omega}{\sigma T_1^4} \tag{4.31}$$

In accordance with the previous assumption of the Planck function $e_\omega(T)$ being independent of wave number within the band, and by making use of Eqs. (4.28) and (4.29), Eqs. (4.30) and (4.31) can be expressed as

$$\frac{\kappa_p(T)}{p} = \frac{e_{\omega c}(T)}{\sigma T^4} S(T) \tag{4.32}$$

and

$$\frac{\kappa_m(T, T_1)}{P} = \frac{e_{\omega c}(T_1)}{\sigma T_1^4} S(T) = \frac{\kappa_p(T_1)}{P} \frac{T_1}{T} \tag{4.33a}$$

It must be noted here that both $\kappa_p(T)/P$, and $\kappa_m(T, T_1)/P$ are independent of the actual line structure of the band. However, the line structure will influence the range of applicability of the optical thin limit. This is due the fact that the gas must be optically thin for all values of wave number, such that $(\kappa_\omega)_{\max} L << 1$, where $(\kappa_\omega)_{\max}$ denotes the maximum value of κ_ω within the band.

In general, definitions of κ_p and κ_m can be extended to multi-band gases, and through a combination of Eqs. (4.29) through (4.31), the following relation can be established

$$\frac{T\kappa_m(T,T_1)}{T_1\kappa_p(T_1)} = \frac{\sum_{i=1}^{n} e_{\omega i}(T_1)S_i(T_o)F_i(T)}{\sum_{i=1}^{n} e_{\omega i}(T_1)S_i(T_o)F_i(T_1)} \tag{4.33b}$$

where n represents the number of bands. By including the contributions from overtone and combination bands, calculations performed for CO, CO_2, and H_2O indicate [77] that the ratio on the right side of Eq. (4.33b) is approximately equal to unity and, therefore, Eq. (4.33a) can be regarded as an excellent approximation of Eq. (4.33b).

Equation (4.32) is expressed for a multiband system of a homogeneous gas as

$$\kappa_p(T) = P\sum_{i=1}^{n}[e_b(\omega_{ci},T)S_i(T)]/(\sigma T^4) \tag{4.34}$$

This can be modified to apply to a mixture of different gases as

$$\kappa_p(T) = \sum_j P_j\left\{\sum_{i=1}^{n}[e_b(\omega_{ci},T)S_i(T)]\right\}_j/(\sigma T^4) \tag{4.35}$$

where j denotes the number of species in the mixture and P_j is the partial pressure of the jth species.

Several models for the mean absorption coefficient are available in the literature [18, 33, 78]. Since these models account for detailed spectral information of molecular bands, this approach of radiative formulation is referred to as the "pseudo-gray formulation."

For an accurate evaluation of the transmittance (or absorptance) of a molecular band, a convenient line model is used to represent the variation of the spectral absorption coefficient. The line models usually employed are Lorentz, Doppler, and Voigt line profiles. A complete formulation (and comparison) of the transmittance and absorptance by these line profiles is given in [33-37]. In a particular band consisting of many lines, the absorption coefficient varies very rapidly with the frequency. Thus, it becomes very difficult and time-consuming task to evaluate

the total band absorptance over the actual band contour by employing an appropriate line profile model. Consequently, several approximate band models (narrow as well as wide) have been proposed which represent absorption from an actual band with reasonable accuracy [33–37, 79-88]. Several continuous correlations for the total band absorption are available in literature [33-37, 84-88]. These have been employed in many nongray radiative transfer analyses with varying degree of success. A brief discussion is presented here on the total band absorption, band models, and band absorptance correlations.

The absorption within a narrow spectral interval of a vibration rotation band can quite accurately be represented by the so-called "narrow band models." For a homogeneous path, the total absorptance of a narrow band is given by

$$A_N = \int_{\Delta\omega} [1 - \exp(-\kappa_\omega X)] d\omega \tag{4.36}$$

where κ_ω is the volumetric absorption coefficients, ω is the wave number, and $X = py$ is the pressure path length. The limits of integration in Eq. (4.36) are over the narrow band pass considered. The total band absorptance of the so-called "wide band models" is given by

$$A = \int_{-\infty}^{\infty} [1 - \exp(-\kappa_\omega X)] d(\omega - \omega_o) \tag{4.37}$$

where the limits of integration are over the entire band pass and ω_o is the wave number at the center of the wide band. In actual radiative transfer analyses, the quantity of frequent interest is the derivative of Eqs. (4.36) and (4.37).

Four commonly used narrow band models are Elsasser, Statistical, Random Elsasser, and Quasi-Random. The application of a model to a particular case depends upon the nature of the absorbing emitting molecule. Complete discussion on narrow bands models, and expressions for transmittance and integrated absorptance are available in the literature [33-37, 79-81]. Detailed discussions on the wide band models are given in [33-37, 82-88]. The relations for total band

absorptance of a wide band are obtained from the absorptance formulations of narrow band models by employing the relations for the variation of line intensity as [33–37, 85-88]

$$S_j/d = (S/A_o)\exp\{[-b_o|\omega-\omega_o|]/A_o\} \tag{4.38}$$

where S_j is the intensity of the jth spectral line, d is the line spacing, S is the integrated intensity of a wide band, A_o is the band width parameter, and $b_o = 2$ for a symmetrical band and $b_o = 1$ for bands with upper and lower wave number heads at ω_o. The total absorptance of an exponential wide band, in turn, may be expressed by

$$\bar{A}(u,\beta) \equiv A(u,\beta)/A_o = \frac{1}{A_o}\int_{\substack{wide\\band}} [A_N(u,\beta)]d(\omega-\omega_o) \tag{4.39}$$

where $u = SX/A_o$ is the nondimensional path length, $\beta = 2\pi\gamma_L/d$ is the line structure parameter, γ_L is the Lorentz line half-width, and $\bar{A}_N(u,\beta)$ represents the mean absorptance of a narrow band.

By employing the Elsasser narrow band absorptance relation and Eq. (4.38) the expression for the exponential wide band absorptance is obtained as [36, 37].

$$\bar{A}(u,\beta) = \gamma + (1/\pi)\int_o^\pi [\ln\psi + E_1(\psi)]dz \tag{4.40}$$

where $\psi = u\sinh\beta/(\cosh\beta - \cos z)$, γ = 0.5772156 is the Euler's constant, and $E_1(\psi)$ is the exponential integral of the first order. Analytic solution of Eq. (4.40) can be obtained in a series form as [36, 37]

$$\bar{A}(u,\beta) = \sum_{n=1}^{\infty}\{-(A)^n[SUM(mn)]/[n(B+1)^n n!(n-1)!]\} \tag{4.41}$$

where

$$SUM(mn) = \sum_{m=0}^{\infty}[(n+m-1)!(2m-1)!C^m]/\left(2^m(m!)^2\right)$$

$$A = -u\tanh\beta, B = 1/\cosh\beta$$

$$C = 2/(1+\cosh\beta) = 2B/(B+1)\ .$$

The series in Eq. (4.41) converges rapidly. When the weak line approximation for the Elsasser model is valid (i.e. β is large), then Eq. (4.40) reduces to

$$\bar{A}(u) = \gamma + \ln(u) + E_1(u) \ . \tag{4.42}$$

In the linear limit, Eqs. (4.40) and (4.41) reduce to $\bar{A} = u$, and in the logarithmic limit they reduce to $\bar{A} = \gamma + \ln(u)$. It can be shown that Eq. (4.40) reduces to the correct limiting form in the square-root limit. Results of Eqs. (4.40) and (4.41) are found to be identical for all pressures and pathlengths. For p > 1 atm, results of Eqs. (4.40)-(4.42) are in good agreement for all path lengths.

By employing the uniform statistical, general statistical, and random Elsasser narrow band models absorptance relations and Eq. (4.38), three additional expressions for the exponential wide band absorptance were obtained in [36, 37]. The absorptance results of the four wide band models are discussed in detail in [37]. The expression obtained by employing the uniform statistical model also reduces to the relation given by Eq. (4.42) for large β.

Several continuous correlations for the total absorptance of a wide band, which are valid over different values of path length and line structure parameter, are available in the literature. These are discussed, in detail, in [33–37, 85–88] and are presented here in the sequence that they became available in the literature. Most of these correlations are developed to satisfy at least some of the limiting conditions (nonoverlapping line, linear, weak line, and strong line approximation, and square-root, large pressure, and large path length limits) for the total band absorptance [34–37]. Some of the correlations even have experimental justifications [33–83].

The first correlation for the exponential wide band absorptance (a three piece correlation) was proposed by Edwards et al. [35, 82, 83]. The first continuous correlation was proposed by Tien and Lowder [33], and this is of the form

$$\bar{A}(u, \beta) = \ln(uf(t)\{(u+2)/[u+2f(t)]\} + 1) \tag{4.43}$$

where

$$f(t) = 2.94[1 - \exp(-2.60t)], t = \beta/2$$

This correlation does not reduce to the correct limiting form in the square-root limit [34-37], and its use should be made for $\beta \geq 0.1$. Further discussions on correlations proposed by Edwards et al. and by Tien and Lowder are provided in Appendix A.

Another continuous correlation was proposed by Goody and Belton [87], and in terms of the present nomenclature, this is given by

$$\bar{A}(u,\beta) = 2\ln\left\{1 + u/[4 + (\pi u/4t)]^{1/2}\right\}, \beta = 2t \tag{4.44}$$

Use of this correlation is restricted to relatively small β values [34–37]. Tien and Ling [88] have proposed a simple two parameter correlation for $\bar{A}(u,\beta)$ as

$$\bar{A}(u) = \sinh^{-1}(u) \tag{4.45}$$

which is valid only for the limit of large β. A relatively simple continuous correlation was introduced by Cess and Tiwari [34], and this is of the form

$$\bar{A}(u,\beta) = 2\ln\left(1 + u/\left\{2 + \left[u\left(1 + 1/\bar{\beta}\right)\right]^{1/2}\right\}\right) \tag{4.46}$$

where $\bar{\beta} = 4t/\pi = 2\beta/\pi$. By slightly modifying Eq. (4.46), another form of the wide band absorptance is obtained as [36, 37]

$$\bar{A}(u,\beta) = 2\ln\left(1 + u/\left\{2 + [u(c + \pi/2\beta)]^{1/2}\right\}\right) \tag{4.47}$$

where

$$c = \begin{cases} 0.1, & \beta \leq 1 \text{ and all u vlaues} \\ 0.1, & \beta > 1 \text{ and u} \leq 1 \\ 0.25, & \beta > 1 \text{ and u} > 1. \end{cases}$$

Equations (4.46) and (4.47) reduce to all the limiting forms [34].

Based on the formulation of slab band absorptance, Edwards and Balakrishnan [85] have proposed the correlation

$$\bar{A}(u) = \ln(u) + E_1(u) + \gamma + \frac{1}{2} - E_3(u) \tag{4.48}$$

which is valid for large β. For present application, this correlation should be modified by using the technique discussed in [36, 37]. Based upon the formulation of the total band absorptance from the general statistical model, Felske and Tien [86] have proposed a continuous correlation for $\bar{A}(u, \beta)$ as

$$\begin{aligned}\bar{A}(u,\beta) = {} & 2E_1(t\rho_u) + E_1(\rho_u/2) - E_1[(\rho_u/2)(1+2t)] \\ & + \ln\left[(t\rho_u)^2/(1+2t)\right] + 2\gamma\end{aligned} \tag{4.49}$$

where

$$\rho_u = \{(t/u)[1 + (t/u)]\}^{-1/2}$$

The absorptance relation given by Eq. (4.42) is another simple correlation which is valid for all path lengths and for $t = (\beta/2) \geq 1$. The relation of Eq. (4.41) can be treated as another correlation applicable to gases whose spectral behavior can be described by the Elsasser model. In Ref. 37, it was shown that the Elsasser as well as random band model formulations for the total band absorptance reduce to Eq. (4.42) for $t \geq 1$.

Band absorptance results of various correlations are compared and discussed in some detail in [36, 37]. It was found that results of these correlations could be in error by as much as 40% when compared with the exact solutions based on different band models. Felske and Tien's correlation was found to give the least error when compared with the exact solution based on the general statistical model while Tien and Lowder's correlation gave the least error when compared with the exact solution based on the Elsasser model. The results of Cess and Tiwari's correlations followed the trend of general statistical model. Tiwari and Batki's correlation [Eq. (4.41) or

(4.42)] was found to provide a uniformly better approximation for the total band absorptance at relatively high pressures. The sole motivation in presenting the various correlations here is to see if their use in actual radiative processes made any significant difference in the final results.

From the basic information presented in [36, 37], it may be concluded that use of the Tien and Lowder's correlation should be avoided at lower pressures, but its use is justified (at moderate and high pressures) to gases whose spectral behavior can be described by the regular Elasasser band model. For all pressures and path length conditions, use of the Cess and Tiwari's correlations could be made to gases with bands of highly overlapped lines. In a more realistic problem involving flow of an absorbing emitting gas, results of different correlations (except the Tien and Lowder's correlation) differ from each other by less than 6% for all pressures and path lengths. Use of Tien and Lowder's correlations is justified for gases like CO at moderate and high pressures. For gases like CO_2, use of any other correlation is recommended. The Felske and Tien's correlation is useful for all pressures and path lengths to gases having random band structure. Tiwari and Batki's simple correlation could be employed to gases with regular or random band structure but for $P \geq 1.0$ atm.

4.5 Radiative Flux Equations

Following the procedure described in [18], for the physical model illustrated in Figs. 4.1 and 4.2, and integration of the transfer equation, Eq. (4.23a), gives

$$q_{R\omega} = 2B_{1\omega}E_3(\tau_\omega) - 2B_{2\omega}E_3(\tau_{o\omega} - \tau_\omega) + 2\pi\left[\int_o^{\tau_\omega} J_\omega(t)E_2(\tau_\omega - t)dt - \int_{\tau_\omega}^{\tau_{o\omega}} J_\omega(t)E_2(t - \tau_\omega)dt\right] \tag{4.50a}$$

where

$$\tau_\omega = \kappa_\omega y \ , \quad \tau_{o\omega} = \kappa_\omega L \tag{4.50b}$$

$$J_\omega(t) = \frac{e_\omega(t)}{\pi} + \frac{1}{2}\eta\bar{H}(t), \ \eta = \eta_c/\eta_r \tag{4.50c}$$

$$\bar{H}(y) = \frac{-divq_R(y)}{2\pi PS(T)} = \frac{-\int_o^\infty (dq_{R\omega}/dy)d\omega}{2\pi PS(T)} \tag{4.50d}$$

In this equation $\tau_{o\omega}$ is the optical path length and t is a dummy variable for τ_ω. The quantities $B_{1\omega}$ and $B_{2\omega}$ represent the surface radiosities, and $E_n(t)$ are the exponential integral functions. In writing the expression for the source function J_ω, use was made of the relation $e_\omega = \pi B_\omega$. Further, it has been assumed that the spectral absorption coefficient κ_ω is independent of temperature, i.e., restriction is made to moderately small temperature differences within the gas.

Following the procedure outlined in [18], expression for the surface radiosities are obtained as

$$B_{1\omega} = \varepsilon_{1\omega}e_{1\omega} + 2(1 - \varepsilon_{1\omega})\left[B_{2\omega}E_3(\tau_{o\omega}) + \pi\int_o^{\tau_{o\omega}} J\omega(t)E_2(t)dt\right] \tag{4.51a}$$

$$B_{2\omega} = \varepsilon_{2\omega}e_{2\omega} + 2(1 - \varepsilon_{2\omega})\left[B_{1\omega}E_3(\tau_{o\omega}) + \pi\int_o^{\tau_{o\omega}} J\omega(t)E_2(\tau_{o\omega} - t)dt\right] \tag{4.51b}$$

Equations (4.51) constitute two simultaneous equations for $B_{1\omega}$ and $B_{2\omega}$. For black surfaces, $B_{1\omega} = e_{1\omega}$ and $B_{2\omega} = e_{2\omega}$. Under the assumptions of LTE, $J_\omega(t) = e_\omega(t)/\pi$. For these specific situations, the simplified form of Eq. (4.50) should be obvious.

The total radiative flux is given by the expression

$$q_R = \int_o^\infty q_{R\omega} d\omega \tag{4.52}$$

In general, for nongray gases, Eq. (4.50) does not possess a correct optically thick limit. However, a correct large path length limit does exist and it will be discussed in a separate subsection. A correct optically thin limit of Eq. (4.50) exists and is given by [18]

$$\begin{aligned} q_{R\omega}(\tau_\omega) = {} & B_{1\omega}(1 - 2\tau_\omega) - B_{2\omega}(1 - 2\tau_{o\omega} + 2\tau_\omega) \\ & + 2\pi\left[\int_o^{\tau_\omega} J_\omega(t)dt - \int_{\tau_\omega}^{\tau_{o\omega}} J_\omega(t)dt\right] \end{aligned} \tag{4.53}$$

Differentiating Eq. (4.53) with respect to τ_ω and neglecting terms of $0(\tau_{o\omega})$, one finds an expression for the divergence of radiative flux as

$$-div\underset{\sim}{q}_R(y) = -\int_o^\infty \frac{dq_{R\omega}}{dy} d\omega = 2\int_o^\infty \kappa_\omega[B_{1\omega} + B_{2\omega} - 2\pi J_\omega(y)]d\omega \tag{4.54}$$

By noting the assumption on $J_\omega(y)$ as being independent of wave number, and using the definitions of Planck mean and modified Planck mean absorption coefficients as given by Eqs. (4.30) and (4.31), Eq. (4.54) is written in an alternate form as

$$-\left(1 + \frac{\eta_c}{\eta_r}\right)\frac{dq_R}{dy} = 2B_1\kappa_m(T, T_1) + 2B_2\kappa_m(T, T_2) - 4\kappa_p(T)\sigma T^4(y) \tag{4.55}$$

The expressions for surface radiosities corresponding to the optically thin limit are available in [18].

The obvious simplification of NLTE effect in Eq. (4.55) should be noted. As such, all optically thin analyses based on the assumption of LTE can be modified to include the effect

of NLTE simply by multiplying the divergence of the radiative flux by a constant involving the nonequilibrium parameter $\eta = \eta_c/\eta_r$.

Under the assumption of LTE, Eq. (4.50a) may be expressed for black bounding surfaces as

$$q_{R\omega}(\tau_\omega) = e_{1\omega} - e_{2\omega} + 2\left[\int_o^{\tau_\omega} F_{1\omega}(t)E_2(\tau_\omega - t)dt - \int_{\tau_\omega}^{\tau_{o\omega}} F_2(t)E_2(t - \tau_\omega)dt\right] \tag{4.56}$$

where $F_{1\omega}(t) = e_\omega(t) - e_{1\omega}$; $F_2(t) = e_\omega(t) - e_{2\omega}$. A direct differentiation of Eq. (4.56) results in

$$-\frac{dq_{R\omega}}{d\tau_\omega} = -2[F_{1\omega}(\tau_\omega) + F_{2\omega}(\tau_\omega)] + 2\left[\int_o^{\tau_\omega} F_{1\omega}(t)E_1(\tau_\omega - t)dt + \int_{\tau_\omega}^{\tau_{o\omega}} F_{2\omega}(t)E_1(t - \tau_\omega)dt\right] \tag{4.57}$$

Equation (4.56) and (4.57) are the LTE equations for one-dimensional absorbing-emitting medium with diffuse nonreflecting boundaries and are very useful for many engineering applications

4.5.1 Fundamental Approximations and Resulting Equations

An often employed approximation in radiative transfer problems involves replacing the exponential integral $E_n(t)$ by an exponential function. The procedure for obtaining this approximation and its validity is discussed in [18]. For the present situation, the exponential integrals $E_2(t)$ and $E_3(t)$ are approximated by

$$E_2(t) \simeq \frac{3}{4}\exp\left(-\frac{3}{2}t\right) \tag{4.58a}$$

$$E_3(t) = -\int E_2(t)dt \simeq \frac{1}{2}\exp\left(-\frac{3}{2}t\right) \tag{4.58b}$$

Employing these approximations, Eq. (4.50) is expressed in physical coordinates as

$$q_{R\omega} = B_{1\omega}\exp\left(-\frac{3}{2}\kappa_\omega y\right) - B_{2\omega}\exp\left[-\frac{3}{2}\kappa_\omega(L - y)\right] + \frac{3\pi}{2}\left\{\int_o^y J_\omega(z)\kappa_\omega \exp\left[-\frac{3}{2}\kappa_\omega(y - z)\right]dz - \int_y^L J_\omega(z)\kappa_\omega \exp\left[-\frac{3}{2}\kappa_\omega(z - y)\right]dz\right\} \tag{4.59}$$

At the same time Eqs. (4.58) should also be used in Eqs. (4.51) to obtain corresponding expressions for the surface radiosities. In order to avoid writing expressions for the radiosities in the subsequent discussion, attention will be directed only to black bounding surfaces.

Again, by noting the assumptions on $J_\omega(y)$ as being independent of wave number within the band, for black bounding surfaces, a combination of Eqs. (4.52) and (4.59) gives

$$\begin{aligned} q_R &= e_1 - e_2 \\ &+ \frac{3}{2}\int_o^y [\pi J_{\omega c}(z) - e_{1\omega c}] \int_{\Delta\omega} \kappa_\omega \exp\left[-\frac{3}{2}\kappa_\omega(y-z)\right] d\omega dz \\ &- \frac{3}{2}\int_y^L [\pi J_{\omega c}(z) - e_{2\omega c}] \int_{\Delta\omega} \kappa_\omega \exp\left[-\frac{3}{2}\kappa_\omega(z-y)\right] d\omega dz \end{aligned} \tag{4.60}$$

Equation (4.60) may now be formulated in terms of the derivative of the total band absorptance, $A'(y)$, since the kernal of the integrals in this equation have exactly the same form as the derivative of the total band absorptance obtainable from Eq. (4.37). After expressing Eq. (4.60) in terms of $A'(y)$, it should be noted that the correlations for the total band absorptance are available in terms of the dimensionless path length u. Thus it would be convenient to re-express the resulting equation in terms of u. This is done by defining $u_o = (S/A_o)PL$, and by letting u' be the dummy variable for u. After this has been accomplished then by defining the dimensionless independent variable as

$$\xi = \frac{y}{L} = \frac{\tau_\omega}{\tau_{o\omega}} = \frac{u}{u_o};\ \ \xi' = \frac{u'}{u_o} = \frac{z}{L} \tag{4.61}$$

the equation for the radiative flux is expressed in its final form as

$$\begin{aligned} q_R(\xi) &= e_1 - e_2 \\ &+ \frac{3}{2}A_o u_o \left\{ \int_o^\xi F_{1\omega_c}(\xi')\bar{A}'\left[\frac{3}{2}u_o(\xi-\xi')\right] d\xi' \right. \\ &\left. - \int_\xi^1 F_{2\omega_c}(\xi')\bar{A}'\left[\frac{3}{2}u_o(\xi'-\xi)\right] d\xi' \right\} \\ &- \frac{3}{8}\eta \left\{ \int_o^\xi \left(\frac{dq_R}{d\xi'}\right)\bar{A}'\left[\frac{3}{2}u_o(\xi-\xi')\right] d\xi' \right. \end{aligned}$$

$$- \int_{\xi}^{1} \left(\frac{dq_R}{d\xi'}\right) \bar{A}'\left[\frac{3}{2}u_o(\xi' - \xi)\right] d\xi' \Bigg\} \tag{4.62}$$

where $\bar{A}'(u)$ denotes the derivative of the dimensionless band absorptance $\bar{A}(u)$ with respect to u.

Performing spatial integration by parts, Eq. (4.62) can be expressed in an alternate form as

$$\begin{aligned} q_R(\xi) = e_1 - e_2 + A_o \Bigg\{ & \int_{o}^{\xi} \frac{de_{\omega c}}{d\xi'} \bar{A}\left[\frac{3}{2}u_o(\xi - \xi')\right] d\xi' \\ & + \int_{\xi}^{1} \frac{de_{\omega c}}{d\xi'} \bar{A}\left[\frac{3}{2}u_o(\xi' - \xi)\right] d\xi' \Bigg\} \\ & - \frac{3}{8}\eta \Bigg\{ \frac{dq_R}{d\xi'} \bar{A}'\left[\frac{3}{2}u_o(\xi - \xi')\right] d\xi' \\ & - \int_{\xi}^{1} \frac{dq_R}{d\xi'} \bar{A}'\left[\frac{3}{2}u_o(\xi' - \xi)\right] d\xi' \Bigg\} \end{aligned} \tag{4.63}$$

In obtaining this equation it was assumed that $e_{\omega c}(0) = e_{1\omega c}$, and $e_{\omega c}(1) = e_{2\omega c}$, which is correct only in the large path length limit. Consequently, Eq. (4.63) is applicable only in the limit of large u_o.

Since restriction is made to moderately small temperature differences within the gas, Planck function $e_\omega(\xi)$ can therefore be linearized as

$$e_\omega(\xi) \simeq e_{1\omega} + (de_\omega/dT)_{T_1}(T - T_1) \tag{4.64}$$

By employing Eq. (4.64), linearized form of the radiative flux equations, Eqs. (4.62) and (4.63), can be obtained.

Because of the restrictions of two level transitions inherent in the nonequilibrium transfer equation, the radiative flux equations given by Eqs. (4.62) and (4.63) are applicable to gases with only one fundamental band contributing to the radiative process. These equations, therefore, are useful in describing radiative transfer only in diatomic gases where contributions from the overtone bands are not important. For gases with more than one fundamental band, where each band independently contributes to the radiative process, Eq. (4.62) is written in the form

$$q_R(\xi) = e_1 - e_2$$

$$+\frac{3}{2}\sum_{i=1}^{n}A_{oi}u_{oi}\left\{\int_{o}^{\xi}F_{1\omega_i}\bar{A}_i'\left[\frac{3}{2}u_{oi}(\xi-\xi')d\xi'\right]\right.$$
$$\left.-\int_{\xi}^{1}F_{2\omega_i}\bar{A}_i'\left[\frac{3}{2}u_{oi}(\xi'-\xi)\right]d\xi'\right\}$$
$$-\frac{3}{8}\sum_{i=1}^{n}\eta_i\left\{\int_{o}^{\xi}\frac{dq_R}{d\xi'}\bar{A}_i'\left[\frac{3}{2}u_{oi}(\xi-\xi')\right]d\xi'\right.$$
$$\left.-\int_{\xi}^{1}\frac{dq_R}{d\xi'}\bar{A}_i'\left[\frac{3}{2}u_{oi}(\xi'-\xi)\right]d\xi'\right\} \qquad (4.65)$$

Here n denotes the number of fundamental bands. Equation (4.63) can also be written in a similar form.

For the situations where assumptions of LTE are valid, the last two terms on the right hand side of Eq. (4.65) vanish and then there remains no restriction of taking summation over fundamental bands only. However, for the conditions (low pressure and moderate temperature) where NLTE effects are important, fundamental bands are of main importance to the radiative process. Contributions from the combination and overtone bands become significant only at higher temperature and pressure where conditions of LTE usually prevail. As such, Eq. (4.65) could be regarded as a general expression for the radiative flux in nongray gases.

4.5.2 Optically Thin Limit

As pointed out by Sampson [72], the effect of nonequilibrium radiation is more prominent in the optically thin limit. Many physical problems involving nonequilibrium radiation can therefore be formulated in this limit with considerable mathematical simplification. In a particular analysis, this limit is approached when optical thickness τ_o, pressure path length X, or dimensionless path length u_o is small. There are two ways of obtaining this limit. One is to employ the Planck mean and modified Planck mean coefficient and make use of Eq. (4.55), while the alternate method is to directly obtain limiting forms of governing equations. Following the second approach, and

by noting that for $u_o << 1, \bar{A}(u) = u, \bar{A}'(u) = 1$, there is obtained from Eq. (4.62)

$$\frac{dq_R}{d\xi}\left(1 + \frac{3}{4}\eta\right) = \frac{3}{2}A_o u_o\{[e_{\omega c}(\xi) - e_{1\omega c}] + [e_{\omega c}(\xi) - e_{2\omega c}]\} \tag{4.66}$$

Equation (4.66) along with the equation for the conservation of energy will describe a physical problem completely in the optically thin limit. It should be noted that Eq. (4.66) is essentially the same as Eq. (4.55).

4.5.3 The Large Path Length Limit

As discussed in [77, 89, 90], conventional Rosseland (or diffusion) limit does not apply to infrared gaseous radiation. For Rosseland equation to apply, the gas must be optically thick for all values of wave number that contribute to the absorption-emission process. However, there will always be optically non-thick regions in the wings of vibration-rotation bands and this prohibits using Rosseland limit as a proper limit for infrared radiation.

For vibration-rotation bands, even though the Rosseland equation is inapplicable, a large path length limit does exist and is achieved when $u_o >> 1$ for each band of importance. As shown in [77, 89, 90], in this limit $\bar{A}(u) = \ln(u)$, $\bar{A}'(u) = 1/u$, such that their substitution in Eqs. (4.62) and (4.63) gives

$$\begin{aligned} q_R(\xi) = {} & e_1 - e_2 \\ & + A_o\left[\int_o^\xi F_{1\omega}(\xi')\frac{d\xi'}{\xi - \xi'} + \int_\xi^1 F_{2\omega}(\xi')\frac{d\xi'}{\xi - \xi'}\right] \\ & - \frac{1}{4u_o}\eta\left[\int_o^1 (dq_R/d\xi')\frac{d\xi'}{\xi - \xi'}\right] \end{aligned} \tag{4.67}$$

and

$$\begin{aligned} q_R(\xi) = {} & e_1 - e_2 \\ & + A_o\left\{\int_o^\xi \frac{de_\omega}{d\xi'}\ln\left[\frac{3}{2}u_o(\xi - \xi')\right]d\xi' + \int_\xi^1 \frac{de_\omega}{d\xi'}\ln\left[\frac{3}{2}u_o(\xi' - \xi)\right]d\xi'\right\} \\ & - \frac{1}{4u_o}\eta\left[\int_o^1 (dq_R/d\xi')\frac{d\xi'}{\xi - \xi'}\right] \end{aligned} \tag{4.68}$$

In order to obtain the divergence of the radiative heat flux and to compare the order of magnitude of each term in the resulting equation, it seems convenient to work with Eq. (4.68). Differentiation of Eq. (4.68) is performed by using the Cauchy principle and there is obtained

$$\frac{dq_R}{d\xi} = A_o \int_o^1 \frac{de_{\omega c}}{d\xi'} \frac{d\xi'}{\xi - \xi'} + \frac{1}{4u_o}\eta \int_o^1 \frac{dq_R}{d\xi'} \frac{d\xi'}{(\xi - \xi')^2} \,. \tag{4.69}$$

Since, for the gas models considered here, the quantity $\eta = \eta_c/\eta_r$ will not be much higher than of order one, in the limit of large u_o, Eq. (4.69) reduces to

$$\frac{dq_R}{d\xi} = A_o \int_o^1 \left(de_{\omega c}/d\xi'\right) \frac{d\xi'}{\xi - \xi'} \tag{4.70}$$

which is purely an equilibrium result. The vanishing of nonequilibrium effects in this limit can further be seen from the consideration of the source function. It should be recalled, from the discussion of Sec. 4.2, that the NLTE effects come only through the source function. The source function, as given by Eq. (4.50c), can be expressed in the following form

$$J_\omega(\xi) = \frac{e_\omega(\xi)}{\pi} - \frac{\eta}{4\pi u_o A_o} \frac{dq_R}{d\xi} \,. \tag{4.71}$$

A combination of Eqs. (4.69) and (4.71) results in

$$J_\omega(\xi) = \frac{e_\omega(\xi)}{\pi} - \frac{1}{4\pi}\eta \left\{ \frac{1}{u_o} \int_o^1 \frac{de_{\omega c}}{d\xi'} \frac{d\xi'}{\xi - \xi'} + \frac{1}{4A_o u_o^2} \int_o^1 \frac{dq_R}{d\xi'} \frac{d\xi'}{(\xi - \xi')^2} \right\} \tag{4.72}$$

From a comparison of the order of magnitude of each term in this equation, it is noted that in the large u_o limit the source function $J_\omega(\xi)$ becomes the Planck function $e_\omega(\xi)/\pi$, and according to the Kirchhoff's law the conditions of LTE prevail.

From a physical point of view, it should be noted that the large u_o limit is achieved by either going to higher pressures or to larger path lengths. In case of high pressures, the energy levels are

populated mainly by collisions (a collision dominated process) and consequently the conditions of LTE prevail. On the other hand, when the large u_o limit is achieved as a result of large path length, then LTE is assured by the conditions for optically thick radiation (photon continuum).

4.5.4 Gray Gas Formulation

Under the assumption of LTE, a combination of Eqs. (4.52) and (4.59) results in (for black bounding surfaces and gray gas approximation)

$$q_R(\tau) = F(\tau) + \Gamma\left\{\int_o^\tau T^4(t)\exp\left[-b(\tau - t)\right]dt - \int_\tau^{\tau_o} T^4(t)\exp\left[-b(t-\tau)\right]dt\right\} \tag{4.73}$$

where

$$F(\tau) = \sigma T_1^4 \exp\left(-b\tau\right) - \sigma T_2^4 \exp\left[-b(\tau_o - \tau)\right]$$

and $b = 3/2$ and $\Gamma = b\sigma$. Differentiation of Eq. (4.73) twice by using the Leibnitz formula results in

$$\frac{d^2 q_R}{d\tau^2} = \frac{d^2 F}{d\tau^2} + 2\Gamma\frac{dT^4}{d\tau} + \Gamma b^2\left\{\int_o^\tau T^4(t)\exp\left[-b(\tau - t)\right]dt - \int_\tau^{\tau_o} T^4(t)\exp\left[-b(t-\tau)\right]dt\right\} \tag{4.74}$$

Eliminating the integrals between Eqs. (4.73) and (4.74), one obtains

$$\frac{d^2 q_R}{d\tau^2} - b^2 q_R(\tau) = 2\Gamma\frac{dT^4}{d\tau} + \frac{d^2 F}{d\tau^2} - b^2 F(\tau) \tag{4.75}$$

Equation (4.75) is the general differential equation for radiative flux for gray gas approximation. For the specific relation of $F(\tau)$ as defined in Eq. (4.73), there is obtained $d^2F/d\tau^2 + b^2F(\tau) = 0$. Consequently, Eq. (4.75) reduces to

$$\frac{d^2 q_R}{d\tau^2} - \frac{9}{4}q_R = 3\sigma\frac{dT^4}{d\tau} \tag{4.76}$$

This is an appropriate relation for radiative flux for gray gas analyses of the present physical problem.

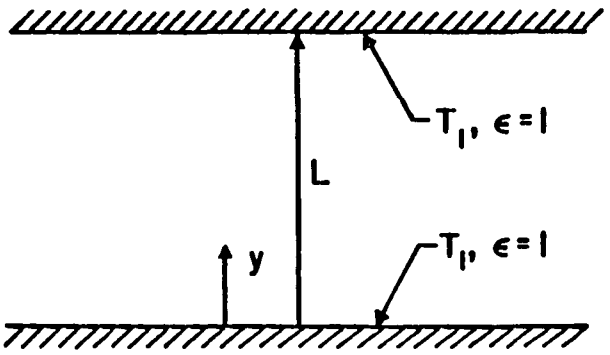

Figure 4.1 Physical model for radiative interaction

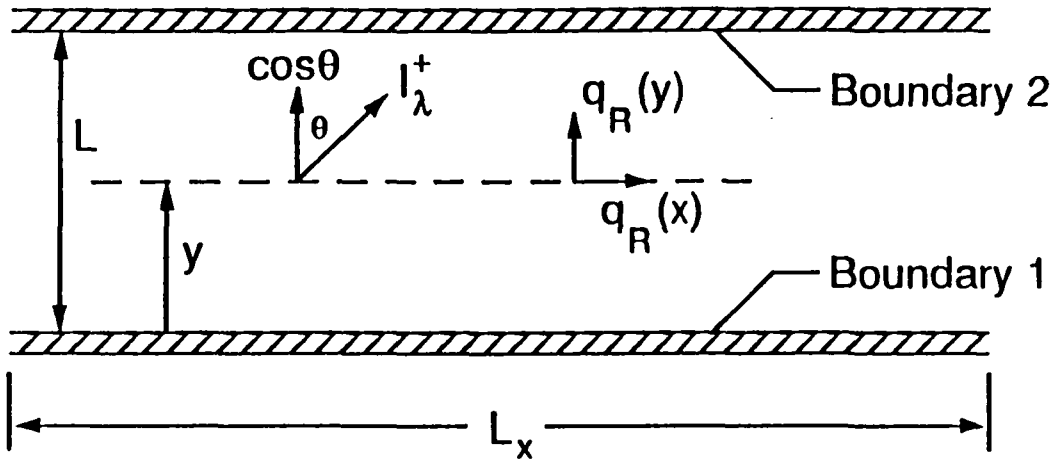

Figure 4.2 Plane radiating layer between parallel boundaries

5. RADIATIVE INTERACTION IN GASES WITH VIBRATIONAL NONEQUILIBRIUM

In this section, basic features of infrared radiative heat transfer in nongray nonisothermal gases are investigated. A general band absorptance model analysis is presented for diatomic and polyatomic gases. This model, at least in an approximate manner, accounts for the line structure behavior of the band and takes into consideration radiation in the wing regions. Other approximate band models were considered in [77]. The particular gases selected are CO, CO_2, H_2O, and CH_4 mainly because the required spectroscopic information for these gases is easily available. The effect of nonequilibrium is investigated for diatomic gases in general and for CO in particular. It is further pointed out that for CO_2 fundamental bands, at room temperature, the assumption of LTE is valid even down to a pressure of 1/100 atmosphere. Under the assumption of LTE, radiative contribution from the combination and overtone bands of CO_2 and CO is investigated. It was indicated in [71] that if band centers of two adjacent bands are separated by more than about 100 Be cm^{-1} then these bands can be treated as independent bands and any overlapping in the large path length limit can be neglected.

5.1 Infrared Radiation Transfer in Gases with Internal Heat Source

The physical model and the coordinate system are as shown in Figs. 4.1 and 5.1 except that the plate surfaces are assumed to be black and to have the same uniform temperature T_1. There is a uniform heat source (or sink) per unit volume Q within the gas. The model as stated here, would at first appear to be quite unrealistic, but it serves a very useful purpose in the investigation of the basic features of infrared radiative heat transfer. This is analogous to the problem of slug flow convection in a parallel plate channel.

5.1.1 General Formulation

From the conservation of energy, there is obtained

$$\frac{dq_R}{d\xi} = Q \tag{5.1}$$

where q_R is the total radiative flux over all wave numbers and is given by Eq. (4.65). From symmetry of the problem, it follows that $q_R = 0$ at $y = L/2$, and Eq. (5.1) may be integrated to yield

$$q_R = \frac{QL}{2}\left(2\frac{y}{L} - 1\right) \tag{5.2}$$

For the ith vibration-rotation band, a combination of Eqs. (4.61), (4.62), (5.1), and (5.2) yields

$$\begin{aligned}\frac{QL}{2}(2\xi - 1) = &\\ &+ \frac{3}{2}\int_o^\xi \left[A_{oi}u_{oi}\left[F_{1\omega_i}(\xi')\right] - (\eta_i)\frac{Q}{4}\right]\bar{A}_i'(I)d\xi' \\ &- \frac{3}{2}\int_\xi^1 \left[A_{oi}u_{oi}\left[F_{1\omega_i}(\xi')\right] - (\eta_i)\frac{Q}{4}\right]\bar{A}_i'(II)d\xi'\end{aligned} \tag{5.3}$$

where

$$\bar{A}_i'(I) = \bar{A}_i'\left[\frac{3}{2}u_{oi}(\xi - \xi')\right], \quad \bar{A}_i'(II) = \bar{A}_i'\left[\frac{3}{2}u_{oi}(\xi' - \xi)\right]$$

The integro-differential equation expressed in this form is valid for gases with only one fundamental band, i.e., to diatomic molecules. By defining a dimensionless quantity

$$\phi(\xi) = \frac{e_\omega(\xi) - e_{1\omega}}{QL/A_o u_o} = \frac{e_\omega(\xi) - e_{1\omega}}{Q/A_o C_o^2 P} \tag{5.4}$$

Eq. (5.3) may be expressed as

$$\begin{aligned}\xi - \frac{1}{2} = &\\ &+ \frac{3}{2}\int_o^\xi \left[\phi_i(\xi') - 0.25(\eta_i)\right]\bar{A}_i'(I)d\xi' \\ &- \frac{3}{2}\int_\xi^1 \left[\phi_i(\xi') - 0.25(\eta_i)\right]\bar{A}_i'(II)d\xi'\end{aligned} \tag{5.5}$$

The quantity $\phi(\xi)$ represents the temperature profile within the gas. The parameters in this equation are, the dimensionless pathlength u_o, the nonequilibrium parameter $(\eta = \eta_c/\eta_r)$ and the line structure parameter β which enters through the empirical correlation for the total band absorptance $A(u)$.

For the conditions where the assumption of LTE is justified, a combination of Eqs. (4.61), (4.64), (4.65), and (5.2) results in a linearized form of integro-differential equation for gases with n-vibration rotation bands as

$$\xi - \frac{1}{2} = \frac{3}{2}\sum_{i=1}^{n}(H_i u_{oi}/H)\left[\int_o^{\xi} \phi^*(\xi')\bar{A}_i'(I)d\xi' - \int_{\xi}^{1} \phi^*(\xi')\bar{A}_i'(II)d\xi'\right] \tag{5.6}$$

where the following definitions were employed

$$H_i = A_{oi}\left(\frac{de_{\omega i}}{dT}\right)_{T_1} \tag{5.7a}$$

$$H = \sum_{i=1}^{n} H_i = \sum_{i=1}^{n} A_{oi}\left(\frac{de_{\omega i}}{dT}\right)_{T_1} \tag{5.7b}$$

$$\phi^* = (T - T_1)/(QL/H) \tag{5.7c}$$

The quantity ϕ^* represents the temperature profile for linearized radiation under the assumption of LTE.

Note that, for a multiband system, a combination of Eqs. (4.61), (4.65), and (5.2) would have resulted in a nonlinear integral equation. However, consistent with the assumption of a temperature independent absorption coefficient, the problem was linearized through the use of Eq. (4.64). Further, it should be noted that for a single band gas if ϕ^* is available then ϕ can be obtained from the relation

$$\phi = \phi^* + \frac{1}{4}(\eta) \tag{5.8}$$

By making use of the correlation for the total band absorptance as given by the Eq. (4.43), numerical solutions of Eqs. (5.5), and (5.6) were obtained. Spectroscopic information of Tables A1 and A2 was used, and for the relaxation time of CO fundamental band, Eq. (4.8) was employed. The solutions were obtained by the method of undetermined parameters. A polynomial solution for ϕ was assumed, and the constants were evaluated by satisfying the integral equation at equally spaced locations. Both quadratic and quartic solutions were utilized, with the two solutions yielding virtually identical results. Simpson as well as Romberg techniques of numerical integration were employed. The results are presented and discussed in Sec. 5.3.

5.1.2 Large β Solution

For gases where detailed spectroscopic information about the line structure behavior of individual bands is not available, radiative effects can be investigated in the limit of large β. This limit is approached when spectral lines are sufficiently pressure broadened such that the total band absorptance is no longer a function of pressure. The line structure function in Eq. (4.43) for this case becomes $f(\beta) = 2.94$, and β now ceases to be a parameter in the integro-differential equations, Eqs. (5.5) and (5.6). It should be noted that for the conditions where the assumption of large β is valid, the assumption of LTE is also justified except for small values of u_{oi}. Formulations in this limit are especially useful in determining the contributions from combinations and overtone bands.

The spectroscopic information required for this limit is the rotational constant, the band width parameter, and the integrated band intensity. For important molecules, rotational constants and band intensities are available in the literature [70, 91]. The band width parameter A_o can be evaluated by the method presented in Appendix A. Large β solutions were obtained for CO, CO_2, H_2O, and CH_4, and these are discussed along with the general band absorptance results

in Sec. 5.3.

5.1.3 Optically Thin Limit

As discussed in [18], an exact formulation of the nongray problem is possible in the optically thin limit. For the physical model considered here, the divergence of radiative flux for this limit is obtained from Eq. (4.55) as

$$-(1+\eta)\frac{dq_R}{dy} = 4\sigma\left[\kappa_m(T,T_1)T_1^4 - \kappa_p(T)T^4\right] \tag{5.9}$$

Combining this with Eqs. (4.33) and (5.1), there is obtained

$$\kappa_p(T)T^4 - \kappa_p(T_1)\frac{T_1^5}{T} = \frac{Q}{4\sigma}(1+\eta) \tag{5.10}$$

It should be noted that Eq. (5.9) is a completely general equation and is applicable to gases with multiple bands. From the discussion of Sec. 4.4, Eq. (5.10) can also be regarded as a general equation. However, the presence of the nonequilibrium parameter η in these equations should restrict their applicability to gases with fundamental bands only. Since, in the optically thin limit, only fundamental and pure rotation bands contribute significantly to radiation, and since rotational energy is assumed to be described by the kinetic temperature, Eq. (5.10) can be treated as a general equation for the nonequilibrium conditions. In applying Eq. (5.10) to multiband gases, the nonequilibrium parameter η must be summed over all bands. Alternately, by making use of Eq. (4.33b), a rigorous formulation in the optically thin limit can be presented for multiband gases.

Employing Eq. (4.32), and by noting that for fundamental and pure rotation bands $S(T) \sim 1/T$, Eq. (5.10) can be expressed as

$$\frac{e_{\omega i}(T) - e_{\omega i}(T_1)}{Q/PS_i(T)} = \phi_i = \frac{1}{4}(1+\eta_i) \tag{5.11}$$

where the result ϕ = 1/4 was obtained in [77] for this limit under the assumption of LTE.

Equation (5.11) could also be obtained by first allowing the spectral coefficient to be temperature dependent, and then going to the limit of small temperature differences. This would not be the case, however, if one employs Eq. (5.10) and then assumes that the Planck mean absorption coefficient is independent of temperature. In other words the correct formulation for small temperature differences corresponds to assuming that the spectral coefficient, and not the Planck mean, is independent of temperature.

The optically thin limit can also be obtained by taking the limit of the integro-differential equation, Eq. (5.5), as the dimensionless path length u_o becomes very small. Alternately, this amounts to combining Eqs. (4.66) and (5.1) to obtain

$$\frac{e_{\omega i}(T) - e_{\omega i}(T_1)}{Q/PS_i(T)} = \frac{1}{3} + \frac{1}{4}\eta_i \tag{5.12}$$

The differences between Eqs. (5.11) and (5.12) are due to the fact that Eq. (5.11) was obtained from an exact formulation while exponential kernal substitutions were made in obtaining Eq. (5.12). The exponential kernal approximation, as given by Eq. (4.58), produces the greatest error for optically thin conditions.

Further discussion about formulating the radiative problems in the optically thin limit is given in [18, 77].

5.1.4 Large Path Length Limit

From the discussion of subsection 4.5.1, it should be recalled that in the large path length limit the assumption of LTE is justified. Since in this limit $\bar{A}(u_i) = \ln(u_i)$, and $\bar{A}'(u_i) = 1/u_i$, then there is obtained from Eq. (5.6)

$$\xi - \frac{1}{2} = \int_o^1 \phi^*(\xi') \frac{d\xi'}{\xi - \xi'} \tag{5.13}$$

Aside from the obvious simplification in form in going from Eq. (5.6) to Eq. (5.13), there are other more striking consequences associated with Eq. (5.13). For example, of the three correlation quantities A_{oi}, C_{oi}^2, and B_i^2, only A_{oi} remains in Eq. (5.13) through the definition of $\phi^*(\xi)$ as given by Eq. (5.7). The dependence upon this single correlation quantity in the large path length limit has also been illustrated by Edwards et al. [35] in dealing with laminar flow between parallel plates.

The absence of the line structure quantity B_i^2 is obvious, since the line structure of the band plays no role when radiative transfer occurs solely in the wings of the band. Since the individual band intensities correspond to $A_{oi}C_{oi}^2$, the absence of C_{oi}^2 illustrates that the radiative transfer process is independent of the band intensities in the large path length limit. This is physically reasonable, since the central portion of the band does not contribute to radiative transfer in this limit.

A further simplication associated with Eq. (5.13) is that the temperature profile within the gas is independent of pressure. This is not the case with the general formulation, Eq. (5.6), for which pressure appears both in the dimensionless band path length u_{oi} and in the line structure parameter β_i. This invariance with pressure can also be found from the results of Edwards et al. [35].

The solution of Eq. (5.13) was obtained by Cess and Tiwari [89] as

$$\phi^*(\xi) = \frac{1}{\pi}\sqrt{\xi(1-\xi)} \tag{5.14}$$

It should be noted that this temperature profile yields the result that the gas temperature at the surface is equal to the surface temperature, and this absence of a temperature slip is characteristic of optically thick radiation. This, of course, is due to the fact that optically thick radiation is occurring in certain spectral regions. As previously discussed, optically nonthick radiation exists

in other spectral regions, with the result that Eq. (5.14) differs substantially from the temperature profile which would be predicted using a Rosseland type (or diffusion) equation [77].

The dimensionless centerline temperature follows from Eq. (5.14) to be

$$\frac{T_c - T_1}{QL/H} = \frac{1}{2\pi} = 0.159 \tag{5.15}$$

5.2 Energy Transfer by Conduction and Radiation

The sole purpose of this subsection is to investigate the effects of including thermal conduction as another mode of energy transfer in the physical system already considered in Sec. 5.1. The physical model is still somewhat unrealistic, but the results will be of qualitative use in assessing the relative importance of thermal radiation and molecular conduction as energy transport mechanisms for other real physical systems to be treated in Sec. 6.

For the sake of brevity, band absorptance model solutions are obtained only for CO, and the radiative contribution of the overtone band is investigated in the limit of large u_o. Furthermore, for the CO fundamental band, effects of vibrational nonequilibrium are studies in the presence of molecular conduction. Limiting solutions of governing integro-differential equations are obtained in general, and values of interaction parameters in the optically thin and large u_o limits are evaluated for different gases.

5.2.1 General Formulation

The physical model for the present problem is taken to be the same as considered in Sec. 5.1. Here, in addition to uniform heat generation within the gas, thermal conduction is also included.

From conservation of energy, Eq. (2.10), the temperature profile within the gas is described by

$$k\frac{d^2T}{dy^2} - \frac{dq_R}{dy} + Q = 0 \tag{5.16}$$

Upon integrating this equation once, and by noting that $dT/dy = 0$ and $q_R = 0$ at $y = L/2$, there results

$$q_R = k\frac{dT}{dy} + (y - L/2)Q \tag{5.17}$$

In this case, the appropriate equation for the radiative heat flux is Eq. (4.65). For linearized radiation a combination of Eqs. (4.64) and (4.65) yields, for the ith band

$$\begin{aligned} q_R(\xi) = {} & \frac{3}{2}A_{oi}u_{oi}\left(\frac{de_{\omega i}}{dT}\right)_{T_1}\left\{\int_o^{\xi} \left[T(\xi') - T_1\right]\bar{A}_i'(I)d\xi'\right. \\ & \left. - \int_{\xi}^{1} \left[T(\xi') - T_1\right]\bar{A}_i'(II)d\xi'\right\} \\ & - \frac{3}{8}\eta\left\{\int_o^{\xi} \left(\frac{dq_R}{d\xi'}\right)\bar{A}_i'(I)d\xi' - \int_{\xi}^{1} \left(\frac{dq_R}{d\xi'}\right)\bar{A}_i'(II)d\xi'\right\} \end{aligned} \tag{5.18}$$

where $\bar{A}_i'(I)$ and $\bar{A}_i'(II)$ are as defined in Eq. (5.3).

Upon letting

$$\theta = (T - T_1)/(QL^2/k) \tag{5.19}$$

and employing definitions of Eqs. (5.7a) and (5.7b), then for a multiband system, Eqs. (5.16) through (5.18) combine to yield the integro differential equation

$$\begin{aligned} & \frac{d\theta}{d\xi} + \xi - \frac{1}{2} = \\ & + \frac{3}{2}\frac{L}{k}\sum_{i=1}^{n} H_i u_{oi}\left[\int_o^{\xi} \theta(\xi')\bar{A}_i'(I)d\xi' - \int_{\xi}^{1} \theta(\xi')\bar{A}_i'(II)d\xi'\right] \\ & - \frac{3}{8}\sum_{i=1}^{n}\eta_i\left[\int_o^{\xi} \left(1 + \frac{d^2\theta}{d\xi'^2}\right)\bar{A}_i'(I)d\xi' - \int_{\xi}^{1} \left(1 + \frac{d^2\theta}{d\xi'^2}\right)\bar{A}_i'(II)d\xi'\right] \end{aligned} \tag{5.20}$$

Since the presence of conduction implies continuity of temperatures at the boundaries, the boundary condition for this equation is

$$\theta(0) = 0 \tag{5.21}$$

For the conditions where the assumption of LTE is justified, the second term on the right hand side of Eq. (5.20) drops out. Furthermore, note that for negligible radiation transfer, Eq. (5.20) yields the temperature profile

$$\theta = \frac{1}{2}(\xi - \xi^2) \tag{5.22}$$

Following the identical procedures discussed in Sec. 5.1, numerical solutions of Eq. (5.20) have been obtained for CO and results are presented in Sec. 5.3.

5.2.2 Optically Thin Limit

In the present notation, the optically thin limit corresponds to $u_{oi} << 1$ for each band of importance. Noting that $\tilde{A}_i'(u_i) = 1$ for $u_{oi} << 1$, Eq. (5.20) reduces to

$$\begin{aligned}
&\frac{d\theta}{d\xi} + \xi - \frac{1}{2} = \\
&+ \frac{3}{2}\frac{L}{k}\sum_{i=1}^{n} H_i u_{oi}\left[\int_o^{\xi} \theta(\xi')d\xi' - \int_{\xi}^{1} \theta(\xi')d\xi'\right] \\
&- \frac{3}{8}\sum_{i=1}^{n}\eta_i\left[\int_o^{\xi} \left(1 + \frac{d^2\theta}{d\xi'^2}\right)d\xi' - \int_{\xi}^{1} \left(1 + \frac{d^2\theta}{d\xi'^2}\right)d\xi'\right]
\end{aligned} \tag{5.23}$$

Differentiating this once, and upon letting

$$N = \frac{PL^2}{k}\sum_{i=1}^{n} A_{oi}C_{oi}^2\left(\frac{de_{\omega i}}{dT}\right)_{T_1} \tag{5.24a}$$

and

$$\tilde{N} = N/\left(1 + \frac{3}{4}\eta_i\right) \tag{5.24b}$$

the optically thin form of the energy equation becomes

$$\frac{d^2\theta}{d\xi^2} - 3\tilde{N}\theta = -1 \tag{5.25}$$

with boundary conditions

$$\theta(0) = 0,\ \theta'(1/2) = 0$$

Note that in Eq. (5.24b), the summation over the nonequilibrium parameter was not taken simply because NLTE effects are investigated only for the fundamental band of CO. Equation (5.25) possesses an elementary solution, and the centerline temperature is found to be

$$\frac{T_c - T_1}{QL^2/k} = \frac{1}{3\tilde{N}}\left\{1 - 2\left[\frac{\exp\left(-\frac{1}{2}\sqrt{3\tilde{N}}\right)}{1+\exp\left(-\sqrt{3\tilde{N}}\right)}\right]\right\} . \tag{5.26}$$

It readily follows that the dimensionless parameter N (or $\tilde{N}$) characterizes the relative importance of radiation versus conduction within the gas. For particular values of P and L, it is actually the dimensional gas property

$$\frac{N}{PL^2} = \frac{1}{k}\sum_{i=1}^{n} A_{oi}C_{oi}^2\left(\frac{de_{\omega i}}{dT}\right)_{T_1} \tag{5.27}$$

which denotes the relative importance of radiation to conduction. This quantity was evaluated for a number of gases and is illustrated in Fig. 5.2. For CO, CO_2, H_2O, and CH_4, Eq. (5.27) was evaluated using the correlation quantities given in Table A1. For N_2O and NH_3, the band intensities, $A_{oi}C_{oi}^2$, were taken from Table A2. Thermal conductivity values were obtained from Tsederberg [92] and information given in Appendix B. It was noted that inclusion of weaker overtone and combination bands of these gases did not make any significant change in the values of the quantity N/PL^2. It should be emphasized that this quantity characterizes the radiation-conduction interaction only in the optically thin limit, and that the nonequilibrium interaction in this limit comes through the definition of $\tilde{N}$. For the range of pressure and temperature considered here, the difference between N and $\tilde{N}$ should be quite small for all gases except CO.

5.2.3 Large Path Length Limit

As noted earlier, in the large u_{oi} limit, the assumption of LTE is justified, and with $\bar{A}_i'(u_i) = 1/u_i$ for each band of importance, Eq. (5.20) reduces to

$$\frac{d\theta}{d\xi} + \left(\xi - \frac{1}{2}\right) = M\int_o^1 \theta(\xi')\frac{d\xi'}{\xi - \xi'} \tag{5.28}$$

where Eq. (5.21) is again the appropriate boundary condition, and

$$M = \frac{HL}{\lambda} = \frac{L}{\lambda} \sum_{i=1}^{n} A_{oi} \left(\frac{de_{\omega i}}{dT} \right)_{T_1} \tag{5.29}$$

The dimensionless parameter M constitutes the radiation-conduction interaction parameter for the large path length limit, and the dimensional gas property M/L is illustrated in Fig. 5.3. For each molecule, the number of bands included in evaluating Eq. (5.29) are listed in Table A2. Contributions from weaker bands were seen to be significant at higher temperatures, and therefore, they were included in evaluating the quantity M/L. For CO, CO_2, H_2O, and CH_4, this quantity was evaluated by using the values for A_{oi} as given in Table A1. For weaker bands of CO_2, H_2O, and CH_4, and for all bands of N_2O and NH_3, Eq. (A.10) for A_{oi} was employed.

A comparison of Figs. 5.2 and 5.3 shows a considerable difference in the radiation-conduction interaction for the optically thin limits as opposed to the large path length limit. For example, in the optically thin limit CO_2 possesses a large radiation interaction relative to the other gases, while the reverse is true in the large path length limit. On the other hand, just the opposite trend is observed for H_2O. Since the thermal conductivities of the various gases do not differ appreciably, this behavior is due to differences in the radiative transfer for the optically thin and large path length limits, and a discussion to this effect has been given in [89].

Equation (5.28) does not appear to possess a closed form solution. A numerical solution has thus been obtained, and the results for dimensionless centerline temperature are presented in Sec. 5.3.

5.3 Results and Discussion

The results are presented first for the case of infrared radiation heat transfer in gases with internal heat source, and this is followed by the results for combined conduction, uniform heat

generation, and radiative interaction. For the sake of brevity, most of the results are expressed in terms of the centeline temperature.

5.3.1 Radiation Transfer in Gases with Internal Heat Source

Numerical solutions of Eq. (5.5) are illustrated in Figs. 5.4 and 5.5 for $\beta = 0.1$, and $\beta = \infty$, and for a range of the nonequilibrium parameter $\eta = \eta_c/\eta_r$. Because of the limitation noted earlier, these results are only applicable to diatomic gases. Also shown are results for the large u_o limit, Eq. (5.15), and for the optically thin limit, Eq. (5.12). Optically thin results are shown only for the case of LTE. It should be noted that a lower centerline temperature implies a greater ability of the gas to transfer energy.

For conditions where the assumption of LTE is justified, all modes of energies are described by a single equilibrium temperature (referred here as kinetic temperature). In the presence of vibrational nonequilibrium, however, there would be a continuous exchange of energies between the vibrational and the kinetic modes. As a consequence, there would be attained a new temperature which would be higher than the temperature corresponding to the conditions of LTE. This behavior is evident from the results of Figs. 5.4 and 5.5. As would be expected the nonequilibrium effects are significant in the regions of small path lengths, and for the values of the parameter η higher than unity. For large values of u_o, the assumption of LTE is seen to be justified.

For CO fundamental, the vibrational noneqilibrium parameter η is illustrated in Fig. 5.6. Values of η_c and η_r were obtained from Eqs. (4.8) and (4.27) respectively. It is seen that at a pressure of one atmosphere and a temperature of 500K, the nonequilibrium parameter has a value of about eight, indicating that for these conditions the assumption of LTE will prove to be highly in error. It was pointed out by Hooker and Millikan [49] that at a pressure of one atmosphere, the spontaneous radiation process should dominate the vibrational relaxation process

for temperatures lower than 600K. At a temperature of 1000K, the assumption of LTE will be justified for pressure higher than 1/10th of an atmosphere.

Information on relaxation time for the fundamental bands of CO_2 is obtained from the discussion and results presented in [62, 64]. According to these references, at room temperature, both the bending mode (vibration of wave number 667 cm^{-1}) and the asymmetric mode (wave number 2349 cm^{-1}) have a value of $P\eta_c$ of 7 atm-μ sec. At a mean translational temperature of 500K, the values are 2.9 and 3.6 atm-μ sec, and at 1000K they are 0.93 and 1.4 atm-μ sec, respectively. Employing the values of η_r from Table A2 for bending and asymmetric modes the quantity $P(\eta_c/\eta_r)$, at room temperature, is found to be (3.26×10^{-5}) and (3.21×10^{-3}) atm, respectively. Consequently, for CO_2 at room temperature, the assumption of LTE will be justified at least down to a pressure of 10^{-3} atm, and at higher temperatures, the assumption will be justified even to much lower pressures.

Information on relaxation time for N_2O is available in [62]. Nitrous oxide has very similar physical properties to carbon dioxide and, therefore, the above conclusions should also apply to N_2O.

For CO fundamental, LTE and NLTE band absorptance results are illustrated in Figs. 5.7 through 5.9 for temperature of 500K, 1000K, and 2000K, and for a range of pressures. In evaluation of these results, spectroscopic information of Tien and Lowder [33] was employed. Since the abscissa variable is the pressure path length, PL, then the separate influence of pressure upon the LTE centerline temperature curves is due solely to the alteration of the line structure of the bands as a consequence of pressure broadening. As the pressure is increased, the discrete line structure is eliminated and pressure ceases to be a parameter in the high pressure limit.

From a comparison of LTE and NLTE results in Figs. 5.7 through 5.9, one arrives at the conclusions mentioned earlier, i.e., at a temperature of 500K, the assumption of LTE is not justified up to a pressure of about 8 to 10 atmosphere. However, at a temperature of 2000K, the

assumption of LTE will be valid for pressures higher than 1/100th of an atmosphere.

Under the assumption of LTE, for CO, CO_2, H_2O, and CH_4, general band absorptance and large β results, as obtained from the numerical solutions of Eq. (5.6), are shown in Figs. 5.10 through 5.13 for different temperatures and for a pressure of one atmosphere. These results were obtained by considering the contributions from the three bands of CO_2, five bands of H_2O, and two bands of CH_4, and spectroscopic information of Table A1 was employed. For the CO fundamental band, spectroscopic information of Tien and Lowder [33] was used. General band absorptance results for these gases at various pressures were reported, along with results in the large path length limit, by Cess and Tiwari [89].

It is seen from Figs. 5.10 through 5.13 that large β and band absorptance results approach to be the same in both optically thin and large path length limits, and that maximum differences occur for the intermediate values of path lengths. The reasons for this can be given on the physical grounds. In the optically thin limit results become independent of pressure because the radiative transfer process in this limit depends solely upon the area under κ_ω/P versus wave number curve. In the large path length limit the total band absorptance reduces to the logarithmic asymptote $\bar{A} = \ln u$, and is thus independent of β. It has been further explained in [77] that the line structure of bands has maximum influence only for the intermediate values of path lengths. It should be noted that for gases like CO_2 and H_2O, large β solutions, for the most part, are very good approximations to the general band model results. However, this is not so for gases like CO and CH_4. Further, for CO_2 differences between the two results seem to disappear at higher temperatures. This is because the quantity $B_i^2(T)$ is proportional to the square root of temperature, and at higher temperatures this results in a larger value for β.

A comparison of the relative ability of the various gases to transmit radiant energy is shown in Fig. 5.14 for a temperature of 1000K and a pressure of one atmosphere. From previous discussions, for these conditions, the assumption of LTE would be justified. As discussed in

[89] CO_2, having the largest Planck mean coefficient, is the best transmitter of radiant energy in the optically thin limit, although just the opposite is true for the large path length limit.

Radiative contributions from overtone and combination bands of CO and CO_2 were investigated and results are illustrated in Figs. 5.15 and 5.16. For CO, band absorptance results were obtained by using the information of Table A1. Employing spectroscopic information of Tables A1 and A2, large β solutions were obtained for CO_2. For the three weaker bands of CO_2, the band width parameter A_o was calculated by using the relation given in Appendix A, i.e., Eq. (A.10).

Figures 5.15 and 5.16 indicate that contributions from overtone and combination bands are significant only for large path lengths and at higher temperatures. This is because at a particular pressure, if the path length is increased there becomes available more molecules to participate in the transfer process and at higher temperatures a significant number of molecules make transitions to higher energy levels.

From the results presented in this section it may be concluded that in the large path length limit the assumption of LTE is justified and that nonequilibrium has the largest effect in the optically thin limit. At a pressure of one atmosphere, the assumption of LTE for CO is not valid for temperatures below 600K, while for gases like CO_2 and N_2O, the assumption is justified at room temperatures. Large β results represent good approximation to general band absorptance results for CO_2 and H_2O, and at moderate temperatures, contributions from weaker combination and overtone bands can usually be neglected.

5.3.2 Energy Transfer by Conduction and Radiation

The variations in radiation-conduction interaction parameters for optically thin and large path length conductions are illustrated in Figs. 5.2 and 5.3, respectively. General results for the centerline temperature as a function of the interaction parameter are shown for the optically thin

radiation in Fig. 5.17 and for the large path length interaction in Fig. 5.18. Dimensionless centerline temperatures for CO as obtained from the numerical solution of Eq. (5.20), are illustrated in Figs. 5.19 through 5.21 for wall temperatures of 500K and 1,000K, and for a range of pressures. Since the centerline temperature for pure conduction follows from Eq. (6.7) to be $(T_c - T_1)/(QL^2/k) = 0.125$, then Figs. 5.17 through 5.21 serve to illustrate the influence of radiative transfer upon the temperature profile within the gas.

Figure 5.17 illustrates the influence of nonequilibrium in the optically thin limit. It is seen that for a fixed value of the interaction parameter N, the radiative contribution decreases as the nonequilibrium parameter ($\eta = \eta_c/\eta_r$) increases. This is consistent with the discussion given in Sec. 5.1 that the presence of nonequilibrium will result in a higher centerline temperature. This behavior is also observed from the results of Figs. 5.19 and 5.20. Once again, it is concluded that for CO at one atmospheric pressure the assumption of LTE is not justified for a temperature of 500K; however, at 1,000K the assumption is valid even for a pressure of 0.01 atmosphere.

Also shown in Figs. 5.19 and 5.20 are the large path length limit (large u_{oi} limit) results, as obtained from Fig. 5.18 together with the M/L values from Fig. 5.3. It can be seen that the large path length limit is essentially a limiting solution for large pressures. As would be expected, the importance of radiation becomes more pronounced as the pressure, or the plate spacing, or both are increased.

The radiative contribution from the 1st overtone band of CO was investigated in the presence of molecular conduction, and results obtained in the large u_o limit indicate a significant contribution only at a higher temperature and for a larger plate separation (Fig. 5.21).

For this problem, under the assumption of LTE, band absorptance and limiting solutions were also obtained for CO_2, H_2O, and CH_4 by Cess and Tiwari [90]. The band absorptance results were based on the Tien and Lowder correlation, Eq. (4.43). From a comparison of the entire results it was concluded that the large path length limit constitutes an upper bound

upon the influence of radiative transfer on the temperature profile within the gas. This same conclusion applies to the optically thin limit since self-absorption is neglected. This fact that both limiting solutions constitute upper bounds on the radiative interaction can be employed to estimate whether or not, for a given gas, the interaction of radiation may be of importance.

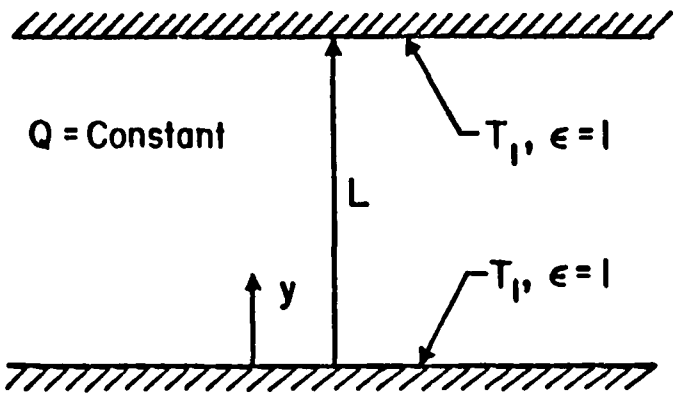

Figure 5.1 Physical model for radiation transfer in gases with internal heat source

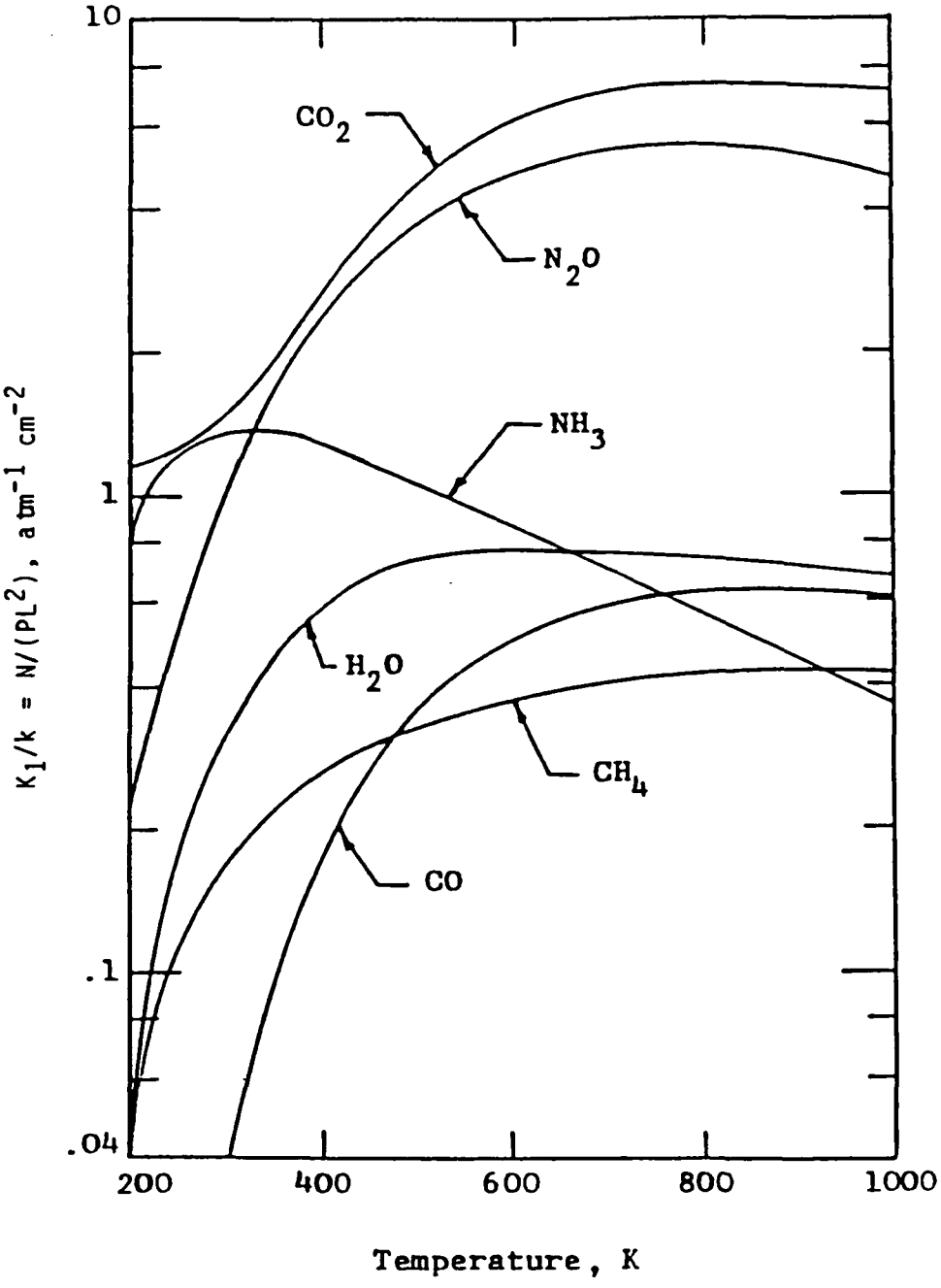

Figure 5.2 Interaction parameter for optically thin radiation

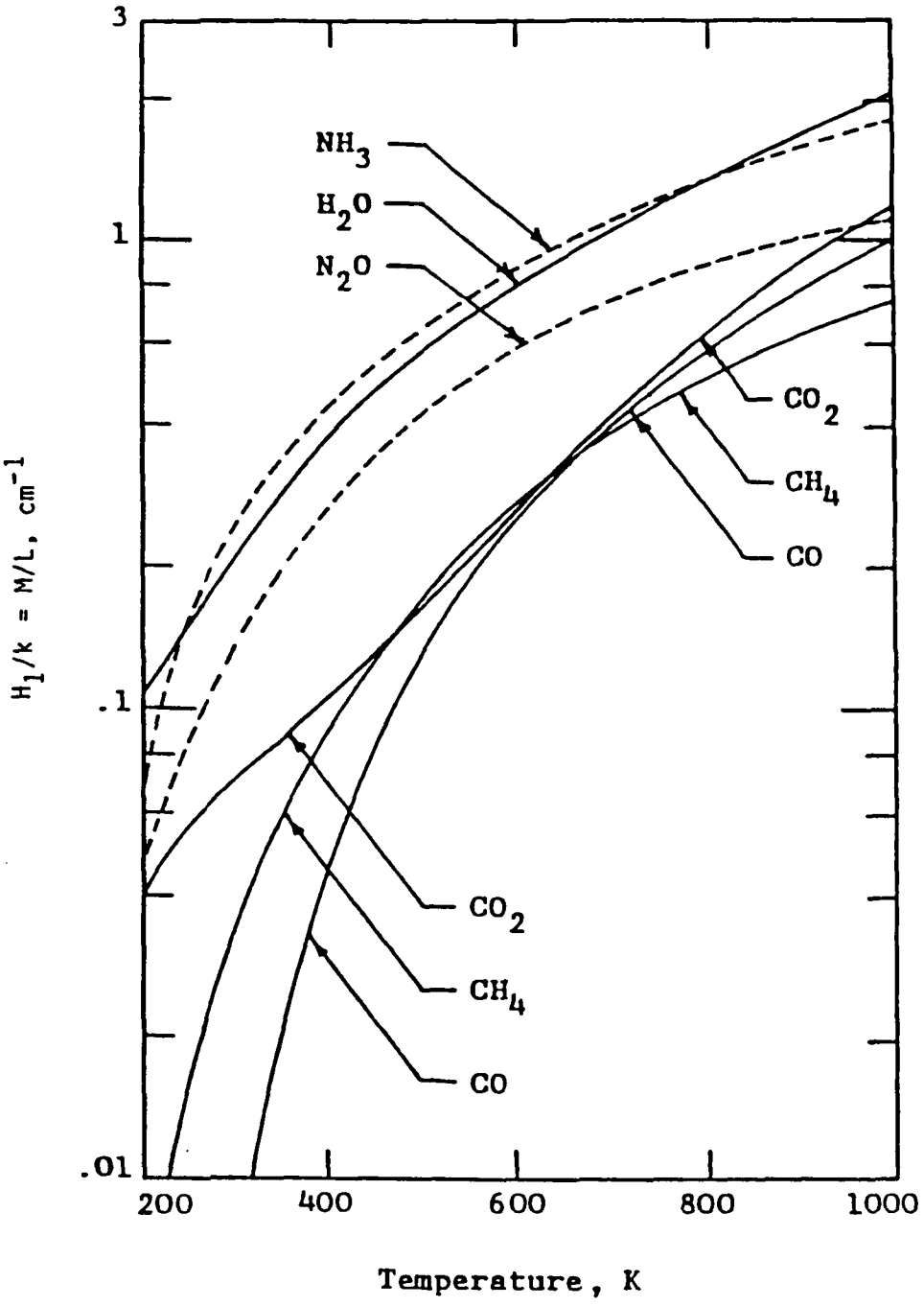

Figure 5.3 Interaction parameter for large path length limit

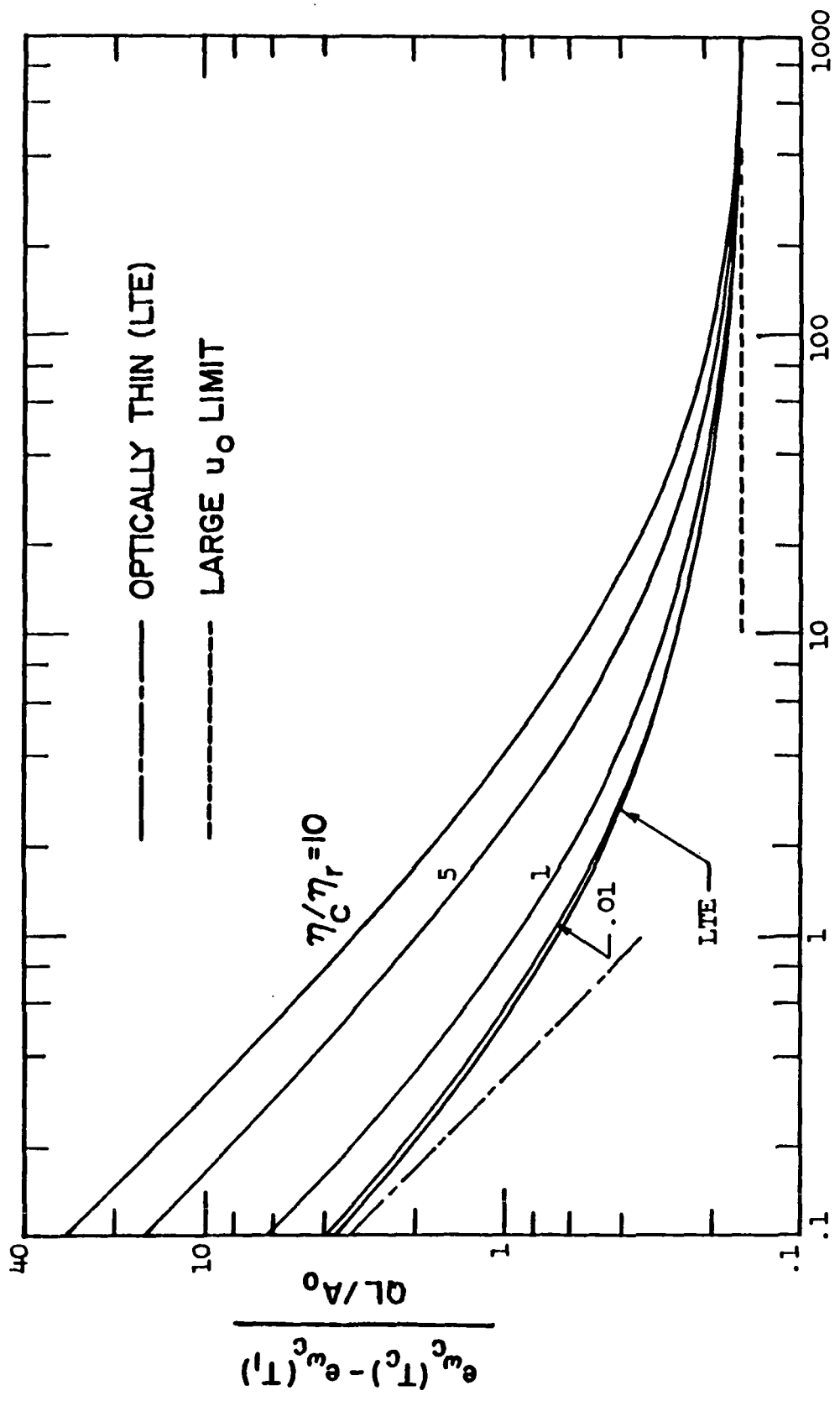

Figure 5.4 Non-LTE (NLTE) results for β = 0.1

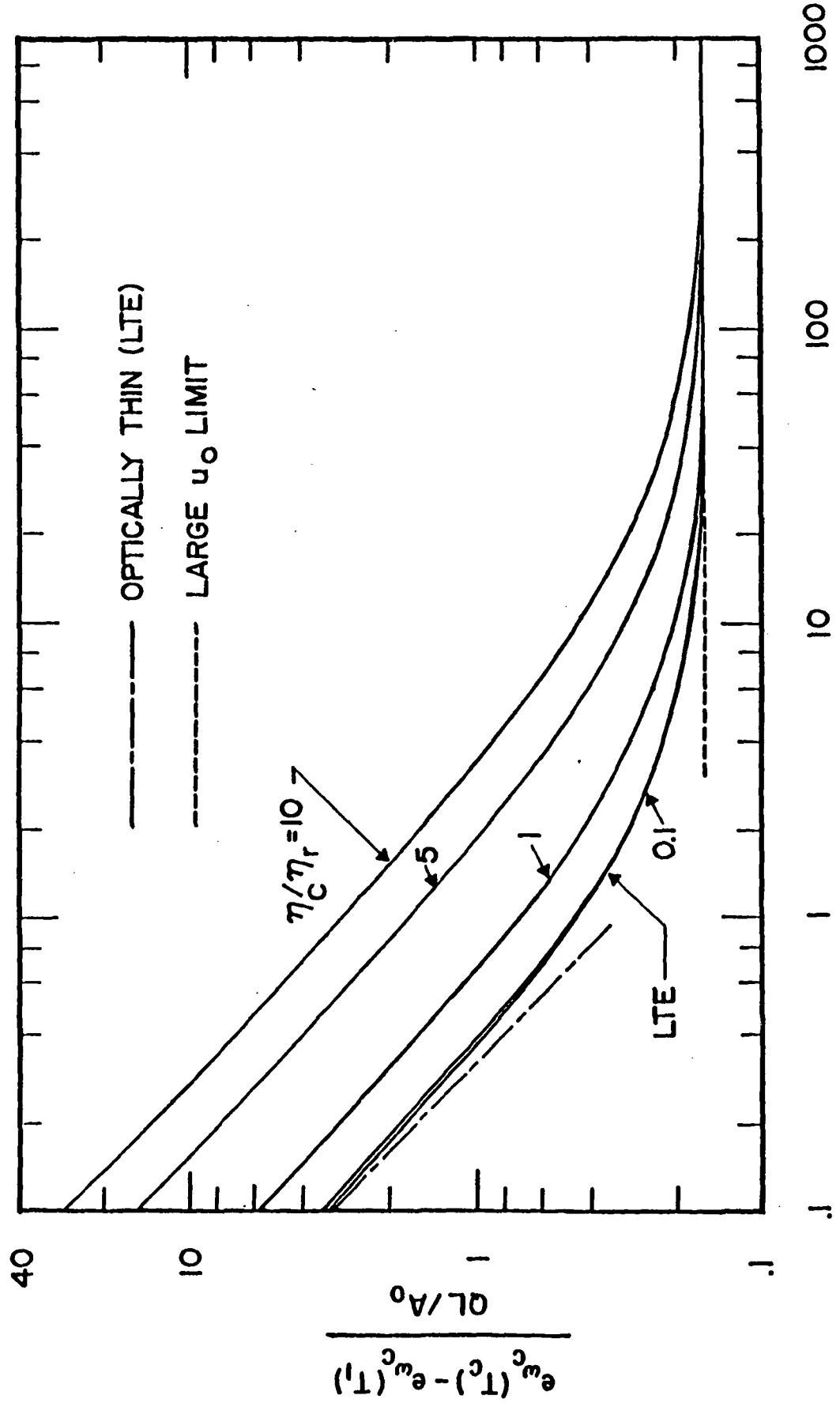

Figure 5.5 Non-LTE (NLTE) results for $\beta = \infty$

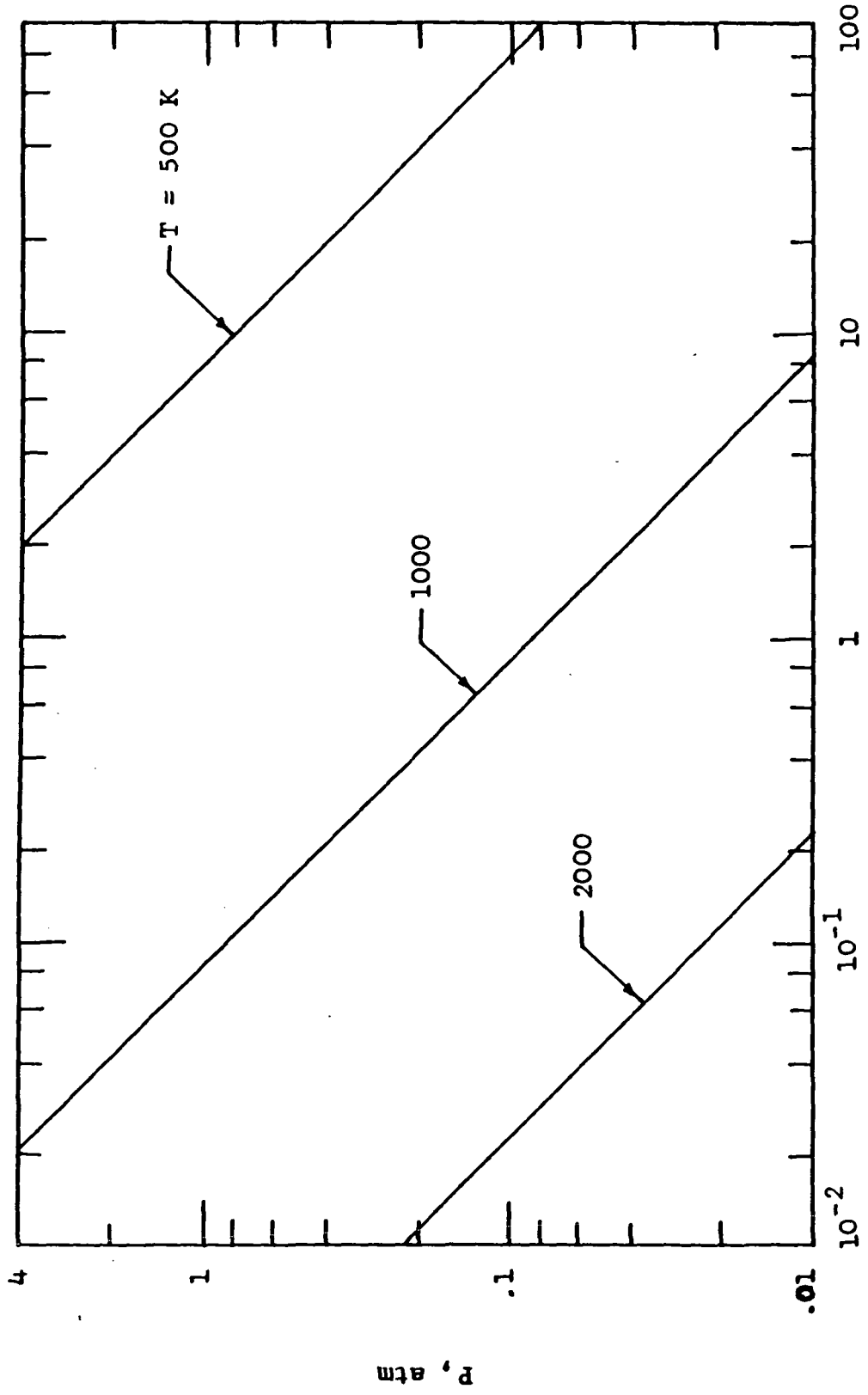

Figure 5.6 Vibrational nonequilibrium parameter for CO

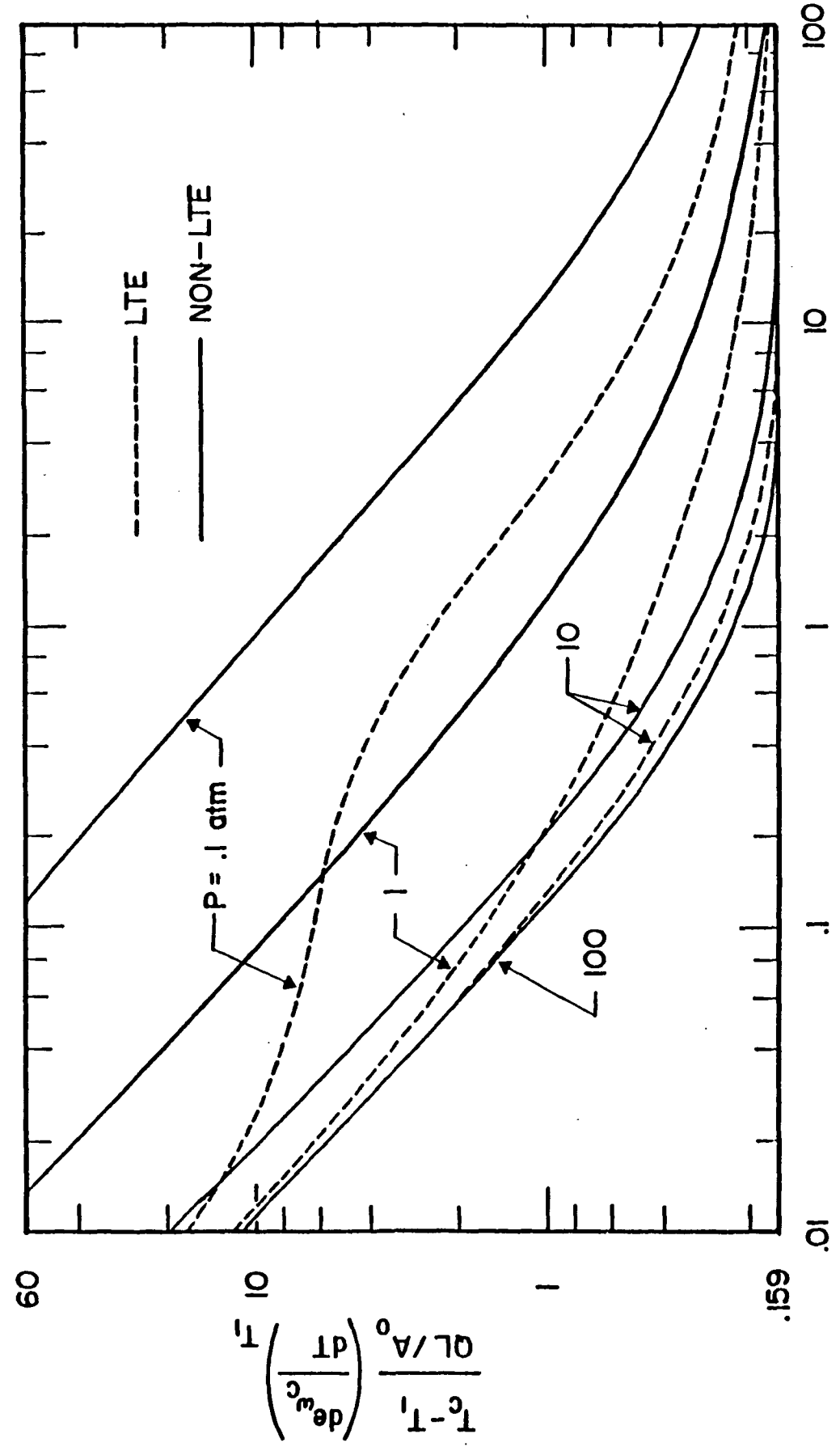

Figure 5.7 LTE and non-LTE (NLTE) results for CO with T_1 = 500 K

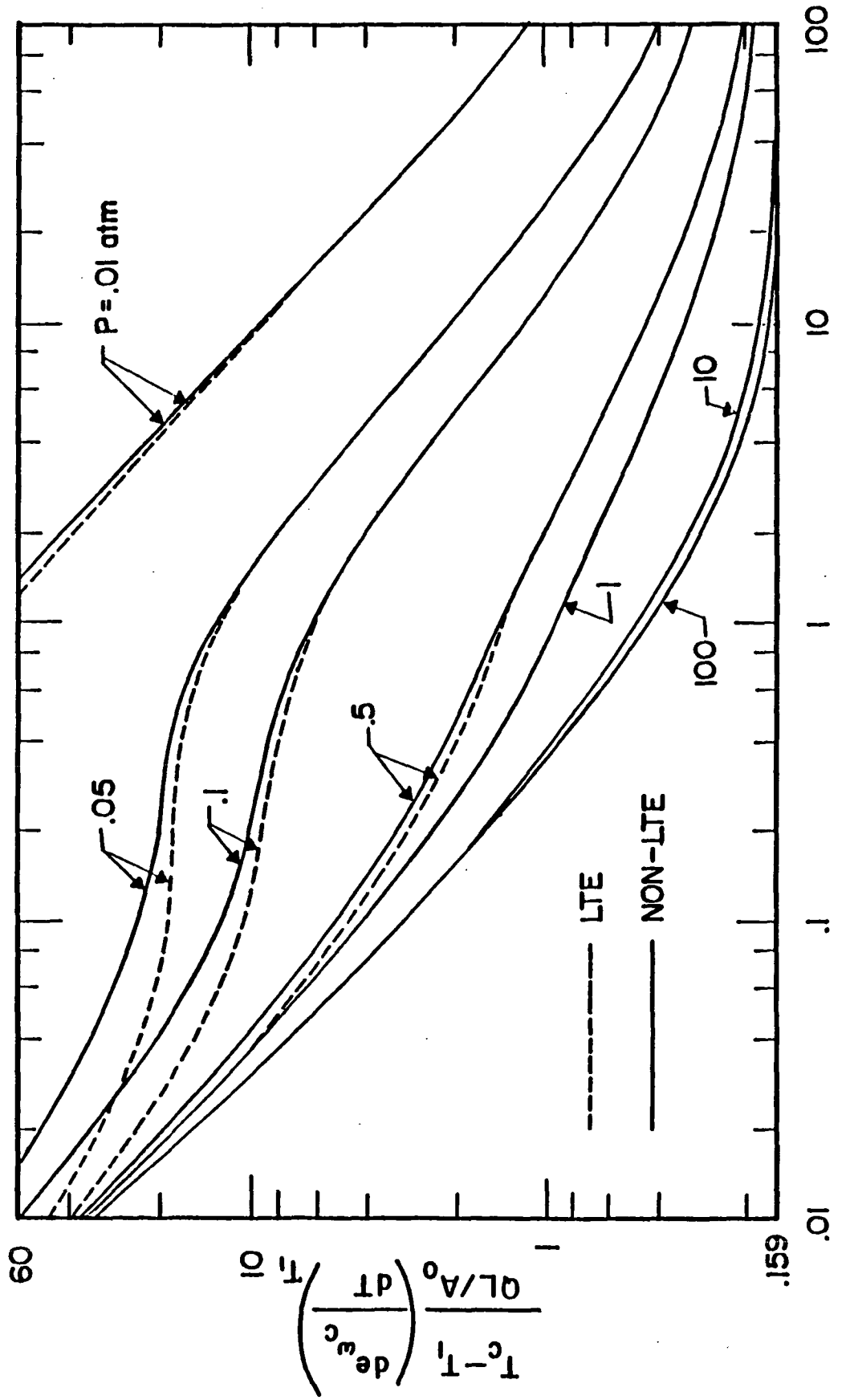

Figure 5.8 LTE and non-LTE (NLTE) results for CO with T_1 = 1,000 K

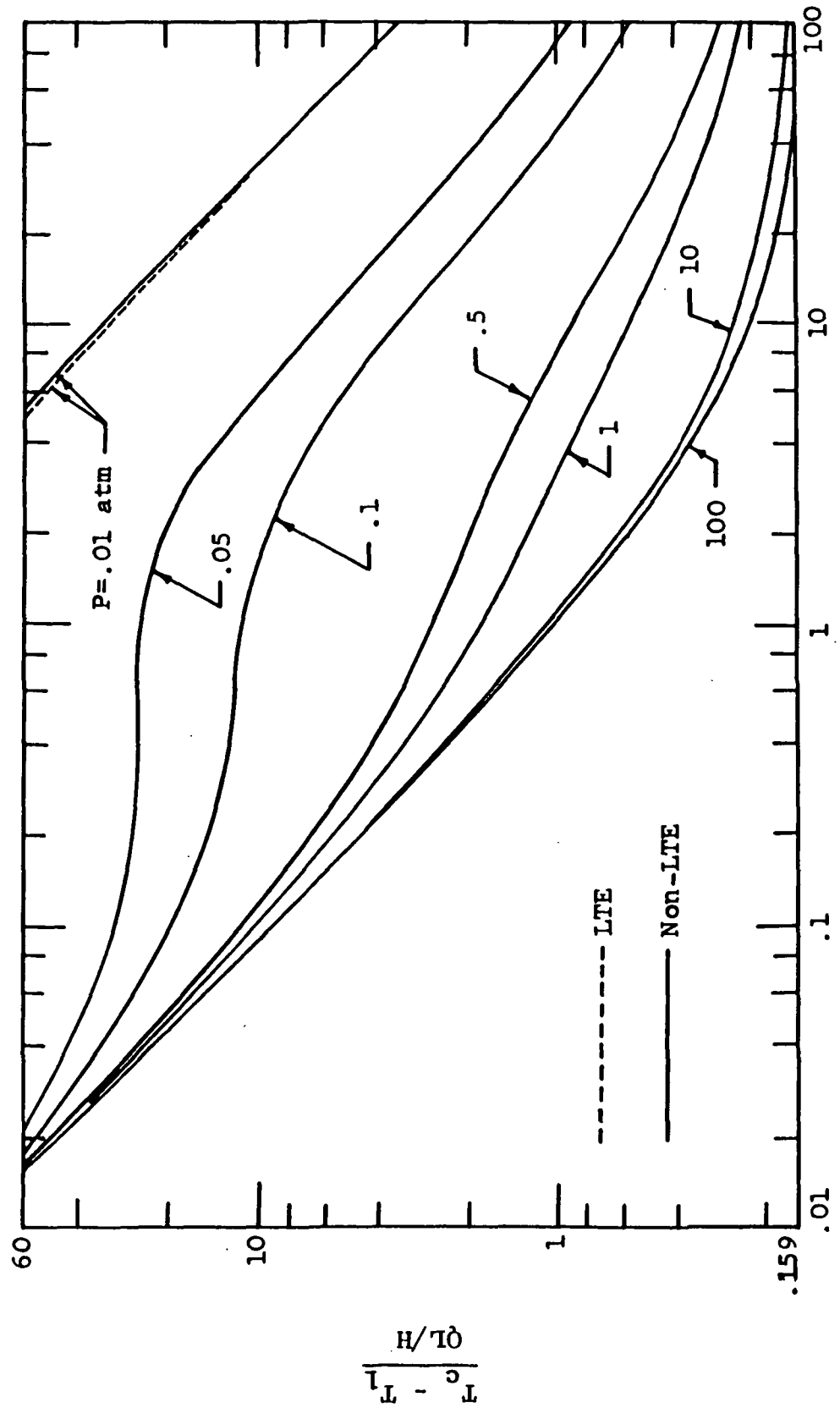

Figure 5.9 LTE and non-LTE (NLTE) results for CO with T_1 = 2,000 K

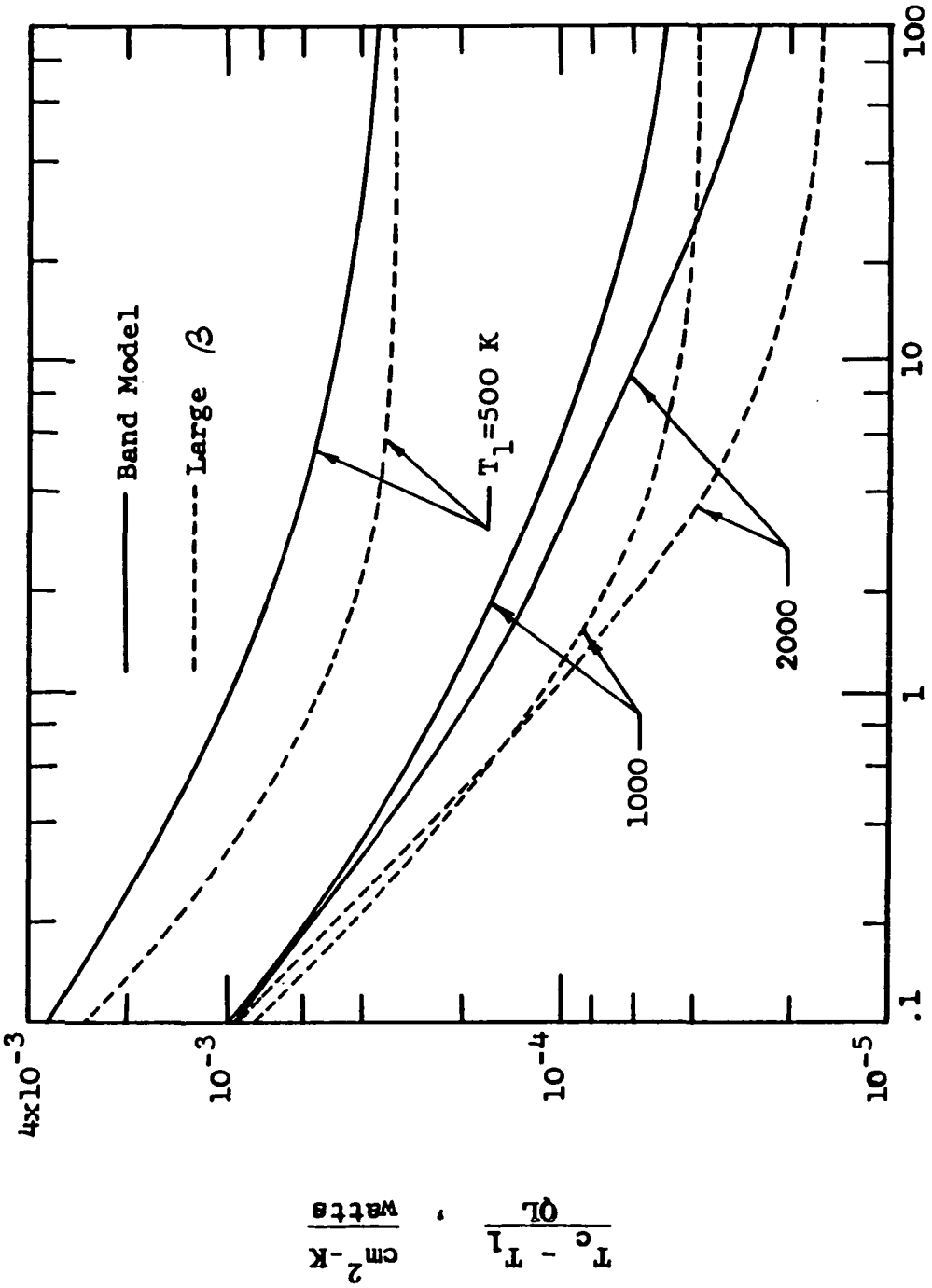

Figure 5.10 Comparison of results for CO (fundamental band) with P = 1 atm

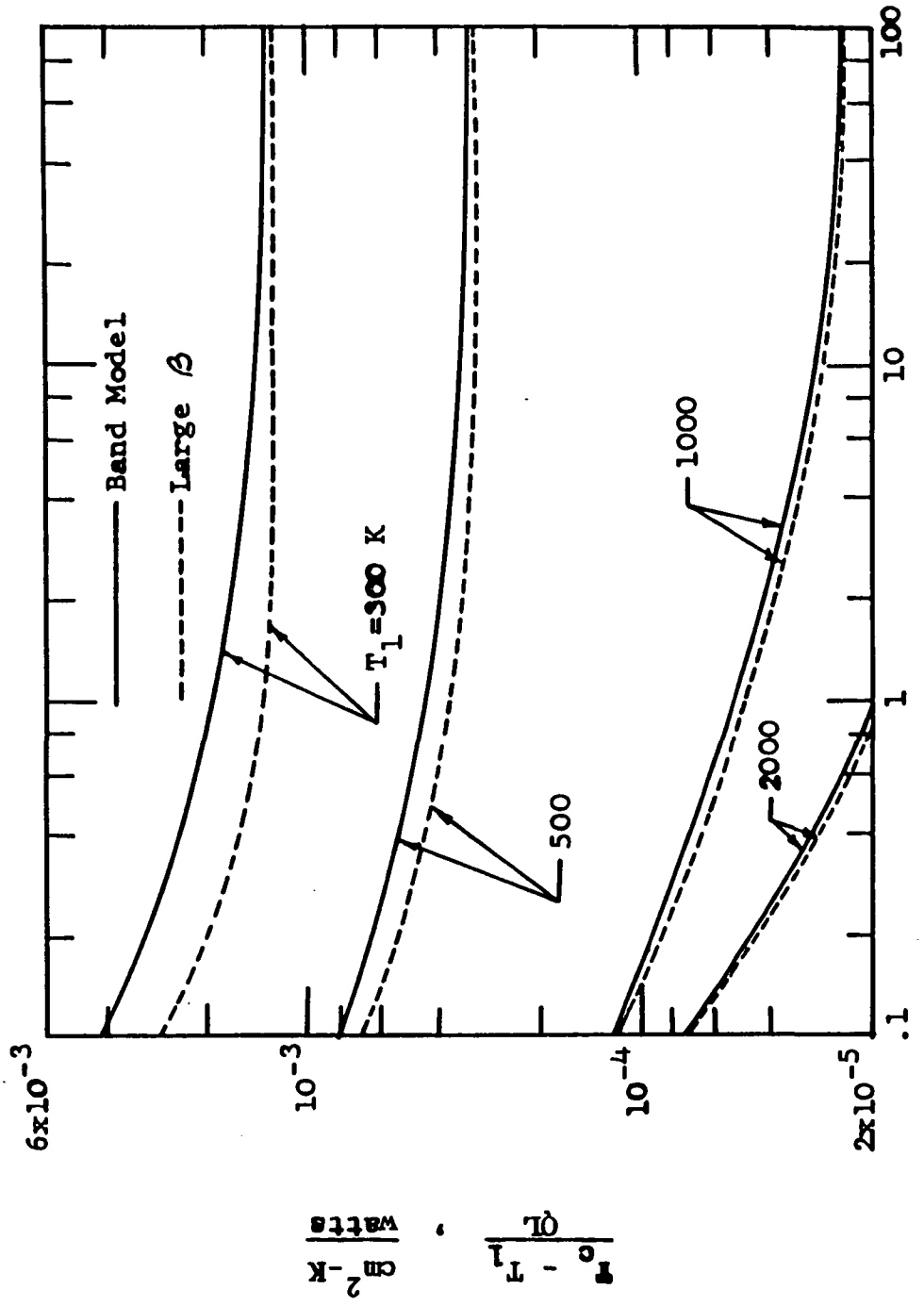

Figure 5.11 Comparison of results for CO_2 (three bands) with P = 1 atm

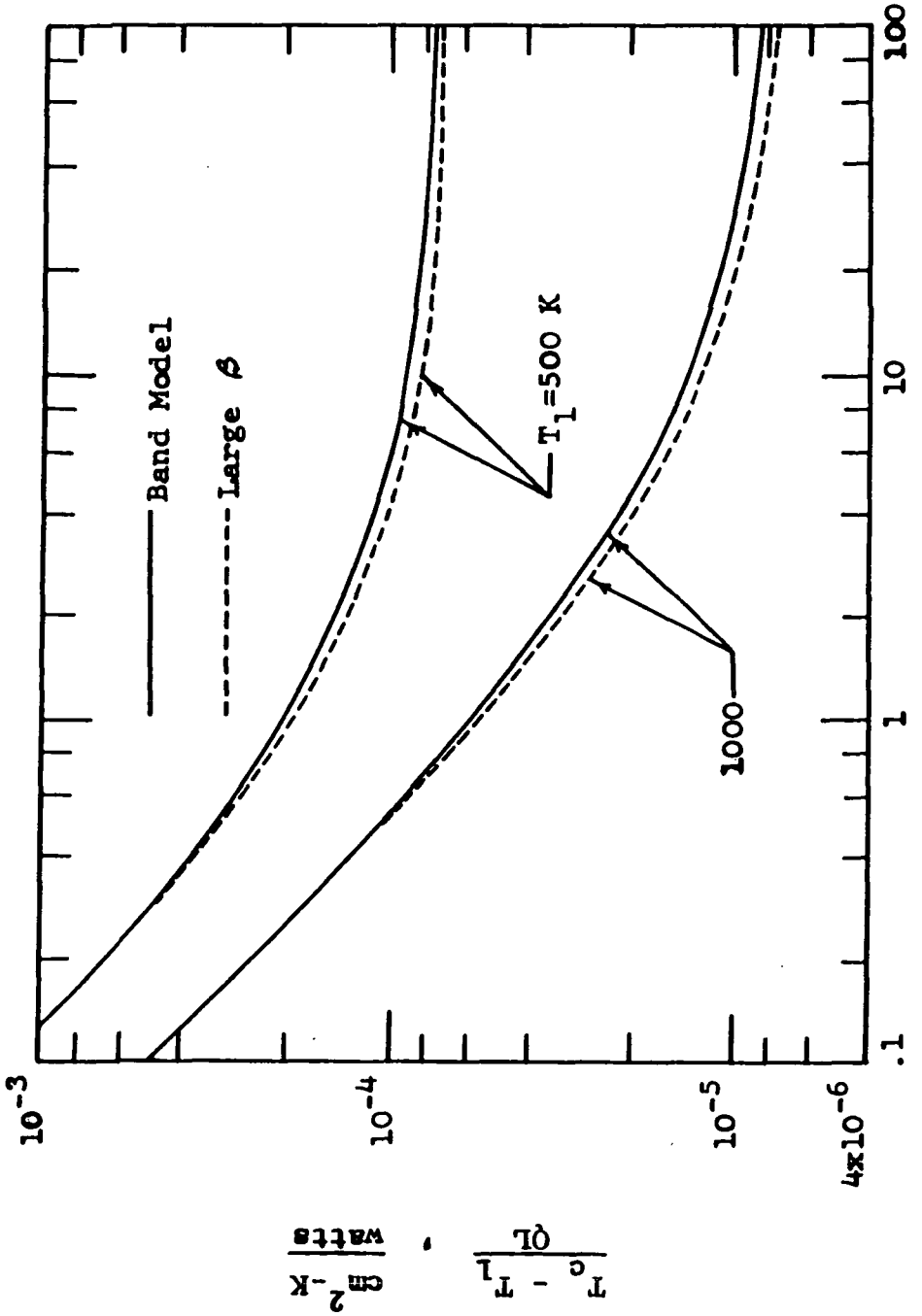

Figure 5.12 Comparison of results for H_2O (five bands) with P = 1 atm

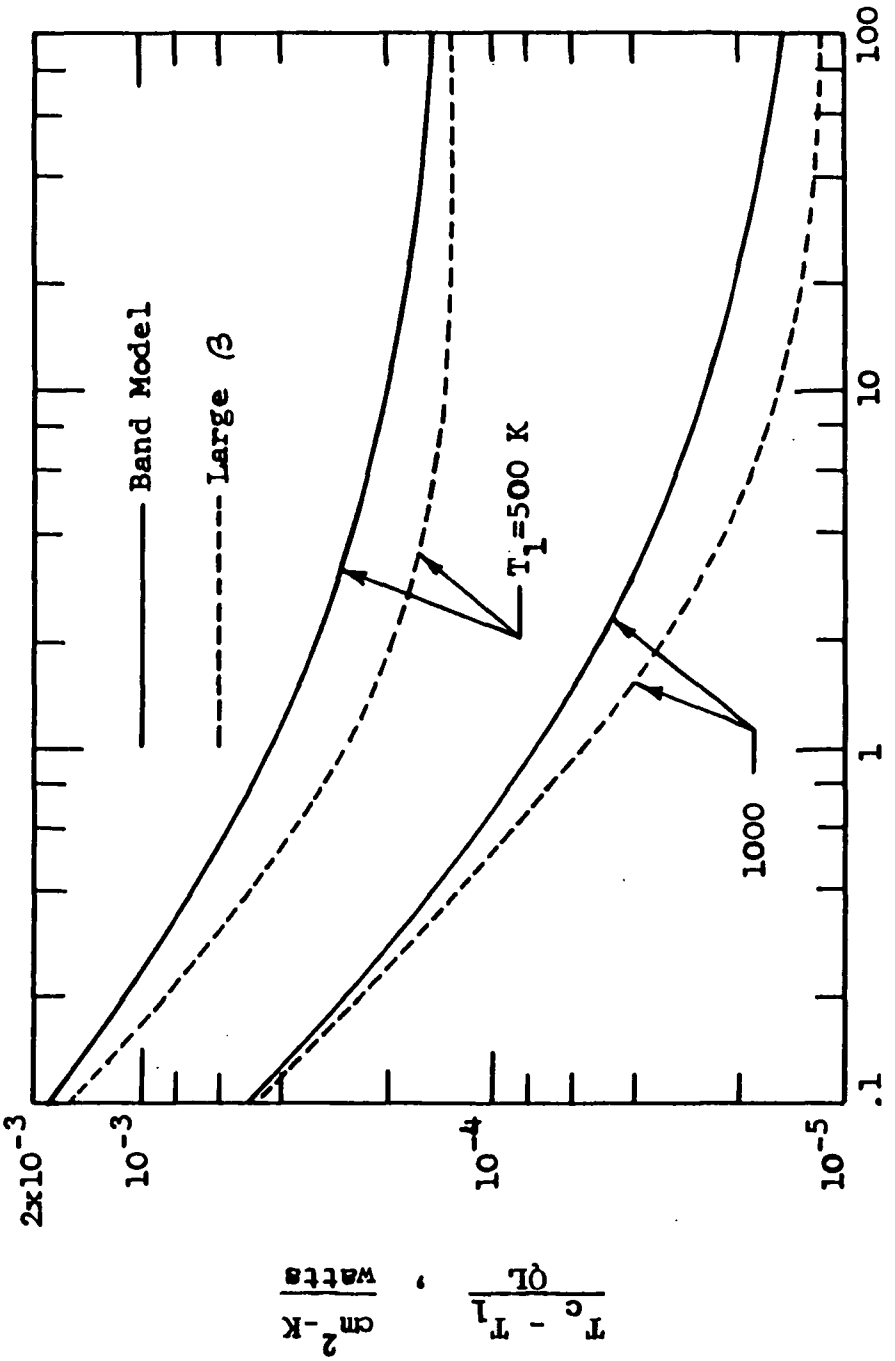

Figure 5.13 Comparison of results for CH_4 (two bands) with P = 1 atm

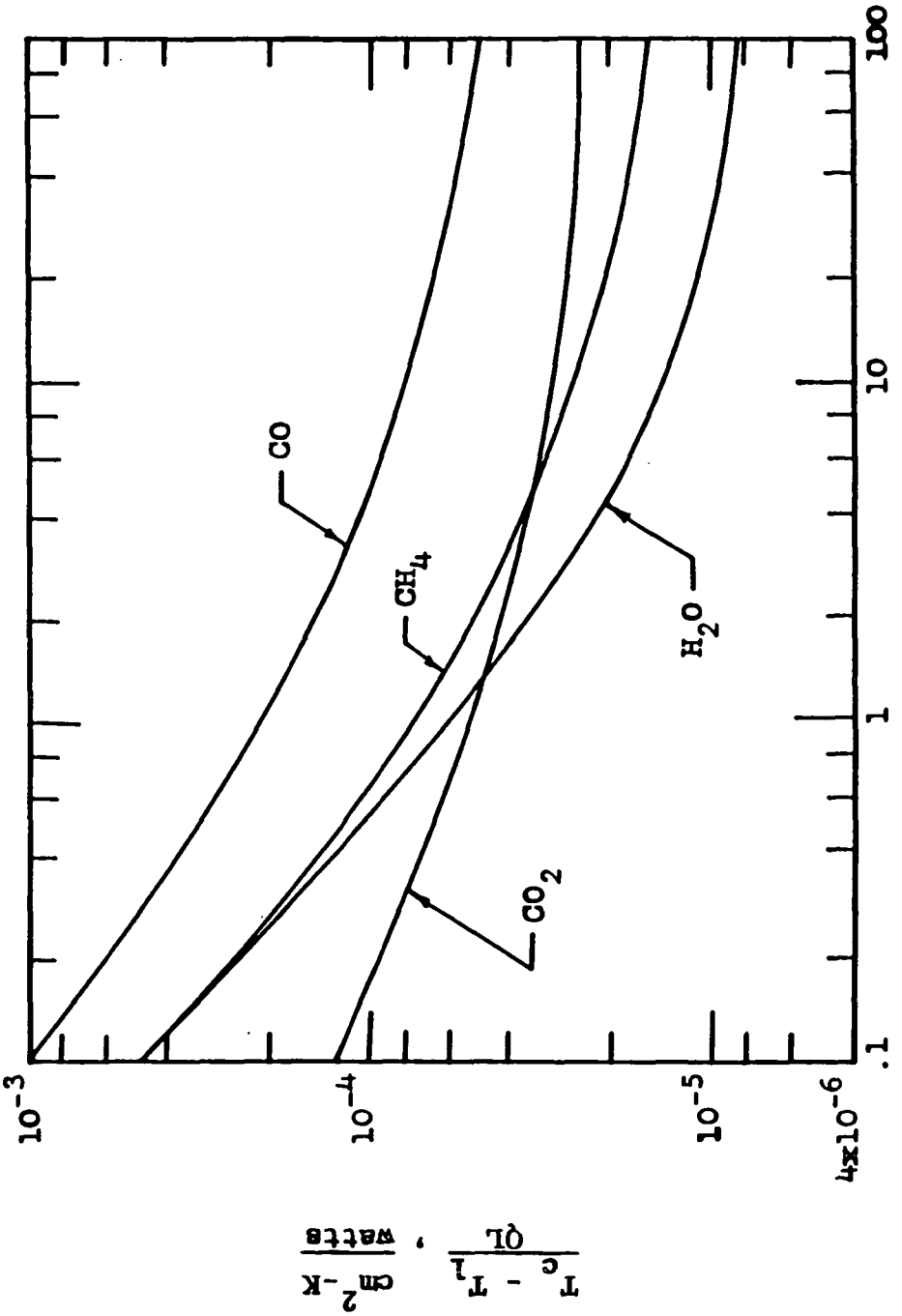

Figure 5.14 Comparison of results for P = 1 atm and T_1 = 1,000 K

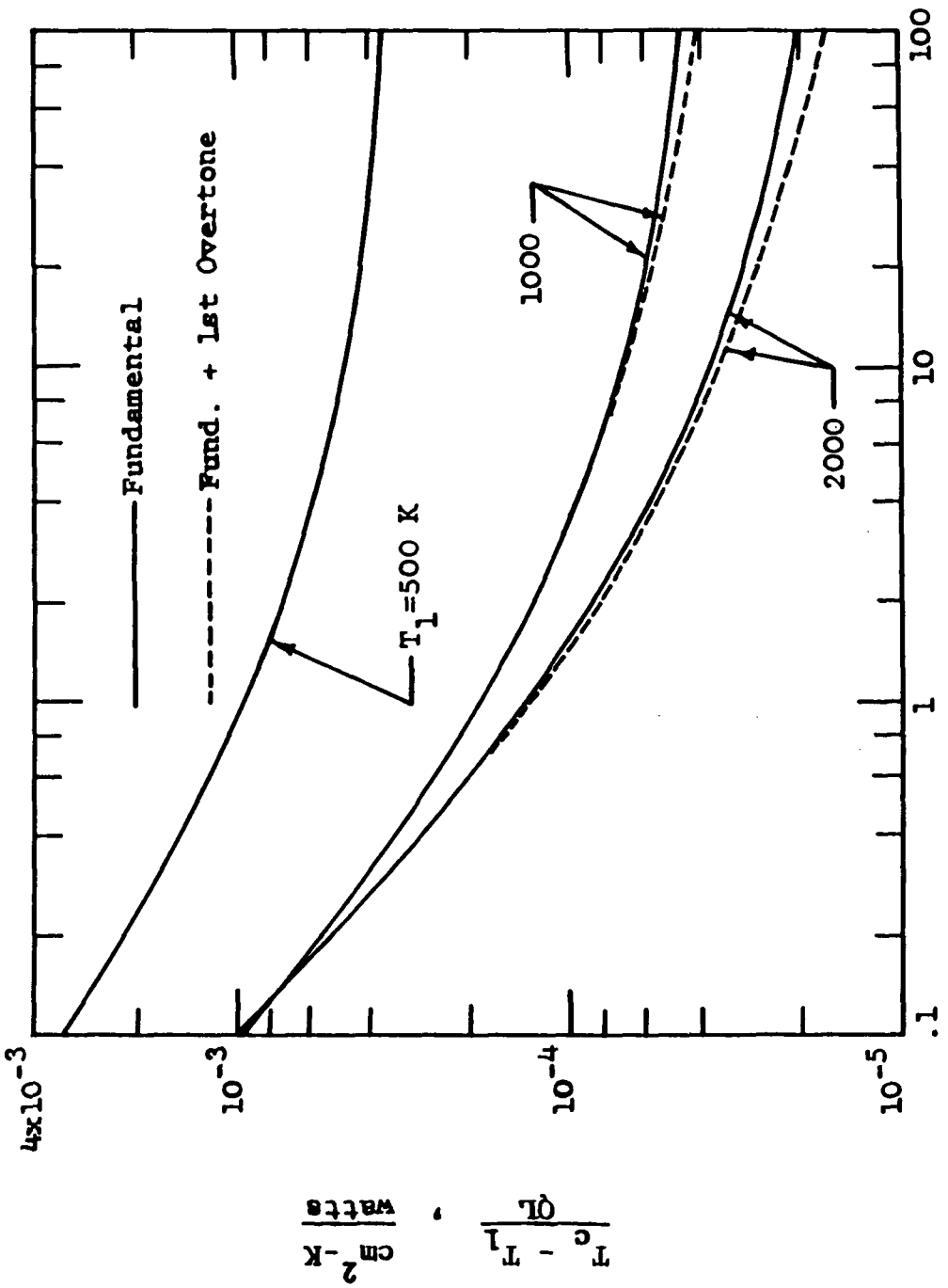

Figure 5.15 Results for CO with P = 1 atm

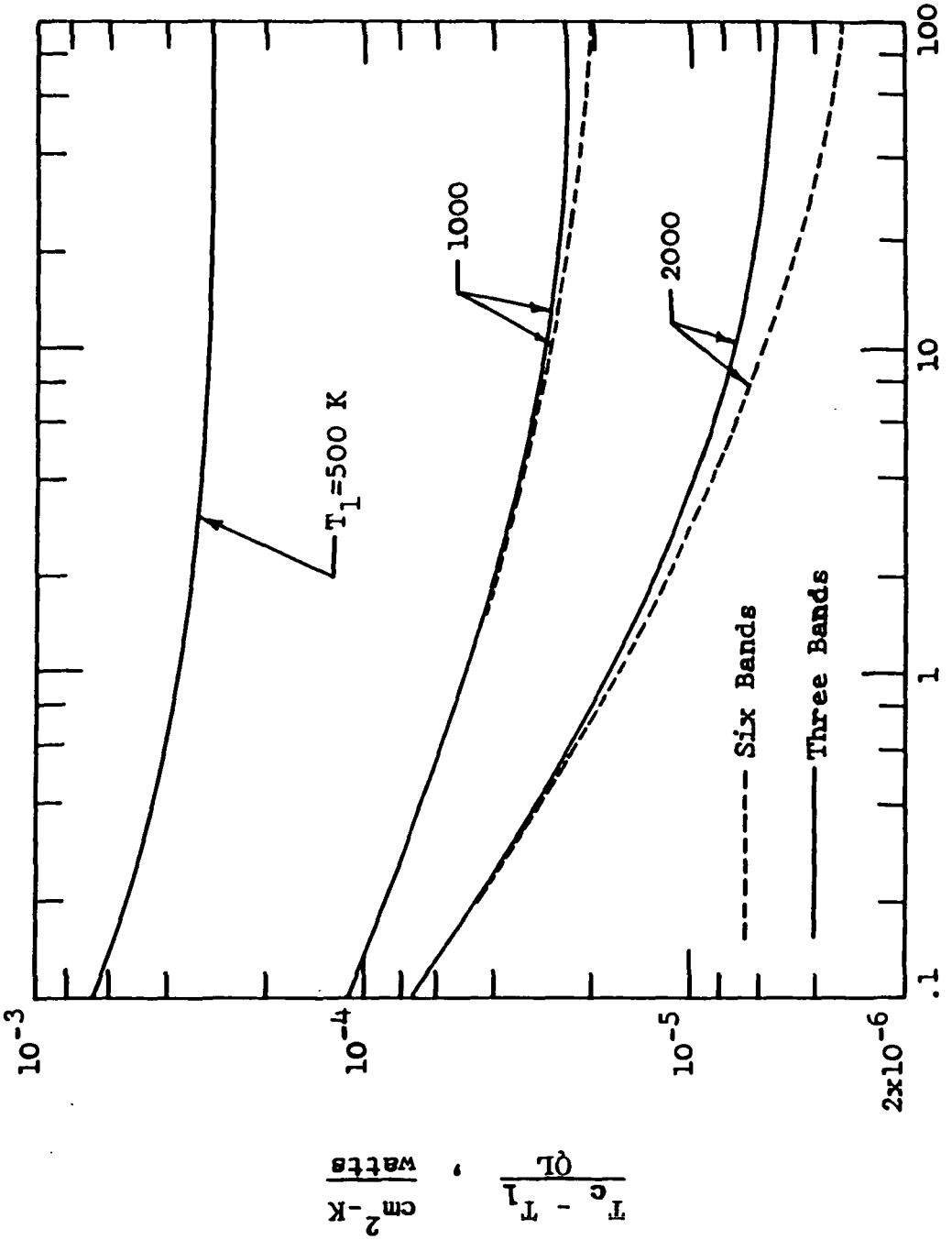

Figure 5.16 Results for CO_2 in the limit of large β

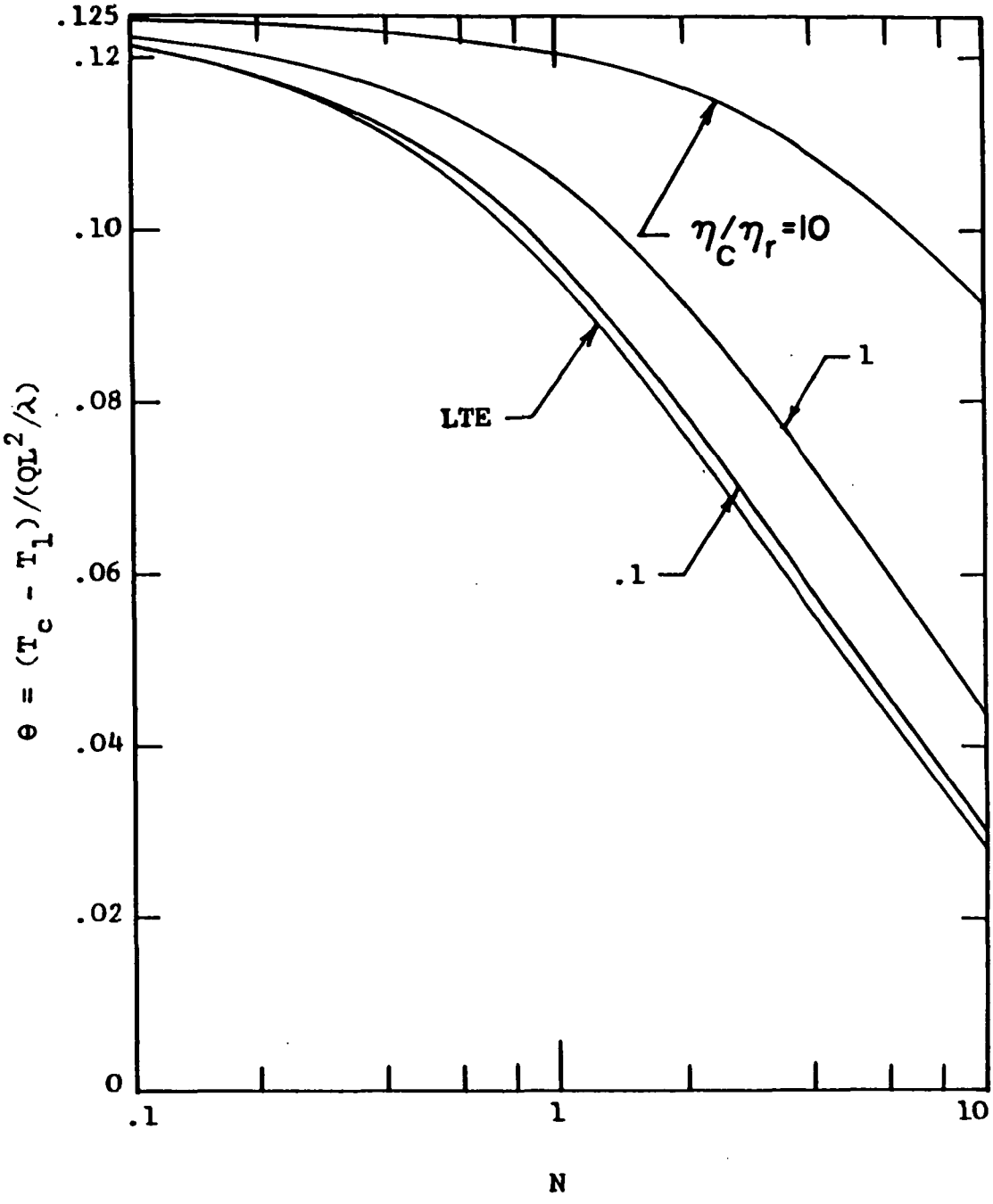

Figure 5.17 Results for conduction-radiation interaction in the optically thin limit

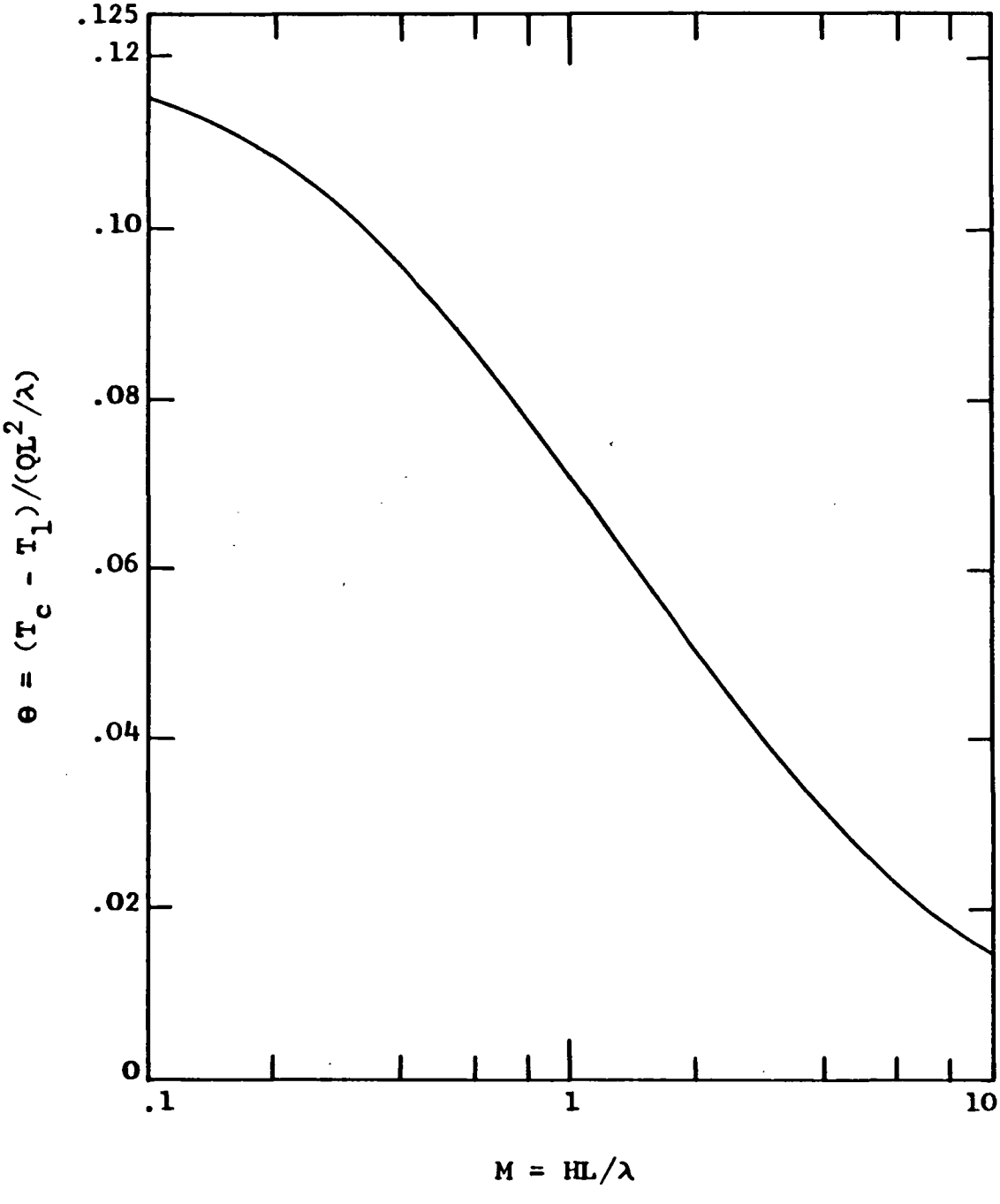

Figure 5.18 Results for conduction-radiation interaction for the large path length limit

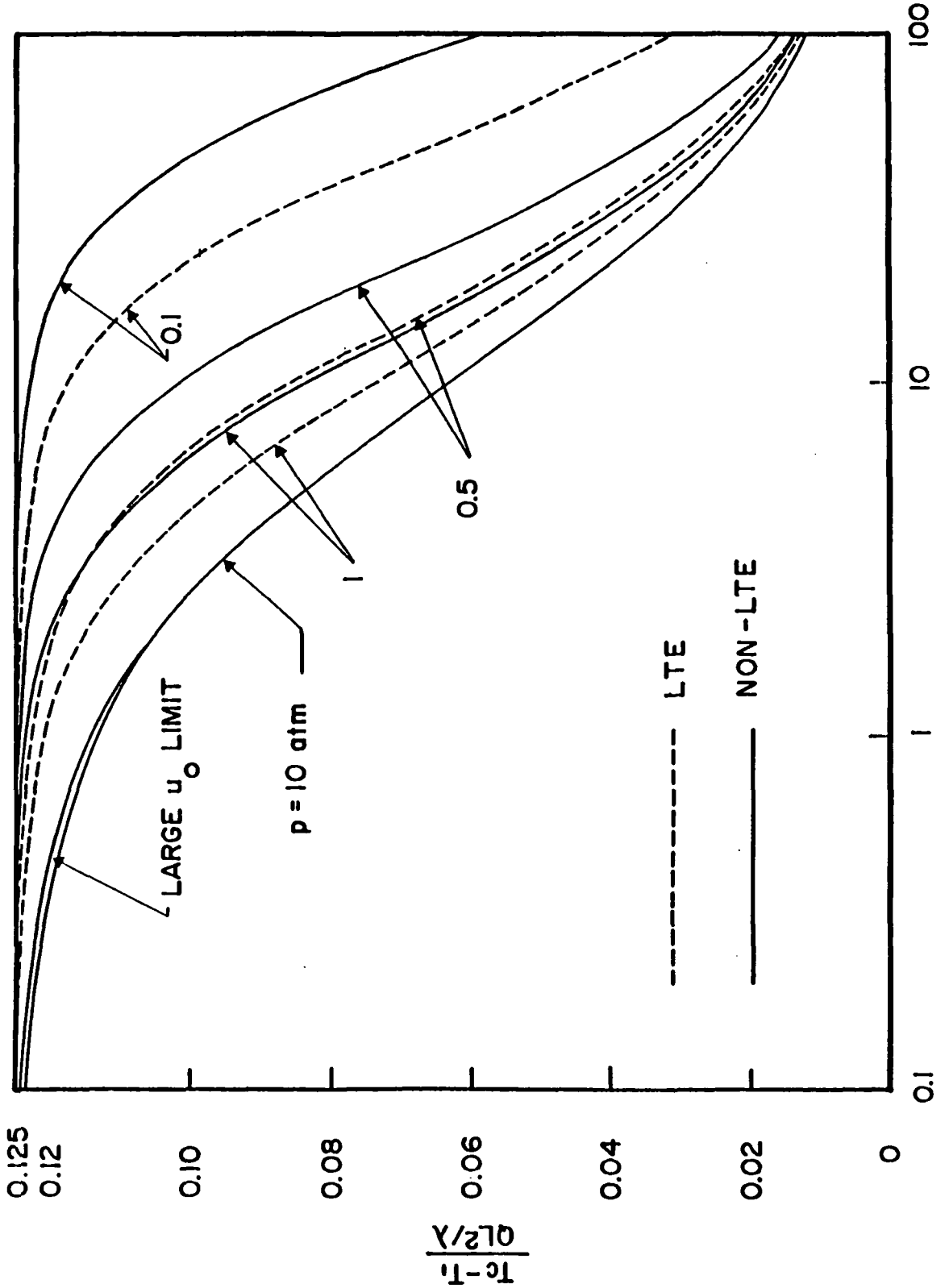

Figure 5.19 Results for combined conduction and radiation for CO (fundamental band) with T_1 = 500 K

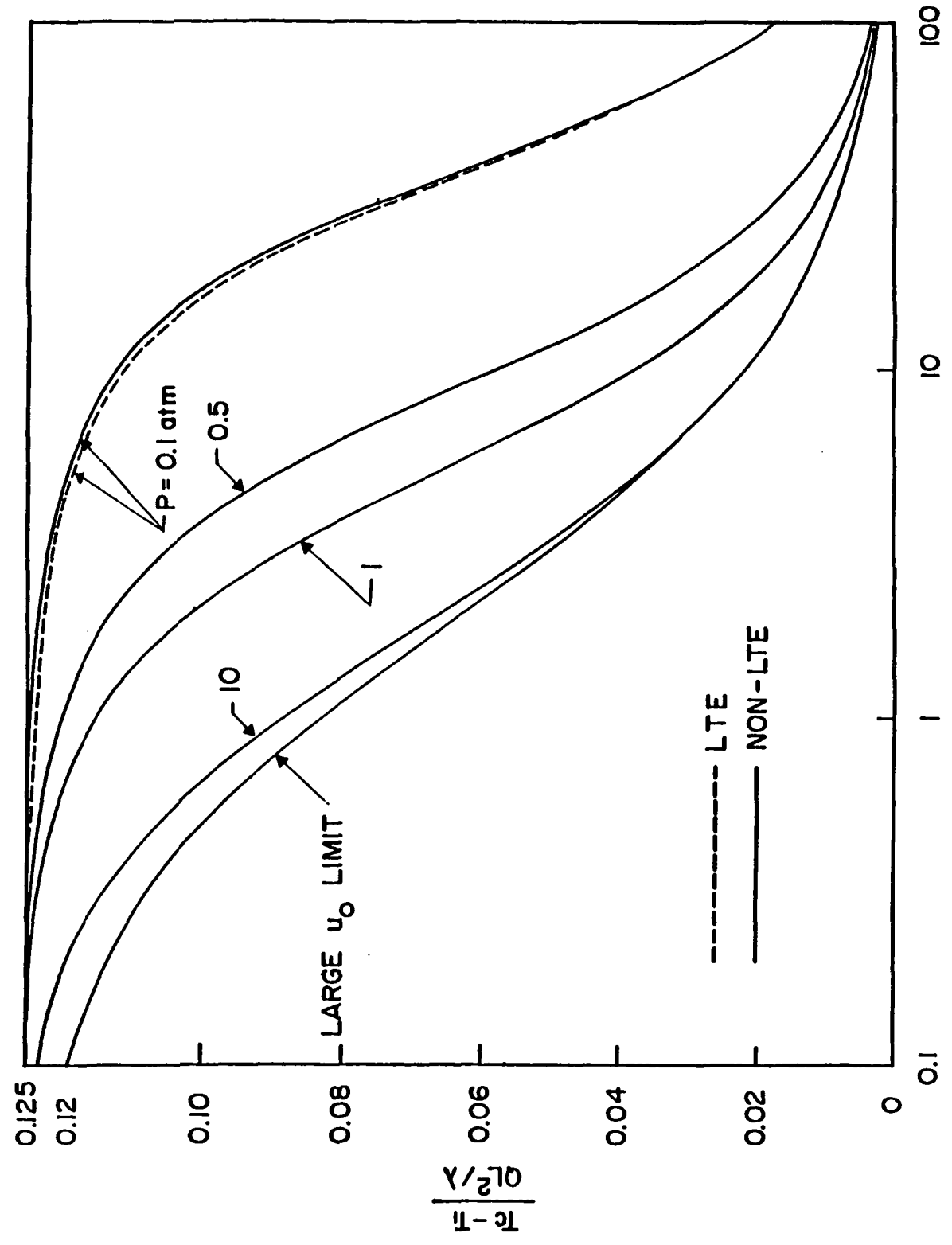

Figure 5.20 Results for combined conduction and radiation for CO (fundamental band) with T_1 = 1,000 K

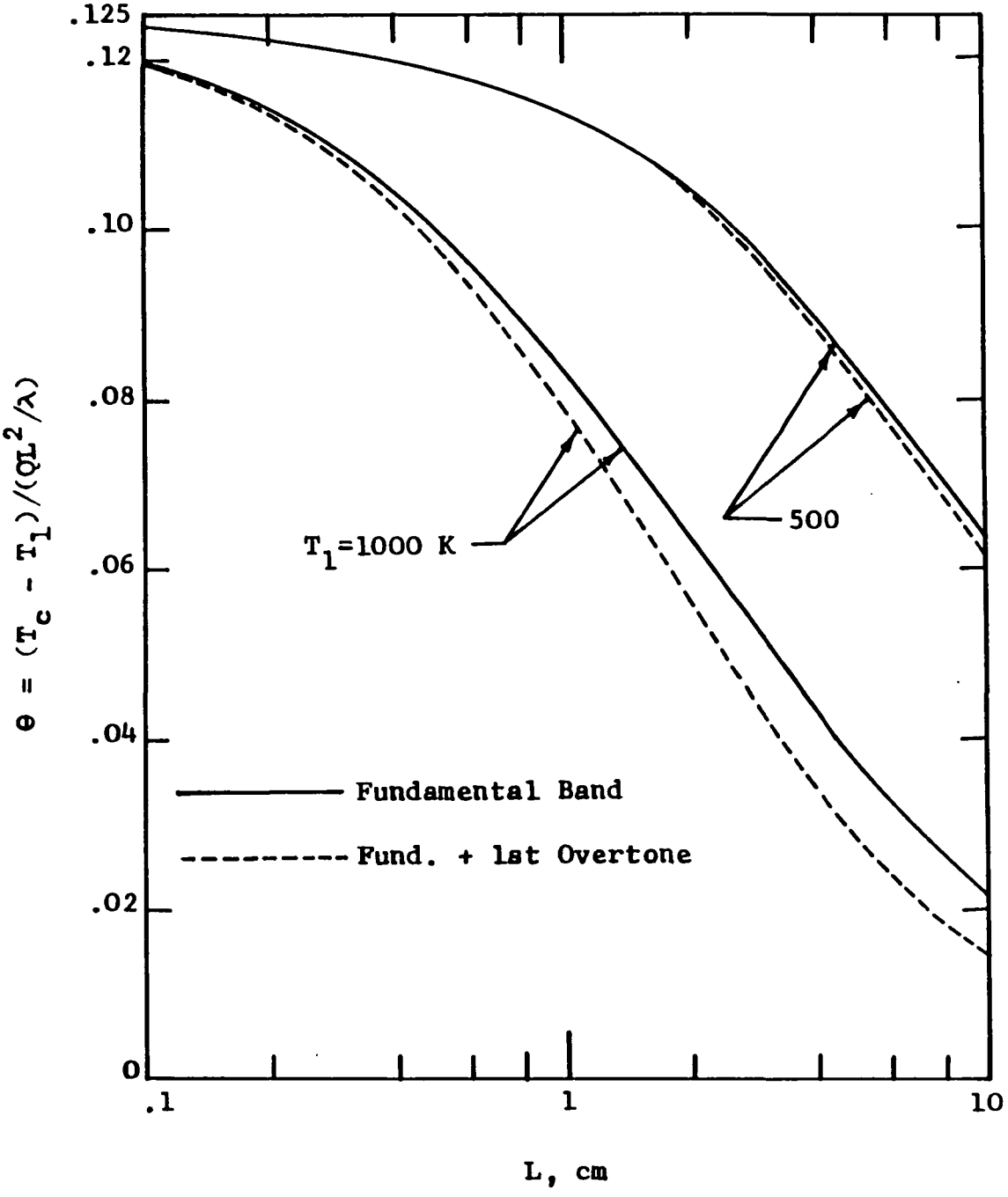

Figure 5.21 Comparison of large path length limit results for combined conduction and radiation for CO

6. HEAT TRANSFER TO LAMINAR FLOW OF RADIATING GASES IN DUCTS

The methods developed in the previous sections will now be applied to the more realistic problem of combined conduction convection and radiation for laminar flow between two parallel plates and within a circular tube. Analyses will be restricted to the conditions where the assumption of LTE is justified. Gray as well as nongray treatments are presented and the effects of surface emittance upon radiative transfer are also investigated for this problem. For the parallel plate geometry nongray results for CO and CO_2 have been obtained by employing various band model correlations for comparative purposes.

Radiative interactions in duct flows have been investigated extensively during the past two decades with certain inherent simplifying assumptions. Some important works are summarized in [32-40] and details are available in cited references. Certain specific studies related to the present problem are available in [93-114]. The main objective here is to provide gray as well as nongray formulations in a systematic manner, discuss relevant solution procedures, present results for some specific cases, and suggest certain areas for further research.

6.1 Heat Transfer in Laminar Flow of Absorbing-Emitting Gases between Parallel Plates

The physical model consists of laminar flow between two infinite parallel gray plates, each of which has the same emissivity ε. The boundary condition along each of the plate surfaces is taken to be that of a uniform heat flux, and thus the temperature of the plates, T_1, varies in the axial direction (Fig. 6.1). Only fully developed flow and heat transfer are considered. Attention will additionally be restricted to small temperature differences, such that constant properties and linearized radiation may be assumed.

6.1.1 Basic Formulation

Since the wall temperature varies in the axial direction, there will exist radiative transfer between wall elements located at different axial positions, and in general this would preclude

the possibility of achieving fully developed heat transfer. For linearized radiation, however, it is easily shown that fully developed heat transfer can be obtained, with the subsequent result that there will be no net radiative transfer between wall elements.

Within the confines of the foregoing assumptions, the energy equation for the present problem can be obtained from Eq. (2.10) as

$$v_x \frac{\partial T}{\partial x} = \alpha \frac{\partial^2 T}{\partial y^2} - \frac{1}{\rho C_p} \frac{\partial q_R}{\partial y} \tag{6.1}$$

where the parabolic velocity profile is described by Eq. (3.11) which for the present case is expressed as

$$v_x = 6 v_m \left[(y/L) - (y/L)^2 \right] \tag{6.2}$$

where the mean velocity $v_m = u_m$ is given by Eq. (3.1). For a uniform wall heat flux and fully developed heat transfer $\partial T/\partial x$ is a constant and is given by Eq. (3.21). Consequently, Eq. (6.1) can be written in dimensionless form as

$$12(\xi - \xi^2) = \frac{d^2 \theta p}{d\xi^2} - \frac{1}{q_w} \frac{dq_R}{d\xi} \tag{6.3a}$$

where ξ is defined by Eq. (4.61) and

$$\theta_p = (T - T_1)/(q_w L/k) \tag{6.3b}$$

Upon integrating this equation once, and by noting that $d\theta_p/d\xi = 0$ and $q_R = 0$ at $\xi = 1/2$, one finds

$$\frac{d\theta_p}{d\xi} - 2(3\xi^2 - 2\xi^3) + 1 = \frac{q_R}{q_w} \tag{6.4}$$

The expression for the total radiative flux for gray surfaces and a single band gas was developed by Tiwari and Cess [94], which can easily be extended to include multi-band gases,

and for the present problem there is obtained

$$\frac{q_R}{q_w} = \frac{3}{2}\frac{L}{k}\sum_{i=1}^{n} H_i u_{oi}\Bigg\{\int_o^{\xi} \theta_p(\xi')\bar{A}_i'(I)d\xi' - \int_{\xi}^{1} \theta_p(\xi')\bar{A}_i'(II)d\xi' + \int_o^{1} \theta_p(\xi')\sum_{m=0}^{\infty}(1-\varepsilon)^{m+1}\Big(\bar{A}_i'\Big[\frac{3}{2}u_{oi}(\xi'+\xi+m)\Big] - \bar{A}_i'\Big[\frac{3}{2}u_{oi}(\xi'-\xi+1+m)\Big]\Big)d\xi'\Bigg\} \tag{6.5}$$

Note that for black plates, this coincides with the expression for the total radiative heat flux, under the assumption of LTE, as given by Eq. (5.20).

The temperature profile within the gas, $\theta_p(\xi)$, is thus defined by the combination of Eqs. (6.4) and (6.5). The boundary condition for the resulting equation follows to be $\theta_p(0) = 0$. For flow problems, the quantity of primary interest is the bulk temperature of the gas, which is defined by Eq. (3.9). Employing Eq. (6.2) and the dimensionless quantities defined earlier, the bulk temperature can be expressed in a dimensionless form as

$$\theta_{bp} = \frac{T_b - T_1}{q_w L/k} = 6\int_o^{1} \theta_p(\xi)(\xi - \xi^2)d\xi \tag{6.6}$$

which is equivalent to Eq. (3.35).

The heat transfer q_w is given by the expression, $q_w = h_c(T_1 - T_b)$, where h_c is the equivalent heat transfer coefficient watts/m^2–k. As mentioned in Sec. 3, the heat transfer results are expressed usually in terms of the Nusselt number Nu defined in terms of the hydraulic diameter D_h. For the present geometry D_h = 2L. Eliminating the effective heat transfer coefficient h_c from the expressions for q_w and Nu, a relation between the Nusselt number and the bulk temperature is obtained as

$$Nu = \frac{2Lq_w}{k(T_1 - T_b)} = \frac{-2}{\theta bp} \tag{6.7}$$

Equation (6.7) is essentially the same as Eq. (3.37).

By employing the techniques similar to that discussed in Sec. 5 and described in detail in [109-114], numerical solutions yielding results for θ_{bp} have been obtained for several illustrative cases, and these are discussed in Sec. 6.4. It should be pointed out here that the number of terms (m values) required in Eq. (6.5), for proper convergence, increases as values of wall emittance decreases. For example, with $\epsilon = 0.5$ it was necessary to consider only three terms, while with $\epsilon \approx 0.1$ a minimum of ten terms were required. The numerical procedure is described here briefly.

The numerical solutions of combined form of Eqs. (6.4) and (6.5) are obtained by the method of undetermined parameters. For this case, a polynomial solution for $\theta_p(\xi)$ is assumed as

$$\theta_p(\xi) = a_o + a_1\xi + a_2\xi^2 + a_3\xi^3 + a_4\xi^4 \tag{6.8}$$

After employing the conditions $\theta_p(0) = 0$, $\theta_p'(1/2) = 0$, and $\theta_p'(1) = \theta_p'(0)$, Eq. (6.8) becomes

$$\theta_p(\xi) = a_1(\xi - 2\xi^3 + \xi^4) + a_2(\xi^2 - 2\xi^3 + \xi^4) \tag{6.9}$$

The constants a_1 and a_2 are obtained by satisfying the governing integro-differential equation at two locations $\xi = 0$ and $\xi = 1/4$. A combination of Eqs. (6.6) and (6.9) results in

$$\theta_{bp} = \frac{1}{70}(17a_1 + 3a_2) \tag{6.10}$$

Thus, with a_1 and a_2 known, the bulk temperature (or the Nusselt number) is obtained from Eq. (6.10). The procedure for evaluating the constants a_1 and a_2 is described in detail in [109, 114].

6.1.2 Limiting Solutions

For negligible radiation, there will be obtained from Eq. (6.3a)

$$\theta_p = 2\xi^3 - \xi^4 - \xi \tag{6.11}$$

and substitution of this in Eq. (6.6) will yield

$$\theta_{bp} = -17/70 \tag{6.12}$$

This is analogous to the result given in Eq. (3.36).

As discussed before, in the optically thin limit (i.e. the limit of small u_{oi}) $\bar{A}'(u) = 1$, and from a combination of Eqs. (6.4) and (6.5), there is obtained in this limit

$$\frac{d\theta_p}{d\xi} - 2(3\xi^2 - 2\xi^3 + 1) = \frac{3}{2}\frac{L}{k}\sum_{i=1}^{n} H_i u_{oi}\left\{\int_o^{\xi} \theta_p(\xi')d\xi' - \int_{\xi}^{1} \theta_p(\xi')d\xi'\right\} \tag{6.13}$$

After differentiating once, this equation can be expressed in the following form

$$\frac{d^2\theta_p}{d\xi^2} - 3N\theta_p(\xi) = 12(\xi - \xi^2) \tag{6.14}$$

with boundary conditions

$$\theta_p(0) = 0, \quad \theta_p'(1/2) = 0$$

The optically thin interaction parameter N in this equation is the same as defined by Eq. (5.24a). It should be noted here that, under optically thin conditions the effect of surface emittance upon the radiative transfer vanishes. Explanation to this effect has been given in [94].

Equation (6.14) possesses an elementary solution, and the result expressed in terms of the bulk temperature is found to be

$$\theta_{bp} = \frac{1}{(3N)^3}\left\{\frac{576}{\sqrt{3N}}\left[\frac{1 - \exp\left(-\sqrt{3N}\right)}{1 + \exp\left(-\sqrt{3N}\right)}\right] - 21.6N^2 + 72N - 288\right\} \tag{6.15}$$

This result is illustrated in Fig. 6.2. Again, note that the parameter N characterizes the relative importance of radiation versus conduction, for the present problem, in the optically thin limit.

The large path length limit is obtained by replacing $\bar{A}'(u)$ by $1/u$ in Eq. (6.5), and the corresponding energy equation becomes

$$\frac{d\theta_p}{d\xi} - 2(3\xi^2 - 2\xi^3) + 1 = \frac{L}{k}\sum_{i=1}^{n} H_i\left\{\int_0^1 \theta_p(\xi')\frac{d\xi'}{\xi - \xi'} + \sum_{m=0}^{\infty}(1 - \varepsilon_i)^{m+1} \times \int_0^1 \theta_p(\xi')\left[\frac{1}{\xi' + \xi + m} - \frac{1}{\xi' - \xi + 1 + m}\right]d\xi'\right\} \tag{6.16}$$

where quantity $(L/k)\sum_{i=1}^{n} H_i = M$, as defined by Eq. (5.29). Note that, written in this form, Eq. (6.16) can also be applied to investigate the effects of nongray wall emittance. This, however, will be treated in Sec. 6.2 while dealing with the problem of flow through specific circular tubes.

Numerical solution of Eq. (6.16) has been obtained by following the procedure described for the general case, and θ_{bp} results are given in Fig. 6.3 as a function of interaction parameter M. For a particular physical system, the value of M can be obtained from Fig. 5.3.

6.1.3 Gray Gas Approximation

The gray gas assumption is probably the greatest approximation for the real gas. This assumption replaces the wave-number dependent absorption coefficient by a wave-number averaged quantity. For lack of a more rational choice, this average coefficient will be taken to be $\kappa_p(T_1)$.

Employing Eq. (4.32) and using the information of Table A2, the Planck mean absorption coefficient was calculated for a number of gases and is illustrated in Fig. 6.4. Values of κ_p for higher temperatures than those given in Fig. 6.4, can be obtained from Refs. 18 and 33.

In this section, for convenience, attention will be directed only to black bounding surfaces. Replacing κ_ω by κ_p in Eq. (4.59), integrating over the wave number, and utilizing the linearized expression

$$T^4 - T_1^4 = 4T_1^3(T - T_1)$$

there is obtained for the present problem

$$q_R = 6\sigma\kappa_p T_1^3 \left\{ \int_0^y [T(z) - T_1] \exp\left[-\frac{3}{2}\kappa_p(y - z)\right] dz - \int_y^L [T(z) - T_1] \exp\left[-\frac{3}{2}\kappa_p(z - y)\right] dz \right\} \tag{6.17}$$

Upon differentiating this equation twice, the integrals repeat themselves and may be eliminated, and the resulting equation can be expressed as

$$\frac{d^2 q_R}{d\xi^2} - \frac{9}{4}\tau_o^2 q_R = \gamma_1 q_w \frac{d\theta_p}{d\xi} \tag{6.18a}$$

where

$$\gamma_1 = \frac{3\tau_0^2}{\bar{N}} \quad ; \quad \bar{N} = \frac{k\,\kappa_p}{4\sigma T_1^3} \quad ; \quad \tau_o = \kappa_p L \tag{6.18b}$$

Equation (6.18a) is, in fact, simply one form of the well-known differential approximation [16, 18] and is analogous to Eq. (4.75). The boundary conditions for this equation are found to be

$$q_R(1/2) = 0 \quad ; \quad \frac{3}{2} q_R(0) = \frac{1}{\tau_o}(dq_R/d\xi)_{\xi=0} \tag{6.18c}$$

The simultaneous solution of Eqs. (6.4) and (6.18) is straightforward, and the final result for the dimensionless bulk temperature is expressed as (see Appendix C)

$$\begin{aligned}\theta_{bp} = {} & C_1\left[24 - 12M_1 + M_1^3 + \left(M_1^3 - 12M_1 - 24\right)e^{-M_1}\right] \\ & - \frac{12}{5}\frac{\gamma_1}{M_1^4} + \frac{17}{70}\frac{\gamma_1}{M_1^2} - \frac{17}{70}\end{aligned} \tag{6.19}$$

where

$$C_1 = \frac{\gamma_1}{M_1^8}\left[\frac{48 - 3\tau_o M_1^2 + 36\tau_o}{3\tau_o(1 - e^{-M_1}) + 2M_1(1 + e^{-M_1})}\right]$$

$$M_1^2 = 3\tau_o^2\left(\frac{3}{4} + \frac{1}{\bar{N}}\right)$$

The governing parameters for this equation are $\bar{N}$, and τ_o. Note that $\bar{N}$ characterizes the relative importance of radiation versus conduction for gray gas. The results of this equation are illustrated in Fig. 6.5. For a particular physical system, values of τ_o and $\bar{N}$ can be obtained from Eq. (6.18b) by utilizing the result for κ_p as given in Fig. 6.4.

For optically thin conditions ($\tau_o \to 0$), $M_1^2 \to \gamma_1$, and Eq. (6.19) reduces to

$$\theta_{bp} = \frac{1}{\gamma_1^3}\left\{\frac{576}{\sqrt{\gamma_1}}\left[\frac{1-\exp\left(-\sqrt{\gamma_1}\right)}{1+\exp\left(-\sqrt{\gamma_1}\right)}\right] - 2.4\gamma_1^2 + 24\gamma_1 - 288\right\} \tag{6.20}$$

and from the definition of γ_1 it is seen that in this limit the governing parameter is $\bar{N}/\tau_o^2$. For small values of γ_1, by expanding the exponential $\exp\left(-\sqrt{\gamma_1}\right)$ in series, it can be shown that the transparent limit ($\tau_o = 0$) corresponds to the result with no radiation, Eq. (6.12), see Appendix C.

Under optically thick conditions, since $\tau_o >> 1$, then $M_1 >> 1$, and Eq. (6.19) reduces to

$$\theta_{bp} = \frac{-17/70}{1+(4/3\bar{N})} \tag{6.21}$$

and it is seen that this limit is characterized by the parameter $\bar{N}$.

From a comparison of Eqs. (6.5) and (6.19) it is noted that, while the band absorptance model formulation involves three basic parameters, band intensity S(T), band width A_o, and line structure β, the gray gas formulation is governed only by two parameters $\bar{N}$, and τ_o. The line structure parameter β has no significance in a gray gas analysis. From Eq. (6.13) it may be seen that the optically thin limit of the band model involves the single parameter N/u_o^2, which is analogous to the gray gas parameter $\bar{N}/\tau_o^2$. On the other hand, the large u_o limit parameter A_o is not analogous to the gray gas counterpart $\bar{N}$. This again illustrates that the large u_o limit for a vibration-rotation band differs from the conventional optically thick limit.

6.1.4 Results and Discussion

Bulk temperature results are presented in terms of the dimensional quantities L and P. For CO, CO_2, H_2O, and CH_4, the band absorptance results obtained by using the Tien and Lowder correlation are illustrated in Figs. 6.6 through 6.11. The limiting value of $\theta_{bP} = -0.243$, Eq. (6.12), corresponds to negligible radiation, and effect of radiation increases with increasing

plate spacing. As would be expected radiative transfer is more pronounced for higher pressures and wall temperatures.

Figures 6.3 and 6.6 illustrate the effects of variable wall emittance upon radiative transfer. Shown in Fig. 6.6 are the band absorptance results for CO_2 at P = 1 atm and T_1 = 500 K. Radiative contribution is seen to become smaller for lower wall emittances. This is because a lower surface emittance corresponds to a reduction in the energy transfer capability between the gas and the surface.

For the sake of convenience and brevity, the results are presented only for the case of black bounding surfaces in Figs. 6.7 through 6.11. Also shown in these figures are the limiting solutions for large u_o. As in Sec. 5.2, the large u_o solutions for individuals gases are obtained from the results of Fig. 6.3 together with the M/L values from Fig. 5.3. It is again seen that for a given wall temperature, the large u_o limit can be obtained either by going to large values of L or to high pressures. Furthermore, these results indicate that at a particular wall temperature, the large u_o limit for CO_2 is achieved at a relatively lower pressure than for other gases. As a matter of fact, for most practical purposes involving CO_2, at room temperature, the result at one atmosphere can be regarded as a result for the large u_o limit.

A comparison of the band absorptance results for the four gases is shown in Fig. 6.11 for a pressure of one atmosphere and a wall temperature of 1000 K. The relative order of the four curves, for small values of L, is characteristic of the interaction parameter for optically thin radiation (see Fig. 5.2). As the value of L is increased the results approach to the solution obtained for the large u_o limit, and the relative order of the curves become as indicated by the large u_o interaction parameter of Fig. 5.3.

For CO_2, H_2O, and CH_4, a comparison of various solutions are illustrated in Figs. 6.12 through 6.14 for a wall temperature of 500 K and a pressure of one atmosphere. The gray solutions were obtained from a combination of the results of Figs. 6.4 and 6.5, and the optically

thin solutions were obtained from the results of Fig. 6.2 together with the N values from Fig. 5.2.

For CO_2 it is seen from Fig. 6.12 that, when radiation is of importance, the radiative transfer process very nearly corresponds to the large path length limit. Conversely, this indicates that when the radiation is optically thin, it is in turn negligible relative to conduction, such that the optically thin limit does not constitute a useful limiting solution for the conditions illustrated in Fig. 6.12. For H_2O and CH_4, however, a greater departure from the large path length limit is noticed (Figs. 6.13 and 6.14), and optically thin limit is seen to be the appropriate limiting solution for small values of L. Furthermore, when radiation is of importance (i.e., at relatively larger value of L), the optically thin limit greatly overestimates the influence of radiation, indicating that for these conditions the actual radiative process is not optically thin.

Note that the gray gas solution also overestimates the importance of radiation. As explained in [77], the reason for this is that the optical thickness of the gas based upon the Planck mean coefficient can be several orders of magnitude less than that based upon the maximum absorption coefficient within the vibration-rotation band. Correspondingly, the gray gas assumption may predict optically thin radiation under conditions for which the real process is not optically thin.

Gray, optically thin as well as large u_o solutions can be obtained with considerable mathematical simplifications. Since these results overestimate the influence of radiation, they can be utilized to estimate whether or not, for a given gas, the interaction of radiation is going to be of importance.

Bulk temperature results for CO (fundamental band) and CO_2 (15μ, 4.3μ, and 2.7μ bands) as obtained by employing the various correlations for band absorptance, are illustrated in Figs. 6.15 through 6.18. Results for CO are illustrated in Figs. 6.15 and 6.16 for wall temperatures of 500 K and 1,000 K, respectively. It is evident from these figures that, except for the results of Tien and Lowder correlation, results of other correlations differ from each other by less than 6% for all pressures and path lengths. For P = 0.1 and 1 atm, results differ by not more than 3%.

The largest difference of about 6% occurs for P = 10.0 atm and T_1 = 1,000 K. From a close observation of all results presented in Figs. 6.15 and 6.16, it may be concluded that, for low to moderate pressures (say up to 5 atm), any one of the correlations (No. 2, 3, 5, or 6) could be employed in radiative transfer analyses. At high pressures, however, use of correlations 5 or 7 is recommended.

From Ref. 101 and the results presented in Figs. 6.7, it is noted that for CO the limit of large u_o is approached at P = 10 atm for T_1 = 500 K and at 100 atm for T_1 = 1,000 K. This trend is also evident, in general, from the results of Figs. 6.15 and 6.16. The results of Tien and Lowder correlation, however, follow this trend more closely than any other result. As such, use of Tien and Lowder correlation is justified for radiative transfer analyses involving gases like CO (i.e., diatomic gases with single fundamental band having uniform distribution of spectral lines) at moderate and high pressures.

For CO_2, results of different correlations are illustrated in Figs. 6.17 and 6.18 for P = 0.01, 0.1, 1 and 10 atm, and for T_1 = 500 K and 1,000 K, respectively. From the results presented in Fig. 6.8, it may be noted that for CO_2 the limit of large u_o (LLU) is approached at 2 atm for T_1 = 300 K, at about 4 atm for T_1 = 500 K, and at about 10 atm for T_1 = 1,000 K. Thus, results for 10 atm in Figs. 6.17 and 6.18 essentially are LLU results. For clarity, results of P = 1 and 10 atm are not plotted on the same graph.

As was the case with CO, the results of all correlations (except Tien and Lowder) almost are identical for CO_2 also for P = 0.01 and 0.1 atm. This, however, would be expected because the low pressure (small β) situation corresponds to the case of square-root limit and most correlations are developed to satisfy this limit. It was pointed out earlier and in [34, 37] that the square-root limit is not satisfied by the Tien and Lowder correlation. At low pressures, therefore, use of the Tien and Lowder correlation certainly is not justified. Other results of CO_2 (shown in Figs. 6.17 and 6.18) follow the same general trend as for CO in Figs. 6.15 and 6.16. The maximum

difference between the results of different correlations is about 6% for P = 1 atm and T_1 = 1,000 K. For the most part, results of correlations 3, 5, 6, and 7 are identical for P = 10 atm. This again would be expected because for CO_2, the LLU is approached at relatively lower pressures and most correlations are developed to satisfy the logarithmic limit. For gases like CO_2, therefore, use of any one of the correlations 2, 3, 5 and 6 is recommended at low and moderate pressures, and of 3, 5, 6, and 7 at high pressures. Use of the correlations 2, 3, 6, and 7, in a particular radiative transfer analysis, provides a greater mathematical flexibility and simplicity.

6.2 Radiative Interaction in Laminar Flow through a Circular Tube

This section is concerned with the heat transfer to absorbing-emitting gases in laminar flow through a circular tube. With the single exception of a circular geometry, this problem is exactly the same as treated in the previous chapter. As before, fully developed laminar flow and heat transfer have been assumed, and the boundary condition at the tube wall has been taken to be that of a uniform surface heat flux (see Figs. 3.6 and 6.19).

In addition to the consideration of gray wall emittance, effects of nongray wall emittance upon radiative exchange have also been investigated. Specific results have been obtained for the flow of CO_2 through stainless steel tubes of various compositions. Furthermore, based on the gray gas analysis for black bounding surfaces, a correlation between the parallel plate and the tube results has been established.

6.2.1 Governing Equations

For this problem, the energy equation, Eq. (2.10), can be expressed as

$$v_x \frac{\partial T}{\partial x} = \frac{\alpha}{r}\frac{\partial}{\partial r}\left(r\frac{\partial T}{\partial r}\right) - \frac{1}{\rho c_p}\frac{1}{r}\frac{\partial}{\partial r}(rq_R) \tag{6.22}$$

where the velocity profile is given by Eq. (3.14) and is expressed here as

$$v_x = 2v_m\left[1 - (r/r_o)^2\right] \tag{6.23}$$

The mean velocity $v_m = u_{\max}/2$, and $u_{\max}$ is defined by Eq. (3.15). Noting again that for a uniform wall heat flux and fully developed heat transfer, $\partial T/\partial x$ is given by Eq. (3.41), a combination of Eqs. (6.22) and (6.23) yields

$$4(\xi - \xi^3) = \frac{d}{d\xi}\left(\xi \frac{d\theta_T}{d\xi}\right) - \frac{1}{q_w}\frac{d}{d\xi}(\xi q_R) \tag{6.24a}$$

where

$$\theta_T = \frac{T - T_w}{q_w r_o/k} \quad ; \quad \xi = \frac{r}{r_o} = \frac{u}{u_o} \tag{6.24b}$$

Upon integrating this equation, and noting that $d\theta_T/d\xi = 0$ and $q_R = 0$ at $\xi = 0$, there is obtained

$$\frac{d\theta_T}{d\xi} + \xi^3 - 2\xi = \frac{q_R}{q_w} \tag{6.25}$$

and the boundary condition for this is given as $\theta_T(1) = 0$.

For a circular geometry, the spectral radiative heat flux is given by the expression [98, 100, 115-119]

$$\begin{aligned} q_{R_\omega} = \frac{4}{\pi}\int_o^{\pi/2} \Bigg\{ & \int_{r\sin\gamma}^{r} \left[e_\omega(r') - e_\omega(T_w)\right]\kappa_\omega a e^{-\frac{b\kappa_\omega}{\cos\gamma}(r-r')}dr' \\ & - \int_r^{r_o} \left[e_\omega(r') - e_\omega(T_w)\right]\kappa_\omega a e^{-\frac{b\kappa_\omega}{\cos\gamma}(r'-r)}dr' \\ & + \int_{r\sin\gamma}^{r_o} \left[e_\omega(r') - e_\omega(T_w)\right]\kappa_\omega a e^{-\frac{b\kappa_\omega}{\cos\gamma}(r+r'-2r\sin\gamma)}dr' \\ & + \left[B_\omega(T_w) - e_\omega(T_w)\right]\frac{a}{b}\cos\gamma\left[e^{-\frac{b\kappa_\omega}{\cos\gamma}(r+r_o-2r\sin\gamma)}dr'\right. \\ & \left. - e^{-\frac{b\kappa_\omega}{\cos\gamma}(r_o-r)}\right]\Bigg\}d\gamma \end{aligned} \tag{6.26}$$

where constants a and b have values of unity and 5/4 respectively, and the expression for the radiosity is found to be

$$\begin{aligned} B_\omega(T_w) = \Bigg\{ & \varepsilon e_\omega(T_w) + \frac{4a}{\pi}(1-\varepsilon)\int_o^{\pi/2}\int_{r_o\sin\gamma}^{r_o} \kappa_\omega e_\omega(r') \\ & \times \left[e^{-\frac{b\kappa_\omega}{\cos\gamma}(r_o+r'-2r_o\sin\gamma)} + e^{-\frac{b\kappa_\omega}{\cos\gamma}(r_o-r')}\right]dr'd\gamma\Bigg\}/DEN \end{aligned} \tag{6.27a}$$

where

$$DEN = \left\{1 - \frac{4a}{\pi b}(1-\varepsilon)\int_o^{\frac{\pi}{2}} \cos\gamma \exp\left[-\frac{2b\kappa_\omega r_o}{\cos\gamma}(1-\sin\gamma)\right]d\gamma\right\} \tag{6.27b}$$

In order to be able to apply the technique developed in [94] for combining Eqs. (4.52), (6.26), and (6.27), it would be necessary to obtain an exact solution for the integral appearing in Eq. (6.27b). However, this innocent looking integral does not appear to possess a closed form solution and therefore it has been approximated by an exponential as

$$\int_o^{\pi/2} \cos\gamma \exp\left[-\left(\frac{1-\sin\gamma}{\cos\gamma}\right)X\right]d\gamma \simeq C_1 \exp\left(-C_2 X\right)$$

where C_1 and C_2 are constants and $X = 2b\ \kappa_\omega\ r_o$. Evaluation of the constants in the limit when X approaches zero gives, $C_1 = 1$, and $C_2 = (\pi/2) - 1$. With these values for the constants, the exponential will be expected to be a good approximation of the integral only for small values of X. However, from a comparison of the numerical solution of the integral with the exponential result using $C_1 = 1$, and $C_2 = 1/2$, an excellent agreement between the two solutions has been found for all values of X. Using this approximation, and by noting that $4a/\pi b \simeq 1$, and following the identical procedure outlined in [94], Eq. (6.27) can now be expressed as

$$\begin{aligned} B_\omega(T_w) - e_\omega(T_w) = \frac{4}{\pi}(1-\varepsilon)\int_o^{\pi/2}\int_{r_o\sin\gamma}^{r_o} \left[e_\omega(r') - e_\omega(T_w)\right] \\ \times \sum_{m=0}^{\infty}(1-\varepsilon)^m \kappa_\omega \left\{\exp\left[-b\kappa_\omega\left(\frac{r_o + r' - 2r_o\sin\gamma}{\cos\gamma} + mr_o\right)\right]\right. \\ \left. + \exp\left[-b\kappa_\omega\left(\frac{r_o - r'}{\cos\gamma} + mr_o\right)\right]\right\} dr' d\gamma \end{aligned} \tag{6.28}$$

Following the procedures adopted in the previous sections, Eqs. (6.25)-(6.28) are combined and there is obtained the final form of the energy equation as

$$\frac{d\theta_T}{d\xi} + \xi^3 - 2\xi =$$
$$+ \frac{4r_o}{\pi k}\sum_{i=1}^{n} H_i u_{oi} \int_o^{\pi/2} \left\{ \int_{\xi \sin\gamma}^{\xi} \theta_T(\xi') \bar{A}_i' \left[\frac{bu_{oi}}{\cos\gamma}(\xi - \xi') \right] d\xi' \right.$$
$$- \int_{\xi}^{1} \theta_T(\xi') \bar{A}_i' \left[\frac{bu_{oi}}{\cos\gamma}(\xi' - \xi) \right] d\xi' + \int_{\xi \sin\gamma}^{1} \theta_T(\xi') \bar{A}_i' \left[\frac{bu_{oi}}{\cos\gamma}(\xi + \xi' - 2\xi \sin\gamma) \right] d\xi'$$
$$\left. + \sum_{m=0}^{\infty} (1 - \varepsilon_i)^{m+1} \cos\gamma \int_o^{\frac{\pi}{2}} \int_{\sin\gamma'}^{1} \theta_T(\xi')[BRAKT] d\xi' d\gamma' \right\} d\gamma \qquad (6.29)$$

where

$$[BRAKT] = \bar{A}_i' \left[bu_{oi} \left(\frac{1 + \xi - 2\xi \sin\gamma}{\cos\gamma} \right.\right.$$
$$\left.\left. + \frac{1 + \xi' - 2\sin\gamma'}{\cos\gamma'} + m \right) \right] + \bar{A}_i' \left[bu_{oi} \left(\frac{1 + \xi - 2\xi \sin\gamma}{\cos\gamma} + \frac{1 - \xi'}{\cos\gamma'} + m \right) \right]$$
$$- \bar{A}_i' \left[bu_{oi} \left(\frac{1 - \xi}{\cos\gamma} + \frac{1 + \xi' - 2\sin\gamma'}{\cos\gamma'} + m \right) \right] - \bar{A}_i' \left[bu_{oi} \left(\frac{1 - \xi}{\cos\gamma} + \frac{1 - \xi'}{\cos\gamma'} + m \right) \right]$$

This equation along with the boundary condition $\theta_T(1) = 0$ defines the temperature within the gas.

The bulk temperature for this problem is defined by Eq. (3.44) and is expressed here as

$$T_b = \frac{1}{v_m \pi r_o^2} \int_o^{2\pi} \int_o^{r_o} v_x T(r d\psi dr) = \frac{4}{r_o^2} \int_o^{r_o} T \left(1 - \frac{r^2}{r_o^2} \right) r dr \qquad (6.30a)$$

By employing the dimensionless quantities defined earlier, this can be expressed as

$$\theta_{bT} = (T_b - T_w)/(q_w r_o/k) = 4 \int_o^1 \theta_T(\xi - \xi^3) d\xi \qquad (6.30b)$$

For negligible radiation, Eq. (6.29) yields the temperature profile

$$\theta_T = \xi^2 - \frac{1}{4}(\xi^4 + 3)$$

and the bulk temperature is found to be

$$\theta_{bT} = -11/24 \qquad (6.31)$$

In the large path length limit, Eq. (6.29) reduces to

$$\frac{d\theta_T}{d\xi} + \xi^3 - 2\xi$$
$$= \frac{4r_o}{\pi bk}\sum_{i=1}^{n} H_i \int_o^{\pi/2} \left\{ \cos\gamma \int_{\xi\sin\gamma}^{1} \theta_T(\xi') \left[\frac{d\xi'}{\xi - \xi'} + \frac{d\xi'}{\xi + \xi' - 2\xi\sin\gamma} \right] \right.$$
$$+ \sum_{m=0}^{\infty} (1-\varepsilon_i)^{m+1} \cos\gamma \int_o^{\frac{\pi}{2}} \int_{\sin\gamma'}^{1} \theta_T(\xi') \left[\left(\frac{1+\xi-2\xi\sin\gamma}{\cos\gamma} + \frac{1+\xi'-2\sin\gamma'}{\cos\gamma'} + m \right)^{-1} \right.$$
$$+ \left(\frac{1+\xi-2\sin\gamma}{\cos\gamma} + \frac{1-\xi'}{\cos\gamma'} + m \right)^{-1} - \left(\frac{1-\xi}{\cos\gamma} + \frac{1+\xi'-2\sin\gamma'}{\cos\gamma'} + m \right)^{-1}$$
$$\left. \left. - \left(\frac{1-\xi}{\cos\gamma} + \frac{1-\xi'}{\cos\gamma'} + m \right)^{-1} \right] d\xi' d\gamma' \right\} d\gamma \qquad (6.32)$$

In the form presented, Eqs. (6.29) and (6.32) can be utilized to investigate the effects of nongray wall emittance upon radiation.

Employing the Haselgrove technique for numerical integration of multidimensional integrals, and following the procedure described in previous sections, numerical solutions of Eqs. (6.29) and (6.32) can be obtained and results expressed in terms of the bulk temperature.

6.2.2 Gray Medium Approximation

As in Sec. 6.1, assumption of gray gas means replacing the wave number dependent absorption coefficient by a wave number averaged quantity $\kappa_p(T)$. Note that inherent in this approximation is the fact that κ_p is independent of temperature, which actually is not realistic and a discussion to this effect has been given in [77].

The expression involving the total radiative heat flux can be obtained from the differential approximation [16, 18], and for this problem one finds from Eq. (4.75)

$$\frac{d}{dr}\left[\frac{1}{r}\frac{d}{dr}(rq_R)\right] - \frac{9}{4}\kappa_p^2 q_R = 3\sigma\kappa_p \frac{dT^4}{dr} \qquad (6.33)$$

For linearized radiation

$$\frac{dT^4}{dr} = 4T_w^3 \frac{dT}{dr}$$

and Eq. (6.33) may now be expressed as

$$\frac{d}{d\xi}\left[\frac{1}{\xi}\frac{d}{d\xi}(\xi q_R)\right] - \frac{9}{4}\bar{\tau}_o^2 q_R = \gamma_2 q_w \frac{d\theta_T}{d\xi} \tag{6.34a}$$

where

$$\gamma_2 = 3\bar{\tau}_o^2/\bar{N} \quad , \quad \bar{N} = \frac{k\kappa_p}{4\sigma T_w^3} \quad , \quad \bar{\tau}_o = \kappa_p r_o \tag{6.34b}$$

Equation (6.34) is analogous to Eq. (6.18) for the parallel plate geometry. For a black tube, the boundary conditions for Eq. (6.34) are found to be

$$\frac{3}{2}q_R(1) = -\frac{1}{\bar{\tau}_o}\left[\frac{1}{\xi}\frac{d}{d\xi}(\xi q_R)\right]_{\xi=1} \quad , \quad q_R(0) = 0 \tag{6.34c}$$

From a combination of Eqs. (6.25) and (6.34), there is obtained

$$\xi^2\frac{d^2 q_R}{d\xi^2} + \xi\frac{dq_R}{d\xi} - \left(M_2^2\xi^2 + 1\right)q_R = \gamma_2 q_w\left(2\xi^3 - \xi^5\right) \tag{6.35}$$

where

$$M_2^2 = \frac{9}{4}\bar{\tau}_o^2 + \gamma_2$$

First Eq. (6.35) is solved for q_R, and then from Eq. (6.25) the solution is obtained for θ_T, and finally from Eq. (6.30b) the result for the bulk temperature is obtained as (see Ref. 113 and Appendix D)

$$\begin{aligned}\theta_{bT} = {} & C_2\left[M_2\left(8 - M_2^2\right)I_o(M_2) - 16I_1(M_2)\right] \\ & + \frac{11}{24}\frac{\gamma_2}{M_2^2} - \frac{8}{3}\frac{\gamma_2}{M_2^4} - \frac{11}{24}\end{aligned} \tag{6.36}$$

where

$$C_2 = \frac{\gamma_2}{M_2^8}\left[\frac{3\bar{\tau}_o M_2^2 - 24\bar{\tau}_o - 32}{2M_2 I_o(M_2) + 3\bar{\tau}_o I_1(M_2)}\right]$$

and I_o and I_1 represent the modified Bessel functions of the first kind.

For optically thin conditions ($\tau_o \to 0$), $M_2^2 \to \gamma_2$, and Eq. (6.36) reduces to

$$\theta_{bT} = \frac{1}{\gamma_2^3}\left\{\frac{256}{\sqrt{\gamma_2}}\left[\frac{I_1\left(\sqrt{\gamma_2}\right)}{I_o\left(\sqrt{\gamma_2}\right)}\right] - \frac{8}{3}\gamma_2^2 + 16\gamma_2 - 128\right\} \tag{6.37}$$

Employing the series expansion of the modified Bessel functions for small values of the argument γ_2, Eq. (6.37) can be written in an alternate form and by letting $\gamma_2 \rightarrow 0$ in that form there is obtained the result in the transparent limit $\theta_{bT} = -11/24$.

The optically thick limit of Eq. (6.36) is obtained by letting $\tau_o \rightarrow \infty$ in the asymptotic series of the modified Bessel functions for large values of M_2. Consequently, one obtains

$$\theta_{bT} = \frac{-11/24}{1 + (4/3\bar{N})} \tag{6.38}$$

As in Sec. 6.1, it is also evident from the above equations that, optically thin and optically thick limits are characterized by the parameters $\bar{N}/\tau_o^2$, and $\bar{N}$ respectively. The gray results are illustrated in Fig. 6.20. Note that in this figure, both θ_{bT} and τ_o are expressed in terms of the diameter of the tube, and the solutions, as obtained by Eq. (6.36), are shown by the solid lines.

6.2.3 Results and Discussion

For the case of gray wall emittance, a general solution (θ_{bT} versus M) of Eq. (6.32) was obtained and the results are illustrated in Fig. 6.21 by the solid lines. For a particular physical system the value of M can be obtained from Fig. 5.3 simply by replacing L with either the radius r_o or with the diameter of the tube.

As discussed in Sec. 6.1, the influence of radiation decreases with a decrease in the value of the wall emittance. This decrease in radiative effect is seen to be higher for the parallel plate geometry than for the tube. The reason for this is based on the fact that the reflection of radiant energy from the bounding surfaces plays a greater role at lower values of wall emittance, and under identical conditions the number of reflections resulting from a circular geometry will be relatively higher than those from the parallel plates.

The assumption of a gray wall emittance is analogous to replacing κ_ω by κ_p. This, as discussed before, is not a very realistic assumption. In general, the wall emittance varies with

the wave number and with the surface temperature. However, its variation with the temperature is not as serious as with the wave number. As an example consider polished steel [18], for which between the wave lengths of 0.5 to 9.3 microns, the wall emittance varies from a value of 0.45 to 0.07; whereas, for a range of temperatures between 100-500°F, the average value of the wall emittance varies only from 0.07 to 0.1.

The matter of considering nongray wall emittance becomes crucial in the analyses involving real gas models. This is because at wave numbers, where for a particular gas the important vibration-rotation bands are located, if the values of surface emittance are relatively higher, then the results obtained on the assumption of gray wall emittance will greatly underestimate the influence of radiation. On the other hand, at those wave numbers where wall emittance is higher but there are no absorption-emission bands located, the analyses based on gray wall emittance will overestimate the influence of radiation.

In Fig. 6.22, the spectral distribution of surface emittance for stainless steel of various composition is shown. Using ε_i values from this figure, numerical solutions of Eq. (6.32) were obtained for CO_2 at temperatures of 300, 500 and 1000 K, and the bulk temperature results are illustrated in Figs. 6.23 and 6.24 along with the result for the black tube. One again, it can be seen from Figs. 6.23 and 6.24 that the importance of radiation becomes more pronounced at higher temperatures and for larger tube diameters. Consider, for example, the result for stainless steel tube of type 304 having a diameter of 2.5 cm, the radiative contribution is found to be only about 5.5% at the room temperature, while it is 9.7% at 500 K and 37.4% at 1000 K. These results are very close to the results for gray wall emittance with $\varepsilon_w = 0.1$ (Figs. 5.3 and 6.21). For the same conditions, if the tube surface is considered to be black, then the radiative contributions are found to be 8.4%, 15.8%, and 49.5%, respectively.

The nongray analysis in this section was directed to the specific case of gas CO_2 with three important vibration-rotation bands contributing significantly in the radiative process. The

solutions were obtained only in the large path length limit simply because for CO_2 at room temperature the large path length limit is achieved at a pressure of one atmosphere, and because it is relatively easier to obtain numerical solutions in this limit. For other gases, under the assumption of gray wall emittance, solutions in this limit can be obtained through a combination of results presented in Figs. 5.3 and 6.21. For specific problems involving real gases other than CO_2, the general band absorptance results can be obtained from a numerical solution of Eq. (6.29).

6.3 Correlation Between Parallel Plate and Circular Tube Results

In the present case involving flow through a circular tube, it is not always an easy affair to obtain the numerical solution of the governing equation, Eq. (6.29). Even the simplified form of this equation, in the large path length limit, requires a considerable amount of numerical computation before actual results are obtained.

As an alternate approach it was found that, for black bounding surfaces and for surfaces with higher wall emittance, a correlation, established from the consideration of gray results, serves a very useful purpose in extending all nongray results for the parallel plate geometry to the present case of flow through a circular tube. A discussion pertaining to such a correlation is presented in this section.

Consider flow of a gray gas through black bounding surfaces and let $\tau_o = \kappa_P D$ denote the gray gas optical thickness for the circular tube. Note the difference between this definition of τ_o and that given by Eq. (6.34). In order to be consistent with the present definition, let

$$\Theta_{bT} = \theta_{bT}/2 = (T_b - T_1)/(q_w D/k) \tag{6.39}$$

The notations for the case of parallel plate geometry are taken to be the same as defined in Sec. 6.1.3.

From the gray results presented earlier, it follows that, in the transparent limit

$$\theta_{bP} = -17/70 \ , \ \Theta_{bT} = -11/48$$

while in the optically thick limit, θ_{bP} is given by Eq. (6.21), and Θ_{bT} can be obtained from Eq. (6.38) by replacing the constant 11/24 by 11/48. In both limits the following relation between θ_{bP} and Θ_{bT} is found to exist

$$\Theta_{bT} = 0.943 \, \theta_{bP} \tag{6.40}$$

The reason that this applies to both $\tau_o = 0$ and $\tau_o >> 1$ is because in either case energy transport within the gas is a diffusion process. For $\tau_o = 0$, this process is solely conduction, while for $\tau_o >> 1$ it is combined conduction and optically thick radiation.

It now remains to extend Eq. (6.40) to include all values of τ_o. From a comparison of gray results (Figs. 6.5 and 6.20), it was found that the circular tube solution could be closely approximated by the expression

$$\Theta_{bT}(\tau_o) = 0.943 \, \theta_{bP}(2\tau_o/3) \tag{6.41}$$

In other words, the circular tube is equivalent to a parallel plate geometry having an optical thickness which is two-thirds that of the tube. The tube results obtained by using this correlation are illustrated in Fig. 6.20 by the broken lines.

For infrared radiation in nongray gases, the spectral thickness can cover a large range of values for one given system. Correspondingly, the obvious utility of Eq. (6.41) for all values of optical thickness suggests that this same procedure should apply to nongray gases. As an example, to extend the parallel plate results shown in Figs. 6.7 through 6.11 to the circular tube geometry, the ordinate would be replaced by $\Theta_{bT}/0.943$, while in the abscissa L would be replaced by 2D/3. For Fig. 6.3, this amounts to redefining M for a cylindrical geometry as $M = 2HD/3k$.

Using the correlation of Eq. (6.41) and the parallel plate results of Fig. 6.3, solutions for the circular tube were obtained and are illustrated in Fig. 6.21 by the dashed curves. It is noticed that for a gray wall emittance higher than 0.5, there is no difference between the actual tube result and the result obtained by using the correlation. For values of ε_w below 0.5, however, the correlation does not seem to be satisfactory. The reason for this could be that the present correlation is established on the basis of results obtained for black bounding surfaces. Furthermore, as discussed in Sec. 6.2.3, in the case of a circular tube the possibilities of multiple reflections are higher than those for the parallel plate geometry.

In conclusion it should be emphasized that the correlation given by Eq. (6.41) can be utilized, along with the nongray solutions of the parallel plate geometry, to obtain qualitative results for most physical systems involving circular tubes.

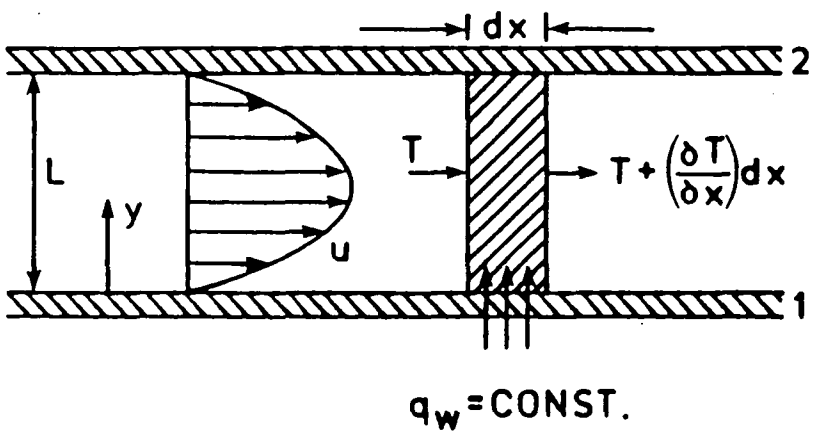

Figure 6.1 Physical model for flow of radiating gases between parallel plates with constant wall heat flux

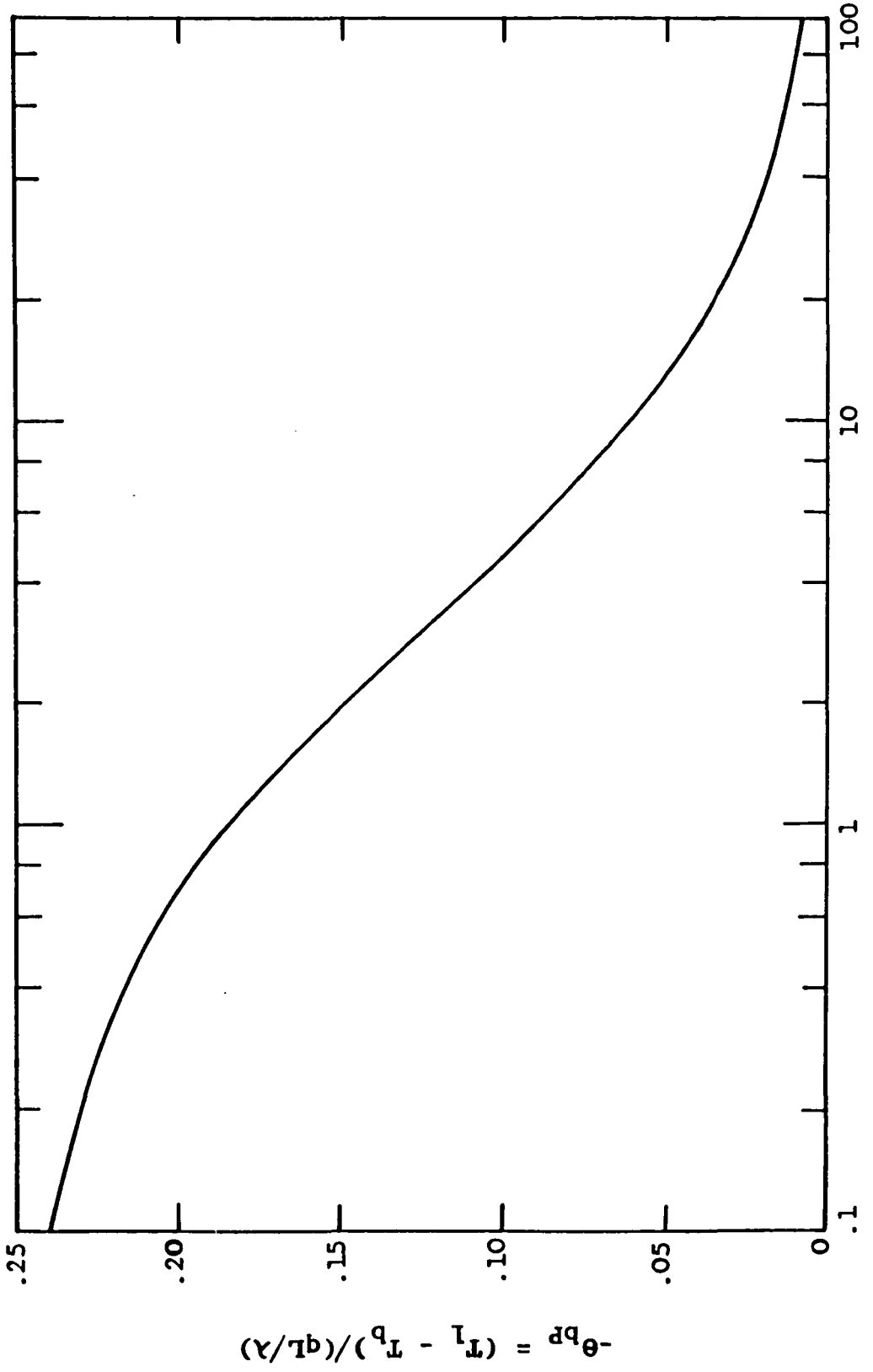

Figure 6.2 Bulk temperature results in the optically thin limit

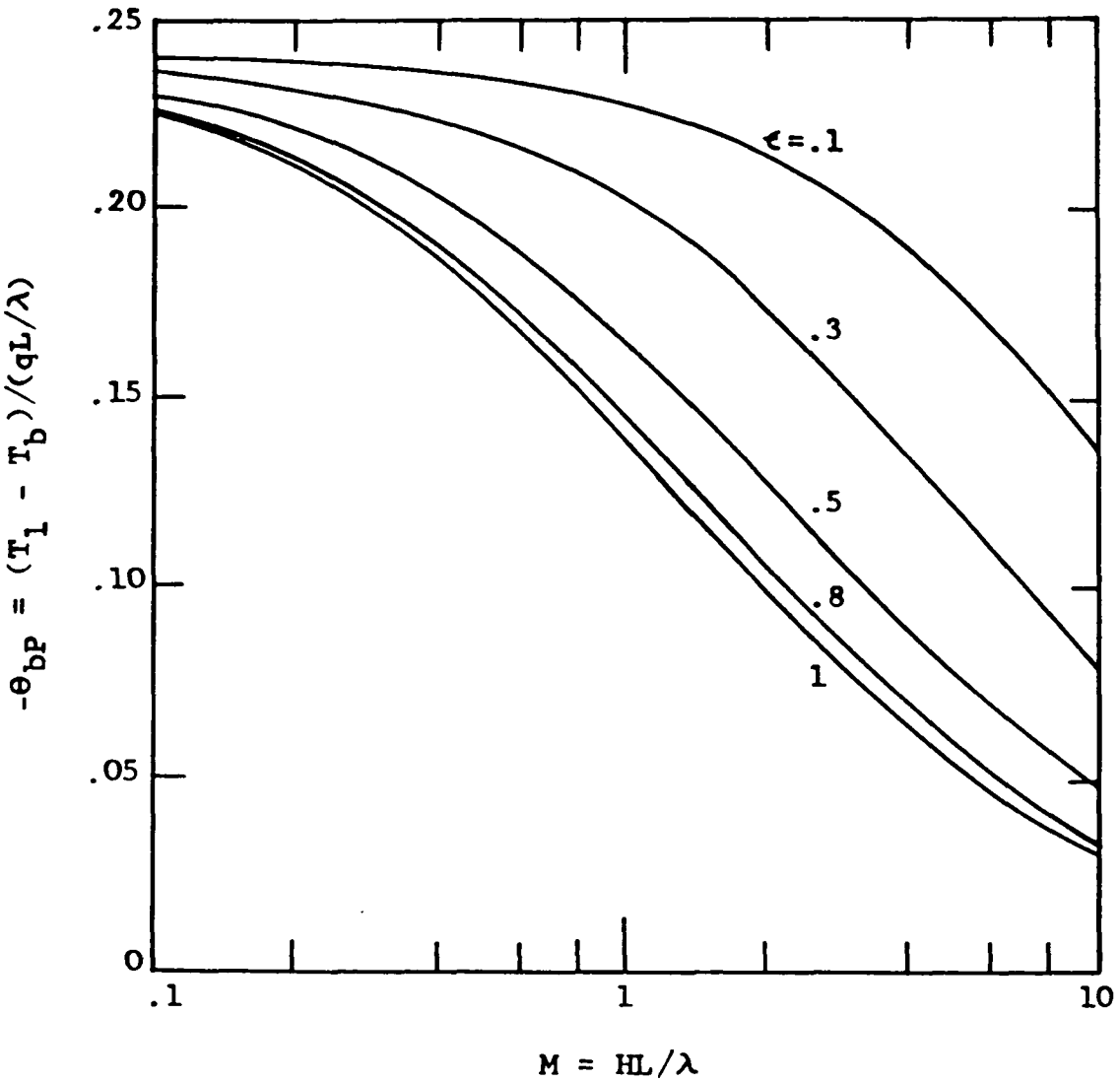

Figure 6.3 Bulk temperature results for the large path length limit

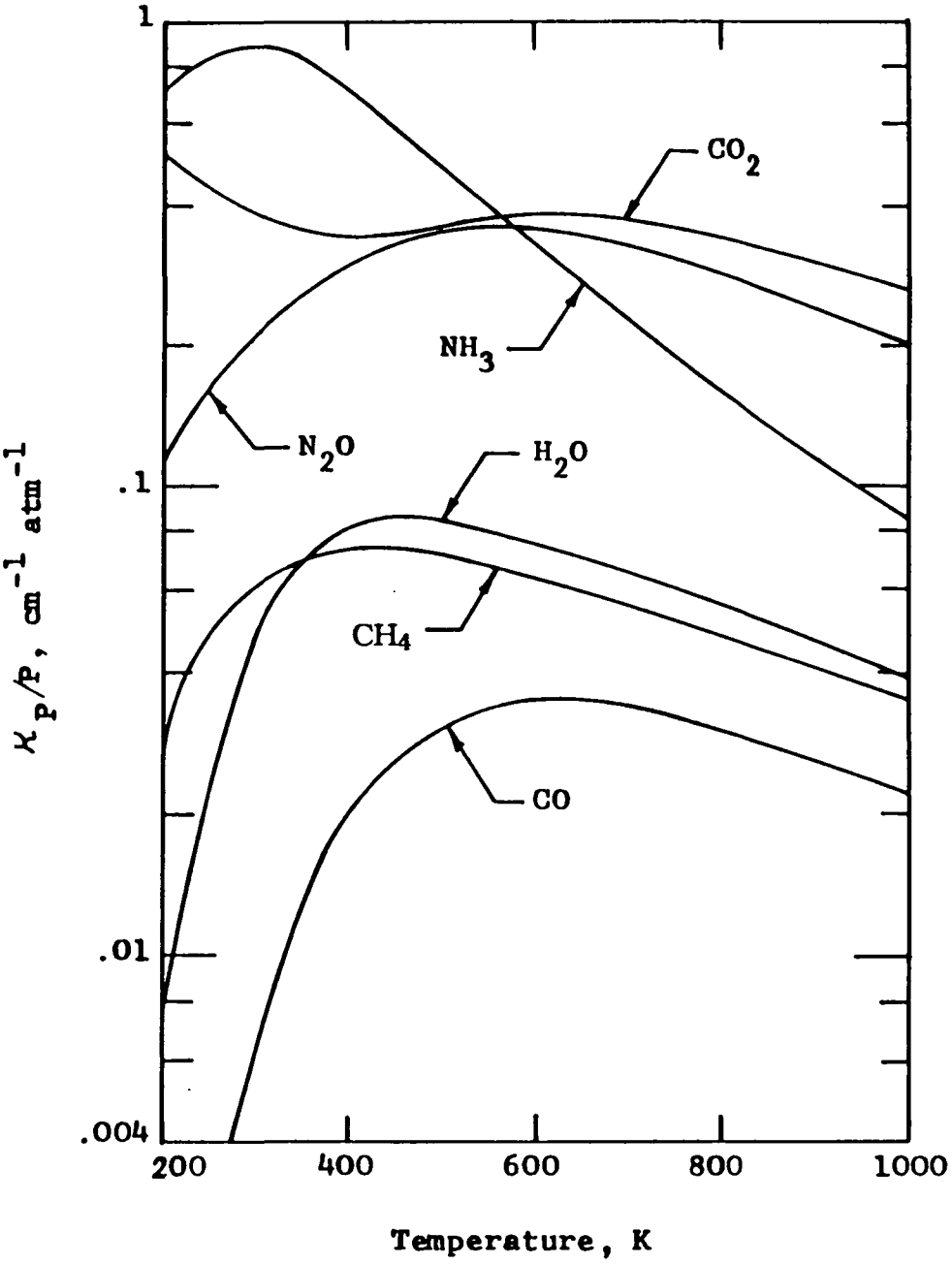

Figure 6.4 Planck mean absorption coefficients

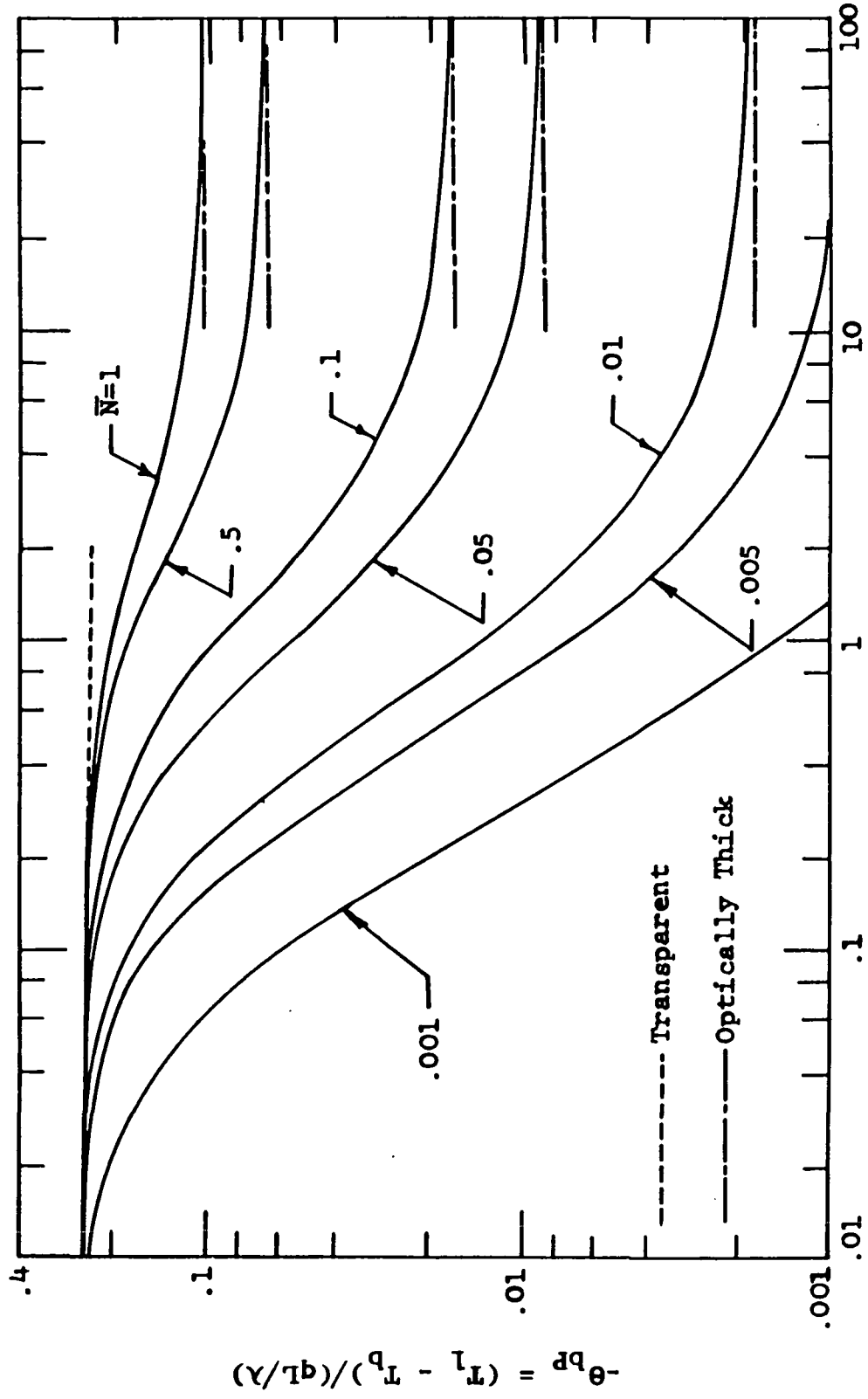

Figure 6.5 Gray results for flow between parallel plates, $\varepsilon_1 = 1$

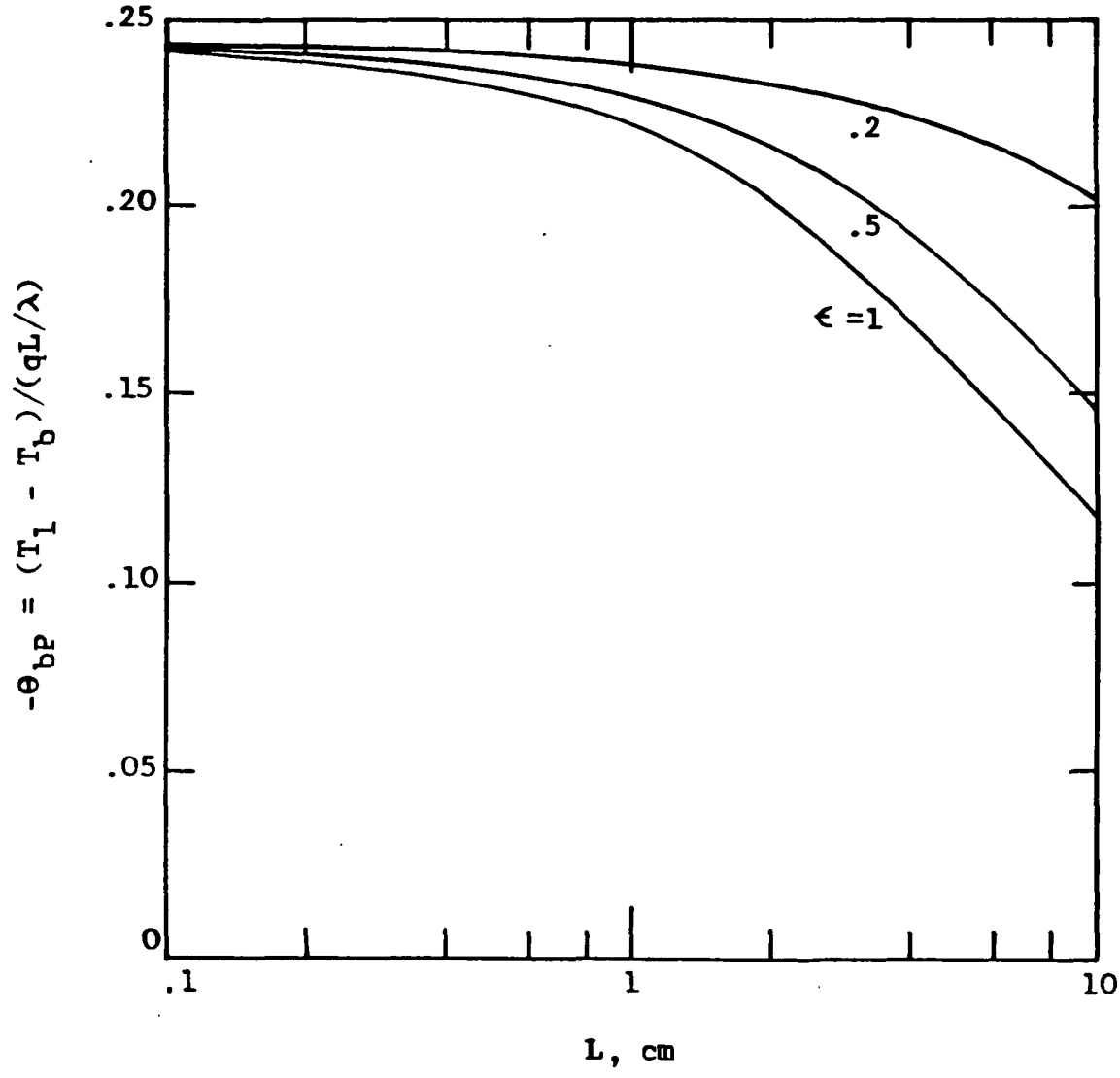

Figure 6.6 Bulk temperature results for CO_2 (three bands) with T_1 = 500 K and P = 1 atm

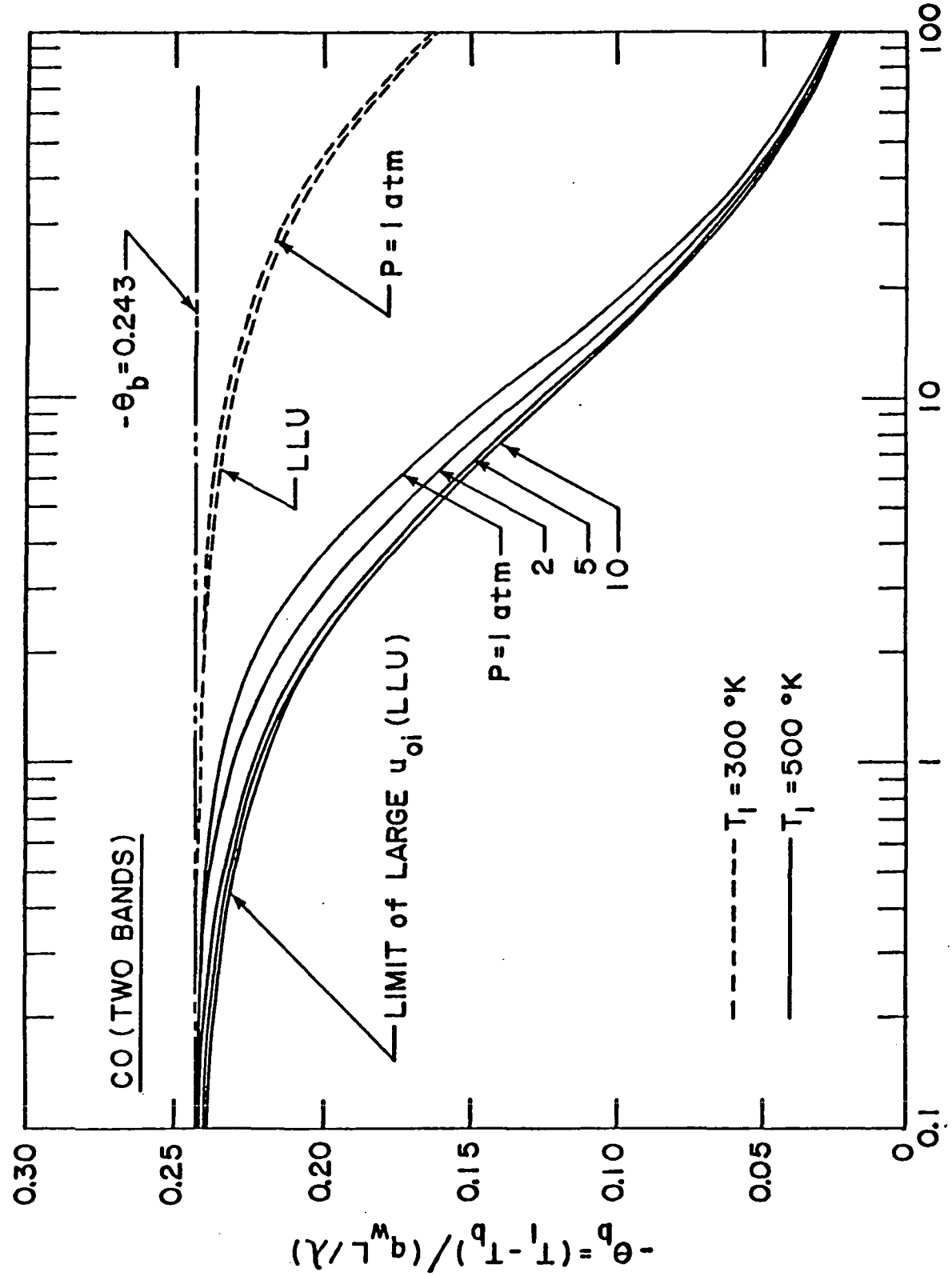

Figure 6.7a Variation of bulk temperature with plate spacing for CO; T_1 = 300 K and 500 K

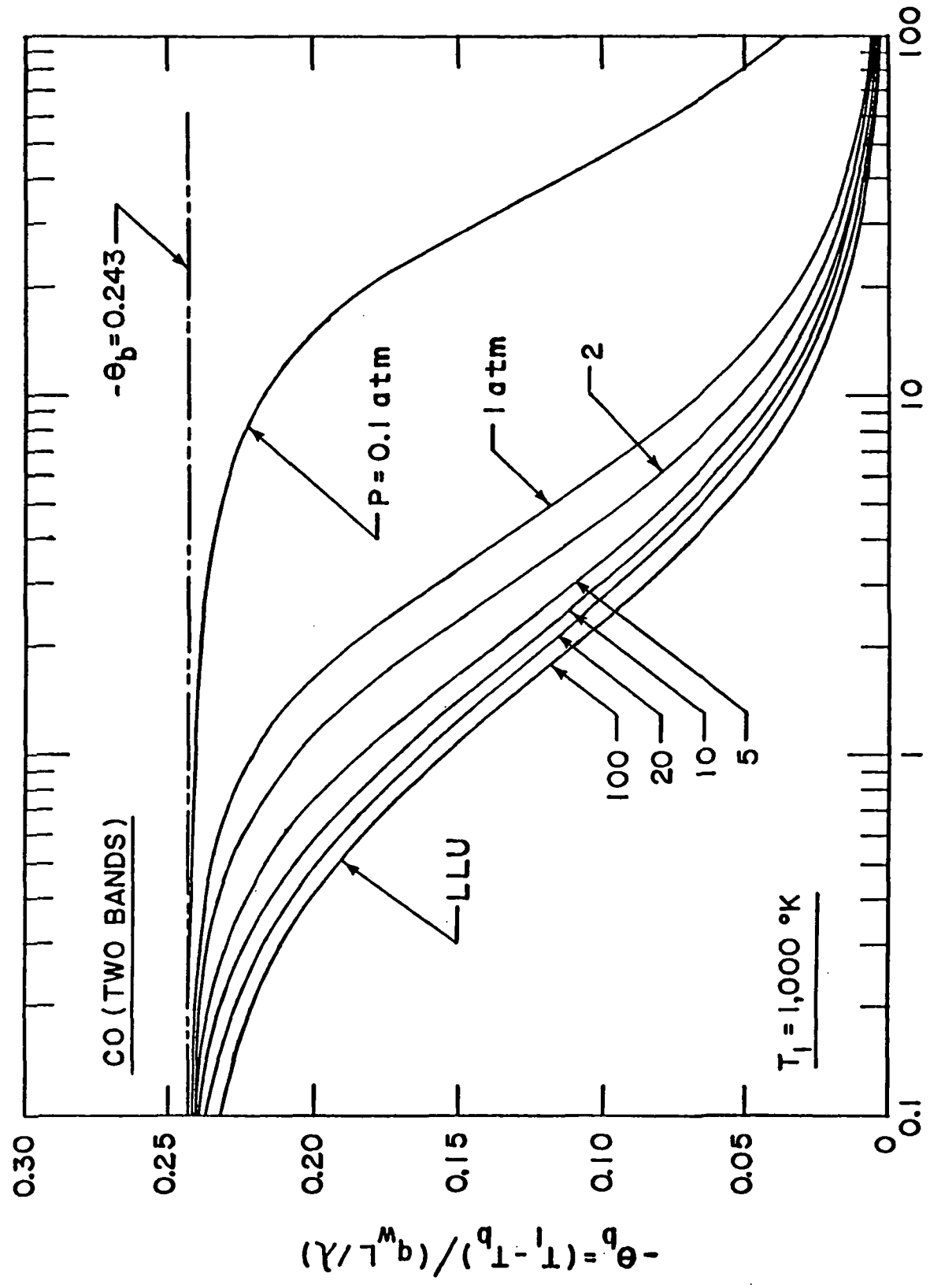

Figure 6.7b Variation of bulk temperature with plate spacing for CO; T_1 = 1,000 K

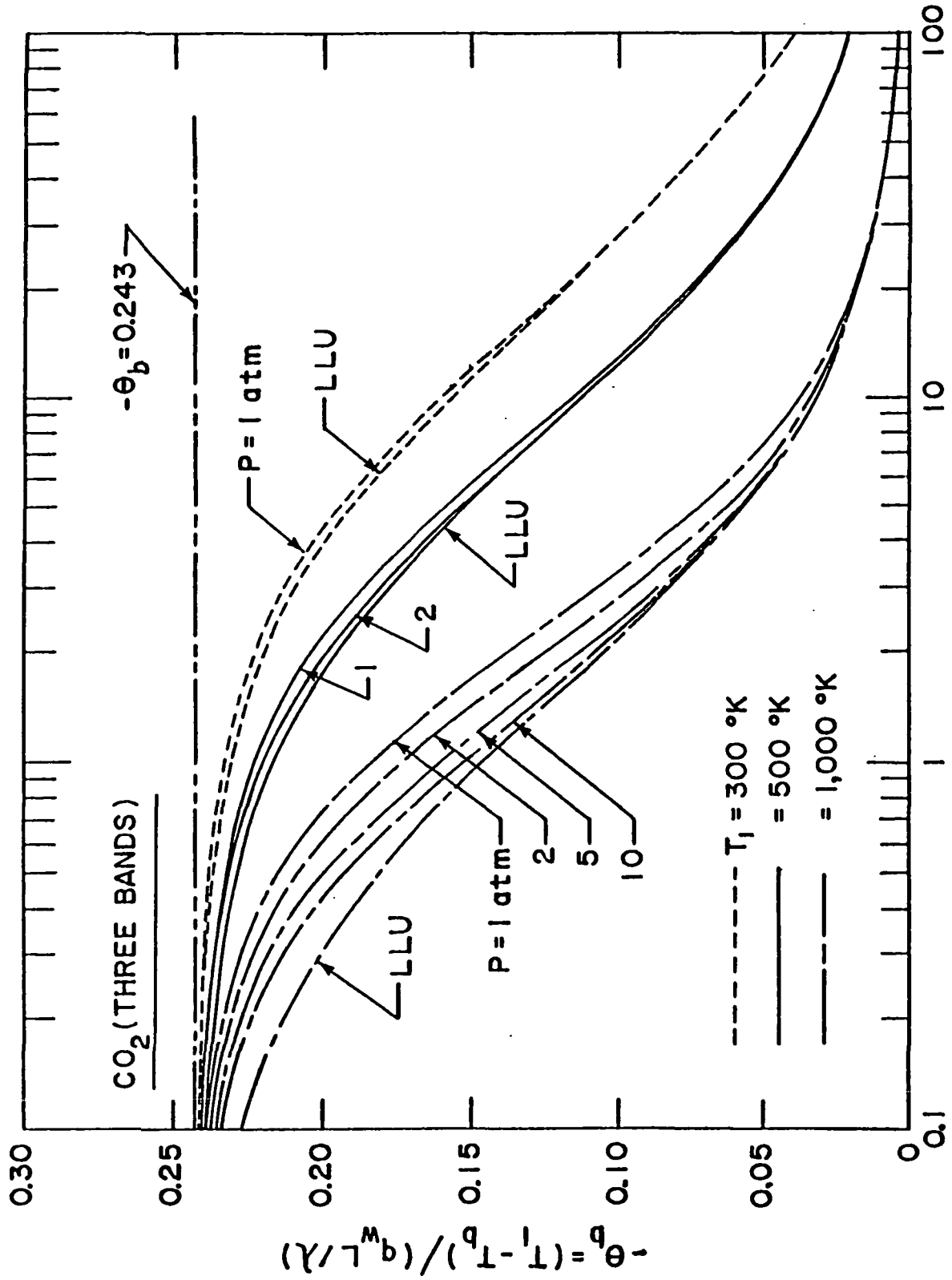

Figure 6.8 Variation of bulk temperature with plate spacing for CO_2; T_1 = 300 K, 500 K and 1,000 K

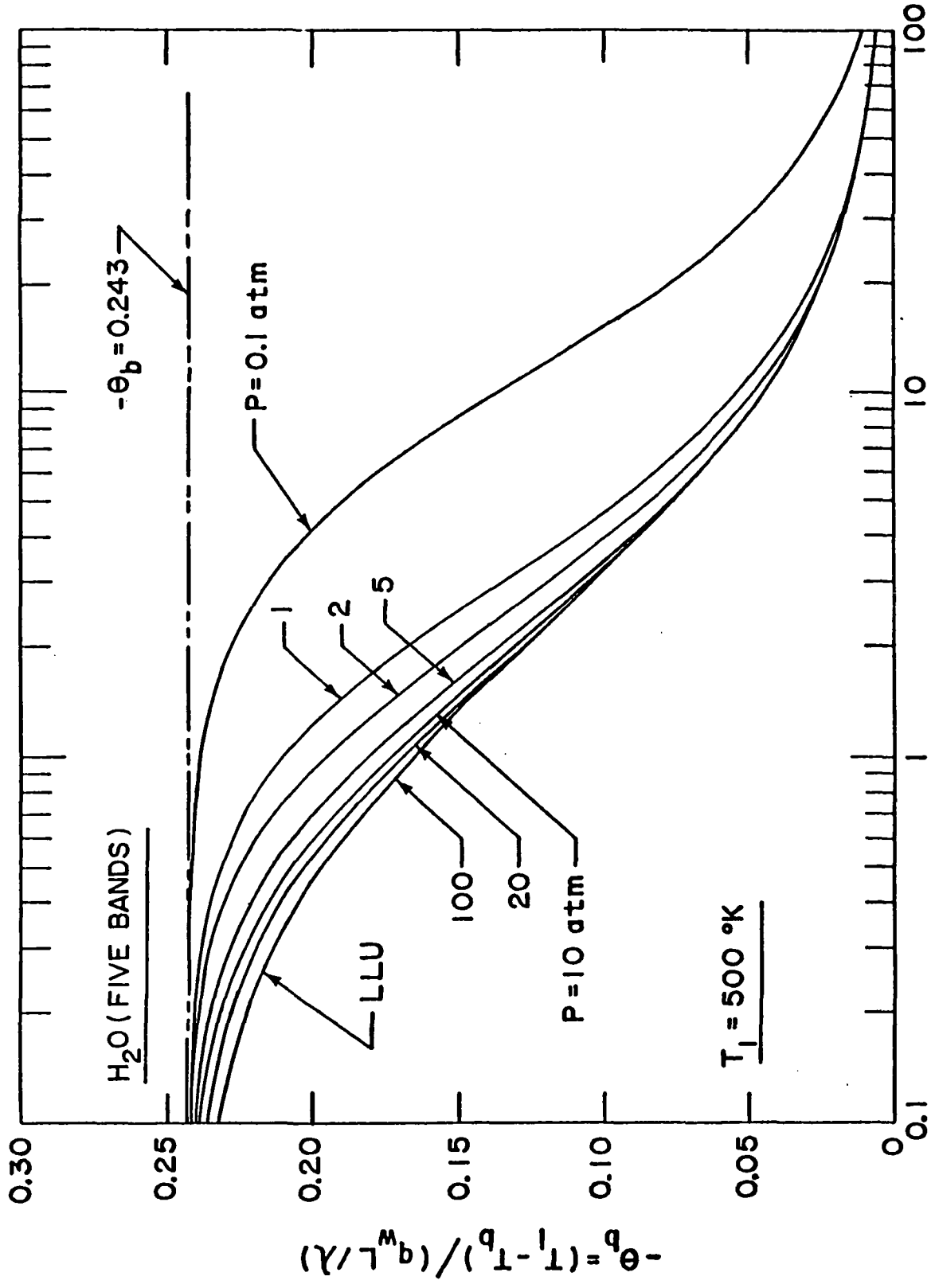

Figure 6.9a Variation of bulk temperature with plate spacing for H_2O; T_1 = 500 K

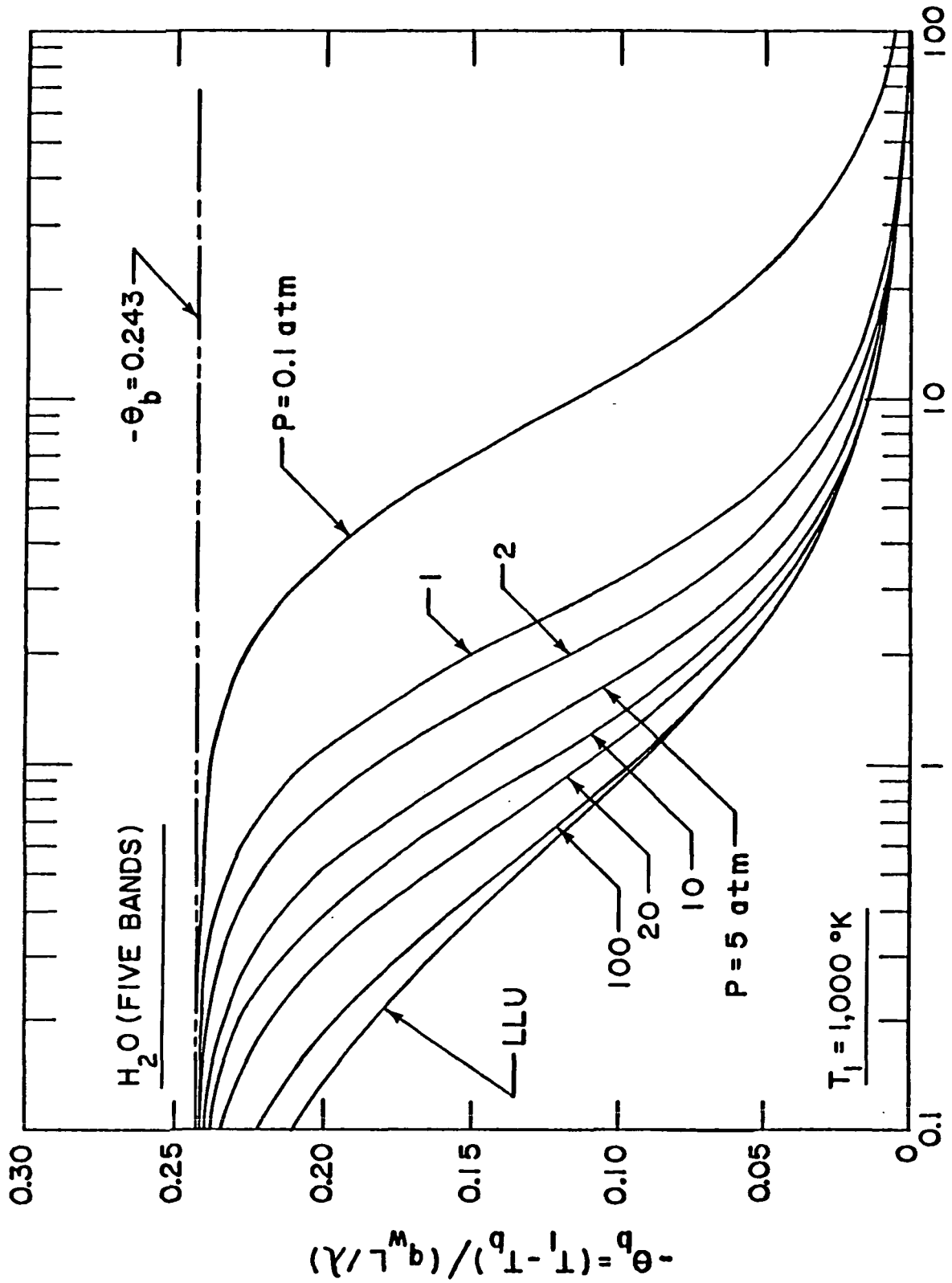

Figure 6.9b Variation of bulk temperature with plate spacing for H_2O; T_1 = 1,000 K

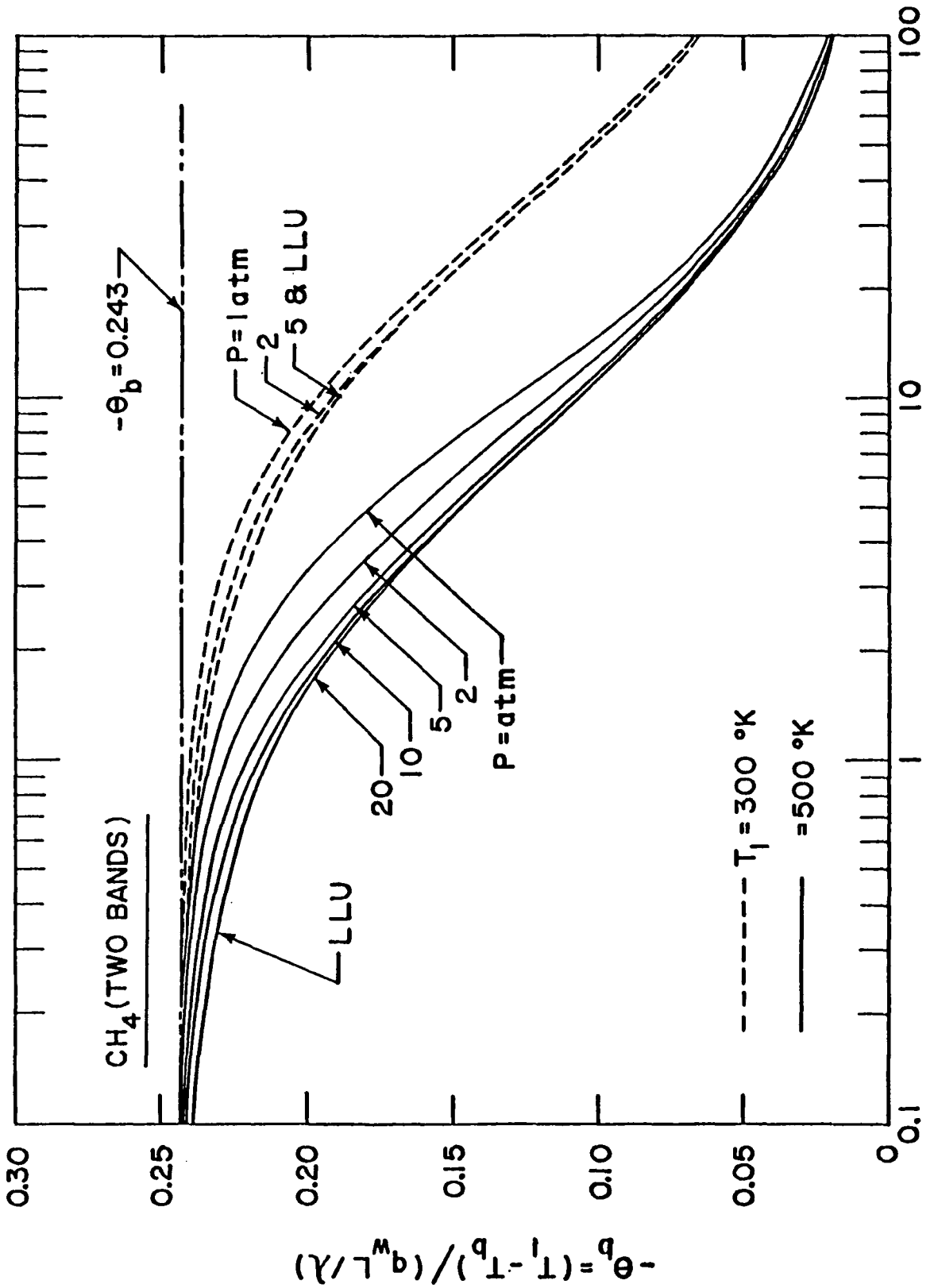

Figure 6.10a Variation of bulk temperature with plate spacing for CH_4; T_1 = 300 K and 500 K

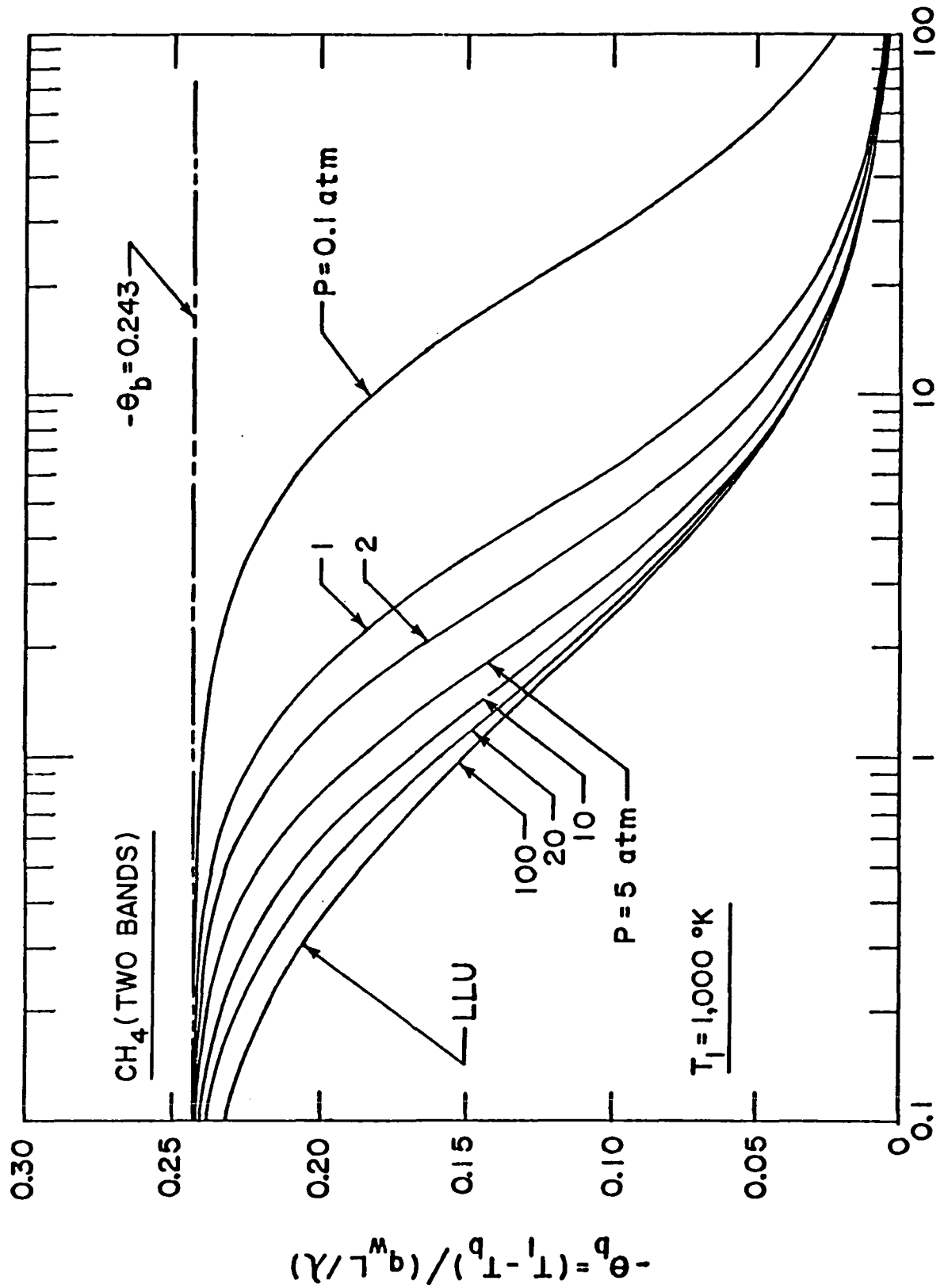

Figure 6.10b Variation of bulk temperature with plate spacing for CH_4; T_1 = 1,000 K

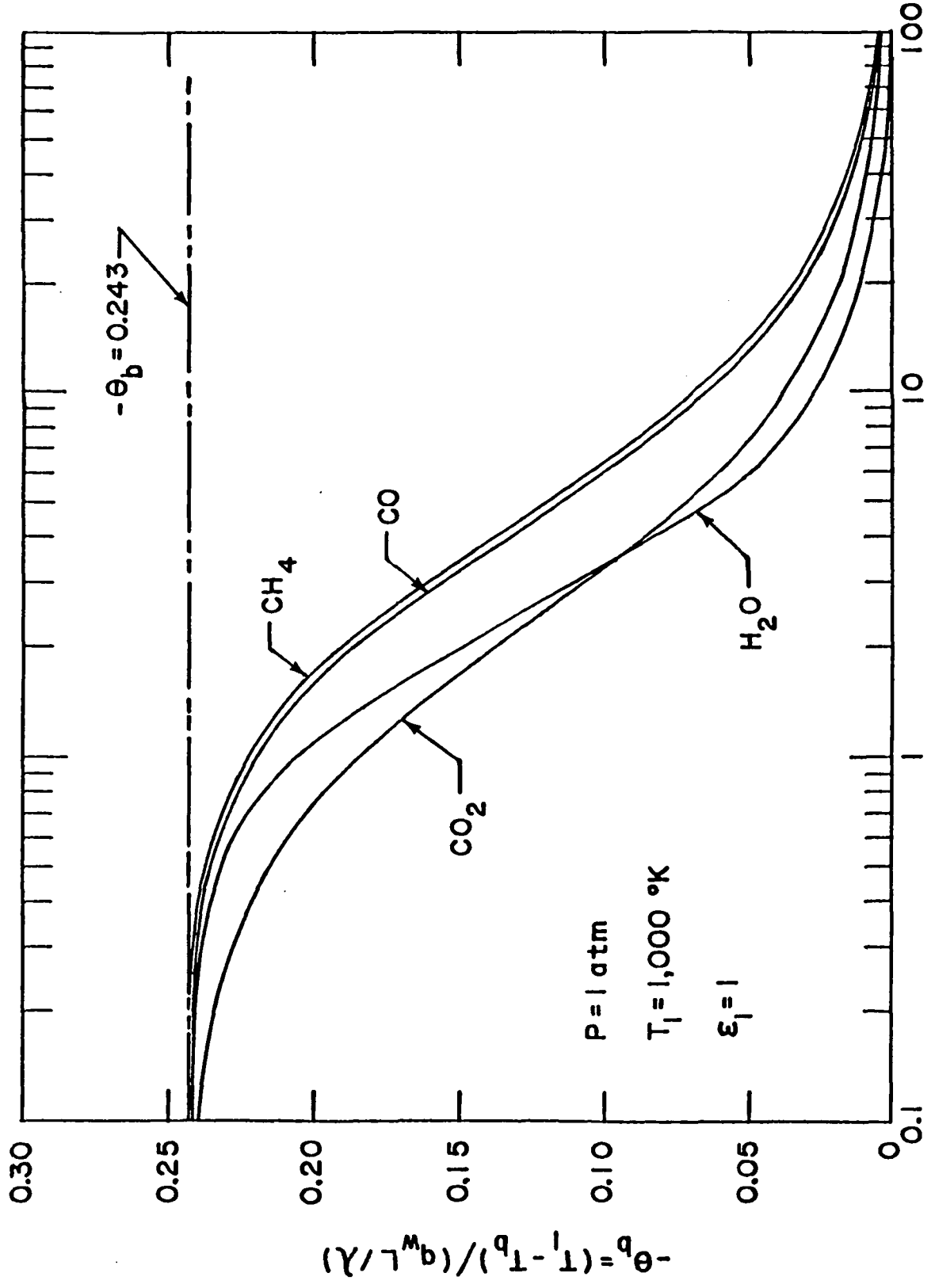

Figure 6.11 Comparison of bulk temperature results for parallel plates; P = 1 atm and T_1 = 1,000 K

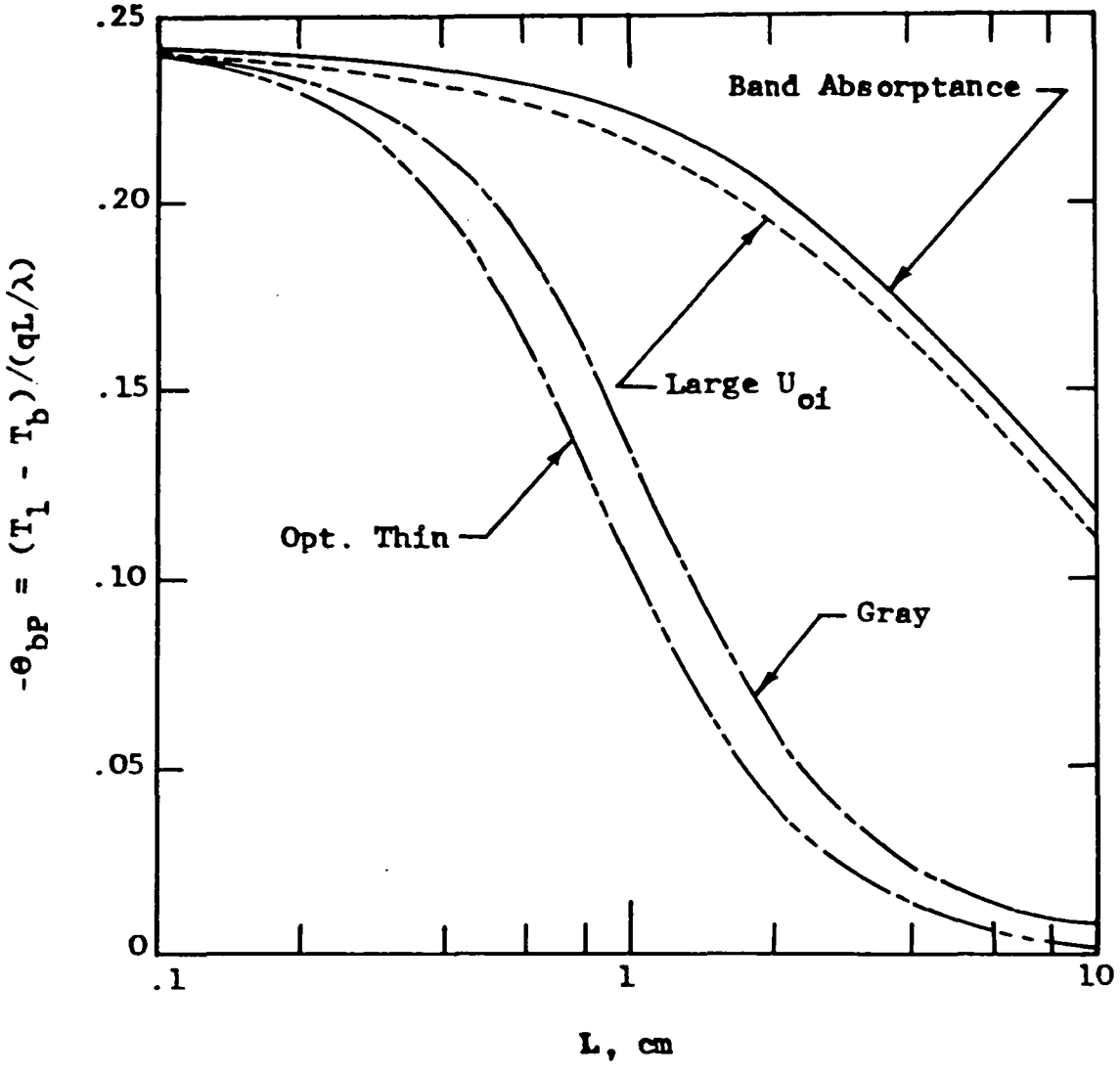

Figure 6.12 Comparison of bulk temperature results for CO_2 (three bands) with P = 1 atm and T_1 = 500 K

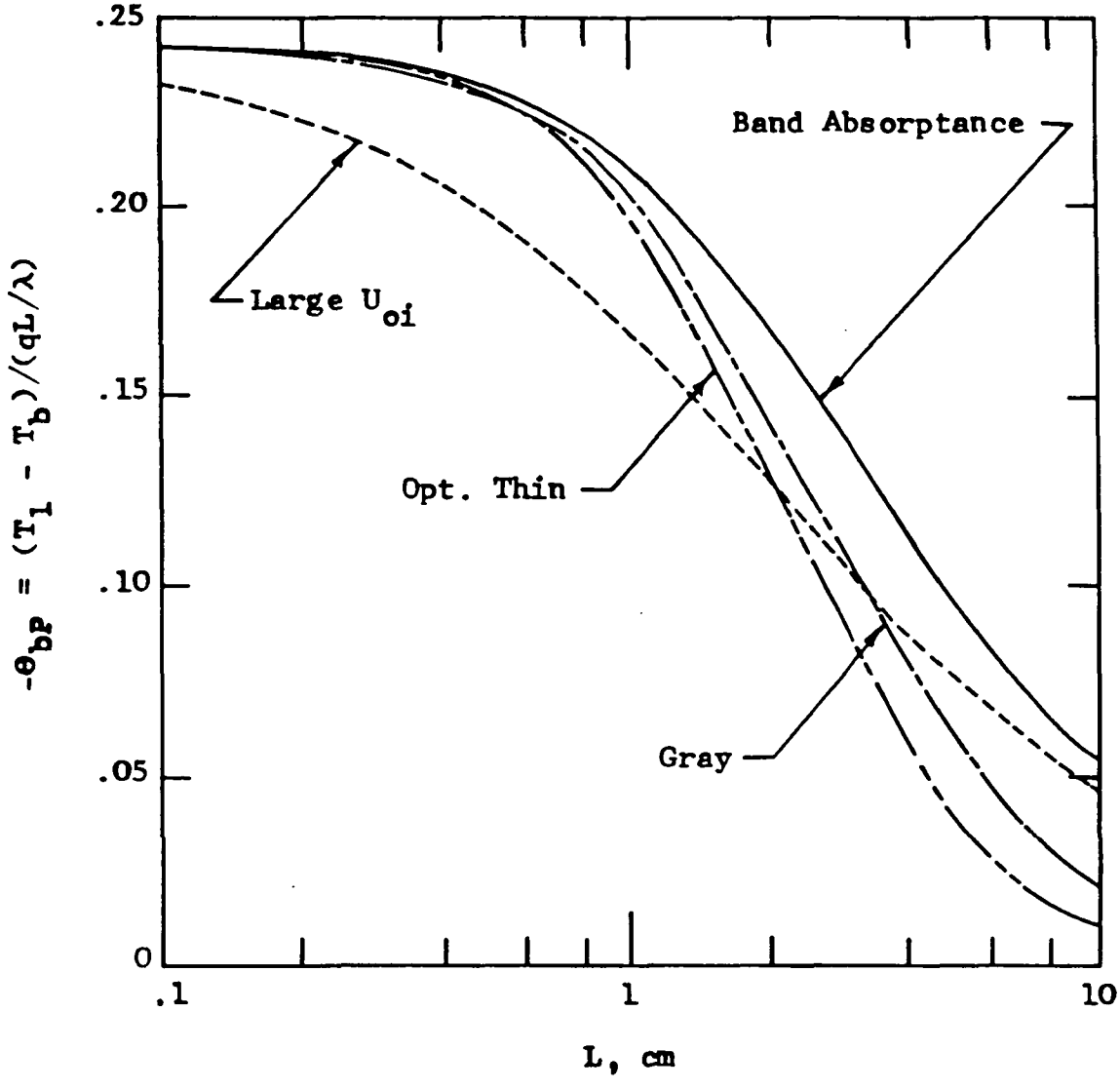

Figure 6.13 Comparison of bulk temperature results for H_2O (five bands) with P = 1 atm and T_1 = 500 K

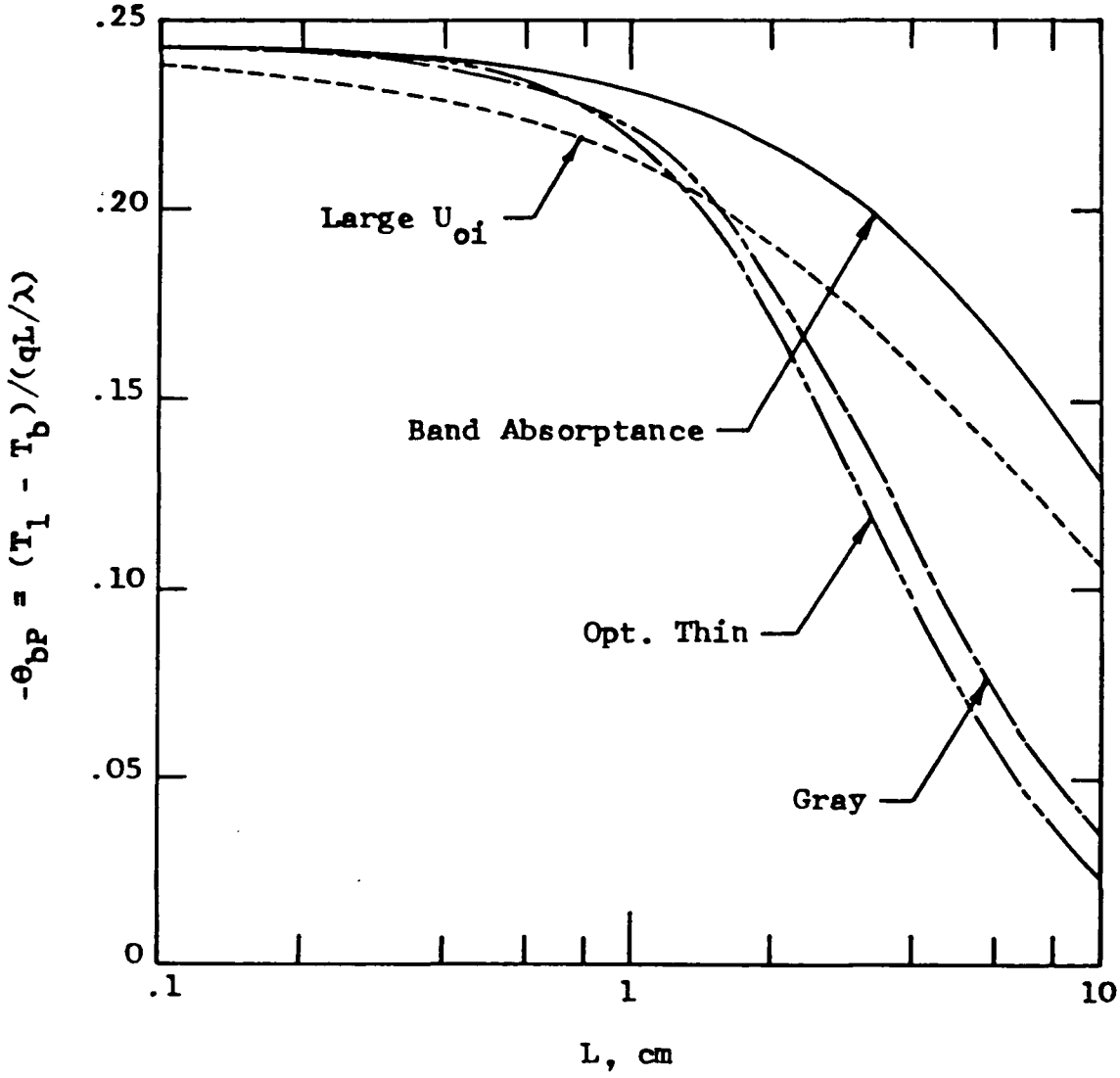

Figure 6.14 Comparison of bulk temperature results for CH_4 (two bands) with P = 1 atm and T_1 = 500 K

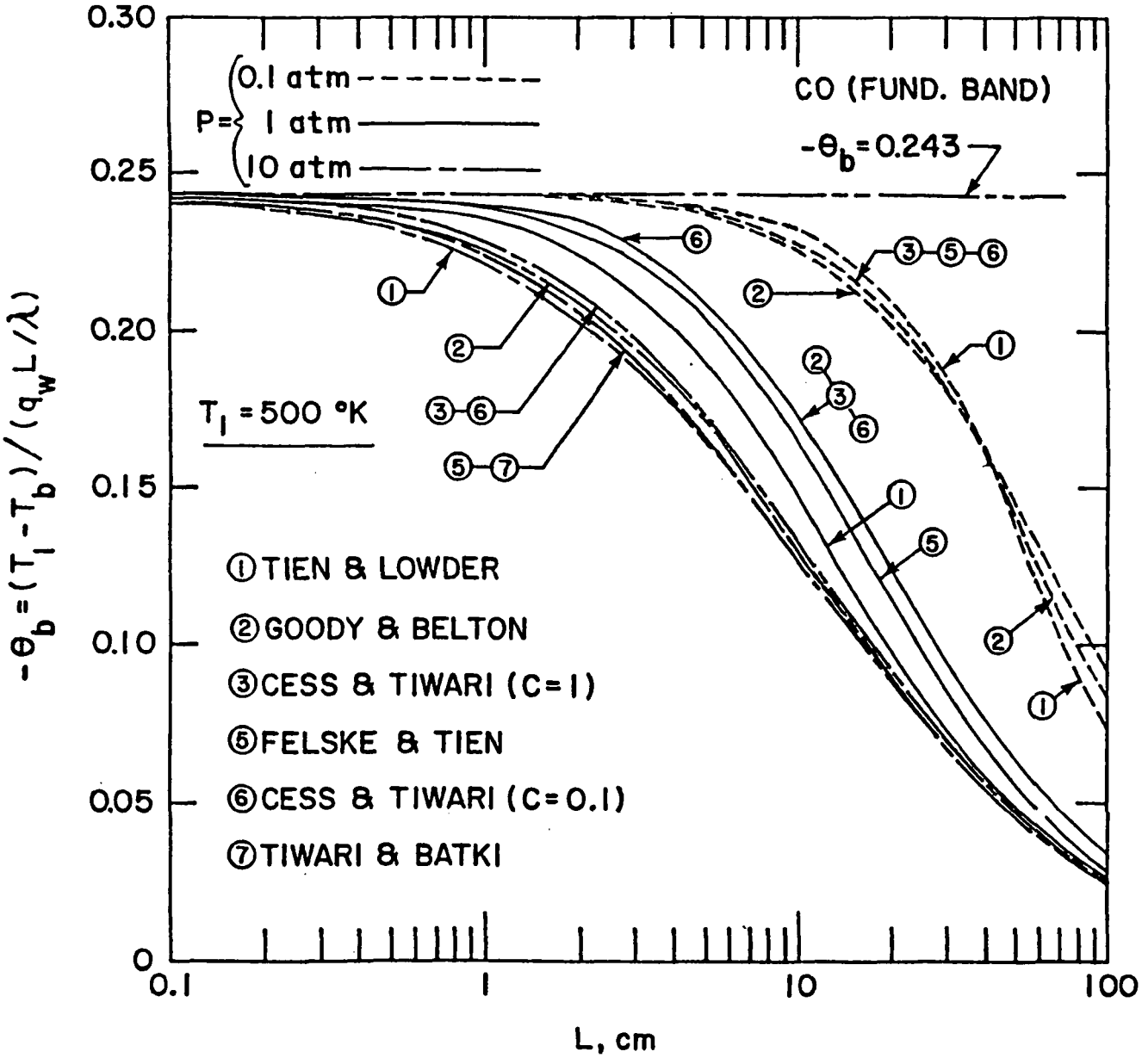

Figure 6.15 Bulk temperature results for CO (fundamental band) with T_1 = 500 K

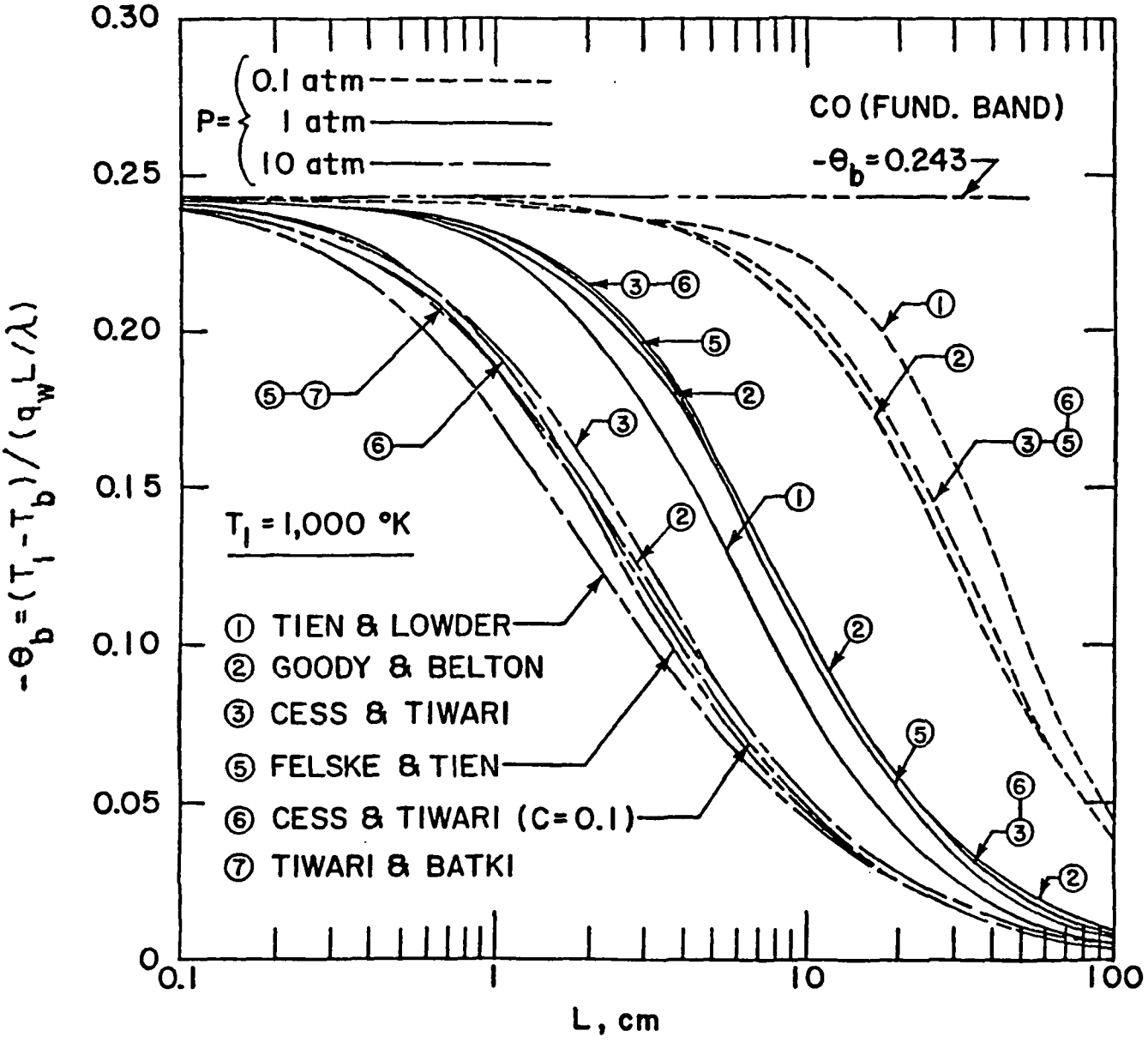

Figure 6.16 Bulk temperature results for CO (fundamental band) with T_1 = 1,000 K

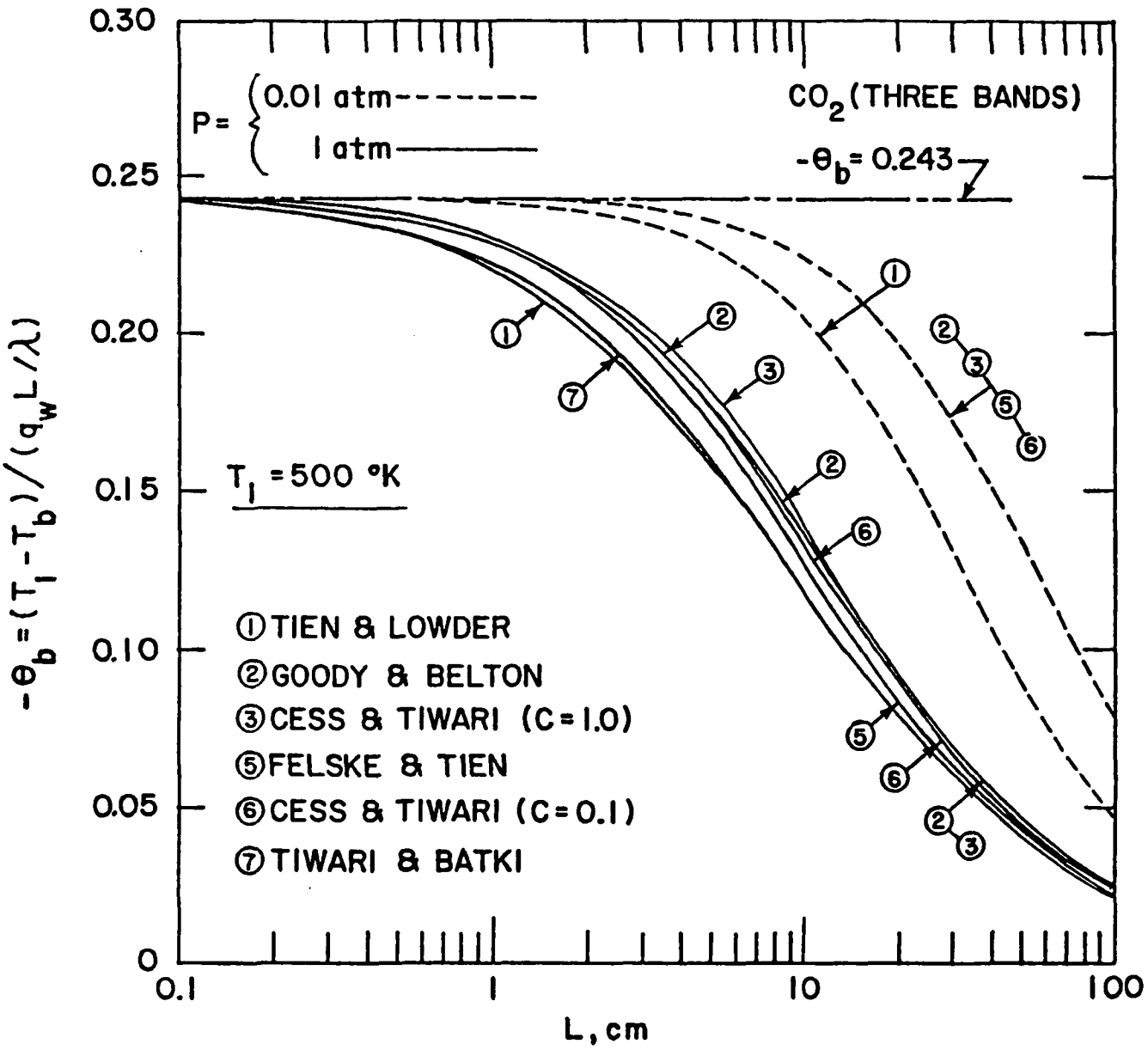

Figure 6.17a Bulk temperature results for CO_2 (three bands) with T_1 = 500 K; P = 0.01 atm and 1 atm

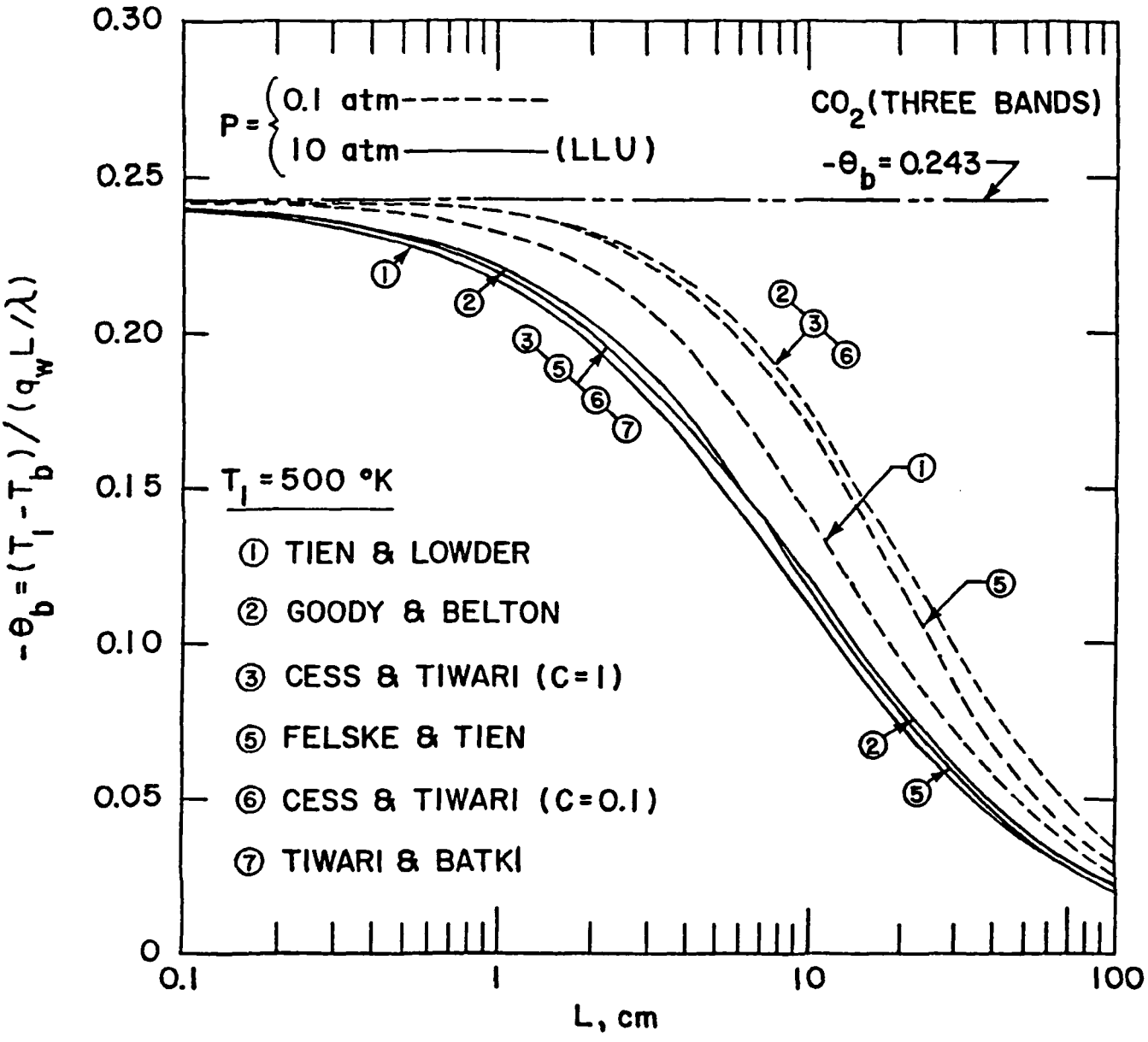

Figure 6.17b Bulk temperature results for CO_2 (three bands) with T_1 = 500 K; P = 0.1 atm and 10 atm

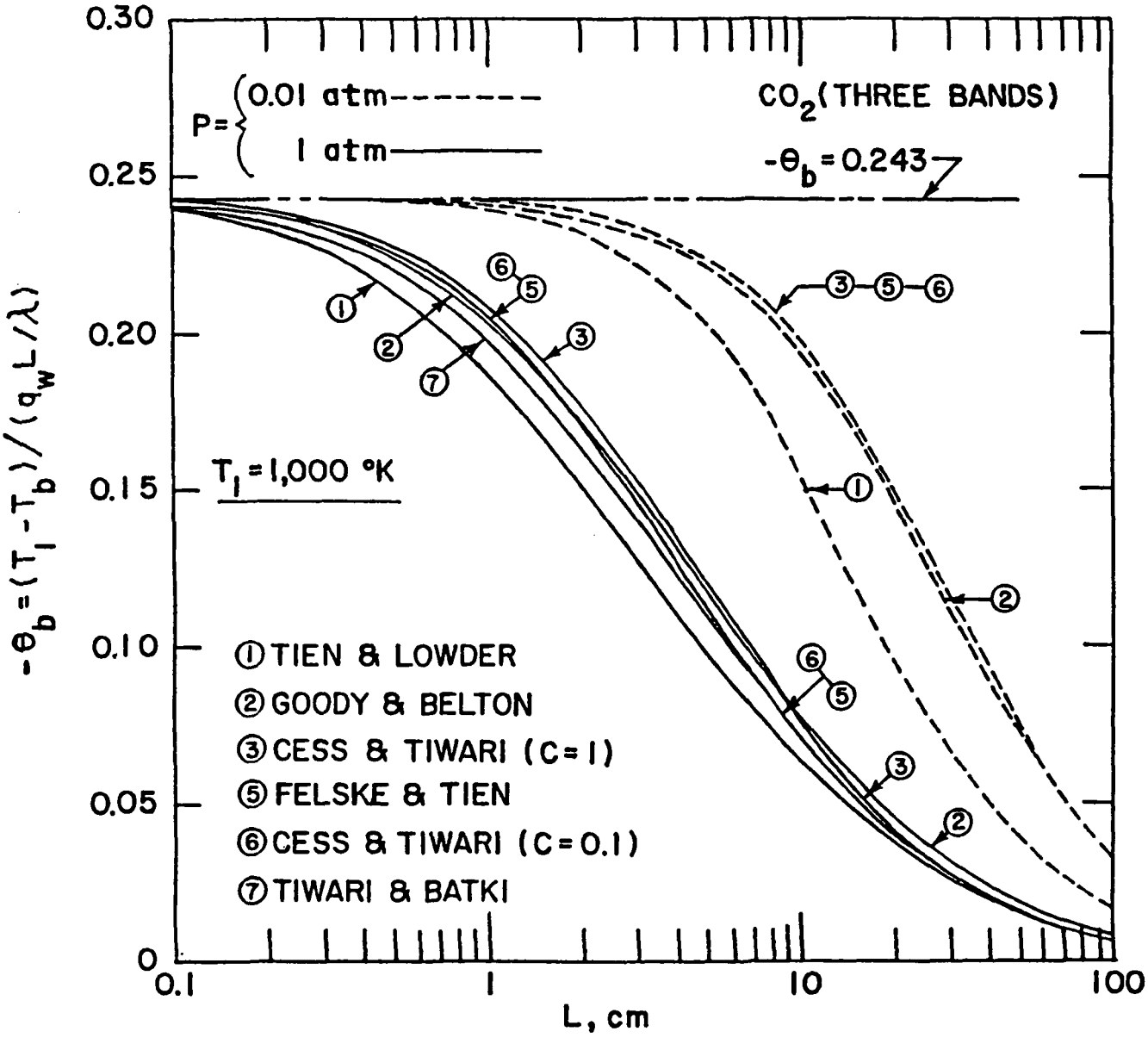

Figure 6.18a Bulk temperature results for CO_2 (three bands) with T_1 = 1,000 K; P = 0.01 atm and 1 atm

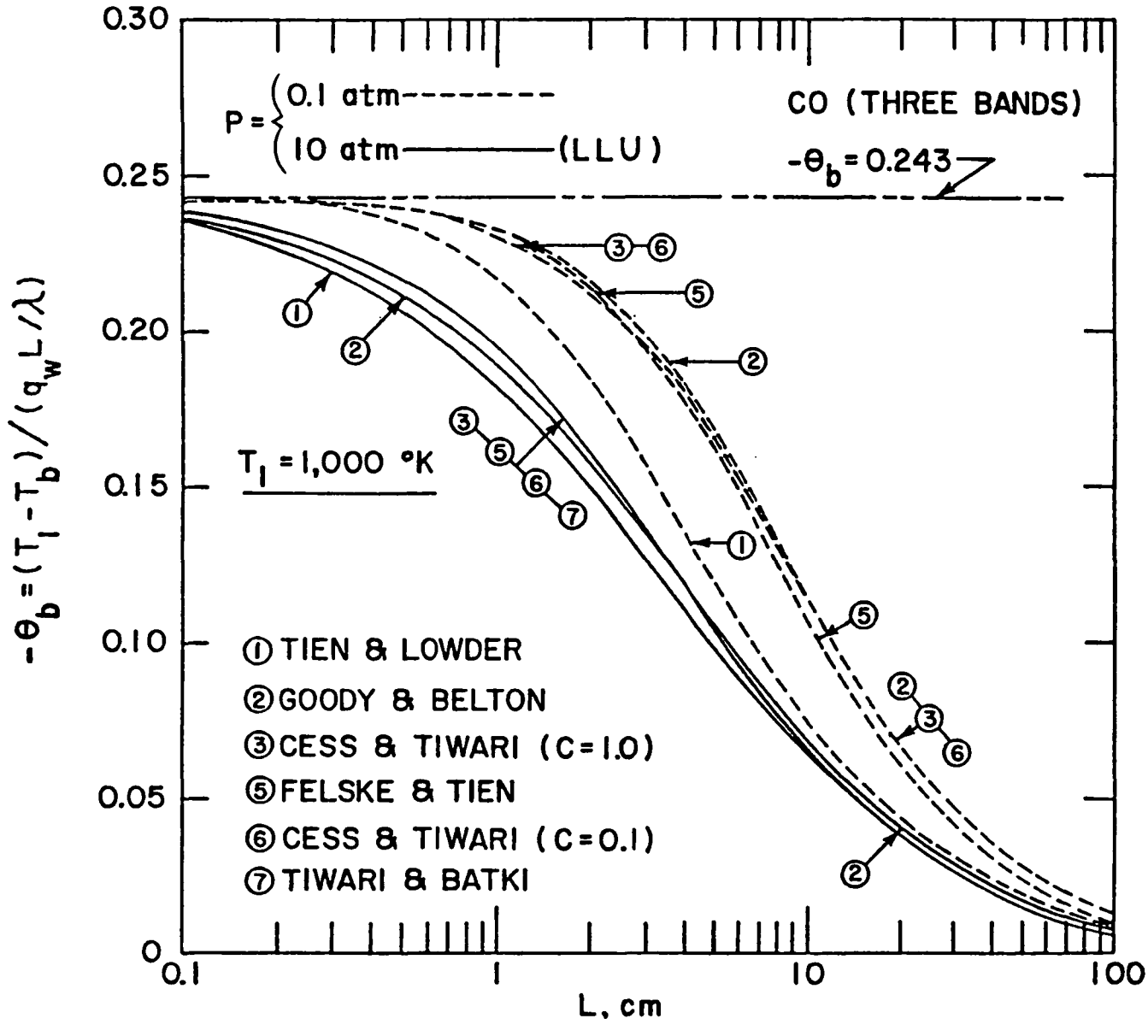

Figure 6.18b Bulk temperature results for CO_2 (three bands) with T_1 = 1,000 K; P = 0.1 atm and 10 atm

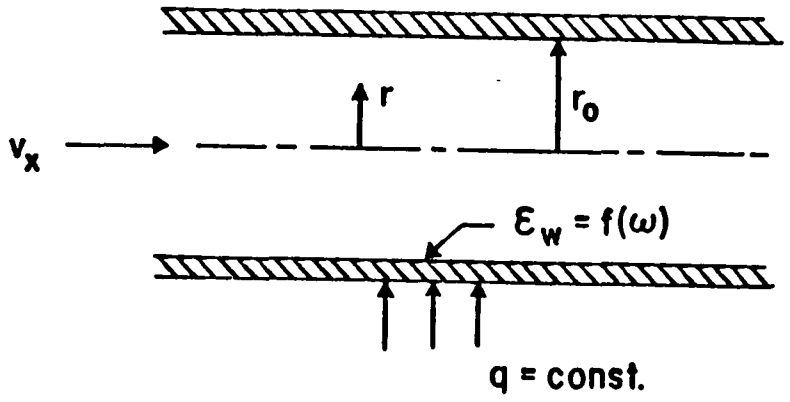

Figure 6.19 Physical model for flow of radiating gases in a circular tube with constant wall heat flux

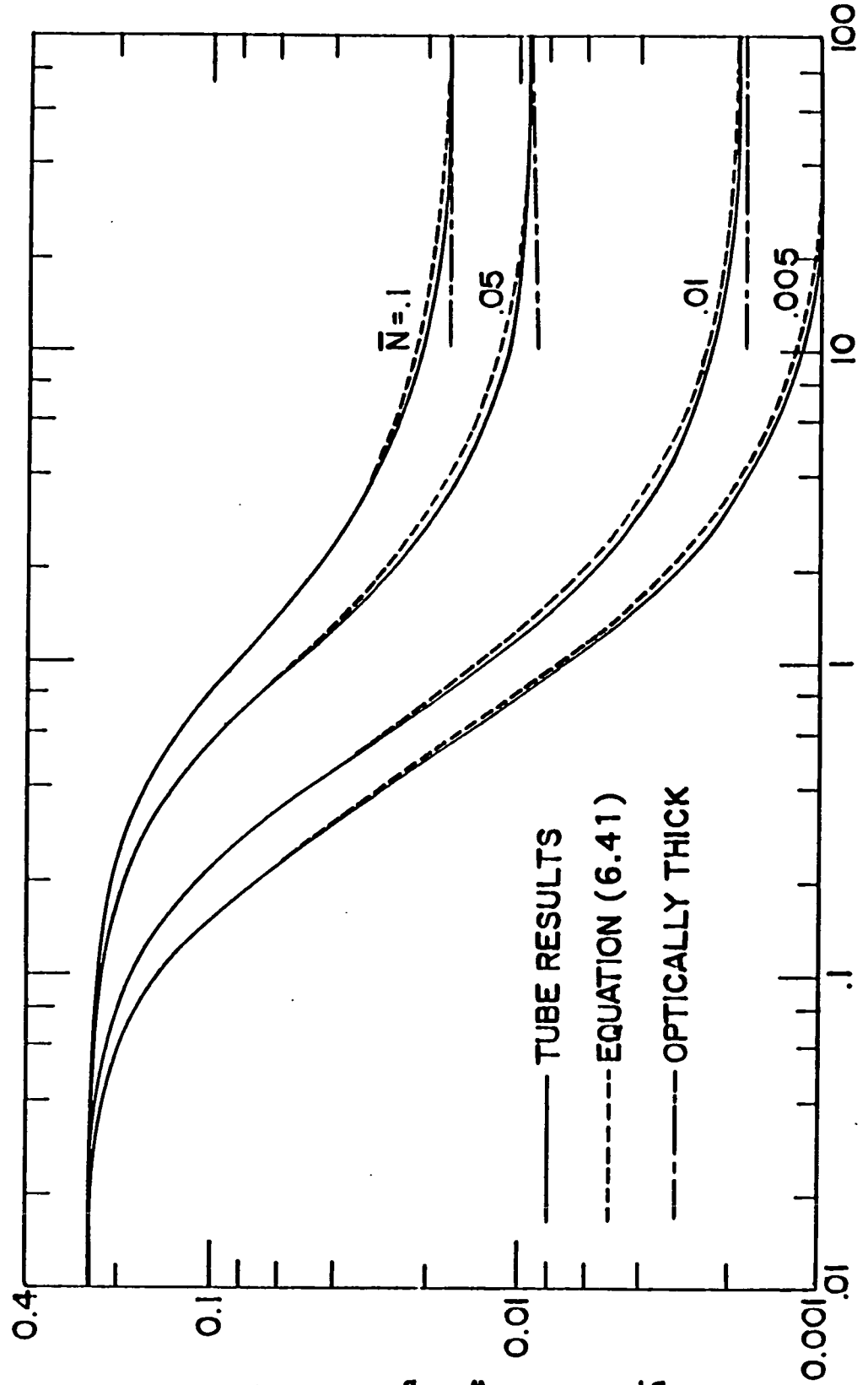

Figure 6.20 Comparison of gray results for flow through a circular tube

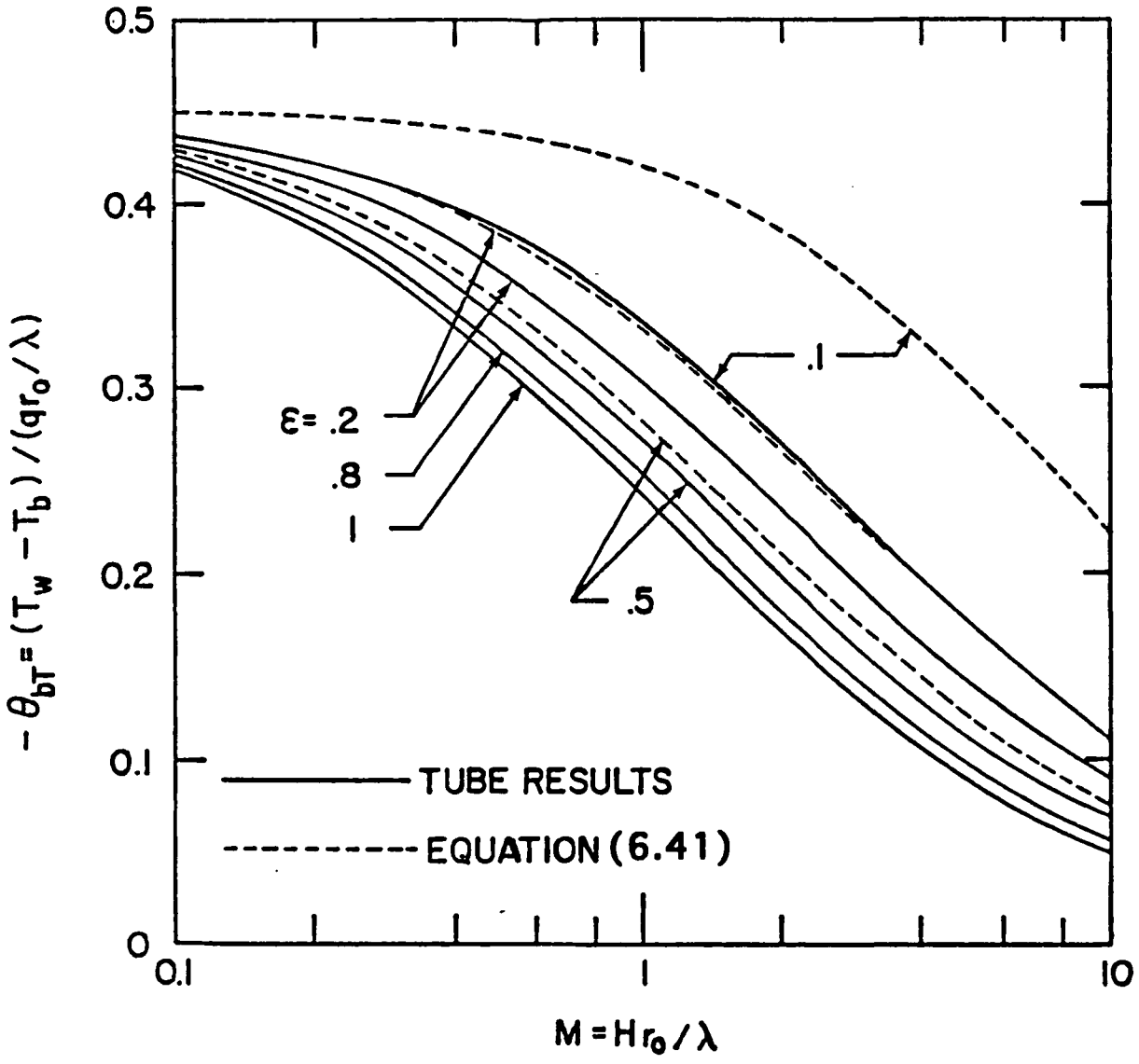

Figure 6.21 Nongray results for flow through a circular tube

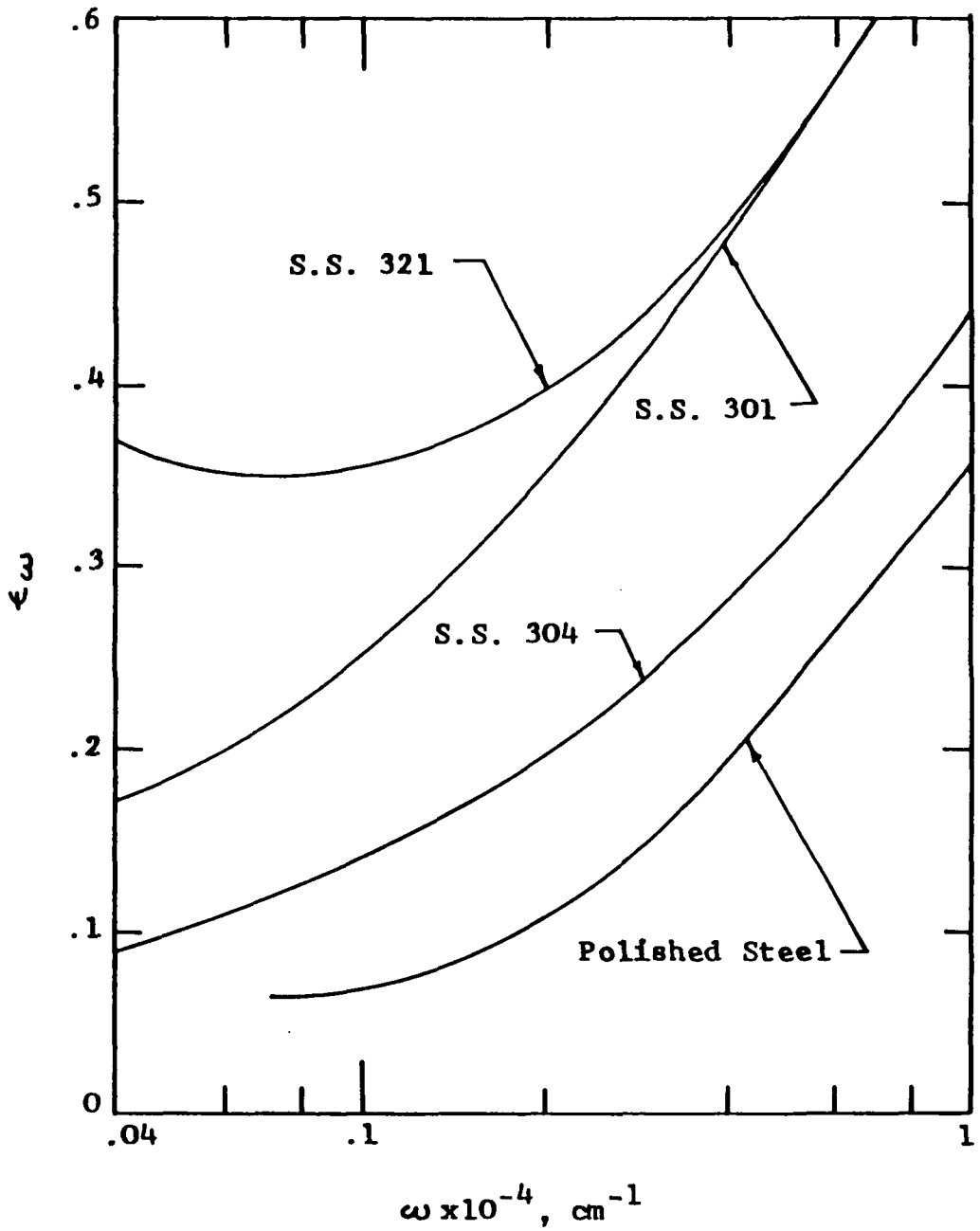

Figure 6.22 Spectral distribution of surface emittance

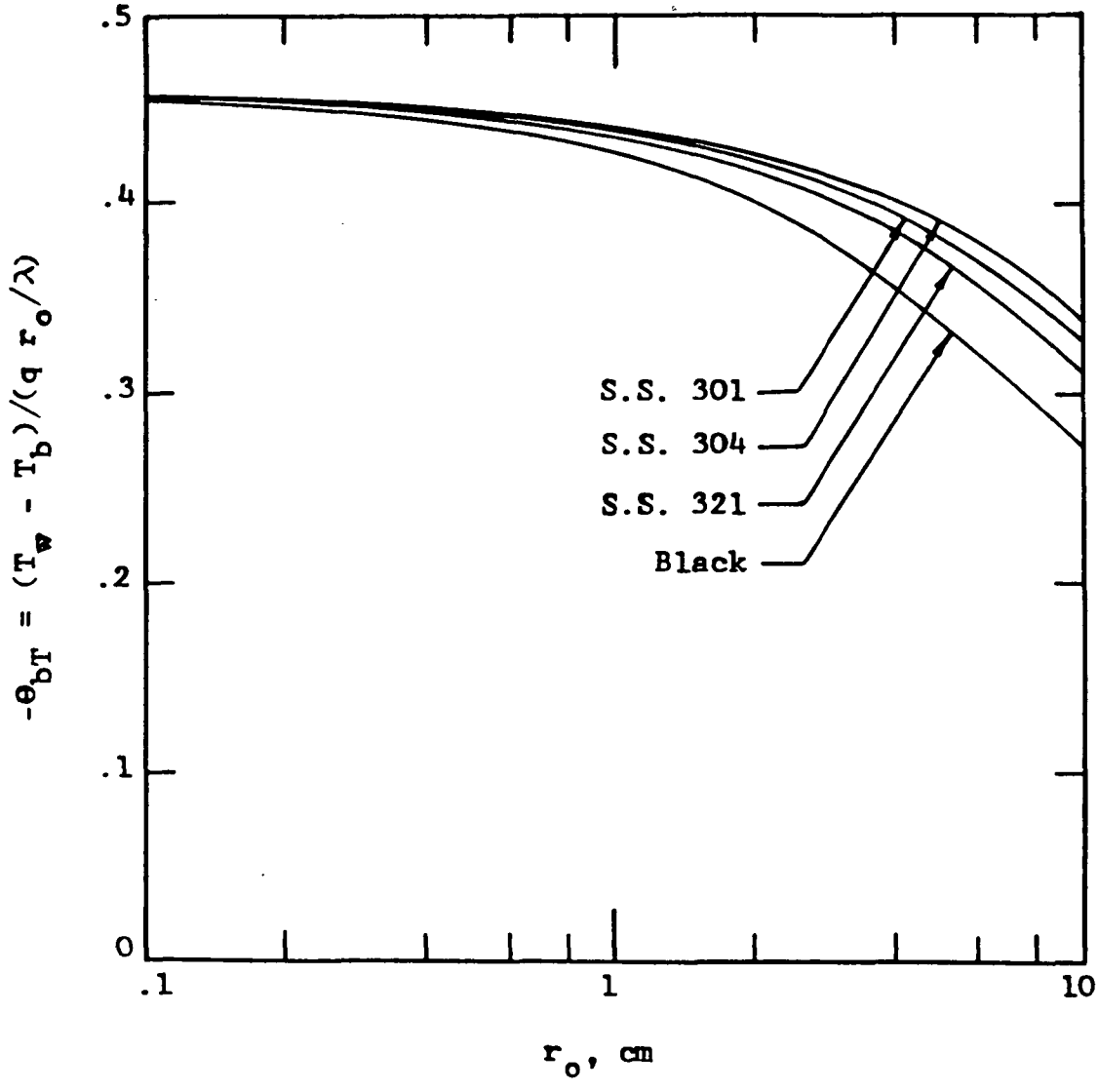

Figure 6.23 Variation of bulk temperature with radius for CO_2 (three bands); large u_{oi} results with T_w = 300 K

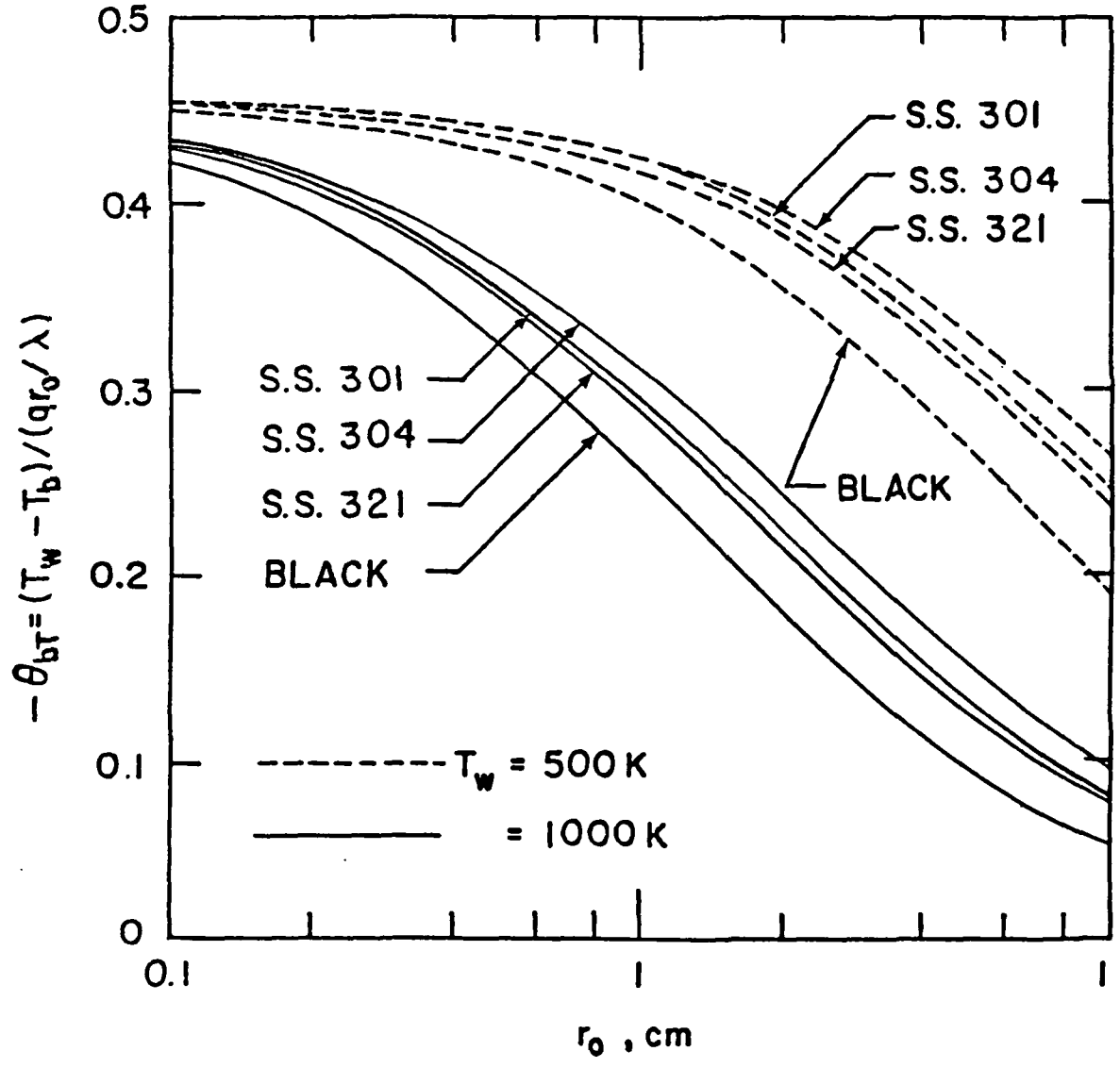

Figure 6.24 Variation of bulk temperature with radius for CO_2 (three bands); large u_{oi} results with T_w = 500 K and 1,000 K

7. CONCLUDING REMARKS

Radiative interactions in molecular gases were investigated under different physical and flow conditions. It was found that at a pressure of one atmosphere, the assumption of local thermodynamic equilibrium (LTE) for a gas such as CO is not valid for temperature below 600K, while for gases like CO_2 and N_2O, the assumption is justified at room temperature. The LTE results indicate that the gas such as CO_2 is a very poor transmitter of radiant energy, relative to other absorbing-emitting gases, in the large path length limit, although just the opposite is true under optically thin conditions. Large β results represent a good approximation to general band absorptance results for CO_2 and H_2O. It was noted that at moderate temperatures, radiative contributions from weaker combination and overtone bands can usually be neglected. For CO_2, at room temperature, it was found that the large path length (large u_o) limit is achieved approximately at the atmospheric pressure. The effect of radiation was seen to become smaller for lower wall emittance. Gray, optically thin, as well as large u_o results overestimate the influence of radiation, and this fact can be utilized to see whether or not, for given gas, the interaction of radiation is going to be of importance. The accuracy of various correlations for the total band absorptance was examined and specific recommendations were made for their use. The entire procedure developed in this study can be easily adopted to investigate radiative interactions in complex problems involving molecular radiating species. Some recent applications are presented in Appendices E and F.

REFERENCES

1. Schlichting, H., Boundary-Layer Theory, McGraw-Hill Book Company, New York, 1950 (2nd ed.), 1960 (4th ed.), 1968 (6th ed.), and 1979 (7th ed.).

2. Rosenhead, L. (editor), Laminar Boundary Layers, Oxford University Press, London, 1963.

3. Batchelor, G. K., An Introduction to Fluid Dynamics, Cambridge University Press, London, 1967.

4. White, F. M., Viscous Fluid Flow, McGraw-Hill Book Company, New York, 1974.

5. Bird, R. B., Stewart, W. E., and Lightfoot, E. N., Transport Phenomena, John Wiley and Sons, Inc., New York, 1960.

6. Rohsenow, W. H. and Choi, H. Y., Heat, Mass, and Momentum Transfer, Prentice-Hall, Englewood Cliffs, New Jersey, 1961.

7. Eckert, E.R.G. and Drake, R. M., Analysis of Heat and Mass Transfer, McGraw-Hill Book Company, New York, 1972.

8. Kays, W. M. and Crawford, M. E., Convection Heat and Mass Transfer, second edition, McGraw-Hill Book Company, New York, 1980.

9. Anderson, D. A., Tannehill, J. C., and Pletcher, R. M., Computational Fluid Mechanics and Heat Transfer, Hemisphere Publishing Corporation, New York, 1984.

10. Shah, R. K. and London, A. L., Laminar Forced Convection in Ducts, Advances in Heat Transfer, Academic Press, New York, 1978.

11. Chandrasekhar, S., Radiative Transfer, Dover Publications, Inc., New York, 1960.

12. Kourganoff, V., Basic Methods in Transfer Problems, Dover Publications, Inc., New York, 1963.

13. Sobolev, V. V., A Treatise on Radiative Transfer, D. Van Nostrand Company, Inc., Princeton, New Jersey, 1963.

14. Goody, R. M., Atmospheric Radiation I: Theoretical Basis, Oxford University Press, London and New York, 1964.

15. Preisendorfer, R. W., Radiative Transfer on Discrete Spaces, Pergamon Press, London and New York, 1965.

16. Vincenti, W. G. and Kruger, C. H., Introduction to Physical Gas Dynamics, John Wiley & Sons, Inc., New York, 1965. Printed and Published by Robert E. Krieger Publishing Co., Inc., Huntington, N.Y.

17. Pai, Shih-I., Radiation Gas Dynamics, Springer-Verlag New York Inc., New York, 1966.

18. Sparrow, E. M. and Cess, R. D., Radiation Heat Transfer, Brooks/Cole, Belmont, Calif., 1966 and 1970. New Augmented Edition, Hemisphere Publishing Corp., Washington, D.C., 1978.

19. Zel'dovich, Y. B. and Raizer, Y. P., Physics of Shock Waves and High-Temperature Hydrodynamic Phenomena, Vols. I and II, Academic Press, New York, 1967.

20. Hottel, H. C. and Sarofim, A. F., Radiative Transfer, McGraw-Hill Book Co., New York, 1967.

21. Love, T. J., Radiative Heat Transfer, Charles E. Merrill Publishing Co., Columbus, Ohio, 1968.

22. Penner, S. S. and Olfe, D. B., Radiation and Reentry, Academic Press, New York, 1968.

23. Kondratyev, K. Ya., Radiation in Atmosphere, Academic Press, New York, 1969.

24. Siegel, R. and Howell, J. R., Thermal Radiation Heat Transfer, McGraw-Hill Book Co., New York, 1971; Second Edition, 1981.

25. Ozisik, M. N., Radiative Transfer and Interactions with Conduction and Convection, John Wiley and Sons, Inc., New York, 1973.

26. Pomraning, G. C., Radiation Hydrodynamics, Pergamon Press, London and New York, 1973.

27. Paltridge, G. and Platt, C., Radiation Process in Meteorology and Climatology, American Elsevier Publishing Co., Inc., New York, 1976.

28. Rybicki, G. B. and Lightman, A. P., Radiative Processes in Astrophysics, John Wiley and Sons, Inc., New York, 1979.

29. Liou, K. N., An Introduction to Atmospheric Radiation, Academic Press, 1980.

30. Cess, R. D., "The Interaction of Thermal Radiation with Conduction and Convection Heat Transfer," Advances in Heat Transfer, Vol. 1, Academic Press, New York, 1964.

31. Sparrow, E. M., "Radiation Heat Transfer between Surfaces," Advances in Heat Transfer, Vol. 2, Academic Press, New York, 1965.

32. Viskanta, R., "Radiative Transfer and Interaction of Convection with Radiation Heat Transfer," Advances in Heat Transfer, Vol. 3, Academic Press, New York, 1966.

33. Tien, C. L., "Thermal Radiation Properties of Gases," Advances in Heat Transfer, Vol. 5, Academic Press, New York, 1968.

34. Cess, R. D. and Tiwari, S. N., "Infrared Radiative Energy Transfer in Gases," Advances in Heat Transfer, Vol. 8, Academic Press, New York, 1972.

35. Edwards, D. K., "Molecular Gas Band Radiation," Advances in Heat Transfer, Vol. 12, Academic Press, New York, 1976; also Radiation Heat Transfer Notes, Hemisphere Publishing Corporation, Washington, D.C., 1981.

36. Tiwari, S. N. "Band Models and Correlations for Infrared Radiation," Radiative Transfer and Thermal Control (Progress in Astronautics and Aeronautics), Vol. 49, American Institute of Aeronautics and Astronautics, New York, 1976.

37. Tiwari, S. N., "Models for Infrared Atmospheric Radiation," Advances in Geophysics, Vol. 20, Academic Press, New York, 1978.

38. Viskanta, R., "Radiation Heat Transfer," Fortschrift der Verfahrenstechnik, Vol. 22A, 1984, pp. 51-81.

39. Viskanta, R. and Menguc, M. P., "Radiation Heat Transfer in Combustion Systems," Progress in Energy Combustion Sciences, Vol. 13, No. 2, 1987, pp. 97-160.

40. Howell, J. R., "Thermal Radiation in Participating Media: The Past, the Present, and Some Possible Futures," Journal of Heat Transfer (Transaction of the ASME), Vol. 110, November 1988, pp. 1220-1229.

41. Northup, L. L. and Hsu, C. T., "Vibrational Energy Relaxation with Multiple Quantum Transitions," Physics of Fluids, Vol. 11, No. 6, June 1968, pp. 1375-1377.

42. Bazley, N. W. and Montroll, E. W., "Vibrational Relaxation of a System of Anharmonic Oscillators," Journal of Chemical Physics, Vol. 28, No. 4, April 1957, pp. 700-704.

43. Schwartz, R. N., Slawsky, Z. I., and Herzfeld, K. F., "Calculation of Vibrational Relaxation Times in Gases," The Journal of Chemical Physics. Vol. 20, 1952, pp. 1591-1599.

44. Schwartz, R. N. and Herzfeld, K. F., "Vibrational Relaxation Times in Gases (Three-Dimensional Treatment)," The Journal of Chemical Physics, Vol. 22, No. 5, May 1954, pp. 767-773.

45. Matthews, D. L., "Vibrational Relaxation of Carbon Monoxide in the Shock Tube," The Journal of Chemical Physics, Vol. 34, No. 2, February 1961, pp. 639-642.

46. Cottrell, T. L. and Matheson, A. J., "Transition Probability in Molecular Encounters," Faraday Society (London) Transactions, Vol. 58, 1962, pp. 2336-2341.

47. Millikan, R. C., "Infrared Resonance Fluorescence in the Fundamental Vibration-Rotation Band of Carbon Monoxide," Physical Review Letters, Vol. 8, No. 6, March 1962, pp. 253-254.

48. Woodmansee, W. E. and Decius, J. C., "Vibrational Relaxation in Carbon Monoxide by the Spectrophone Frequency Response Method," The Journal of Chemical Physics, Vol. 36, No. 7, April 1962, pp. 1831-1837.

49. Hooker, W. J. and Millikan, R. C., "Shock Tube Study of Vibrational Relaxation in Carbon Monoxide for the Fundamental and First Overton," The Journal of Chemical Physics, Vol. 38, No. 1, January 1963, pp. 214-220.

50. Millikan, R. C. and White, D. R., "Vibrational Energy Exchange Between N_2 and CO: The Vibrational Relaxation of Nitrogen," The Journal of Chemical Physics, Vol. 39, No. 1, July 1963, pp. 98-101.

51. Madigosky, W. M., "Vibrational Relaxation in High Density Methane," The Journal of Chemical Physics, Vol. 39, No. 10, November 1963, pp. 2704-2708.

52. Millikan, R. C. and White, D. R., "Systematics of Vibrational Relaxation," Journal of Chemical Physics, Vol. 39, No. 12, December 1963, pp. 3209-3213.

53. Camac, M., "CO_2 Relaxation Processes in Shock Waves," Fundamental Phenomena in Hypersonic Flow (Hall, J. G., Editor), Proceedings of the International Symposium Sponsored by Cornell Aeronautical Laboratory, June 25-26, 1964, Cornell Univ., Press, Ithaca, New York, 1966.

54. Read, A. W., "Vibrational Relaxation in Gases," Progress in Reaction Kinetics, Oxford Univ., Press, Vol. 3, 1965, pp. 203-235.

55. Stretton, J. L., "Calculation of Vibrational Relaxation Times in Polyatomic Gases," Faraday Society (London) Transactions, No. 61, January-June 1965, pp. 1053-1067.

56. Richards, L. W. and Sigafoos, D. H., "Vibrational Relaxation of Methane," The Journal of Chemical Physics, Vol. 43, No. 2, July 1965, pp. 492-497.

57. Parker, J. G. and Swope, R. H., "Vibrational Relaxation in Methane-Oxygen Mixtures," The Journal of Chemical Physics, Vol. 43, No. 12, December 1965, pp. 4427-4434.

58. Cottrell, T. L., Macfarlane, I. M., Read, A. W., and Young, A. H., "Measurement of Vibrational Relaxation Times by the Spectrophone," Faraday Society (London) Transactions, No. 62, July-December 1966, pp. 2655-2666.

59. Cottrell, T. L., Macfarlane, I. M., and Read, A. W., "Measurement of Vibration Relaxation Times by the Spectrophone," Faraday Society (London) Transactions, No. 63, September 1967, pp. 2093-2097,

60. Carnevale, E. H., Carey, C., and Larson, G., "Ultrasonic Determination of Rotational Collisional Numbers and Vibrational Relaxation Times of Polyatomic Gases at High

Temperatures," The Journal of Chemical Physics, Vol. 47, No. 8, October 1967, pp. 2829-2835.

61. Weaner, D., Roach, J. F., and Smith, W. R., "Vibrational Relaxation Times in Carbon Dioxide," The Journal of Chemical Physics, Vol. 47, No. 8, October 1967, pp. 3096-3102.

62. Simpson, C.J.C.M., Bridgman, K. D., and Chandler, T.R.D., "Shock-Tube of Vibrational Relaxation in Carbon Dioxide," The Journal of Chemical Physics, Vol. 49, No. 2, July 1968, pp. 513-522.

63. Yardly, J. T. and Moore, C. B., "Vibrational Energy Transfer in Methane," The Journal of Chemical Physics, Vol. 49, No. 3, August 1968, pp. 1111-1125.

64. Hodgson, J. P. and Hine, R. J., "Measurement of the Relaxation Frequency of the Asymmetric Stretching Mode of Carbon Monoxide," Journal of Fluid Mechanics, Vol. 35, January 1969, pp. 171-183.

65. Houghton, J. T., "Absorption and Emission by Carbon Dioxide in the Mesosphere," Quarterly Journal of the Royal Meteorological Society, Vol. 95, No. 403, January 1969, pp. 1-20.

66. Tiwari, S. N. and Cess, R. D., "The Influence of Vibrational Nonequilibrium Upon Infrared Radiative Energy Transfer," Journal of Quantitative Spectroscopy and Radiative Transfer, Vol. 11, 1971, pp. 273-248.

67. Tiwari, S. N. and Manian, S. V., "Evaluation of Upwelling Infrared Radiance in a Nonhomogeneous and Nonequilibrium Atmosphere," NASA CR-149090, November 1976; also, MS Thesis by S. V. Manian, Old Dominion University, Norfolk, Virginia, December 1976.

68. Gilles, S. E., "Flow with Coupled Radiative and Vibrational Nonequilibrium in a Diatomic Gas," Ph.D. Dissertation, Stanford University, California, 1968; also, Gilles, S. E. and Vincenti, W. G., "Coupled Radiative and Vibrational Nonequilibrium in a Diatomic Gas with Application to Gas Dynamics," Journal of Quantitative Spectroscopy and Radiative Transfer, Vol. 10, No. 2, February 1970, pp. 71-97.

69. Wang, L. S., "An Integral Equation of Radiative Equilibrium in Infrared Radiating Gases," Journal of Spectroscopy and Radiative Transfer, Vol. 8, No. 2, February 1968, pp. 851-863.

70. Penner, S. S., Quantitative Molecular Spectroscopy and Gas Emissivities, Addison-Wesley Publishing Co., Reading, Mass., 1959.

71. Penner, S. S. and Varanasi, P., "Approximate Band Absorption and Total Emissivity Calculations for CO_2," Journal of Quantitative Spectroscopy and Radiative Transfer, Vol. 4, No. 6, November/December 1964, pp. 799-806,

72. Sampson, D. H., Radiative Contributions to Energy and Momentum Transport in a Gas, Interscience Publishers, New York, 1965.

73. McClatchey, R. A., Benedict, W. S., Clough, S. A., Burch, D. E., Calfee, R. F., Fox, K., Rothman, L. S., and Garing, J. S., "AFCRL Atmospheric Line Parameters Compilation," Air Force Cambridge Research Laboratories, Bedford, Mass., AFCRL-TR-73-0096, January 1973 (also, NTIS AD A762904).

74. Ludwig, C. G., Malkmus, W., Reardon, J. E., and Thomas, J. A. L., Handbook of Infrared Radiation from Combustion Gases, R. Goulard and J. A. L. Thomson (Editors), NASA SP-3080, 1973.

75. Ludwig, C. G. (Editor), Atmospheric Effects on Radiative Transfer, Proceedings of the Society of Photo-Optical Instrumentation Engineers, Vol. 195, August 1979.

76. Rothman, L. S., Gamache, R. R., Barbe, A., Goldman, A., Gillis, J. R., Brown, L. R., Toth, R. A., Flaud, J. M., and Camy-Peyret, C., "AFCRL Atmospheric Absorption Line Parameters Compilation: 1982 Edition," Applied Optics, Vol. 22, No. 15, August 1983, pp. 2247-2256.

77. Cess, R. D., Mighdoll, P., and Tiwari, S. N., Infrared Radiative Heat Transfer in Nongray Gases," International Journal of Heat and Mass Transfer, Vol. 10, No. 11, November 1967, pp. 1521-1532.

78. Patch, R. W., "Effective Absorption Coefficients for Radiant Energy Transport in Nongray Nonscattering Gases," Journal of Quantitative Spectroscopy and Radiative Transfer, Vol. 7, No. 4, July/August 1967, pp. 611-637.

79. Plass, G. N., "Models for Spectral Band Absorption," Journal of the Optical Society of America, Vol. 8, No. 10, October 1958, pp. 690-703.

80. Plass, G. N., "Useful Representation for Measurements of Spectral Band Absorption," Journal of the Optical Society of America, Vol. 50, No. 9, September 1960, pp. 868-875.

81. Wyatt, P. J., Stull, V. R., and Plas, G. N., "Quasi-Random Model of Band Absorption," Journal of the Optical Society of America, Vol. 52, No. 11, November 1962, pp. 1209-1217.

82. Edwards, D. K. and Menard, W. A., "Comparison of Methods for Correlation of Total Band Absorption," Applied Optics, Vol. 3, No. 5, May 1964, pp. 621-625.

83. Edwards, D. K., Glassen, L. K., Hauser, W. C., and Tucher, J. S., "Radiation Heat Transfer in Nonisothermal Nongray Gases," Journal of Heat Transfer, Vol. 89C, No. 3, August 1967, pp. 219-229.

84. Edwards, D. K. and Balakrishnan, A., "Slab Band Absorptance for Molecular Gas Radiation," Journal of the Qualitative Spectroscopy and Radiative Transfer, Vol. 12, No. 10, October 1972, pp. 1379-1387.

85. Edwards, D. K. and Balakrishnan, A., "Thermal Radiation by Combustion Gases," International Journal of Heat and Mass Transfer, Vol. 16, No. 1, January 1973, pp. 25-40.

86. Felske, J. D. and Tien, C. L., " A Theoretical Closed Form Expression for the Total Band Absorptance of Infrared Radiating Gases," International Journal of Heat and Mass Transfer, Vol. 17, No. 1, January 1974, pp. 155-158.

87. Goody, R. M. and Belton, M. J. S., "Radiative Relaxation Times for Mars (A Discussion of Martian Atmospheric Dynamics)," Planetary and Space Science, Vol. 15, No. 2, February 1967, pp. 247-256.

88. Tien, C. L. and Ling, G. R., "On a Simple Correlation for Total Band Absorptance of Radiating Gases," International Journal of Heat and Mass Transfer, Vol. 12, No. 9, September 1969, pp. 1179-1181.

89. Cess, R. D. and Tiwari, S. N., "The Large Path Length Limit for Infrared Gaseous Radiation," Applied Scientific Research, Vol. 19, No. 6, November 1968, pp. 439-449.

90. Cess, R. D. and Tiwari, S. N., The Interaction of Thermal Conduction and Infrared Gaseous Radiation," Applied Scientific Research, Vol. 20, No. 1, January 1969, pp. 25-39.

91. Herzberg, G., Molecular Spectra and Molecular Structure. I. Spectra of Diatomic Molecules (1950), II. Infrared and Raman Spectra of Polyatomic Molecules (1945), Van Nostrand, Co., New York.

92. Tsederberg, N. V., Thermal Conductivity of Gases and Liquids, M.I.T. Press, Cambridge, Mass., 1965.

93. Cess, R. D. and Tiwari, S. N., "Heat Transfer to Laminar Flow of an Absorbing-Emitting Gas Between Parallel Plates," Heat and Mass Transfer-USSR, Vol. 1, May 1968, pp. 229–283.

94. Tiwari, S. N. and Cess, R. D., "The Effect of Surface Emissivity Upon Infrared Gaseous Radiation," International Journal of Heat and Mass Transfer, Vol. 11, No. 11, November 1968, pp. 1731-1734.

95. Pearce, B. E. and Emery, A. F., "Heat Transfer by Thermal Radiation and Laminar Forced Convection to an Absorbing Fluid the Entry Region of a Pipe," Journal of Heat Transfer, Vol. 92C, No. 2, May 1970, pp. 221-230.

96. Kurosaki, Y., "Radiation Heat Transfer in a Flow Between Flat Plates with Temperature Slip at the Walls," Fifth International Heat Transfer Conference, Vol. 1, Tokyo, 1971, pp. 98-107.

97. Echigo, R., Hasegawa, S., and Miyazaki, Y., "Composite Heat Transfer with Thermal Radiation in Nongray Medium-Part I: Interaction of Radiation with Conduction," International Journal of Heat and Mass Transfer, Vol. 14, No. 12, December 1971, pp. 2001-2015.

98. Tiwari, S. N. and Cess, R. D., "Heat Transfer to Laminar Flow of Nongray Gases Through a Circular Tube," Applied Scientific Research, Vol. 25, No. 3/4, December 1971, pp. 155-170.

99. Greif, R. and McEligot, D. M., "Thermally Developing Laminar Flows with Radiative Interaction Using the Total Band Absorptance Model," Applied Scientific Research, Vol. 25, December 1971, pp. 234-244.

100. Edwards, D. K. and Wassel, A. T., "The Radial Radiative Heat Flux in a Cylinder," Journal of Heat Transfer, Vol. 95, Series C. No. 2, May 1973, pp. 276-277.

101. Donovan, T. E. and Greif, R., "Laminar Convection with an Absorbing and Emitting Gas, Applied Scientific Research, Vol. 31, No. 3, August 1975, pp. 110-122.

102. Martin, J. K. and Hwang, C. C., "Combined Radiant and Convective Heat Transfer in Laminar Steam Flow Between Gray Parallel Plates with Uniform Heat Flux," Journal of Quantitative Spectroscopy and Radiative Transfer, Vol. 15, December 1975, pp. 1071-1081.

103. Jeng, D. R., Lee, E. J., and DeWitt, K. J., "A Study of Two Limiting Cases in Convective and Radiative Heat Transfer with Nongray Gases," International Journal of Heat and Mass Transfer, Vol. 20, No. 7, July 1977, pp. 741-751.

104. Tiwari, S. N., "Applications of Infrared Band Model Correlations to Nongray Radiation," International Journal of Heat and Mass Transfer, Vol. 20, No. 7, July 1977, pp. 741-751.

105. Greif, R., "Laminar Convection with Radiation: Experimental and Theoretical Results," International Journal of Heat and Mass Transfer, Vol. 21, No. 4, April 1978, pp. 477-480.

106. Balakrishnan, A. and Edwards, D. K., "Molecular Gas Radiation in the Thermal Entrance Region of a Duct," Journal of Heat Transfer, Vol. 101, August 1979, pp. 489-495.

107. Kobiyama, M., Taniguchi, H. and Saita, T., "The Numerical Analyses of Heat Transfer Combined with Radiation and Convection," Bulletin of the Japanese Society of Mechanical Engineering, Vol. 22, No. 167, May 1979, pp. 707-714.

108. Im, K. H. Ahluwalia, R. K., "Combined Convection and Radiation in Rectangular Ducts," International Journal of Heat and Mass Transfer, Vol. 27, No. 2, February 1984, pp. 221-231.

109. Tiwari, S. N., "'Radiative Interactions in Transient Energy Transfer in Gaseous System," NASA CR-176644 NAS 1.26:176644, December 1985.

110. Tiwari, S. N. and Singh, D. J., "Interaction of Transient Radiation in Nongray Gaseous Systems," NASA CR-181389 NAS 1.26: 181389, January 1987; also AIAA Paper 87-0323, January 1987.

111. Tiwari, S. N. Singh, D. J. "Interaction of Transient Radiation ion Fully Developed Laminar Flows," AIAA Paper 87-1521, June 1987; also "Transient Radiative Energy Transfer in Incompressible Laminar Flows," NASA CR-182605 NAS 1.26:182605, June 1987.

112. Tiwari, S. N. and Singh, D. J., "Radiation Interactions in Transient Energy Transfer in Fully Developed Laminar Flows," Applied Scientific Research, Vol. 47, No. 2, April 1990, pp. 151-176.

113. Trivedi, P. A. and Tiwari, S. N., "Radiative Interactions in Laminar Duct Flows," Institute for Computational and Applied Mechanics (ICAM), Old Dominion University, Norfolk, Virginia, ODU/ICAM Report 90-101, December 1990.

114. Tiwari, S. N., "Infrared Radiative Energy, Transfer in Gaseous System," Institute of Computational and Applied Mechanics (ICAM), Old Dominion University, Norfolk, Virginia, ODU/ICAM Report 91-102, September 1991.

115. Kesten, A. S., "Radiant Heat Flux Distribution in a Cylindrically Symmetric Nonisothermal Gas with Temperature Dependent Absorption Coefficient," Journal of Quantitative Spectroscopy and Radiative Transfer, Vol. 81, No. 1, January 1968, pp. 419-434.

116. Habib, I. S. and Greif, R., "Nongray Radiative Transport in a Cylindrical Medium," Journal of Heat Transfer, Transaction of the ASME, Series C, Vol. 92, No. 1, February 1970, pp. 28-32.

117. Wassel, A. T. and Edwards, D. K., "Molecular Gas Band Radiation in Cylinders," Journal of Heat Transfer, Transactions of the ASME, Series C, Vol. 96, No. 2, February 1974, pp. 21-26.

118. Wassel, A. T., Edwards, D. K., and Catton, I., "Molecular Gas Radiation and Laminar or Turbulent Heat Diffusion in Cylinder with Internal Heat Generation," International Journal of Heat and Mass Transfer, Vol. 18, No. 11, November 1975, pp. 1267-1276.

119. Pandey, D. K., "Combined Conduction and Radiation Heat Transfer in Concentric Cylindrical Media," Journal of Thermophysics and Heat Transfer, Vol. 3, No. 1, January 1989, pp. 75-82.

APPENDICES

APPENDIX A

INFORMATION ON WIDE-BAND MODEL CORRELATIONS

Some relevant information on the wide-band model correlations proposed by Edwards et al. [35, 82, 83] and by Tien and Lowder [33] are provided in this appendix.

After considering various models for the band absorption of vibration-rotation bands, Edwards and Menard proposed the use of an exponential wide band model [82, 83]. Three functional forms for the total band absorptance were suggested and these are, the linear, the square root and the logarithmic, corresponding to the small, the medium, and the large path length regions respectively. The three regions are characterized by three correlation constants, and in the notations of Edwards et al. [35, 82, 83] these are the band intensity constant C_1, the line width constant C_2, and the constant for the band width C_3. At sufficiently large pressures, rotational lines are pressure broadened and the line width constant C_2 ceases to be a parameter. Further, at sufficiently large path lengths, the central portion of the band becomes opaque and radiation transfer within the gas takes place solely in the wing regions of the band. This is characterized by the band width parameter C_3. For important bands of CO, CO_2, H_2O, and CH_4, values of correlation constants C_1, C_2, and C_3, were computed by Edwards et al. from reported experimental data and are available in [33, 35, 83].

Using the detailed information on the three regions of the exponential wide band model and by adopting an approach based on a set of mathematical properties of the total band absorptance, a continuous correlation was introduced by Tien and Lowder [33]

$$A = A_o \ln\left\{uf(t)\left[\frac{u+2}{u+2f(t)}\right]+1\right\} , \tag{A.1a}$$

where

$$u = C_o^2 Py; \quad t = \left[C_2^2/(4C_1C_3)\right]P_e \equiv B^2 P_e , \tag{A.1b}$$

$$f(t) = 2.94[1 - \exp(-2.60t)] \ . \tag{A.1c}$$

Note that Eq. (A.1) is exactly same as Eq. (4.43). Quantities u, t, B^2, and P_e are all dimensionless. The band width parameter $A_o = C_3$, and is a function of temperature only. The correlation quantity C_o^2 is proportional to (C_1/C_3). It can be shown [33] that

$$A_o C_o^2 = S(T) \ . \tag{A.2}$$

The quantity t is the line structure parameter, and P_e is the equivalent (effective) broadening pressure and is given by the relation

$$P_e = [(P_B + bP_A)/P_o]^n \ , \ P_o = 1 \ atm \ , \tag{A.3}$$

where P_A is the partial pressure of the absorbing gas, P_B the partial pressure of the broadening gas, and b the self-broadening power of the A-molecule with respect to the B-molecule (N_2 in all cases here). The pressure parameter n, which is always less than or equal to unity, accounts for the partial overlapping of bands with different lower states [35]. The quantities b and n are estimated experimentally by using various gas compositions.

By using the information on C_1, C_2, and C_3, quantities A_o, C_o^2, and B^2 were evaluated and expressed in the units employed here. These are given in the Table A1. The procedure for converting the correlation constants C_1, C_2, and C_3 from the data of Edwards et al. [35, 82, 83] into the relations and units of quantities A_o, C_o^2, and B^2 is discussed here briefly. As noted earlier, $A_o = C_3$, and C_o^2 is proportional to (C_1/C_3) such that

$$S(T) = A_o C_o^2 = C_1[(\rho/P) \times 10^4] \tag{A.4}$$

where P, ρ, and $S(T)$ have units of atm, gm/cm^3, and cm^{-2}/atm, respectively. The factor 10^4 enters into the relation of Eq. (A.4) because the unit for C_1 involves meter instead of centimeter.

The correlation constant C_2 represents the square-root coefficient and is proportional to $(2A_oC_oB)$ such that the quantity $[10^4(\rho/P)C_2^2]$ has the units of $\text{atm}^{-1} - \text{cm}^{-3}$.

For perfect (ideal) gases,

$$P = \rho RT = \rho(\bar{R}/M)T \tag{A.5}$$

where $\bar{R}$ is the universal gas constant (= 1545.33 ft-lbv/lb mole-R) and M is the molecular weight of the gas. Thus, $R = \bar{R}/M$ has the units of ft-lb/lbm-R, and one may express

$$\begin{aligned} R = \bar{R}/M &= (1545.33/M), \ \ (ft - lbf/lbm - R) \\ &= (1545.33/M)(9/5), \ \ (ft - lbf/lbm - K) \\ &= (1545.33/M)(9/5)\left(\frac{atm}{14.6959 \times 144}\right)\left[\frac{(12 \times 2.54)^3}{453.6}\left(\frac{cm^3}{gm}\right)\right] \end{aligned}$$

Consequently, Eq. (A.5) is expressed as

$$P/\rho = 82.055(T/M) \tag{A.6}$$

where units of P, ρ, and T are atm, gm/cm^3, and K, respectively. Thus, a combination of Eqs. (A.4) and (A.6) results in

$$S(T) = 121.869(M/T)C_1, \ atm^{-1} - cm^{-2} \tag{A.7}$$

where values of C_1 for different gases are as listed in [33, 35, 82, 83]. It should be noted that the reference temperature T_o is taken to be 100 K in the cited references.

The correlation quantity $B^2(\omega, T)$ represents the mean line-width to spacing ratio at one atmospheric pressure and is given by relation

$$B^2 = \pi(\gamma_L/d) = C_2^2/(4C_1C_3) \tag{A.8}$$

Since B^2 is a nondimensional quantity, its value can be determined exactly from the tabulated values of C_1, C_2 and C_3.

For gases, where detail band information is not available, the radiative transfer capability can be determined in the limit of large path length. As pointed out earlier, in this limit, radiation is governed solely by the band width parameter A_o. By comparing various molecular models (rigid rotator, arbitrary, and non-rigid rotator) as suggested by Edwards and Menard [82], and after personal communications with Dr. D. K. Edwards, it was decided to adopt the following two relations for A_o:

$$A_o = \frac{1}{2}\Gamma^2\left(\frac{3}{4}\right)\left[\left(\frac{4kT}{hc}\right)B_e\right]^{1/2} \tag{A.9}$$

$$A_o = 0.9\ \Gamma^2\left(\frac{3}{4}\right)\left(\frac{2kTB_e}{hc}\right)^{1/2} \tag{A.10}$$

where B_e is the equivalent rotational constant, c is the speed of light, h is the Planck constant, and k is the Boltzmann constant. The two relations given by Eqs. (A.9) and (A.10) are identical except that in Eq. (A.9) the coefficient will be 0.707 instead of 0.9 as it is in Eq. (A.10). Edwards suggests that the relation given by Eq. (A.10) will give a better agreement between the simple theory and the experimental data. The information on rotational constants for selected molecules is provided in Table A3.

It should be noted that in Eqs. (A.9) and (A.10), B_e, c, h and k are constants and do not depend on the temperature. Thus, Eq. (A.10) may be expressed as:

$$A_o(T) = CONST\ (T)^{1/2} \tag{A.11a}$$

where

$$CONST = 0.9\ \Gamma^2\left(\frac{3}{4}\right)\left(\frac{2kB_e}{hc}\right)^{1/2} \tag{A.11b}$$

By evaluating Eq. (A.11a) at a reference temperature T_{ref}, the value of $A_o(T_{ref})$ can be determined and, therefore, Eq. (A.11a) may be expressed alternately as:

$$A_o(T) = A_o(T_{ref})\left(T/T_{ref}\right)^{1/2} \tag{A.12}$$

Equation (A.12) is a convenient form to compare its results with experimental values.

By noting that $\Gamma^2\left(\frac{3}{4}\right) = [\Gamma(3/4)]^2$ and substituting values for c, h, and k, Eq. (A.11) can be expressed as:

$$A_o(T) = 1.59313(B_eT)^{1/2} \tag{A.13}$$

where A_o and B_e have units of cm^{-1} and T is in degrees Kelvin. For a particular gas, $A_o(T_{ref})$ can be obtained from Eq. (A.13) and then Eq. (A.12) can be used to determine $A_o(T)$ at other temperatures. For example, for CO the rotational constant is 1.931 cm^{-1} and at a reference temperature of 300 K, $A_o(T_{ref} = 300K) = 38.344$ cm^{-1}. This compares very well with the experimental value of 38.1 given in Refs. 33 and 35 and presented in Table A.1. Similarly, for the 4.3μ band of CO_2, the equivalent rotational constant is 0.3906 cm^{-1} and, therefore, $A_o(T_{ref} = 300K) = 17.246$ cm^{-1}; the experimental value of 19.9 cm^{-1} given in Table A.1 for this band is slightly higher.

Spectral Information for OH

For the fundamental band of OH, the following information is obtained from Ref. 74:

$$\text{Band center}, \omega_c = 3570 \text{ cm}^{-1}$$

$$\text{Band strength at } STP, S(T_o) = \text{cm}^{-2}\text{atm}^{-1}$$

Also, from Ref. 91 the information on equilibrium rotational constant of OH is obtained as:

$$A^2\Sigma^+ \rightarrow 17.355 \text{ cm}^{-1}$$

$$X^2\Pi_i \rightarrow 18.871 \text{ cm}^{-1}$$

Thus, it is suggested to use a value for the equilibrium rotational constant for OH as B_e = 18 cm^{-1}. Using this, a value of $A_o(T_{ref} = 300K)$ is found as

$$A_o(T_{ref} = 300) = 1.59313(B_e T_{ref})^{1/2} = 117.0707 \quad \text{(A.14)}$$

Considering the value of $A_o(T_{ref})$ = 117 cm^{-1}, the relation for $A_o(T)$ for OH is given as:

$$A_o(T) = 117(T/300)^{1/2} \quad \text{(A.15)}$$

By knowing ω_c, $S(T_o)$, and $A_o(T)$, other required spectral information for OH can be evaluated. The pressure parameters for OH not available in the literature.

Spectral Information on NO and N_2O

Spectral information for NO and N_2O obtained by various sources are listed Table A.4. The band width parameters for these molecules are calculated by the following procedure.

For NO, the information on equilibrium constant is obtained by Herzberg 1950 [91], Table 39, page 558 as

$$A^2\Sigma^+ \rightarrow 1.9952 \quad \text{(high vibrational level)}$$

$$X^2\Pi_i \rightarrow 1.7046 \quad \text{(low vibrational level)}$$

According to Herzberg, one could use the value of the lowest vibrational level and this does not cause any serious problem. Consequently, a value of B_e = 1.7046 is selected for NO, and the value of $A_o(T_{ref})$ is found to be

$$A_o(T_{ref} = 300K) = 1.59313(B_e T_{ref})^{1/2} = 36.027 \quad \text{(A.16)}$$

This value of A_o at T_{ref} = 300 K agrees with the value given by Edwards [35]. By adopting the value of $A_o(T_{ref})$ = 36 cm^{-1}, the relation for $A_o(T)$ for NO is given as:

$$A_o(T) = 36(T/300)^{1/2} \quad \text{(A.17)}$$

Other information for NO are available in [35] and, therefore, it is possible to calculate B^2 and β (or t) by using the relations presented in this appendix.

For N_2O, the value of the equilibrium rotational constant, as obtained from Herzberg and listed in Table A3, is B_e = 0.4182 and this is taken to be the same for all bands. Thus, the value of $A_o(T_{ref})$ for N_2O is found to be

$$A_o(T_{ref} = 300K) = 1.59313(B_e T_{ref})^{1/2} = 17.844 \tag{A.18}$$

The relation for $A_o(T)$, therefore, is expressed as

$$A_o(T) = 17.844(T/300)^{1/2} \tag{A.19}$$

The pressure parameters for N_2O are not available in the literature.

The values of $A_o(T)$ for NO and N_2O are tabulated in Table A4 along with other spectral information. Some relevant information on NO are also available in [35].

Table A.1 Exponential Band Model Correlation Quantities**

Molecule	Band μ	Band Center cm^{-1}	Pressure Parameters		$A_o(T)$ cm^{-1}	$C_o^2(T)$ $atm^{-1}\ cm^{-1}$	$B^2(T)$ dimensionless
			b	n			
CO	4.7	2143	1.1	0.8	38.1 $K_1(T)$	6.24 $K_2(T)$	0.314 $\delta_1(T)$
	2.35	4260	1.0	0.8	38.1 $K_1(T)$	0.042 $K_2(T)$	0.300 $\delta_1(T)$
CO_2	15	667	1.3	0.7	22.3 $K_1(T)$	15.2 $K_2(T)$	0.084 $K_1(T)$
	4.3*	2350	1.3	0.8	19.9 $K_1(T)$	98.7 $K_2(T)$	0.329 $K_1(T)$
	2.7	3715	1.3	0.65	41.6 $K_1(T)$	1.72 $K_2(T)\phi_2(T)$	0.111 $\delta_2(T)$
H_2O	I.R	500	5.0	1.0	49.4 $K_1(T)$	771 $K_2(T)\phi_7(T)$	0.073/$K_1(T)$
	6.3	1600	5.0	1.0	90.1 K_1 (T)	3.35 $K_2(T)$	0.130/$K_1(T)$
	2.7	3750	5.0	1.0	112.6 $K_1(T)$	1.52 $K_2(T)$	0.145/$K_1(T)$
	1.87	5350	5.0	1.0	79.7 $K_1(T)$	0.276 $K_2(T)\phi_{011}(T)$	0.118/$K_1(T)$
	1.38	7250	5.0	1.0	79.7 $K_1(T)$	0.230 $K_2(T)\phi_{101}(T)$	0.201/$K_1(T)$
CH_4	7.6	1310	1.3	0.8	39.8 $K_1(T)$	4.58 $K_2(T)$	0.067 $K_1(T)$
	3.3	3020	1.3	0.8	95.3 $K_1(T)$	3.15 $K_2(T)$	0.036 $K_1(T)$

**For notes on Table A.1, see the next page.

Notes on Table A1

1. Correlation quantities are based on the results of Ref. 35. The intensity of the band marked with * was taken from the Ref. 33.

2. Notations: $K_1(T) = (T/300)^{1/2}, K_2(T) = (300/T)^{3/2}$,

   $\delta_1 = [\phi_1^2(T)/K_1(T)] \times 10^{-3}$, $\delta_2 = \phi_3^2(T)/[\phi_2(T)K_1(T)]$

   $h = 6.625\times10^{-27}$ erg-sec, $C = 2.998\times10^{10}$ cm/sec,

   $k = 1.380\times10^{-16}$, erg/K, hc/k = 1.44 cm -K

3. Temperature range: 300 $K \leq T \leq T_{\max}$. For CO, $T_{\max} = 1800$ K.

   For CO_2, $T_{\max} = 1400$ K. For H_2O, $T_{\max} = 1100$ K. For CH_4, $T_{\max} = 830$ K.

4. For CO, $\omega = 2143$ cm^{-1} and

   $\phi_1(T) = \left[15.15 + 0.22(T/T_o)^{3/2}\right][1 - \exp(-hC\omega/kT)], T_o = 100K$

5. For CO_2, $\omega_1 = 1351$ cm^{-1}, $\omega_2 = 667$ cm^{-1}, $\omega_3 = 2396$ cm^{-1}

   $\phi_2(T) = \{1 - \exp[(-hc/k)(\omega_1 + \omega_3)]\}\times$

   $\{[1 - \exp(-hC\omega_1/kT)][1 - \exp(-hC\omega_3/kT)]\}^{-1}, \phi_3(T) = 1+$

   $0.053(T/100)^{3/2}$

6. For H_2O, $\omega_1 = 3652$ cm^{-1}, $\omega_2 = 1595$ cm^{-1}, $\omega_3 = 3756$ cm^{-1}

   $\phi_{v_1}v_2v_3(T) = \{1 - \exp[-hC(v_1\omega_1 + v_2\omega_2 + v_3\omega_3)/kT]\}\times$

   $\{[1 - \exp(-hC\omega_1/kT)][1 - \exp(-hCw_2/kT)][1 - \exp(-hC\omega_3/kT)]\}^{-1}$

   $\phi_7(T) = \exp\left[-17.6(T/100)^{-1/2}\right]$

Table A.2 Integrated Band Intensities of Important Molecules and the Radiative Lifetime of Their Vibrational States†

Molecule	Band (μ)	Band Center (cm^{-1})	Vibrational Transition	$S(T_o)$ cm^{-2} – atm^{-1}	$\eta_r \times 10^2$ (seconds)
CO	4.7	2143	0-1	289 ± 30	2.97
	(2.35)	4260	0-2	2.3 ± .28	
CO_2	15	667	000-010	362 ± 90	21.5
	4.3	2349	000-001	2970	0.22
	2.7	3715	000-101	67	
	(2.06)	4860.5	000-041	0.272*	
	(2.00)	4983.5	000-121	1.010*	
	(1.96)	5109	000-201	0.426*	
H_2O	20		Rotational	1840	
	6.3	1595	000-010	300 ± 60	4.68
	2.7	3755	000-001	200 ± 20	1.27
			000-100		
	1.87	5331	000-011	26.0	
	1.38	7250	000-101	21.2	
	(1.14)	8807	001-121	1.92	
CH_4	7.6	1306	0000-0001	185	11.3
	(6.5)	1534		2-3	
	3.3	3020	0000-0010	320	1.22

Table A2 (contd.)

NH_3	10.5	950	0000-0100	660	6.0
	6.15	1627	0000-0001	121	11.2
	3.0	3337	0000-1000	22	14.6
	2.9	3448	0000-0010	14.3	21.0
N_2O	17.0	589	000-200	36.2 ± 4	
	8.6	1160	000-120	12.0 ± 1.2*	
	7.8	1285	000-001	270	8.02
	4.5	2224	000-100	2035 ± 204	0.355
	4.1	2462	000-020	11.5 ± 5*	
	3.9	2564	000-010	44.0 ± 6*	11.2

†For notes on Table A.2, see the next page.

Note on Table A2

1. Information provided in Table A2 are based on data available in Refs. 33 and 35 and in cited references.

2. The integrated intensities re evaluated at T_o = 273 except those marked with * where T_o = 300 K.

3. The lifetime of vibrational states for the fundamental bands was calculated by using Eq. (4.27).

4. Intensities of the bands listed in parentheses are small and at moderate temperatures their contributions are generally ignored. However, in the large path length limit contribution from these bands become important. The intensities of three weaker CO_2 bands are given as:

   a. 2.06μ band: S(T) = 0.272 (300/T)ϕ_4

   b. 2.0μ band: S(T) = 1.01 (300/T)ϕ_5

   c. 1.96μ band: S(T) = 0.426 (300/T)ϕ_6

   where $\omega_1 = 1388\ \text{cm}^{-1}$, $\omega_2 = 667\ \text{cm}^{-1}$, $\omega_3 = 2349\ \text{cm}^{-1}$ and

$$\phi_4 = \{1 - \exp[(-hC/kT)(4\omega_2 + \omega_3)]\} \times \left\{[1 - \exp(-hC\omega_2/kT)]^4[1 - \exp(-hC\omega_3/kT)]\right\}^{-1}$$

$$\phi_5 = \{1 - \exp[(-hC/kT)(\omega_1 + 2\omega_2 + \omega_3)]\} \times \left\{[1 - \exp(-hC\omega_1/kT)][1 - \exp(-hC\omega_2/kT)]^2[1 - \exp(-hC\omega_3/kT)]\right\}^{-1}$$

$$\phi_6 = \{1 - \exp[(-hC/kT)(2\omega_1 + \omega_3)]\} \times \left\{[1 - \exp(-hC\omega_1/kT)]^2[1 - \exp(-hC\omega_3/kT)]\right\}^{-1}.$$

Table A.3 Rotational Constants*

Molecule	Moment of Inertia	Type	Rot. Constant Lowest Vibrational Level (cm^{-1})			Rot. Constant Equilibrium Position (cm^{-1})			Equivalent Rot. Constant (cm^{-1})
			$A_{[0]}$	$B_{[0]}$	$C_{[0]}$	A_e	B_e	C_e	
CO	$I_A = 0$ $I_B = I_C \neq 0$	Linear		1.931			1.931		1.931
CO_2	$I_B = I_C \neq 0$	Linear		0.3895			0.3906		0.3906
N_2O	$I_B = I_C \neq 0$	Linear		0.4182			0.4182		0.4182
NH_3	$I_A \neq 0$ $I_B = I_C \neq 0$	Symmeric Top	6.31	9.941		6.31	9.941		9.941
CH_4	$I_A = I_B = I_C$	Spherical Top		5.252			5.252		5.252
H_2O	$I_A \neq I_B \neq I_C$	Asymmetric Top	27.79	14.5	9.28	27.33	14.47	9.49	11.718

* For gases where differences between rotational constants of lowest vibrational level and that of equilibrium position were small or for gases whose equilibrium position rotational constants were not available, corresponding lowest vibrational level values were selected. According to Herzberg [91], the error introduced by doing so is negligible. Except for H_2O and NH_3, values for equivalent rotational constants were taken to be those of equilibrium position. For H_2O, the equivalent rotational constant is obtained by using relation $\bar{B}_e = \sqrt{BC}$. According to Herzberg [91], $\bar{B}_e$ for NH_3 is taken to be 9.941.

Table A.4 Integrated Band Intensities and Band Width Parameter for OH, NO, and N_2O

Molecule	Band (μ)	Band Center (cm^{-1})	Vibrational transitional	$S(T_{ref} = 300K)^*$ $(cm^2 - atm)^{-1}$	$A_o(T)$ (cm^{-1})	Ref.
OH	2.8	3570.0	0-1	110-0	117 $K_1(T)$*	74
	1.4	6974.0	0-2	4.4	"	74
NO	5.3	1876.0	0-1	132.0	36 $K_1(T)$	35, 74
	2.7	3724	0-2	2.2	"	74
N_2O	17.0	588.8	000-010	33.0	17.84 $K_1(T)$	33
	8.6	1167.0	000-020	12.0	"	33
	7.8	1285.0	000-100	383.0	"	33
	4.5	2223.5	000-001	1850.0	"	33
	4.1	2461.5	000-120	11.5	"	33
	3.9	2563.5	000-200	44.0	"	33

*Note that all values are based on T_{ref} = 300K and $K_1(T) = (T/300)^{1/2}$.

APPENDIX B

THERMODYNAMIC AND TRANSPORT PROPERTIES OF SELECTED SPECIES

It is important to consider the variation of thermodynamic and transport properties of various species with temperature and pressure. Quite often, the variation in properties with the pressure is not as crucial as with the temperature. The information on variation of different properties is provided here.

The information on variation of the thermal conductivity with temperature is obtained from Ref. 92 and this is expresses as:

$$\lambda = \lambda_o (T/T_o)^n \tag{B.1}$$

where

T = Temperature, K

λ_o = thermal conductivity at $T_o = 273$ K, k cal/m-hrK

n = constant as given in Table B1

Note that in the main text the notation of k is used for the thermal conductivity. In order to be consistent with the units used in the present work, Eq. (B.1) is expressed as:

$$\lambda = \frac{10^4 \lambda_o}{(36)(23.889)} (T/273)^n, \quad \text{erg/sec-cm-K} \tag{B.2}$$

For Eq. (B.2) the value of λ_o is obtained from Table B.1; the units for λ_o are shown in the table. For example, thermal conductivities of CO and CO_2 are expresses as:

$$\begin{aligned} \text{CO}: \quad \lambda &= (11.627865289 \times 200)(T/273)^{0.8} \\ &= 2325.570579^* \left((TW/273.0)^{**}0.8\right) \end{aligned} \tag{B.3}$$

$$\begin{aligned} \text{CO}_2: \quad \lambda &= (11.627865289 \times 128)(T/273)^{1.23} \\ &= 1488.365171^* \left((TW/273.0)^{**}1.23\right) \end{aligned} \tag{B.4}$$

Thus, for Eq. (B.2), the tabulated values for λ_o should be used without dividing by the factor 10^4.

Thermal conductivities of other species can be calculated in a similar manner. For species not listed in the Table B.1, values should be obtained from Ref. 92 or other sources mentioned in Ref. 111. For higher temperatures, values referred in Ref. 111 should be used. Some of the values used in the present study are listed in Table B.2.

The relations for the constant-pressure specific heat for different ideal gases are available in the literature and these are given in Table B.3 for CO, OH, CO_2, and H_2O.

Table B.1 Constants for Calculation of Thermal Conductivity

Molecule	$\lambda_o \cdot 10^4$ kcal/m-hr-°C	n	Maximum Temperature, °C
CO	200	0.80	1,000
CO_2	128	1.23	1,000
CH_4	264	1.33	600
H_2O	130	1.48	1,000
NH_3	181	1.53	1,000
N_2O	130	1.23	1,000

Table B.2 Thermal Conductivity of Selected Species*, erg/(cm-sec-K)

Temp., K	Molecule			
	OH	CO	CO_2	H_2O
300	(4879.71)	2507.82	1671.43	1738.04
		(2674.22)	(1820.47)	(2925.31)
500	(6993.13)	3773.77	3133.02	3703.67
		(3938.09)	(3339.63)	(4980.15)
1,000	(11504.56)	6570.51	7349.02	10325.76
		(6888.51)	(6716.93)	11588.26)
2,000	(20276.33)	11439.93	17238.37	28803.582
		(11730.56)	(11822.63)	(26302.73)

*Values in parenthesis are from a source mentioned in Ref. 111.

Table B.3 Constant-pressure specific heat for selected ideal gases (from a source mentioned in Ref. 111)

Gas	C_p = kJ/kmole-K, θ = T (Kelvin)/100
CO	$C_p = 69.145 - 0.70463\ \theta^{0.75} - 200.77\ \theta^{-0.5} + 176.76\ \theta^{-0.75}$
OH	$C_p = 81.546 - 59.350\ \theta^{0.25} + 17.329\ \theta^{0.75} - 4.266\ \theta$
CO_2	$C_p = 3.7357 + 30.529\ \theta^{0.5} - 4.1034\ \theta + 0.024198\ \theta^2$
H_2O	$C_p = 143.05 - 183.54\ \theta^{0.25} + 82.751\ \theta^{0.5} - 3.6989\ \theta$

APPENDIX C

GRAY SOLUTION FOR PARALLEL PLATE GEOMETRY

The governing equations for steady, constant properties, fully developed laminar flow of gray radiating gases are given by Eqs. (4.75) and (6.4), and these are repeated here for convenience,

$$\frac{d\theta}{d\xi} - 2\left(3\xi^2 - 2\xi^3\right) + 1 = q_R/q_w \tag{C.1}$$

$$\frac{d^2 q_R}{d\tau^2} - \frac{9}{4} q_R = 3\sigma \frac{dT^4}{d\tau} \tag{C.2}$$

For linearized radiation, $T^4 = 4T_w^3 T - 3T_w^4$ such that $dT^4/d\tau = 4T_w^3 dT/d\tau$, and Eq. (C.2) is expressed as

$$\frac{d^2 q_R}{d\xi^2} - \frac{9}{4}\tau_o^2 q_R = \gamma_1 q_w \frac{d\theta}{d\xi} \tag{C.3}$$

which is exactly the same equation as Eq. (6.18).

A combination of Eqs. (C.1) and (C.3) results in

$$\frac{d^2 q_R}{d\xi^2} - M_1^2 q_R = \gamma_1 q_w \left(6\xi^2 - 4\xi^3 - 1\right) \tag{C.4}$$

where M_1 is same as defined in Eq. (6.19). By obtaining the complimentary and particular solutions, the general solution of Eq. (C.4) is expressed as

$$\begin{aligned} q_R = {} & A\exp\left(M_1\xi\right) + B\exp\left(-M_1\xi\right) \\ & - \left(\gamma_1 q_w/M_1^5\right)\left[M_1^3\left(6\xi^2 - 4\xi^3 - 1\right) + 12M_1(1-2\xi) + 24\right] \end{aligned} \tag{C.5}$$

A substitution of Eq. (C.5) into Eq. (C.1) gives

$$\begin{aligned} \frac{d\theta}{d\xi} = {} & \frac{1}{q_w}\left[A\exp\left(M_1\xi\right) + B\exp\left(-M_1\xi\right)\right] \\ & + \left(\frac{\gamma_1}{M_1^2} - 1\right)4\xi^3 - \left(\frac{\gamma_1}{M_1^2} - 1\right)6\xi^2 - \frac{12\gamma_1}{M_1^4}(1-2\xi) \\ & + \left(\frac{\gamma_1}{M_1^2} - 1\right) - \frac{24\gamma_1}{M_1^5} \end{aligned} \tag{C.6}$$

An integration of this equation results in

$$\theta(\xi) = \frac{1}{q_w}\left[\frac{A}{M_1}\exp(M_1\xi) - \frac{B}{M_1}\exp(-M_1\xi)\right] + \left(\frac{\gamma_1}{M_1^2} - 1\right)\xi^4 + \left(1 - \frac{\gamma_1}{M_1^2}\right)2\xi^3 - \frac{12\gamma_1}{M_1^4}(\xi - \xi^2) + \left(\frac{\gamma_1}{M_1^2} - 1 - \frac{24\gamma_1}{M_1^5}\right)\xi + C \tag{C.7}$$

Note that for $\gamma_1 = 0$ this reduces to the case of convection heat transfer between parallel plates with constant wall heat flux.

By using the boundary condition $q_R(1/2) = 0$ and $\theta'(1/2) = 0$, the relation between coefficients A and B is found from Eqs. (C.5) and (C.6) as

$$A\exp(M_1/2) + B\exp(-M_1/2) = 24\gamma_1 q_w/M_1^5 \tag{C.8}$$

By using the boundary condition $(dq_R/d\xi)_{\xi=0} = (3\tau_o/2)q_R(0)$, there is obtained from Eq. (C.5)

$$A(M_1/\tau_o - 3/2) - B(M_1/\tau_o + 3/2) = (3\gamma_1 q_w/M_1^5)(M_1^3/2 - 6M_1 - 12 - 8M_1/\tau_o) \tag{C.9}$$

By using the condition $\theta(0) = 0$, one obtains from Eq. (C.7)

$$C = (1/q_w M_1)(B - A) \tag{C.10}$$

Equations (C.8)-(C.10) provide three equations to evaluate three constants A, B and C.

Upon substituting the relation for $\theta(\xi)$ into Eq. (6.6) and performing the integrations, there is obtained the result for bulk temperature as

$$\theta_b = (6A/q_w M_1^4)[(M_1 - 2)\exp(M_1) + M_1 + 2] - (6B/q_w M_1^4)[(M_1 + 2)\exp(-M_1) + M_1 - 2] + C - 12\gamma_1/M_1^5 - 151\gamma_1/70M_1^2 - 17/70 \tag{C.11}$$

By evaluating the constants A, B and C from Eqs. (C.8)-(C.10), Eq. (C.11) provides the solutions given by Eq. (6.19).

In the optically thin limit (i.e., in the limit $\tau_o \rightarrow 0$), $M_1 = \sqrt{\gamma}$, and the expression for C_1 becomes

$$C_1 = 24/\left\{\gamma_1^{7/2}[1 + \exp(-\sqrt{\gamma_1})]\right\} \tag{C.12}$$

Consequently, the gray solution for this limit is obtained as given by Eq. (6.20).

For small values of γ_1, the exponential term $\exp(-\sqrt{\gamma_1})$ is expressed as

$$\exp(-\sqrt{\gamma_1}) = 1 - \gamma_1^{1/2} + \frac{\gamma_1}{2} - \frac{\gamma_1^{3/2}}{6} + \frac{\gamma_1^2}{24} - \frac{\gamma_1^{5/2}}{120} + \frac{\gamma_1^3}{720} - \frac{\gamma_1^{7/2}}{5040} + \frac{\gamma_1^4}{40320} - \frac{\gamma_1^{9/2}}{362880} + \ldots \tag{C.13}$$

Thus,

$$\frac{1 - \exp(-\sqrt{\gamma_1})}{1 + \exp(-\sqrt{\gamma_1})} = \frac{\gamma_1^{1/2}}{2} - \frac{\gamma_1^{3/2}}{24} + \frac{\gamma_1^{5/2}}{240} - \frac{17\gamma_1^{7/2}}{40320} + \frac{61\gamma_1^{9/2}}{(70)(41472)} + \ldots \tag{C.14}$$

A substitution of Eq. (C.14) into Eq. (6.20) gives the relation for small values of γ_1 as

$$\theta_b = -\frac{17}{70} + \frac{61\gamma_1}{5040} + \ldots \tag{C.15}$$

For $\gamma_1 = 0$, we obtain the result for the transparent limit (i.e., the case of no radiative interaction) as $\theta_b = -17/70$.

Under optically thick conditions, $\tau_o >> 1$ and, therefore, $M_1 >> 1$, and Eq. (6.19) becomes

$$\theta_b = -17/70 + (17/70)\{4/[\bar{N}(3 + 4/\bar{N})]\} \tag{C.16}$$

This equation is rearranged to give the results of Eq. (6.21).

APPENDIX D

GRAY SOLUTION FOR CIRCULAR TUBE GEOMETRY

The governing equation for steady, constant properties, fully developed laminar flow of gray radiating gases within a black circular tube is given by Eq. (6.35) for linearized radiation. The solution of Eq. (6.35) is found to be

$$q_R(\xi) = AI_1(M_2\xi) + BK_1(M_2\xi) + \left(\gamma_2 q_w/M_2^4\right)\left(M_2^2\xi^3 + 8\xi - 2M_2^2\xi\right) \tag{D.1}$$

where I_1 and K_1 represent the modified Bessel functions of first and second kind. For finite solution as $\xi \to 0$, B must be taken to be zero and Eq. (D.1) becomes

$$q_R(\xi) = AI_1(M_2\xi) + \left(\gamma_2 q_w/M_2^4\right)\left(M_2^2\xi^3 + 8\xi - 2M_2^2\xi\right) \tag{D.2}$$

The constant A in Eq. (D.2) is evaluated by taking the derivative of this equation and invoking the boundary condition given by Eq. (6.34c) as

$$A = \left[\frac{3\tau_o M_2^2 - 24\tau_o - 32}{2M_2 I_o(M_2) + 3\tau_o I_1(M_2)}\right]\left(\frac{\gamma_2 q_w}{M_2^4}\right) \tag{D.3}$$

A combination of Eqs. (6.25) and (D.2) results in

$$\frac{d\theta}{d\xi} = (A/q_w)I_1(M_2\xi) + \left(\gamma_2/M_2^4\right)\left(M_2^2\xi^3 + 8\xi - 2M_2^2\xi\right) + 2\xi - \xi^3 \tag{D.4}$$

Equation (D.4) is integrated once to obtain

$$\theta(\xi) = (A/q_w M_2)I_o(M_2\xi) + \left(\gamma_2/M_2^4\right)\left(M_2^2\xi^4/4 - 4\xi^2 - M_2^2\xi^2\right) + \xi^2 - \xi^4/4 - C \tag{D.5}$$

By using the boundary condition $\theta(1) = 0$, one finds

$$C_4 = (A/q_w M_2) I_o(M_2) + \left(\gamma_2 M_2^4\right)\left(4 - 3M_2^2/4\right) + 3/4 \tag{D.6}$$

Consequently, the temperature distribution within the tube is obtained from a combination of Eqs. (D.5) and (D.6) as

$$\begin{aligned}\theta(\xi) = {} & (A/q_w M_2)[I_o(M_2\xi) - I_o(M_2)] \\ & + \left(\gamma_2/4M_2^4\right)\left(M_2^2\xi^4 + 16\xi^2 - 4M_2^2\xi^2 + 3M_2^2 - 16\right) \\ & + \xi^2 - \xi^4/4 - 3/4\end{aligned} \tag{D.7}$$

The expression for the bulk temperature is obtained by substituting Eq. (D.7) into Eq. (6.30b). The solution is as given by Eq. (6.36).

In the optically thin limit $\tau_o \to 0$ and $M_2^2 \to \gamma_2$. Consequently, the constant C_2 defined in Eq. (6.36) becomes

$$C_2 = -16/\left[\gamma_2^{7/2} I_o(\sqrt{\gamma_2})\right] \tag{D.8}$$

and Eq. (6.36) reduces to the result provided by Eq. (6.37).

For small values of γ_2, the modified Bessel functions are expressed as

$$I_o(\sqrt{\gamma_2}) = 1 + \gamma_2/4 + \gamma_2^2/64 + \gamma_2^3/2304 + \ldots \tag{D.9a}$$

$$I_1(\sqrt{\gamma_2}) = \gamma_2^{1/2}/2 + \gamma_2^{3/2}/16 + \gamma_2^{5/2}/384 + \gamma_2^{7/2}/18432 + \ldots \tag{D.9b}$$

Thus,

$$\frac{I_1(\sqrt{\gamma_2})}{I_o(\sqrt{\gamma_2})} = \gamma_2^{1/2}/2 - \gamma_2^{3/2}/16 + \gamma_2^{5/2}/96 - 11\gamma_2^{7/2}/6144 + \ldots \tag{D.10}$$

Upon substituting Eq. (D.10) into Eq. (6.37), there is obtained for $\gamma_2 = 0$, $\theta_b = -11/24$. This represents the result for the case of no radiative interaction.

In the optically thick limit $\tau_o >> 1$ and $M_2 >> 1$. Asymptotic expansions of modified Bessel functions for large values of M_2 are

$$I_o(M_2) = e^{M_2}/(2\pi M_2)^{1/2}\left[1 + 1/8M_2 + 9/128M_2^2 + \ldots\right] \tag{D.11a}$$

$$I_1(M_2) = e^{M_2}/(2\pi M_2)^{1/2}\left[1 - 3/8M_2 - 15/128M_2^2 + \ldots\right] \tag{D.11b}$$

Upon substituting this equation in Eq. (6.36), it is noted that C_2 times the bracketed term on the RHS approaches zero as $M_2 \to \infty$. Consequently, only the last three terms on the RHS of Eq. (6.36) remain valid for $\tau_o >> 1$, i.e.,

$$\theta_b = 11\gamma_2/24M_2^2 - 8\gamma_2/3M_2^4 - 11/24 \tag{D.12}$$

By using the definitions of γ_2, M_2 and $\bar{N}$, Eq. (D.12) is expressed as Eq. (6.38).

AIAA-92-0122

Radiative Interactions in Nonequilibrium Flows

S. N. Tiwari and R. Chandrasekhar
Old Dominion University,
Norfolk, VA

30th Aerospace Sciences Meeting & Exhibit
January 6-9, 1992 / Reno, NV

RADIATIVE INTERACTIONS IN NONEQUILIBRIUM FLOWS

S. N. Tiwari* and R. Chandrasekhar†
Old Dominion University, Norfolk, VA 23529–0247

ABSTRACT

The influence of vibrational and chemical nonequilibrium upon infrared radiative energy transfer in nonisothermal gases is investigated. Essential information is provided on rate equations, relaxation times, transfer equations, band absorption, and radiative flux equations. The methodology developed is applied to three specific cases. These are, absorbing-emitting species between isothermal parallel plates, radiating gases in the Earth's atmosphere, and supersonic flow of premixed hydrogen and air in an expanding nozzle. The results obtained for different cases reveal that the extent of radiative interactions is reduced significantly under nonequilibrium conditions. The method developed can be easily extended to investigate radiative interactions in complex nonequilibrium flows.

NOMENCLATURE

A	total band absorptance
A_o	band width parameter
B_ω	blackbody intensity, e_ω/π
c	speed of light
E	total internal energy, also upwelling radiance
E_v	total vibrational energy
f_j	mass fraction of jth species
$\bar{H}$	atmospheric heating rate
I_ω	intensity of radiation

* Eminent Professor, AIAA Associate Fellow

† Graduate Research Assistant, AIAA Student Member

J_ω	source function
k	thermal conductivity, also Boltzman constant
L	Plate spacing
P	pressure
Q	heat source or sink per unit volume
q_R	radiative flux
$q_{R\nu}$	spectral radiative flux, also $q_{R\omega}$
S	integrated band intensity
T	temperature
T_v	vibrational temperature
T_1	wall temperature
u_o	dimensionaless path length, SPL/A_o
y	physical coordinate
z	dummy variable for y
β	line structure parameter
γ	specific heat ratio, C_p/C_v
η	nonequilibrium parameter, η_c/η_r
η_c	collisional relaxation time
η_r	radiative life time
θ_v	characteristic vibrational temperarture
κ_ν	absorption coefficient, also κ_ω
ξ	dimensionaless coordinate, y/L
ξ'	dummy variable for ξ
ρ	density
ω	wave number
Ω	solid angle

INTRODUCTION

In order to understand and investigate radiative interactions in nonequilibrium flows, one should be quite familiar with basic transfer processes (mass, momentum, and energy) in gaseous systems. It is also essential to have fundamental knowledge of different numerical and computational procedures. For a basic understanding of these subject areas one should refer to [1-6].

The main objective of this study is to investigate radiative interactions in gaseous systems under nonequilibrium conditions. Attention has been directed specifically towards infrared active diatomic and polyatomic gases, wherein the absorption and emission of thermal radiation occurs as a result of vibration-rotation bands. In order to present a systematic study, it is necessary to assume a suitable model for vibration-rotation bands, and to obtain relevant spectroscopic information for the gases under consideration. The assumption of local thermodynamic equilibrium (LTE) will have to be justified, and any influence of nonequilibrium (non-LTE or NLTE) needs to be investigated.

Basic governing equations and essential information on molecular radiative interactions are provided in [7-10]. Radiative properties for important molecular species are available in [10-14]. In this study, basic equations of fluid mechanics and heat transfer are presented and radiative transport models are provided for molecular radiative interactions. The extent of radiative interactions are investigated under incompressible and compressible flow conditions.

BASIC THEORETICAL FORMULATION

The essential equations for conservation of mass momentum and energy are expresses as [1, 2]

$$\partial\rho/\partial t + \nabla \cdot (\rho \underset{\sim}{u}) = 0 \tag{1}$$

$$\rho \frac{D\underset{\sim}{u}}{Dt} = \rho \underset{\sim}{f} - \nabla p + \frac{\partial}{\partial x_j}\left[u\left(\frac{\partial u_i}{\partial x_j} + \frac{\partial u_j}{\partial x_i}\right) - \frac{2}{3}\delta_{ij}\mu\frac{\partial u_k}{\partial x_k}\right] \tag{2}$$

$$\rho c_p(DT/Dt) = \partial Q/\partial t + \nabla \cdot (k\nabla T) - \nabla \cdot q_R + \beta T(Dp/Dt) + \Phi \tag{3}$$

where Q represents the heat generated (or lost) per unit volume by external agencies, β is the coefficient of thermal expansion of the fluid, and other quantities are defined in the cited references. It should be noted that derivations of Eqs. (1)-(3) assume the conditions of continuum and existence of local thermodynamic equilibrium.

For the case of two-dimensional laminar flow in channels, the energy equation given by Eq. (3) reduces to [8]

$$\rho c_p\left(\frac{\partial T}{\partial t} + u\frac{\partial T}{\partial x} + v\frac{\partial T}{\partial y}\right) = \frac{\partial}{\partial y}\left(k\frac{\partial T}{\partial y}\right) + \beta T u\frac{dP}{dx} + \mu\left(\frac{\partial u}{\partial y}\right)^2 - div\ q_R \tag{4}$$

The energy equation given in this form can be applied to radiatively induced nonequilibrium situation by replacing the divergence of the radiative flux by its nonequilibrium counterpart. At the same time it must be assumed that the departure in population distribution over excited states from the Boltzmann distribution will not significantly change the internal energy, and the transport properties from their equilibrium values [3]. As discussed in [4], this assumption is justified under the conditions where vibrational characteristic temperature $h\nu/k$ is greater than or is of the order of vibrational temperature. Consequently, the temperature appearing in Eq. (4) may be regarded as the kinetic temperature in basic studies.

In obtaining Eq. (4), it has been assumed that the conduction heat transfer in the x direction is negligible compared with the net conduction in the y direction. This represents the physical condition of a large value of the Peclet number. By an analogous reasoning, the radiative heat

transfer in the x direction can be neglected in comparison to that transferred in the y direction. If, in addition, it is assumed that the Eckert number of the flow is small, then Eq. (4) reduces to

$$\frac{\partial T}{\partial t} + u\frac{\partial T}{\partial x} + v\frac{\partial T}{\partial y} = \alpha\frac{\partial^2 T}{\partial y^2} - \frac{1}{\rho C_p}\frac{\partial q_R}{\partial y} \tag{5}$$

In the preceding equation $\alpha = k/\rho C_p$ represents the thermal diffusivity of the fluid and it has been assumed that the fluid properties are constant locally.

Following the nomenclature of the kinetic theory of gases, Eqs. (1)-(3), in general, are referred to as the Navier-Stokes equations. For computational conveniences, it is quite often desirable to express these equations in a compact vector form. For two-dimensional nonequilibrium flows, the governing equations are expressed as [6, 15-19]

$$\frac{\partial U}{\partial t} + \frac{\partial F}{\partial x} + \frac{\partial G}{\partial y} + H = 0 \tag{6}$$

where vectors, U, F, G and H are expressed as

$$U = \begin{bmatrix} \rho \\ \rho u \\ \rho v \\ \rho E_{v_i} \\ \rho E \\ \rho f_j \end{bmatrix}$$

$$F = \begin{bmatrix} \rho u \\ \rho u^2 + p + \tau_{xx} \\ \rho uv + \tau_{xy} \\ \rho u E_{V_i} \\ (\rho E + p)u + \tau_{xx}u + \tau_{xy}v + q_{cx} + q_{Rx} \\ \rho u f_j - \rho D\dfrac{\partial f_j}{\partial x} \end{bmatrix}$$

$$G = \begin{bmatrix} \rho v \\ \rho uv + \tau_{yx} \\ \rho v^2 + p + \tau_{yy} \\ \rho v E_{V_i} \\ (\rho E + p)v + \tau_{xy}v + \tau_{yy}v + q_{cy} + q_{Ry} \\ \rho v f_j - \rho D \dfrac{\partial f_j}{\partial y} \end{bmatrix}$$

$$H = \begin{bmatrix} 0 \\ 0 \\ 0 \\ -\dot{e}_i \\ -\dot{w}_j \end{bmatrix}$$

The total energy E appearing in vectors U, F and G is defined as

$$E = -\frac{P}{\rho} + \frac{u^2 + v^2}{2} + \sum_{j=1}^{m} h_j f_j + \sum_{j=1}^{m} f_j E_{Vj} \tag{7}$$

and other quantities are defined in the cited references. Equation (6) is a very useful equation to study the effect of radiative interactions in compressible thermochemical nonequilibrium flows.

In order to close the system of conservation equations, it is essential to establish relations between the thermodynamic variables p, ρ, T, e, and h and relate these to transport properties μ and k. Since the local thermodynamic state is fixed by any two independent state variables, one may express the equations of state for a simple as

$$p = p(e, \rho) \tag{8a}$$

$$T = T(e, \rho) \tag{8b}$$

For a perfect gas, the following thermodynamic relations are applicable:

$$p = \rho RT, e = c_v T, h = c_p T \tag{9a}$$

$$c_v = R/(\gamma - 1), c_p = \gamma R/(\gamma - 1), \gamma = c_p/c_v \tag{9b}$$

where R is the gas constant, c_v is the specific heat at constant volume, c_p is the specific heat at constant pressure, and γ is the ratio of specific heats. Thus, for a perfect gas, Eq. (8) may be expressed as

$$p = (\gamma - 1)\rho e \tag{10a}$$

$$T = (\gamma - 1)e/R \tag{10b}$$

The transport properties are related to the thermodynamic variables through use of the kinetic theory of gases. The variation in viscosity is given by the Sutherland's formula

$$\mu = c_1 \, T^{3/2}/(T + c_2) \tag{11}$$

where c_1 and c_2 are specific constants for a given gas. The thermal conductivity k usually is determined through use of the Prandtl number defined by $Pr = c_p \, \mu/k$. This is possible because for most gases the ratio c_p/Pr is essentially constant. However, one should be very careful in using appropriate thermodynamic and transport properties under highly nonequilibrium conditions.

RADIATIVE TRANSPORT MODELS

An appropriate model for radiative transport is essential in applying the energy equation to any problem involving participating mediums. This section provides essential information on rate equations and equations for relaxation times, the equation of radiative transfer, band absorption and correlations, and radiative flux equations. Complete information on these topics is available in [20-25] and in the cited references.

Physical Model and Coordinate System

For many engineering and astrophysical applications, the radiative transport equations are formulated for one-dimensional planar system. For this study, the physical model consists of an absorbing-emitting gas bounded by two infinite parallel plates (Fig. 1). The plate surfaces are assumed to emit and reflect in a diffuse manner.

Diatomic and polyatomic gases are considered at sufficiently low temperatures such that the electronic, ionization, and dissociation effects can be neglected. For nonequilibrium analyses, the gas model is considered to be that of a rigid rotator and harmonic oscillator. It is assumed that the translational energy is governed by the Boltzmann law and a local kinetic temperature, referred to simply as the temperature, is defined. Rotational modes requiring only a few collisions to attain equilibrium are assumed to be in equilibrium at the kinetic temperature. Consequently, the governing equations given by Eqs. (4)-(6) are applicable to the case of radiation participating mediums.

Rate Equations and Equations for Relaxation Times

The rate of change of vibrational energy of a system of oscillators can be expressed as [20, 25]

$$\frac{dE_v}{dt} = \left(\frac{dE_v}{dt}\right)_{coll} - \int_0^{\infty} \int_0^{4\pi} \frac{dI_\nu}{ds} d\Omega d\nu \tag{12}$$

where I_ν represents the specific radiation intensity. The vibrational energy of a system of oscillators undergoing a collisional relaxation process is given by the Bethe-Teller relation

$$\frac{dE_v}{dt} = \frac{E_v^* - E_v}{\eta_c} \tag{13}$$

where E_v^* represents the equilibrium value of vibrational energy, and η_c having the dimensions of time is called the vibrational relaxation time. In general, the relaxation time is referred to as the average time required to transfer energy from one mode to another by collision. It is

inversely proportional to the collisional frequency. A simple derivation of Eq. (13) is given in [3, 4]. Since no assumption about the size of the difference $E_v^* - E_v$ was made in its derivation, Eq. (13) should be valid for large departure from the equilibrium. However, the assumption of simple harmonic oscillators restricts its applicability to small departures.

In order to be able to use Eq. (13) an explicit relation for $\eta_c = \eta_c(T, P)$ is required. This is provided by the Landau-Teller relation

$$\eta_c = K_1 P^{-1} \exp\left(K_2 T^{-1/3}\right) \tag{14}$$

where K_1 and K_2 are positive constants and depend on the physical properties of the molecule. It should be noted that the vibrational relaxation time increases with decreasing pressure and temperature. Generally, the product of pressure and relaxation time is plotted against the temperature on a logarithmic scale. Such a plot is known as Landau-Teller plot and for two level transitions it is a straight line for a wide range of temperatures.

Information on collisional relaxation times is available in the literature for some molecular gases, and these are referred to in [20-22, 25]. For diatomic gases, an empirical relation is given by Millikan and White [26, 27]

$$P\eta_c = \exp\left[A\left(T^{-1/3} - 0.015\mu^{1/4}\right) - 18.42\right] \tag{15}$$

where A is a constant and is related to the molecular constants of the colliding species and μ is the reduced mass of the colliding pairs. Values of A and μ are given in the references, and for CO colliding with CO these are A = 175, and μ = 14. The collisional relaxation time for CO_2 is given by the relation [28]

$$P\eta_c = \exp\left(AT^{-1/3} - B\right) \times 10^{-6} \tag{16}$$

where $A = 36.5$ and $B = -3.9$. The collisional relaxation time for methane is given by Richards and Sigafoos as [29]

$$P\eta_c = \exp\left(-5.4 + 40T^{-1/3}\right) \times 10^{-6} \tag{17}$$

In all expressions for η_c, P is the total pressure in atmosphere, η_c is in seconds, and T represents the temperature in degrees Kelvin. Although these relations show a strong dependency of η_c on pressure, in reality it has a larger temperature variation. This is because collisional frequencies are higher at higher temperatures and consequently it takes relatively less time to deactivate the excited states. Further discussions on collisional relaxation times for different colliding pairs are provided by Tiwari and Manian in [22].

For a multicomponent system, Eq. (13) is expressed as

$$\frac{dE_v}{dt} = \frac{E_{vi}^* - E_v}{\eta_{ci}} \tag{18}$$

where

$$E_{vi}^* = \frac{R_i\theta_{vi}}{\exp\left(\theta_{vi}/T - 1\right)}; \quad \theta_{vi} = hc\omega_i/k$$

The equivalent relaxation time η_{ci} of a mixture of gases ($i = 1, j$) is given by the linear mixture rule [30]

$$\frac{1}{\eta_{ci}} = \frac{f_1}{\eta_{ci1}} + \frac{f_2}{\eta_{ci2}} + \frac{f_3}{\eta_{ci3}} + \ldots + \frac{f_j}{\eta_{cij}} \tag{19}$$

where the local vibrational relaxation time η_{cij} of a molecular collision pair (i, j) is given by [26, 27]

$$P\eta_{cij} = \exp\left[0.00116\mu_{ij}^{1/4}\ \theta_{ij}^{4/3}\left(T^{-1/3} - 0.015\mu_{ij}^{1/4}\right) - 18.42\right] \tag{20}$$

where

$$\mu_{ij} = (\mu_{ii})(\mu_{jj})/(\mu_{ii} + \mu_{jj})$$

Note that Eqs. (15)-(17) are special cases of Eq. (20).

The Equation of Radiative Transfer

The equation of radiative transfer is derived for a simple harmonic oscillator on the assumption that rotational and vibrational levels are populated according to the Boltzmann distribution. The rotational energy is characterized by the equilibrium temperature whereas the vibrational energy is described by the nonequilibrium temperature T_v. A complete derivation of the transfer equation is available in [7, 20, 22, 25], and one form this equation is given as

$$\frac{dI_\nu}{ds} = \kappa_\nu\left(\frac{\kappa_\nu^*}{\kappa_\nu}B_\nu\frac{E_v}{E_v^*} - I_\nu\right) = \kappa_\nu^*\left(B_\nu\frac{E_v}{E_v^*} - \frac{\kappa_\nu}{\kappa_\nu^*}I_\nu\right) \tag{21}$$

This is the form of nonequilibrium transfer equation obtained by Goody [7]. It is seen that the quantity $B_\nu(\kappa_\nu^*/\kappa_\nu)(E_\nu/E_v^*)$ is the source function $S(T,T_v)$. Another form of the nonequilibrium transfer equation is derived by Tiwari and Manian in [22].

Under steady-state conditions, for each fundamental band, a combination of Eqs. (12), (13) and (21) yields

$$(E_v/E_v^*)\left[(E_v^*/\eta_c) + \int d\Omega \int \kappa_\nu B_\nu d\nu\right] = (E_v^*/\eta_c) + \int d\Omega \int \kappa_\nu I_\nu d\nu \tag{22}$$

where integration is taken over the frequency range of an individual band and over the solid angle from zero to 4π. Defining a time constant η_r as

$$\eta_r = E_v^*/\left[\int d\Omega \int \kappa_\nu B_\nu d\nu\right] \tag{23}$$

and combining Eqs. (21) and (22), there is obtained

$$\frac{dI_\nu}{ds} = \kappa_\nu(J_\nu - I_\nu) \tag{24a}$$

where

$$J_\nu = B_\nu[(\eta_r + \eta_c X)/(\eta_r + \eta_c)] \tag{24b}$$

$$X = \left(\int d\Omega \int \kappa_\nu I_\nu d\nu\right)/\left(\int d\Omega \int \kappa_\nu B_\nu d\nu\right) \tag{24c}$$

It can be shown [11] that $\eta_r = 1/A(1,0)$ is the radiative lifetime of the vibrational states, where $A(1,0)$ is the Einstein coefficient for spontaneous emission from the first vibration level.

By employing Eqs. (12) and (24), the source function J_ν can be expressed in an alternate form as [25]

$$J_\nu = \frac{B_\nu}{\eta_r + \eta_c}\left\{\eta_r + \eta_c\left[\left(\bar{h} + \int d\Omega \int \kappa_\nu J_\nu d\nu\right)/\left(\int d\Omega \int \kappa_\nu B_\nu d\nu\right)\right]\right\} \tag{25a}$$

where

$$\bar{h} = -\int (dq_{R\nu}/dy)d\nu \tag{25b}$$

It should be noted here that J_ν like B_ν is a slowly varying function of ν and for narrow bands it can be assumed as being independent of ν. The value for B_ν and J_ν are, therefore, taken to be the values evaluated at the band center. Further, by noting that both B_ν and J_ν are isotropic, Eq. (25) is expressed as

$$J_{\nu_c} = B_{\nu_c} + \frac{1}{2}(\eta_c/\eta_r)\bar{H} \tag{26a}$$

where

$$\bar{H} = \bar{h}/\left(2\pi \int \kappa_\nu d\nu\right) \tag{26b}$$

For isotropic radiation, the blackbody intensity of radiation B_ν is related to the Planck function $e_{b\nu}$ by $e_{b\nu} = \pi B_\nu$.

In the limit of very low pressure, the collisional relaxation time η_c is large and in Eq. (24b) η_r can be neglected by comparison. The source function then becomes $J_\nu = B_\nu X$. In the limit of high pressure, on the other hand, the collisional relaxation time approaches zero and the source function, Eq. (24b), becomes the Planck function. This is the situation of LTE usually assumed in most radiation transfer analyses. The degree of nonequilibrium effects is characterized by the order of magnitude of the parameter (η_c/η_r) in the transfer equation. Significant deviations from the LTE results will start when this ratio is unity or higher.

By following the procedure described in [25], an expression for η_r is obtained from Eq. (23) as

$$\eta_r^{-1} = 8\pi(\nu_o/c)^2 \int (\kappa_\nu/n)d\nu = 8\pi c\omega_c^2(P/n) \int (\kappa_\omega/P)d\omega \tag{27}$$

where n is the number density of molecules, and $\omega_c = (\nu_o/c)$ is the wave number corresponding to ν_o. Applying the perfect gas law $P = nkT$, and by using appropriate units for c and k, Eq. (27) is expressed in an alternate form as

$$\eta_r^{-1} = (8\pi\omega_c^2)(4.08 \times 10^{-12})T_o S(T_o) \tag{28}$$

where $S(T_o)$ having the units of cm^{-2} – atm^{-1} is the integrated band intensity, T_o is a reference temperature, and η_r has the units of seconds. For fundamental bands of some important molecules, values of η_r were calculated and these are provided in [25].

Band Absorption and Correlations

The study of radiative transmission in nonhomgeneous gaseous systems requires a detailed knowledge of the absorption, emission, and scattering characteristics of the specific species under investigation. In absorbing and emitting mediums, an accurate model for the spectral absorption coefficient is of vital importance in the correct formulation of the radiative flux equations. A systematic representation of the absorption by a gas, in the infrared, requires the identification of the major infrared bands and evaluation of the line parameters (line intensity, line half-width, and spacing between the lines) of these bands. The line parameters depend upon the temperature, pressure and concentration of the absorbing molecules and, in general, these quantities vary continuously along a nonhomogeneous path in the medium. In recent years, considerable efforts have been expended in obtaining the line parameters and absorption coefficients of important atomic and molecular species [31-33].

Several gray and nongray models are available in the literature to represent the absorption-emission characteristics of a molecular band. Complete discussions on these models, and expressions for transmittance and integrated absorptance are provided in [11-14, 25].

Radiative Flux Equations

Following the procedure described in [8], for the physical model illustrated in Fig. 1, an integration of the transfer equation, Eq. (24a), gives

$$q_{R\omega} = 2B_{1\omega}E_3(\tau_\omega) - 2B_{2\omega}E_3(\tau_{o\omega} - \tau_\omega) + 2\pi\left[\int_o^{\tau_\omega} J_\omega(t)E_2(\tau_\omega - t)dt - \int_{\tau_\omega}^{\tau_{o\omega}} J_\omega(t)E_2(t - \tau_\omega)dt\right] \tag{29a}$$

where

$$\tau_\omega = \kappa_\omega y \ , \quad \tau_{o\omega} = \kappa_\omega L \tag{29b}$$

$$J_\omega(t) = \frac{e_\omega(t)}{\pi} + \frac{1}{2}\eta\bar{H}(t), \ \eta = \eta_c/\eta_r \tag{29c}$$

$$\bar{H}(y) = \frac{-divq_R(y)}{2\pi PS(T)} = \frac{-\int_o^\infty (dq_{R\omega}/dy)d\omega}{2\pi PS(T)} \tag{29d}$$

In this equation $\tau_{o\omega}$ is the optical path length and t is a dummy variable for τ_ω. The quantities $B_{1\omega}$ and $B_{2\omega}$ represent the surface radiosities, and $E_n(t)$ are the exponential integral functions. In writing the expression for the source function J_ω, use was made of the relation $e_\omega = \pi B_\omega$. Further, it has been assumed that the spectral absorption coefficient κ_ω is independent of temperature, i.e., restriction is made to moderately small temperature differences within the gas. The total radiative flux is given by the expression

$$q_R = \int_o^\infty q_{R\omega}d\omega \tag{30}$$

In general, for nongray gases, Eq. (29a) does not possess a correct optically thick limit. However, a correct large path length limit does exist and it is discussed in [25]. A correct optically thin limit of Eq. (29a) exists and is given by [8]

$$q_{R\omega}(\tau_\omega) = B_{1\omega}(1-2\tau_\omega) - B_{2\omega}(1-2\tau_{o\omega}+2\tau_\omega) + 2\pi\left[\int_o^{\tau_\omega} J_\omega(t)dt - \int_{\tau_\omega}^{\tau_{o\omega}} J_\omega(t)dt\right] \tag{31}$$

Differentiating Eq. (31) with respect to τ_ω and neglecting terms of $0(\tau_{o\omega})$, one finds an expression for the divergence of radiative flux as

$$-div\underset{\sim}{q_R}(y) = -\int_o^\infty \frac{dq_{R\omega}}{dy}d\omega = 2\int_o^\infty \kappa_\omega[B_{1\omega}+B_{2\omega}-2\pi J_\omega(y)]d\omega. \tag{32}$$

By noting the assumption on $J_\omega(y)$ as being independent of wave number, and using the definitions of Planck mean and modified Planck mean absorption coefficients as given in [8, 25], Eq. (32) is written in an alternate form as

$$-(1+\eta)\frac{dq_R}{dy} = 2B_1\kappa_m(T,T_1) + 2B_2\kappa_m(T,T_2) - 4\kappa_p(T)\sigma T^4(y) \tag{33}$$

The expressions for surface radiosities corresponding to the optically thin limit are available in [8].

The obvious simplification of NLTE effect in Eq. (33) should be noted. As such, all optically thin analyses based on the assumption of LTE can be modified to include the effect of NLTE simply by multiplying the divergence of the radiative flux by a constant involving the nonequilibrium parameter $\eta = \eta_c/\eta_r$.

An often employed approximation in radiative transfer problems involves replacing the exponential integral $E_n(t)$ by an exponential function. The procedure for obtaining this approximation

and its validity is discussed in [8]. For the present situation, the exponential integrals $E_2(t)$, and $E_3(t)$ are approximated by

$$E_2(t) \simeq \frac{3}{4}\exp\left(-\frac{3}{2}t\right) \tag{34a}$$

$$E_3(t) = -\int E_2(t)dt \simeq \frac{1}{2}\exp\left(-\frac{3}{2}t\right) \tag{34b}$$

Employing these approximations and following the procedure discussed in [25] for black bounding surfaces, a combination of Eqs. (29a) and (30) results in

$$\begin{aligned} q_R(\xi) &= e_1 - e_2 \\ &+ \frac{3}{2}A_o u_o\left\{\int_o^{\xi} F_{1\omega_c}(\xi')\bar{A}'\left[\frac{3}{2}u_o(\xi-\xi')\right]d\xi'\right. \\ &\left. - \int_{\xi}^{1} F_{2\omega_c}(\xi')\bar{A}'\left[\frac{3}{2}u_o(\xi'-\xi)\right]d\xi'\right\} \\ &- \frac{3}{8}\eta\left\{\int_o^{\xi}\left(\frac{dq_R}{d\xi'}\right)\bar{A}'\left[\frac{3}{2}u_o(\xi-\xi')\right]d\xi'\right. \\ &\left. - \int_{\xi}^{1}\left(\frac{dq_R}{d\xi'}\right)\bar{A}'\left[\frac{3}{2}u_o(\xi'-\xi)\right]d\xi'\right\} \end{aligned} \tag{35}$$

where

$$F_{1\omega}(\xi) = e_\omega(\xi) - e_{1\omega}; F_2(\xi) = e_\omega(\xi) - e_{2\omega};$$

$$\xi = \frac{y}{L} = \frac{\tau_\omega}{\tau_{o\omega}} = \frac{u}{u_o}; \xi' = \frac{u'}{u_o} = \frac{z}{L}$$

and $\bar{A}'(u)$ denotes the derivative of the dimensionless band absorptance $\bar{A}(u)$ with respect to u.

Because of the restrictions of two level transitions inherent in the nonequilibrium transfer equation, the radiative flux equations given by Eqs. (29) and (35) are applicable to gases with only one fundamental band contributing to the radiative process. These equations, therefore, are useful in describing radiative transfer only in diatomic gases where contributions from the

overtone bands are not important. For gases with more than one fundamental band, where each band independently contributes to the radiative process, Eq. (35) is written in the form

$$
\begin{aligned}
q_R(\xi) = e_1 - e_2 & \\
& + \frac{3}{2}\sum_{i=1}^{n} A_{oi}u_{oi}\left\{\int_o^{\xi} F_{1\omega_i}\bar{A}_i'\left[\frac{3}{2}u_{oi}(\xi-\xi')d\xi'\right]\right. \\
& \left. - \int_{\xi}^{1} F_{2\omega_i}\bar{A}_i'\left[\frac{3}{2}u_{oi}(\xi'-\xi)\right]d\xi'\right\} \\
& - \frac{3}{8}\sum_{i=1}^{n}\eta_i\left\{\int_o^{\xi}\frac{dq_R}{d\xi'}\bar{A}_i'\left[\frac{3}{2}u_{oi}(\xi-\xi')\right]d\xi'\right. \\
& \left. - \int_{\xi}^{1}\frac{dq_R}{d\xi'}\bar{A}_i'\left[\frac{3}{2}u_{oi}(\xi'-\xi)\right]d\xi'\right\} \qquad (36)
\end{aligned}
$$

where n denotes the number of fundamental bands.

For the situations where assumptions of LTE are valid, the last two terms on the right hand side of Eq. (36) vanish and then there remains no restriction of taking summation over fundamental bands only. However, for the conditions (low pressure and moderate temperature) where NLTE effects are important, fundamental bands are of main importance to the radiative process. Contributions from the combination and overtone bands become significant only at higher temperature and pressure where conditions of LTE usually prevail. As such, Eq. (36) could be regarded as a general expression for the radiative flux in nongray gases. Various limiting forms of Eqs. (35) and (36) are provided in [25].

RADIATIVE INTERACTION IS GASES WITH VIBRATIONAL NONEQUILIBRIUM

The influence of vibrational nonequilibruim upon infrared energy transfer in gases has been investigated in [12, 21, 25]. Certain essential formulation and a few illustrative results of the study are presented here to demonstrate the effect of NLTE in molecular gases. Two cases of the physical model illustrated in Fig. 1 are considered. In the first case radiation is the sole

mode of energy transfer within the gas, and in the second case both molecular conduction and radiation are considered.

For the physical model in which radiation is the only mode of energy transfer, there is a uniform heat source (or sink) per unit volume Q within the gas. The plate surfaces are assumed to be black and to have the same uniform temperature T_1. For this model, the conservation of energy, Eq. (5), provides

$$dq_R/dy = Q \tag{37}$$

From the symmetry of the problem it follows that $q_R(L/2) = 0$, and Eq. (37) is integrated to yield

$$q_R = \frac{QL}{2}\left(2\frac{y}{L} - 1\right) \tag{38}$$

A combination of Eqs. (35) and (38) provides the applicable form of the energy equation as

$$\begin{aligned}\xi - 1/2 = (3u_o/2)\Bigg\{ &\int_o^{\xi} \left[\phi(\xi') - \eta/4u_o\right] \bar{A}'\left[\frac{3}{2}u_o(\xi - \xi')\right] d\xi' \\ &- \int_{\xi}^{1} \left[\phi(\xi') - \eta/4u_o\right] \bar{A}'\left[\frac{3}{2}u_o(\xi' - \xi)\right] d\xi'\end{aligned} \tag{39}$$

where

$$\phi(\xi) = [e_{\omega_c}(T) - e_{\omega_c}(T_1)]/(QL/A_o)$$

The quantity $\phi(\xi)$ in Eq. (39) represents the temperature profile within the gas in terms of the Planck function. The parameters in this equation are the dimensionless path length u_o, the nonequilibrium parameter η, and the line structure parameter β which enters through the correlation for the dimensionless band absorption $\bar{A}(u)$. By letting $\phi^*(\xi)$ denote the value of $\phi(\xi)$ for the case of LTE, it is noted that

$$\phi(\xi) = \phi^*(\xi) + 0.25\,\eta/u_o \tag{40}$$

Thus, if the value of $\phi^*(\xi)$ is available from LTE analyses, then the value of $\phi(\xi)$ can be obtained from Eq. (40).

For the case where molecular conduction is included and there is a uniform heat source within the gas, the energy equation, Eq. (5), is expressed as

$$k\frac{d^2T}{dy^2} - \frac{dq_R}{dy} + Q = 0 \tag{41a}$$

An integration of this equation provides

$$q_R = k(dT/dy) + (y - L/2)Q \tag{41b}$$

In line with the assumption of small temperature differences, Planck's function may be linearized as

$$e_{\omega_c}(T) - e_{\omega_c}(T_1) = (de_{\omega_c}/dT)_{T_1}(T - T_1) \tag{42}$$

Now, a combination of Eqs. (35), (41), and (42) provides the energy equation for this case as

$$\begin{aligned}\frac{d\theta}{d\xi} + \xi - \frac{1}{2} = \frac{3Mu_o}{2}\Bigg\{&\int_o^{\xi} \theta(\xi')\bar{A}'\left[\frac{3}{2}u_o(\xi - \xi')\right]d\xi' \\ &- \int_{\xi}^{1} \theta(\xi')\bar{A}'\left[\frac{3}{2}u_o(\xi' - \xi)\right]d\xi'\Bigg\} \\ &- \frac{3}{8}\eta\Bigg\{\int_o^{\xi} \left(1 + d^2\theta/d\xi'^2\right)\bar{A}'\left[\frac{3}{2}u_o(\xi - \xi')\right]d\xi' \\ &- \int_{\xi}^{1} \left(1 + d^2\theta/d\xi'^2\right)\bar{A}'\left[\frac{3}{2}u_o(\xi' - \xi)\right]d\xi'\Bigg\}\end{aligned} \tag{43}$$

where

$$\theta = (T - T_1)/(QL^2/k); M = (LA_o/k)(de_{\omega_c}/dT)_{T_1}$$

The limiting forms of Eq. (43) for $u_o << 1$ and $u_o >> 1$ are provided in [25].

Equations (39) and (43) represent the energy equation for a gas with a single vibration-rotation band. Analogous expressions can be developed for a multi-band gas and gas mixtures, and these are provided in [25]. Following the procedure discussed in [25], numerical solutions

of Eqs. (39) and (43) have been obtained (along with the limiting solutions for $u_o << 1$ and $u_o >> 1$) by employing the bands absorptance correlation of Tien and Lowder [11]. Selected results are presented here to demonstrate the effects of NLTE on radiative energy transfer.

For the case in which conduction is neglected, numerical solutions of Eq. (39) are illustrated in Fig. 2 for $\beta = \infty$ and for a range of the nonequilibrium parameter $\eta = \eta_c/\eta_r$. As would be expected the NLTE effects are significant in the regions of small path lengths and for η values higher than unity [12, 21]. For large path lengths, the assumption of LTE is seen to be justified. It should be noted that the NLTE results yield higher centerline temperature than the corresponding LTE results. This is a consequence of NLTE reducing the capability of the gas to transmit radiative energy [12, 25].

Specific results are illustrated in Fig. 3 for carbon monoxide with $T_1 = 500$ K. It is seen that NLTE can exert a considerable influence upon the radiative transfer process at low pressures. This is because the value of η varies inversely with pressure. Similar results presented in [12, 25] for $T_1 = 1{,}000$K and 2,000K show that NLTE influence is very small at higher temperatures. This is a consequence of the strong temperature dependence of η, such that the value of η at 1,000K is approximately two orders of magnitude less than the value for 500K [25].

For the case in which molecular conduction is included, numerical solutions of Eq. (43) are illustrated in Fig. 4 for carbon monoxide with $T_1 = 500$K. Recall that NLTE effects are more pronounced under small path length conditions. With reference to Fig. 4, however, this corresponds to the case for which conduction is the predominant mode of energy transfer. Thus, for a given pressure, the NLTE influence upon total energy transfer within the gas will vanish for either small or large values of L. The former corresponds to negligible radiative transfer, while the latter denotes the large path length limit. Further discussions of results obtained for this physical problem are provided in [12, 21, 25].

INFLUENCE OF VIBRATIONAL NONEQUILIBRIUM ON UPWELLING ATMOSPHERIC RADIANCE

In the evaluation of atmospheric radiance, the assumption usually is made that the atmosphere is the LTE. This assumption is justified for most atmospheric constituents at relatively low altitudes. There are situations, however, where this assumption breaks down and conditions of NLTE prevail. Curtis and Goody [7] have concluded that for CO_2 molecules the assumption of LTE is justified at altitudes below 75 km, but not at higher altitudes. As noted earlier, the CO molecules are in the state of nonequilibrium even at moderate values of temperature and pressure. Recently, Mlynczak [34] has presented a study on nonlocal thermodynamic equilibrium process in ozone with special implications for the energy budget of the mesosphere and lower thermosphere. A literature survey on NLTE processes was provided and results were presented to assess the magnitude of atmospheric heating due to NLTE processes involving ozone.

The purpose of this study is to analyze the NLTE effects of CO and CH_4 molecules on the upwelling atmospheric radiation. This information is useful in developing data reduction schemes for the measurement of concentrations of these species in the atmosphere and in assessing the energy budget of the atmosphere.

The expression for the heating rate at any altitude z in the atmosphere is obtained from the combination of Eqs. (25) and (26) as [22]

$$-\bar{H} = B_\omega \bar{\tau}_\omega / [2(1 + \eta \bar{\tau}/4)] \tag{44}$$

where $\bar{\tau}$ represents the average transmittance and is defined as

$$\bar{\tau}_\omega = (1/S) \int_{band} \kappa_\omega \tau_\omega(z, \infty) d\omega \tag{45}$$

Thus, to calculate the NLTE heating rate in the spectral range of a particular band, it is essential to have information on η_c, η_r, and $\bar{\tau}_\omega$. An appropriate absorption model is needed to calculate

$\bar{\tau}_\omega$. In this study, line-by-line as well as quasi-random band models are used to calculate $\bar{\tau}_\omega$. The line parameters needed for these models were obtained from [31-33].

Once the heating rate has been calculated at different altitudes, the source function J_w is evaluated from Eq. (29c). The expression for thermal radiation emerging from a plane parallel atmosphere under nonequilibrium conditions is obtained by modifying Eq. (29a) as [14, 22]

$$E(\omega) = \varepsilon(\omega)B(\omega, T_s)\tau(\omega, 0) + \int_o^h J(\omega, T(z))[d\tau(\omega, z)/dz]dz \tag{46}$$

In Eq. (46), the first term on the right-hand side represents the thermal radiation emitted by the surface with a surface emittance $\varepsilon(\omega)$ and $B(\omega, T_s)$ is the Planck function evaluated at the surface temperature T_s. The second term on the right-hand side represents the thermal emission of the atmosphere.

The upwelling radiation is calculated by dividing the nonhomogeneous atmosphere into a number of homogeneous sublayers. Each sublayer is considered to have constant species, temperature and pressure. If the gas molecules absorbs in a specified spectral region $\Delta\omega$, then the total upwelling radiance is given by

$$E = \int_{\Delta\omega} E(\omega)d\omega \tag{47}$$

The numerical procedures and computer codes for calculation of the heating rates and NLTE upwelling radiance are provided in [22].

The values of collisional relaxation time η_c, NLTE parameter $\eta = \eta_c/\eta_r$, heating rate, and upwelling radiance were calculated for CO, CO_2, and CH_4 for standard atmospheric conditions. Within the specific spectral range of interest, the influence of surface emissivity, interfering molecules, and reflected components of radiation was accounted for in certain calculations. Extensive results are provided in [22] and a few selected results are presented here.

For the CO fundamental band, the values of η_c and η are shown in Fig. 5 for different altitudes. Since the case of LTE is obtained only for $\eta << 1$, it is evident that the source function and Planck function will have a considerable difference for the 4.6μ CO band under atmospheric conditions.

The heating rates are calculated directly by employing Eq. (44) and an appropriate model for $\bar{\tau}_\omega$. The results obtained for the 15μ CO_2 band from 50 to 120 km are compared with the results of Curtis and Goody [7] in Fig. 6. Curtis and Goody applied the method of successive approximation to solve an integral formulation in which the convergence depends on the first approximation selected. The calculation of the heating rate by using Eq. (44) is more accurate and straightforward. The slight difference in the two sets of results in Fig. 6 is because an improved value for the radiative life time was used in the present calculation.

The upwelling radiance at the top of 10 km is shown in Fig. 7 for different CO concentrations. First calculations were carried out for both LTE and NLTE by assuming only CO molecules in the atmosphere. In other words, contributions of the interfering molecules within the spectral range of the CO fundamental band were not considered. It should be noted that the NLTE will tend to reduce the net upwelling radiance. Figure 7 indicates that for the case with no interfering molecules the NLTE effect reduces the upwelling radiance by about six percent for 1 ppmv CO concentrations. For lower concentrations, the effect is even less. This is because as the CO concentrations increases, the average transmittance decreases due to more radiation absorption. This results in higher differences between the Planck and source functions which, in turn, result in larger NLTE effects. The results with H_2O as an interfering gas is also shown in Fig. 7. The upwelling radiance is less than that of pure CO due to increased absorption by the H_2O molecules. The inclusion of H_2O, however, does not tend to increase or decrease the effects of NLTE. This is because H_2O molecules were not considered in the calculation of the atmospheric heating rate. The heating rate was calculated only for CO molecules.

The atmospheric heating rates were also calculated including the interfering molecules. For this case, the upwelling radiance results are shown in Fig. 8. It is seen that the interfering molecules tend to decrease the NLTE effects. This is because inclusion of interfering molecules reduces the value of the average transmittance. This, in turn, reduces the atmospheric heating rate. It is noted from Eq. (29c) that the lower the value of the heating rate, the lower is the difference between the Planck and source functions. This results in lower NLTE effects with increasing number of interfering molecules. Figure 8 shows that only H_2O has the maximum NLTE effect. The reduction in LTE effect due to CO_2 and N_2O molecules, as interfering gases, is very small as compared to the H_2O molecules. This is because H_2O has many more lines in the 4.6μ spectral region of CO than other interfering molecules.

Upwelling radiance calculations were made in the spectral range of 3.3μ CH_4 band to investigate if any NLTE effect existed for this molecule under normal atmospheric conditions. From the results and discussion presented in [22], it was noted that the conditions of LTE is justified for CH_4 up to an altitude of 60 km.

CHEMICALLY REACTING AND RADIATING SUPERSONIC FLOWS

The basic procedure developed and tested in the previous sections are now applied to investigate the NLTE effects in compressible flows. This was the primary motivation of the present study. The two-dimensional elliptic Navier-Stokes equations, Eq. (6), are used to study thermochemical nonequilibrium and radiative interactions in supersonic flows. The specific problem considered is the supersonic flow of premixed hydrogen and air in an expanding nozzle (Fig. 9). A somewhat similar problem was investigated by Gokcen and Park under the assumption of LTE [35], and relevant literatures in the field were cited. The reacting flow consists of seven species, one of which is the inert N_2 molecule. The thermal state of the gas is modeled with one translational-rotational temperature (referred to here as translational

temperature) and five vibrational temperatures. A systematic study of this problem is presented in [36] where relevant information on auxiliary equations and numerical procedures is provided. In essence, this problem involves three competing nonequilibrium processes, thermal, chemical, and radiative.

The radiative flux equations given by Eqs. (29–(33) are appropriate equations to investigate the NLTE effects in chemically reacting supersonic flows. For preliminary study, however, a simplified form of the optically thin formulation, as given by Eq. (33), may be used, and this is expressed as [21, 25]

$$(1 + 0.75\eta)dq_R/d\xi = 3A_o u_o[e_{\omega_c}(\xi) - e_{1\omega_c}] \tag{48}$$

Equations (33) and (48) indicate that the effect of NLTE can be investigated by multiplying the LTE divergence of radiative flux by a constant (1+0.75η). For specific flow conditions the value of $\eta = \eta_c/\eta_r$ must be calculated for all participating species by using the linear mixture rule such as that given by Eq. (19).

The inflow conditions considered for the present physical problem are analogous to the exit conditions of a scramjet combustor. These are, P_∞ = 0.8046 atm, T_∞ = 1,890 K, and M_∞ = 1.4. This problem was studied under equilibrium and nonequilibrium conditions by other investigators cited in [36]. In this study, a seven step finite rate chemistry model for hydrogen air combustion is employed and results are obtained for conditions of chemical nonequilibrium (CNE) and combined thermal and chemical (thermochemical) nonequilibrium (TCNE). The radiation participating species considered are H_2O and OH. The gray gas model is considered for the LTE case, and the optically thin formulation, Eq. (48), is used for the NLTE case. The nozzle wall is considered to be noncatalytic, black and adiabatic. Since the physical problem is symmetric, results were obtained only for the upper half of the geometry. The results corresponding to the centerline are referred to as grid j = 1 results. The results for the top

boundary are designated as $j = j\,\mathrm{max}$ results. The results in the middle of the centerline and top boundary are denoted as $j = j\mathrm{mid}$ results. Extensive results for various cases are provided in [36]. Here, selected results are presented for chemical and thermochemical nonequilibrium conditions with and without LTE and NLTE radiative interactions.

The variations in translational temperature (i.e., translational-rotational temperature) along the nozzle are illustrated in Figs. 10 and 11. The results for the centerline temperature are shown in Fig. 10 for different nonequilibrium models. It is noted that the reaction rates are fairly fast and the chemical potential energy is converted into thermal energy within a short distance from the inlet. The CNE results (solid line) are seen to be significantly higher than the TCNE results. This is because a part of the chemical energy is used to excite the vibrational modes and the vibrational energy relaxes slowly to the equilibrium value. The results for LTE radiative interaction (TCNE+LTE) lie between CNE and TCNE results. This is mainly due to the radiative cooling effect. It was shown in [36] that the concentration of H_2O and OH changes only slightly after $X/L_X = 0.2$. The optically thin NLTE results (TCNE + NLTE) are seen to be close to the CNE results. This is a characteristic of the optically thin radiation where the gas directly exchanges energy with the boundary. In the present case of the adiabatic wall, the wall temperature increases in the direction of the flow. At any x-location, therefore, the net radiative flux between the centerline and wall directly influences the centerline temperature. The results for the general case of NLTE radiative interaction should be lower than the (TCNE + LTE) results. The results for $j = j\mathrm{mid}$ and $j = j\,\mathrm{max}$ are shown in Fig. 11 for different cases along with the centerline results. It is clearly seen that the wall temperature increases in the flow direction. The mid-point results are higher than the centerline results, but they follow the same general trend.

The normalized radiative flux results for different models are illustrated in Figs. 12 and 13. Figure 12 shows the profiles of the streamwise radiative flux q_{Rx} for different y-locations ($j = 1$, $j = j\mathrm{mid}$, and $j = j\,\mathrm{max}$). It is seen that the net q_{Rx} decreases with increasing x

for all models. This is due to cancellation of fluxes in the positive and negative x-directions. The maximum rate of q_{Rx} is predicted by the (CNE + LTE) model at the mid-point location ($j = j\text{mid}$). The results of other models at this location follow the trend of temperature variation exhibited in Fig. 11. The results for other locations follow a similar trend. The profiles of normal radiative flux are illustrated in Fig. 13 for different models at the three y-locations. These results also show a trend similar to the q_{Rx} results. The extent of net q_{Rx} decreases in the flow direction because of cancellation of fluxes in the positive and negative y-directions. Since the walls are assumed to be adiabatic, no energy can be transferred outside the wall. As a result, the wall temperature increases in the flow direction.

CONCLUDING REMARKS

Analytical and numerical procedures have been developed to treat a physical problem where different nonequilibrium processes occur simultaneously. The nonequilibrium processes considered are thermal, chemical, and radiative. The influence of thermal (vibrational) nonequilibrium upon infrared radiative energy transfer was investigated by considering a radiating gas between two parallel plates. The influence of vibrational and nonlocal thermodynamic equilibrium upon the net upwelling infrared atmospheric radiation was investigated by evaluating the upwelling radiances in the spectral ranges of different participating species. The combined effect of the three competing nonequilibrium processes was investigated by considering the flow of chemically reacting and radiating gases in a diverging nozzle. The results demonstrate that nonequilibrium phenomena, in general, tend to reduce the ability of a gas to transfer the radiative energy. The procedure developed can be applied to investigate radiative interactions in challenging multidimensional nonequilibrium problems using sophisticated spectral models for radiation absorption.

ACKNOWLEDGEMENTS

This work was supported by the NASA Langley Research Center through Grants NAG-1-363 and NAG-1-423. Some of the results on atmospheric radiation were obtained by Dr. S. V. Subramanian.

REFERENCES

1. Schlicting, H., Boundary-Layer Theory, McGraw-Hill Book Company, New York, 1950 (2nd ed.), 1960 (4th ed.), 1968 (6th ed.), and 1979 (7th ed.).

2. Bird, R. B., Stewart, W. E., and Lightfoot, E. N., Transport Phenomena, John Wiley and Sons, 1960.

3. Vincenti, W. G. and Kruger, C. H., Introduction to Physical Gas Dynamics, John Wiley & Sons, Inc., New York, 1965. Printed and Published by Robert E. Krieger Publishing Co., Inc., Huntington, N.Y.

4. Zel'dovich, Y. B. and Raizer, Y. P., Physics of Shock Waves and High-Temperature Hydrodynamic Phenomena, Vols. I and II, Academic Press, New York, 1967.

5. Kays, W. M. and Crawford, M. E., Convection Heat and Mass Transfer, Second Edition, McGraw-Hill Book Company, New York, 1980.

6. Anderson, D. A., Tannehill, J. C., and Pletcher, R. M., Computational Fluid Mechanics and Heat Transfer, Hemisphere Publishing Corporation, New York, 1984.

7. Goody, R. M., Atmospheric Radiation I: Theoretical Basis, Oxford University Press, London and New York, 1965.

8. Sparrow, E. M. and Cess, R. D., Radiation Heat Transfer, Brooks/Cole, Belmont, Calif., 1966 and 1970. New Augmented Edition, Hemisphere Publishing Corp., Washington, D.C., 1978.

9. Siegel, R. and Howell, J. R., Thermal Radiation Heat Transfer, McGraw-Hill Book Co., New York, 1971; Second Edition, 1981.

10. Ozisik, M. N., Radiative Transfer and Interactions with Conduction and Convection, John Wiley & Sons, Inc., 1973.

11. Tien, C. L., "Thermal Radiation Properties of Gases," Advances in Heat Transfer, Vol. 5, Academic Press, New York, 1968.

12. Cess, R. D. and Tiwari, S. N., "Infrared Radiative Energy Transfer in Gases," Advances in Heat Transfer, Vol. 8, Academic Press, New York, 1972.

13. Edwards, D. K., "Molecular Gas Band Radiation," Advances in Heat Transfer, Vol. 12, Academic Press, New York, 1976; also Radiation Heat Transfer Notes, Hemisphere Publishing Corporation, Washington, D.C., 1981.

14. Tiwari, S. N., "Models for Infrared Atmospheric Radiation," Advances in Geophysics, Vol. 20, Academic Press, New York, 1978.

15. Anderson, J. D., Jr., Gasdynamic Lasers: An Introduction, Academic Press, New York, 1976.

16. Rakich, J. V., Bailey, H. E. and Park, C., "Computation of Nonequilibrium, Supersonic Three-Dimensional Inviscid Flow Over Blunt-Nosed Bodies," AIAA Journal, Vol. 21, 1983, pp. 834–841.

17. Lee, J. H., "Basic Governing Equations for the Flight Regimes of Aeroassisted Orbital Transfer Vehicles," AIAA Progress in Aeronautics and Astronautics, Vol. 96, edited by H. F. Nelson, 1985, pp. 3-53.

18. Candler, G. V. and MacCormack, R. W., "The Computation of Hypersonic Ionized Flows in Chemical and Thermal Nonequilibrium," AIAA Paper 88-0511, January 1988,

19. Gnoffo, P. A., "Conservation Equations and Physical Models for Hypersonic Air Flows in Thermal and Chemical Nonequilibrium," NASA-TP-2867, February 1989.

20. Gilles, S. E., "Flow with Coupled Radiative and Vibrational Nonequilibrium in a Diatomic Gas," Ph.D. Dissertation, Stanford University, California, 1968; also, Gilles, S. E. and Vincenti, W. G., "Coupled Radiative and Vibrational Nonequilibrium in a Diatomic Gas with Application to Gas Dynamics," Journal of Quantitative Spectroscopy and Radiative Transfer, Vol. 10, No. 2, February 1970, pp. 71–97.

21. Tiwari, S. N. and Cess, R. D., "The Influence of Vibrational Nonequilibrium Upon Infrared Radiative Energy Transfer," Journal of Quantitative Spectroscopy and Radiative Transfer, Vol. 11, 1971, pp. 237–248.

22. Tiwari, S. N. and Manian, S. V., "Evaluation of Upwelling Infrared Radiance in a Non-homogeneous and Nonequilibrium Atmosphere," NASA CR-149090, November 1976; also, MS Thesis by S. V. Manian, Old Dominion University, Norfolk, Virginia, December 1976.

23. Tiwari, S. N., "Radiative Interactions in Transient Energy Transfer in Gaseous Systems," NASA CR-17664 NAS 1.26:176644, December 1985.

24. Tiwari, S. N., "Infrared Radiative Energy Transfer in Gaseous System," Institute of Computational and Applied Mechanics (ICAM), Old Dominion University, Norfolk, Virginia, ODU/ICAM Report 91-102, September 1991.

25. Tiwari, S. N., "Elements of Radiative Interactions in Gaseous Systems," Department of Mechanical Engineering and Mechanics, College of Engineering and Technology, Old Dominion University, Norfolk, Virginia, TR NAG-1-423, December 1991.

26. Millikan, R. C. and White, D. R., "Vibrational Energy Exchange Between N_2 and CO: The Vibrational Relaxation of Nitrogen," The Journal of Chemical Physics, Vol. 39, No. 1, July 1963, pp. 98–101.

27. Millikan, R. C. and White, D. R., "Systematics of Vibrational Relaxation," Journal of Chemical Physics, Vol. 39, No. 12, December 1963, pp. 3209–3213.

28. Camac, M., "CO_2 Relaxation Processes in Shock Waves," Fundamental Phenomena in Hypersonic Flow (Hall, J. G., Editor), Proceedings of the International Symposium Sponsored by Cornell Aeronautical Laboratory, June 25–26, 1964, Cornell University Press, Ithaca, New York, 1966.

29. Richards, L. W. and Sigafoos, D. H., "Vibrational Relaxation of Methane," The Journal of Chemical Physics, Vol. 43, No. 2, July 1965, pp. 492–497.

30. von Rosenberg, C. W., Jr., Bray, K. N. C., and Pratt, N. H., "Shock Tube Vibrational Relaxation Measurements: N_2, Relaxation by H_2O and the CO-N_2 V-V Rate," Journal of Chemical Physics, Vol. 56, No. 7, July 1972, pp.

31. McClatchey, R. A., Benedict, W. S., Clough, S. A., Burch, D. E., Calfee, R. F., Fox, K., Rothman, L. S., and Garing, J. S., "AFCRL Atmospheric Line Parameters Compilation," Air Force Cambridge Research Laboratories, Bedford, Mass., AFCRL-TR-73-0096, January 1973 (also, NTIS AD A762904).

32. Ludwig, C. B., Malkmus, W., Reardon, J. E., and Thomson, J. A. L., Handbook of Infrared Radiation from Combustion Gases, R. Goulard and J. A. L. Thomson (Editors), NASA SP-3080, 1973.

33. Rothman, L. S., Gamache, R. R., Barbe, A., Goldman, A., Gillis, J. R., Brown, L. R., Toth, R. A., Flaud, J. M., and Camy-Peyret, C., "AFCRL Atmospheric Absorption Line Parameters Compilation: 1982 Edition," Applied Optics, Vol. 22, No. 15, August 1983, pp 2247–2256.

34. Mlynczak, M. G., "Nonlocal Thermodynamic Equilibrium Processes in Ozone: Implications for the Energy Budget of the Mesosphere and Lower Thermosphere," Journal of Geophysical Research, Vol. 96, No. D9, September 1991, pp. 17,217–17,228

35. Gokcen, T. and Park, C., "The Coupling of Radiative Transfer to Quasi 1–D Flows with Thermochemical Nonequilibrium," AIAA Paper 91–0570, January 1991.

36. Chandrasekhar, R., Tiwari, S. N., and Drummond, J. P., "Thermochemical Nonequilibrium and Radiative Interactions in Supersonic Hydrogen-Air Combustion," AIAA Paper 92–0340, January 1992.

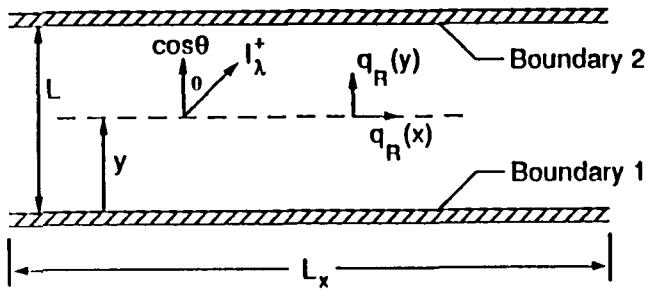

Fig. 1 Physical model and coordinate system.

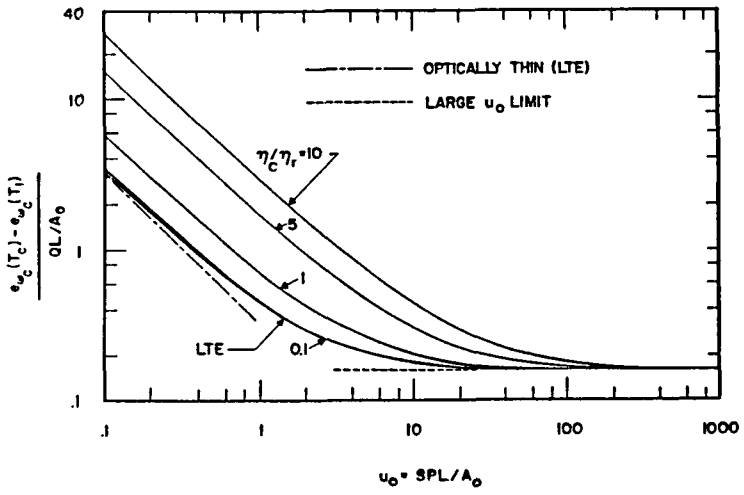

Fig. 2 Non-LTE (NLTE) results for $\beta = \infty$.

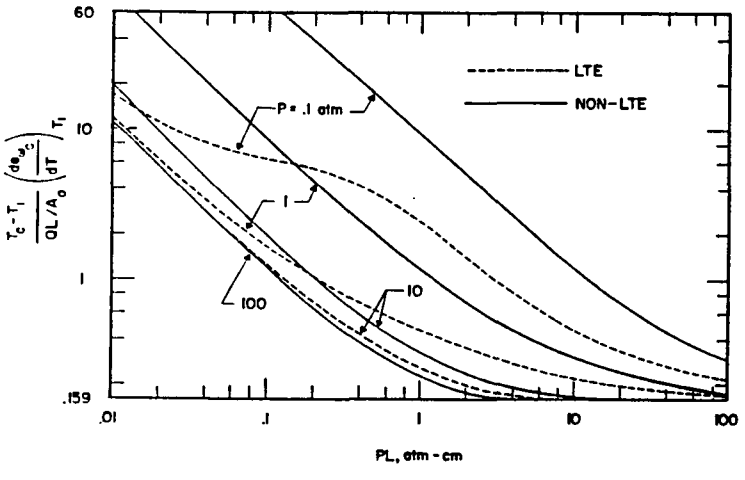

Fig. 3 LTE and non-LTE (NLTE) results for CO with $T_1 = 500$ K.

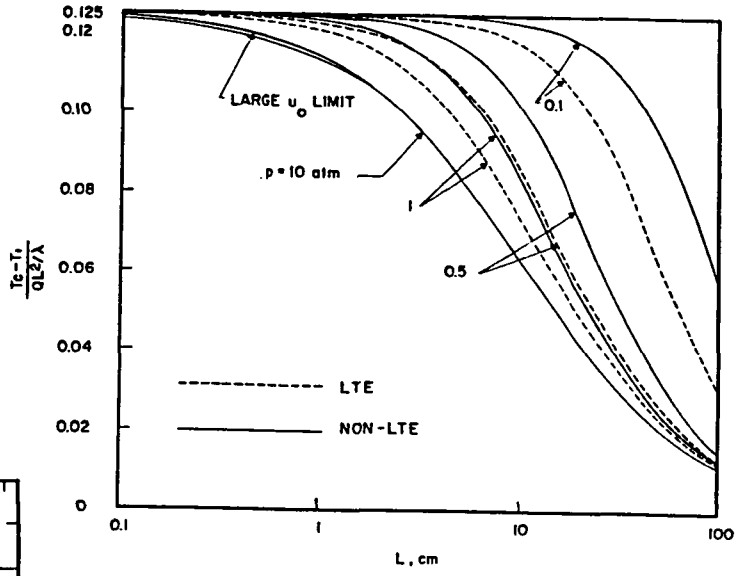

Fig. 4 LTE and non-LTE (NLTE) results for combined conduction and radiation for CO with $T_1 = 500$ K.

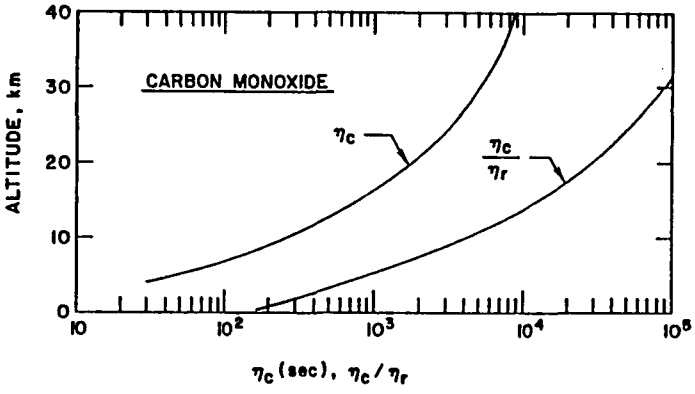

Fig. 5 Variation of collisional relaxation time and NLTE parameter with altitude for CO.

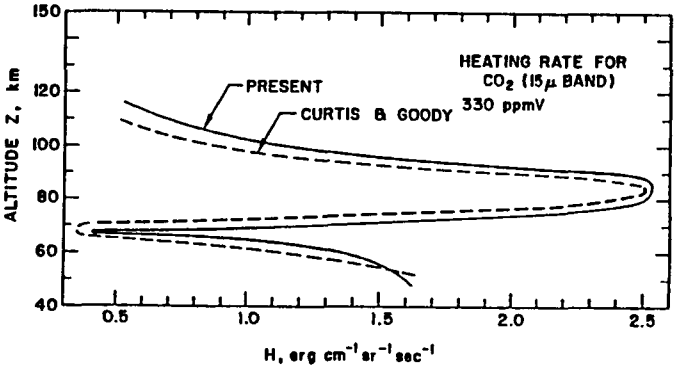

Fig. 6 Heating rates for 15μ CO_2 band at different altitudes.

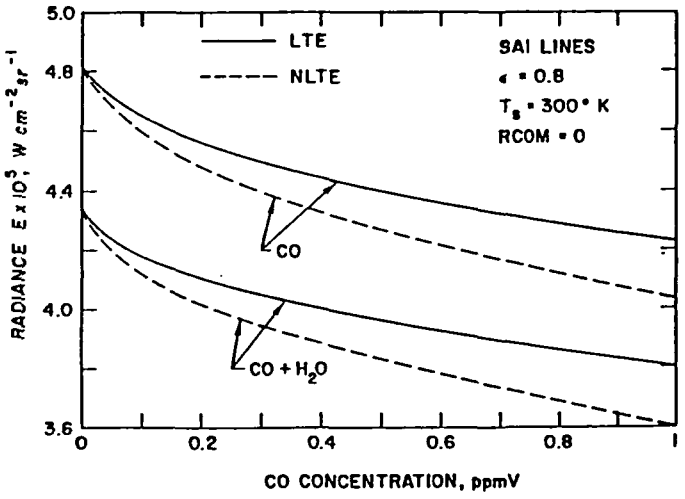

Fig. 7 Upwelling radiance for pure CO and H_2O molecules.

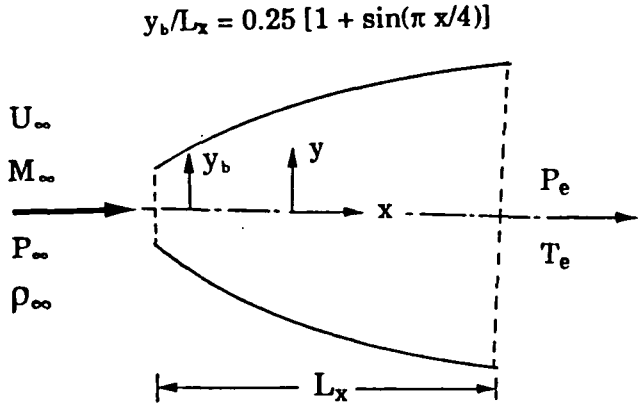

Fig. 9 Physical model of supersonic flow through a nozzle.

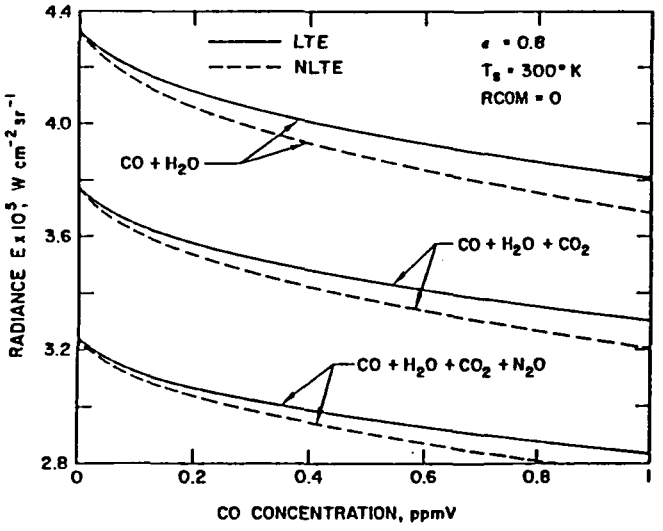

Fig. 8 Upwelling radiance with interfering gases H_2O, CO_2, and N_2O.

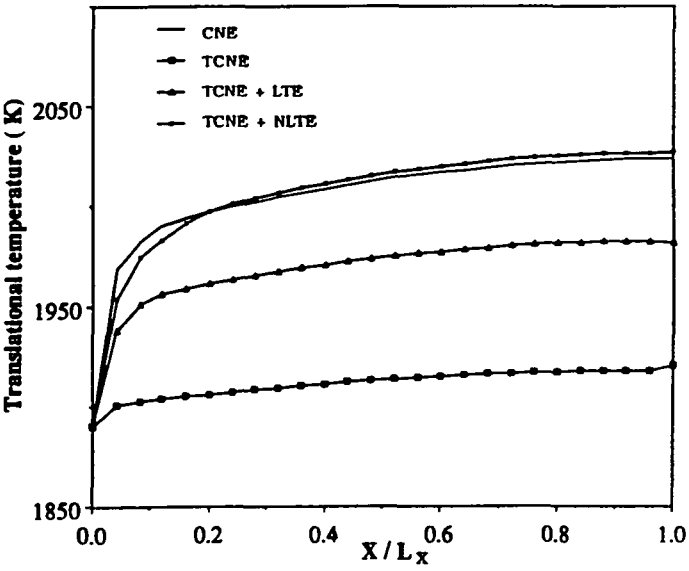

Fig. 10 Centerline translational temperatures (j = 1).

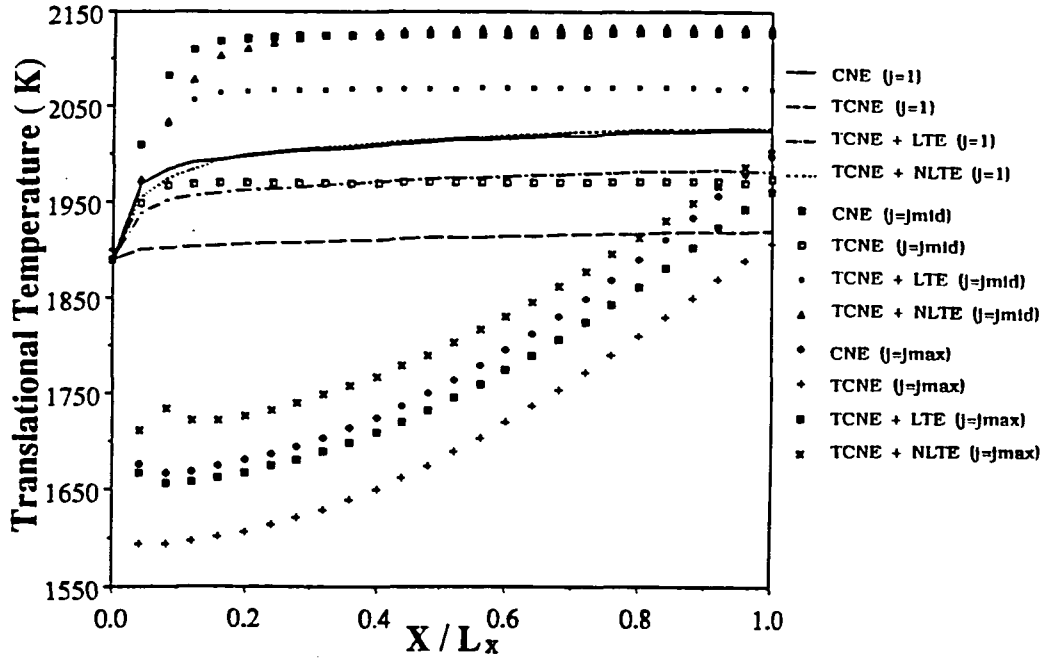

Fig. 11 Profiles of translational temperatures.

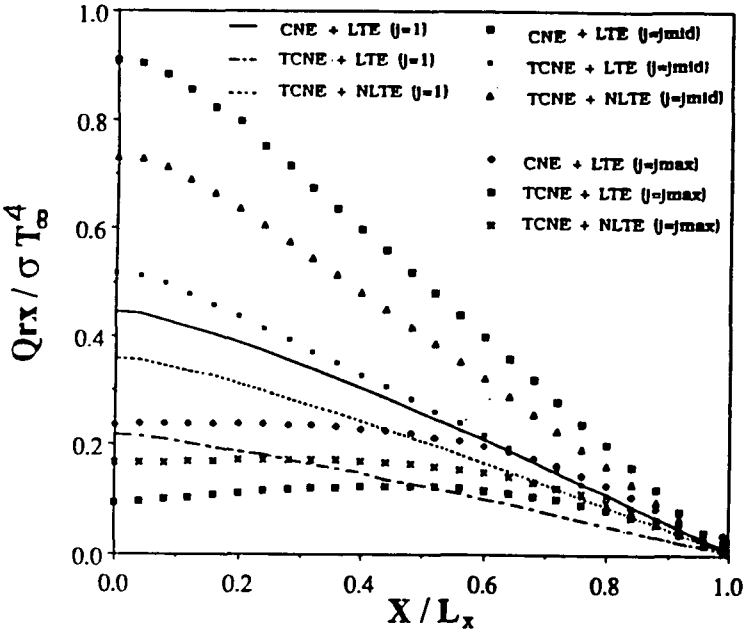

Fig. 12 Variation of streamwise radiative flux.

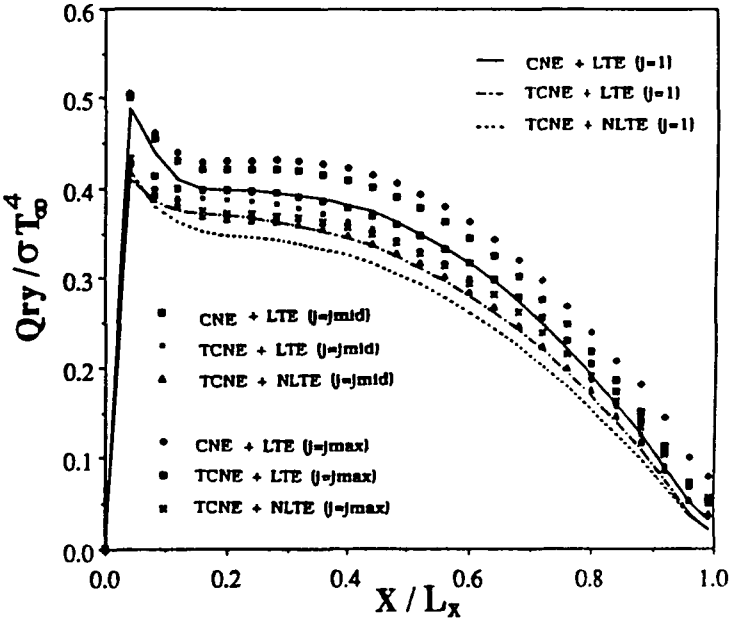

Fig. 13 Variation of normal radiative flux.

AIAA–92–0340

Thermochemical Nonequilibrium and Radiative Interactions in Supersonic Hydrogen-Air Combustion

R. Chandrasekhar and S. N. Tiwari,
Old Dominion University,
Norfolk, VA

30th Aerospace Sciences
Meeting & Exhibit
January 6-9, 1992 / Reno, NV

THERMOCHEMICAL NONEQUILIBRIUM AND RADIATIVE INTERACTIONS IN SUPERSONIC HYDROGEN—AIR COMBUSTION

R. Chandrasekhar* and S. N. Tiwari†
Old Dominion University, Norfolk, VA 23529–0247

Abstract

The two-dimensional, elliptic Navier-Stokes equations are used to investigate supersonic flows with nonequilibrium chemistry and thermodynamics, coupled with radiation, for hydrogen-air systems. The chemistry source term in the species equation is treated implicitly to alleviate the stiffness associated with fast reactions. The explicit, unsplit MacCormack finite-difference scheme is used to advance the governing equations in time, until convergence is achieved. The specific problem considered is the premixed, expanding flow in a supersonic nozzle. The reacting flow consists of seven species, one of which is the inert N_2 molecule. The thermal state of the gas is modeled with one translational-rotational temperature and five vibrational temperatures. The harmonic oscillator model is used in the formulation for vibrational relaxation. The tangent slab approximation is used in the radiative flux formulation. A pseudo-gray model is used to represent the absorption-emission characteristics of the participating species. Results obtained for specific conditions indicate the presence of nonequilibrium in the expansion region. This reduces the radiative interactions and can have a significant influence on the flowfield.

Nomenclature

A *band absorptance*, m^{-1}
A_o *band width parameter*, m^{-1}
C_j *concentration of the* j^{th} *species*, $kg-mole/m^3$
C_p *constant pressure specific heat*, $J/kg-K$
C_o *correlation parameter*, $(N/m^2)^{-1}m^{-1}$
c *speed of light*
E *total internal energy*
E_V *total vibrational energy*
e_ω *Planck's function*
f_j *mass fraction of* j^{th} *species*
H *total enthalpy*, J/kg
h *static enthalpy*, J/kg
$\overline{h}$ *Planck's constant*
k *thermal conductivity*
k_b *backward rate constant*
k_f *forward rate constant*
$\overline{k}$ *Boltzmann's constant*
P *pressure*, N/m^2
P_j *partial pressure of* j^{th} *species*
q_R *total radiative flux*
R *gas constant*
S *integrated band intensity*, $(N/m^2)^{-1}m^{-2}$
T *translational – rotational temperature*, K
T_V *vibrational temperature*, K
u, v *velocity in* $x-$ *and* $y-$ *directions*, m/s
$\dot{w}_j$ *production rate of* j^{th} *species*, kg/m^3-s
x, y *physical coordinates*
γ *ratio of specific heats*
θ_V *characteristic vibrational temperature*
κ_p *Planck mean absorption coefficient*
λ *second coefficient of viscosity*, *wavelength*
μ *dynamic viscosity*, $kg/m-s$
μ_{sr} *reduced molecular mass of colliding pair* (s,r)
ξ, η *computational coordinates*
η_c *vibrational relaxation time*
η_r *radiative lifetime for vibrational states*
ρ *density*
σ *Stefan – Boltzmann constant*
τ *shear stress*
ϕ *equivalence ratio*
ω *wave number*, m^{-1}

Introduction

In recent years there has been a renewed interest in the development of a hypersonic transatmospheric aerospace vehicle capable of flying at suborbital speeds. A hydrogen-fueled supersonic combustion ramjet (scramjet) engine is a strong candidate for propelling such a vehicle. For a better understanding of the complex flowfield in different regions of the engine, both experimental and computational techniques are employed. Several computer programs have been developed [1–4] and applied to gain more insight into the problem involving the flow in the various sections of the scramjet module.

The flowfield in the scramjet combustor consists of a high enthalpy gaseous mixture characterized by very short residence times (order 1.0 msec) and wide temperature and pressure variations (900–3000 K and 1.0–5.0 atmospheres, respectively). This could lead to thermochemical nonequilibrium. In order for molecules to dissociate, they must be excited in all three energy states (rotational, translational and vibrational). After dissociation, the translational and rotational temperatures relax towards equilibrium faster

* Graduate Research Assistant, Department of Mechanical Engineering and Mechanics. Student Member AIAA.
† Eminent Professor, Department of Mechanical Engineering and Mechanics. Associate Fellow AIAA.

than the vibrational temperature. This makes the study of vibrational nonequilibrium an important issue. Several theoretical and computational studies on the nonequilibrium flow of air have been carried out [5–13]. Vibrational relaxation effects are important in mixtures of combusting gases [14–16] and in lasers [17–20]. In recent years, thermochemical nonequilibrium effects in atmospheric re-entry flows have received considerable attention [21–25].

The combustion of hydrogen and air in the scramjet combustor results in gases such as water vapor and hydroxyl radicals. It is known that the presence of water vapor gives rise to rapid relaxation rates [14, 15, 26, 27]. However, the vibrational relaxation effects of hydrogen-air combustion have been investigated only recently [28, 29]. Furthermore, water vapor is an absorbing-emitting gas. Existence of such gases makes it necessary to include the effect of radiation heat transfer. Coupled radiative transfer with chemical nonequilibrium has been studied earlier [30–35]. The effect of radiatively induced vibrational nonequilibrium (non-local thermodynamic equilibrium, or non-LTE) upon radiative energy transfer in hot gases, has also been investigated [36–39].

The objectives of the present study are to investigate vibrational, chemical and radiative nonequilibrium effects in a hydrogen-fueled supersonic combustor. The harmonic oscillator model [40, 41] is used in the formulation for vibrational relaxation. The thermal state of the gas is modeled using one translational-rotational temperature and five vibrational temperatures. The radiative interactions are investigated in both streamwise and transverse directions. The tangent slab approximation is used in the radiative flux formulation. An optically thin assumption is made in the non-LTE model.

The flowfield in the combustor is represented by the Navier-Stokes equations and by the appropriate species continuity equations [2, 3]. Incorporation of the finite-rate chemistry models into the fluid dynamic equations can create a set of stiff differential equations. Stiffness is due to a disparity in the time scales of the governing equations. In the time accurate solution, after the fast transients have decayed and the solutions are changing slowly, taking a larger time step is more efficient. But explicit methods still require small time steps to maintain stability. One way around this problem is to use a fully implicit method. However, this requires the inversion of a block multi-diagonal system of algebraic equations, which is also computationally expensive. The use of a semi-implicit technique [33], provides an alternative to the above problems. This method treats the source term (which is the cause of the stiffness) implicitly, and solves the remaining terms explicitly.

Basic Governing Equations

The physical model for analyzing the flowfield in a supersonic combustor is described by the Navier-Stokes and species continuity equations. For two-dimensional flows, these equations are expressed in physical coordinates as [2, 3]

$$\frac{\partial U}{\partial t} + \frac{\partial F}{\partial x} + \frac{\partial G}{\partial y} + H = 0 \qquad (1)$$

where vectors U, F, G and H are written as

$$U = \begin{bmatrix} \rho \\ \rho u \\ \rho v \\ \rho E_{V1} \\ \rho E_{V2} \\ \rho E_{V3} \\ \rho E_{V4} \\ \rho E_{V5} \\ \rho E \\ \rho f_j \end{bmatrix}$$

$$F = \begin{bmatrix} \rho u \\ \rho u^2 + p + \tau_{xx} \\ \rho uv + \tau_{xy} \\ \rho u E_{V1} \\ \rho u E_{V2} \\ \rho u E_{V3} \\ \rho u E_{V4} \\ \rho u E_{V5} \\ (\rho E + p)u + \tau_{xx}u + \tau_{xy}v + q_{cx} + q_{Rx} \\ \rho u f_j - \rho D \frac{\partial f_j}{\partial x} \end{bmatrix}$$

$$G = \begin{bmatrix} \rho v \\ \rho uv + \tau_{yx} \\ \rho v^2 + p + \tau_{yy} \\ \rho v E_{V1} \\ \rho v E_{V2} \\ \rho v E_{V3} \\ \rho v E_{V4} \\ \rho v E_{V5} \\ (\rho E + p)v + \tau_{xy}v + \tau_{yy}v + q_{cy} + q_{Ry} \\ \rho v f_j - \rho D \frac{\partial f_j}{\partial y} \end{bmatrix}$$

$$H = \begin{bmatrix} 0 \\ 0 \\ 0 \\ -\dot{e}_1 \\ -\dot{e}_2 \\ -\dot{e}_3 \\ -\dot{e}_4 \\ -\dot{e}_5 \\ 0 \\ -\dot{w}_j \end{bmatrix}$$

The viscous stress tensors in the F and G terms are given as,

$$\tau_{xx} = -\lambda\left(\frac{\partial u}{\partial x} + \frac{\partial v}{\partial y}\right) - 2\mu\frac{\partial u}{\partial x} \qquad (2a)$$

$$\tau_{xy} = -\mu\left(\frac{\partial u}{\partial x} + \frac{\partial v}{\partial y}\right) \quad (2b)$$

$$\tau_{yy} = -\lambda\left(\frac{\partial u}{\partial x} + \frac{\partial v}{\partial y}\right) - 2\mu\frac{\partial v}{\partial y} \quad (2c)$$

where $\lambda = -\frac{2}{3}\mu$. The quantities q_{cx} and q_{cy} in the F and G terms are the components of the conduction heat flux and are expressed as

$$q_{cx} = -k\frac{\partial T}{\partial x} \quad ; \quad q_{cy} = -k\frac{\partial T}{\partial y} \quad (3)$$

The molecular viscosity μ is evaluated from the Sutherland's formula. The total internal energy E in Eq. (2) is given by

$$E = -\frac{P}{\rho} + \frac{u^2+v^2}{2} + \sum_{j=1}^{m} h_j f_j + \sum_{j=1}^{m} f_j E_{Vj} \quad (4)$$

Specific relations are needed for the chemistry and radiative flux terms. These are discussed in the following sections.

Chemistry and Thermodynamic Models

Chemical reaction rate expressions are usually determined by summing the contributions from each relevant reaction path to obtain the total rate of change of each species. Each path is governed by a law of mass action expression in which the rate constants can be determined from a temperature dependent Arrhenius expression. The reaction mechanism is expressed in a general form as

$$\sum_{j=1}^{ns} \gamma_{ij}^{'} C_j \quad \underset{k_{b_i}}{\overset{k_{f_i}}{\rightleftharpoons}} \quad \sum_{j=1}^{ns} \gamma_{ij}^{''} C_j \quad , \quad i = 1, nr \quad (5)$$

where ns = number of species and nr = number of reactions. The chemistry source terms $\dot{w}_j$ in Eq. (1) are obtained, on a mass basis, by multiplying the molar changes and corresponding molecular weight as

$$\dot{w}_j = M_j C_j = M_j \sum_{i=1}^{nr} \left(\gamma_{ij}^{''} - \gamma_{ij}^{'}\right)[k_{fi} \prod_{m=1}^{ns} C_m^{\gamma_{im}^{'}} - k_{bi} \prod_{m=1}^{ns} C_m^{\gamma_{im}^{''}}], \quad j = 1, ns \quad (6)$$

The reaction rate constants k_{fi} and k_{bi} appearing in Eqs. (5) and (6) are determined from an Arrhenius rate expression as

$$k_{f_i} = A_i T^b exp\left(-\frac{E_i}{RT}\right) \quad (7)$$

where

$$k_{b_i} = \frac{k_{f_i}}{k_{eq_i}} \quad (8)$$

$$k_{eq_i} = \left(\frac{1}{RT}\right)^{\Delta n} exp\left(\frac{-\Delta G_{R_i}}{RT}\right) \quad (9)$$

The coefficients A , b and E appearing in Eq. (7) are given in Table 1. The term Δn in Eq. (9) denotes the difference in the number of moles of reactants and products. In order to account for the effect of vibrational relaxation on the chemical reaction rates, the temperature T in Eqs. (7)—(9) is expressed as [40]

$$T = \sqrt{T_{trans.-rot.} T_V} \quad (10)$$

The Gibbs energy term in Eq. (9) is calculated from the relation

$$\Delta G_{R_i} = \sum_{j=1}^{ns} \gamma_{ij}^{''} g_i - \sum_{j=1}^{ns} \gamma_{ij}^{'} g_i \ , \quad j = 1, nr \quad (11)$$

where

$$\frac{g_j}{R} = A_j(T - lnT) + \frac{B_j}{2}T^2 + \frac{C_j}{6}T^3 + \frac{D_j}{12}T^4 + \frac{E_j}{20}T^5 + F_j + G_j T \quad (12)$$

The gas constant for the mixture is evaluated by a mass-weighted summation over all species as

$$\overline{R} = \sum_{j=1} f_j R_j \quad (13)$$

$$P = \rho \overline{R} T \quad (14)$$

Vibrational Model

A simplified thermodynamic model for the mixture of gases is necessary. Each species contains translational and rotational energy states in thermodynamic equilibrium and the vibrational energy is described by a harmonic oscillator, which is not in equilibrium [40, 41]. A Landau-Teller model is used to determine the effect of vibrational relaxation on the energy production. Furthermore, ionization effects are ignored. It should be noted that monoatomic species like O and H are not vibrationally excited.

The vibrational source terms in Eq. (1) are expressed as

$$\dot{e}_i = \frac{E_{V_i}^{*} - E_V}{\eta_{ci}} \quad (15)$$

where

$$E^{*}_{Vi} = \frac{R_i \theta_{vi}}{exp(\theta_{vi}/T) - 1} \quad (16)$$

and

$$\theta_{vi} = \frac{\bar{h} c \omega_i}{\bar{k}} \quad (17)$$

In Eq. (15), the equivalent relaxation time η_{ci} of a mixture of gases (i = 1, j) is given by the linear mixture rule [14, 15]

$$\frac{1}{\eta_{ci}} = \frac{f_1}{\eta_{ci1}} + \frac{f_2}{\eta_{ci2}} + \frac{f_3}{\eta_{ci3}} + ... + \frac{f_j}{\eta_{cij}} \quad (18)$$

where the local vibrational relaxation time η_{cij} of a molecular collision pair (i, j) is given by an empirical correlation [42]

$$\eta_{cij} = p^{-1} exp[0.00116 \mu_{ij}^{1/4} \theta_{vi}^{4/3} (T^{-1/3} - 0.015 \mu_{ij}^{1/4}) - 18.42] \quad (19)$$

where

$$\mu_{ij} = \frac{\mu_{ii} \cdot \mu_{jj}}{\mu_{ii} + \mu_{jj}} \quad (20)$$

and values of θ_{vi} for N_2, O_2 and H_2O are obtained from [43] and for H_2 and OH from [44] and [45], respectively.

Radiation Transfer Model

Evaluation of the energy equation presented in Eq. (1) requires an appropriate expression for the radiative flux term, q_R . Therefore, a suitable radiative transport model is needed. Various models are available in the literature to represent the absorption-emission characteristics of the molecular species [33]. The equations of radiative transport are expressed generally in integro-differential forms. The integration involves both the frequency spectrum and physical coordinates. In many realistic three-dimensional physical problems, the complexity of the radiative transport equations can be reduced by introduction of the tangent-slab approximation. This approximation treats the gas layer as a one-dimensional slab in evaluation of the radiative flux (Fig. 1a).

Detailed derivations of radiative flux equations for gray as well as nongray radiation have been carried out previously [33]. For a multiband gaseous system, the nongray radiative flux in the normal direction is expressed as

$$q_R(y) = e_1 - e_2 + \sum_{i=1}^{n} A_{oi} \{ \int_0^y \left[\frac{de_{\omega_i}(z)}{dz} \right] x \bar{A}_i \left[\frac{3}{2} \frac{u_{oi}}{L} (y - z) \right] dz + \int_y^L \left[\frac{de_{\omega_i}(z)}{dz} \right] \bar{A}_i \left[\frac{3}{2} \frac{u_{0i}}{L} (z - y) \right] dz \} \quad (21)$$

The information on the band absorptance $\bar{A}_i$ and other quantities is available in the cited references.

For a gray medium, the spectral absorption coefficient κ_ω is independent of the wave number, and an expression for the radiative flux is obtained as [33, 46]

$$q_R(y) = e_1 - e_2 + \frac{3}{2} \{ \int_0^y [e(z) - e_1] e^{-\frac{3\kappa(y-z)}{2}} \kappa dz - \int_y^L [e(z) - e_2] e^{-\frac{3\kappa(y-z)}{2}} \kappa dz \} \quad (22)$$

It is computationally more efficient to use Eq. (22) in the general energy equation than Eq. (21). This is because by differentiating Eq. (22) twice (using the Leibnitz formula) the integrals are eliminated and the following inhomogenous ordinary differential equation is obtained :

$$\frac{1}{\kappa^2} \frac{d^2 q_R(y)}{dy^2} - \frac{9}{4} q_R(y) = \frac{3}{\kappa} \frac{de(y)}{dy} \quad (23)$$

The solution of Eq. (23) requires two boundary conditions which are given for non-black diffuse surfaces as [46]

$$\left(\frac{1}{\epsilon_1} - \frac{1}{2} \right) [q_R(y)]_{y=0} - \frac{1}{3\kappa} \left[\frac{dq_R}{dy} \right]_{y=0} = 0 \quad (24a)$$

$$\left(\frac{1}{\epsilon_2} - \frac{1}{2} \right) [q_R(y)]_{y=L} + \frac{1}{3\kappa} \left[\frac{dq_R}{dy} \right]_{y=L} = 0 \quad (24b)$$

For black surfaces $\epsilon_1 = \epsilon_2 = 1$ and Eqs. (24) reduce to simpler forms.

An appropriate model for a gray gas absorption coefficient is required in Eqs. (22) — (24). This is represented by the Planck mean absorption coefficient, which is expressed for a multi-band system as [33, 46]

$$\kappa = \kappa_P = \frac{P_j}{\sigma T^4(y)} \sum_{i=1}^{n} e_{\omega_i}(T) S_i(T) \quad (25)$$

It should be noted that κ_P is a function of the temperature and the partial pressures P_j of the species.

Relevant information on relaxation processes, nonequilibrium transfer equations and radiative flux equations is provided in [47]. The basic equations developed can be used to investigate radiative interactions of gray as well as nongray gases under nonequilibrium conditions. In this study, however, the nonequlibrium radiative interactions are considered only in the optically thin conditions. A brief discussion of applicable equations is provided here.

The nonequilibrium radiative transfer equation for two level transitions between vibrational states may be written as [36–39]

$$\frac{dI_\omega}{ds} = \kappa_\omega (J_\omega - I_\omega) \tag{26}$$

where J_ω is the nonequilibrium source function

$$J_\omega = B_\omega \left[\frac{\eta_r + \eta_c X}{\eta_r + \eta_c} \right] ; \qquad X = \frac{\int d\Omega \int \kappa_\omega I_\omega d\omega}{\left(\int d\Omega \int \kappa_\omega B_\omega d\omega \right)} \tag{27}$$

It should be noted that absorption is an equilibrium process, whereas the nonequilibrium influence comes only through the emission process (source function).

The time constant η_r in Eq. (27) is the radiative lifetime of vibrational states, and this is expressed as [36]

$$\frac{1}{\eta_r} = 8 c \omega^2 \left(\frac{P}{n} \right) S \tag{28}$$

where S represents the integrated band intensity of a vibration-rotation band.

The influence of nonequilibrium radiation is most apparent in the optically thin limit, wherein the divergence of the radiative flux can be derived as [36]

$$\frac{dq_R}{d\xi} \left(1 + \frac{3}{4} \frac{\eta_c}{\eta_r} \right) = 3 A_o u_o [e_\omega(\xi) - e_{1\omega}(\xi)] \tag{29}$$

where A_o is the band width parameter and u_o is the nondimensional path length, and these are defined in the cited references. It can be seen from Eq. (29) that the contribution of the non-LTE (non-local thermodynamic equilibrium) is obtained simply by adding a correction involving the nonequilibrium parameter $\frac{\eta_c}{\eta_r}$ to the divergence of the radiative flux.

Method of Solution

The governing equations are transformed from the physical domain (x , y) to a computational domain (ξ , η), using an algebraic grid generation technique similar to the one used by Smith and Weigel [48]. In the computational domain, Eq. (1) is expressed as

$$\frac{\partial \hat{U}}{\partial t} + \frac{\partial \hat{F}}{\partial \xi} + \frac{\partial \hat{G}}{\partial \eta} + \hat{H} = 0 \tag{30}$$

where

$$\hat{U} = UJ , \quad \hat{F} = F y_\eta - G x_\eta , \quad \hat{G} = G x_\xi - F y_\xi , \quad \hat{H} = HJ , \quad J = x_\xi y_\eta - y_\xi x_\eta \tag{31}$$

Once the temporal discretization has been performed, the resulting system is spatially differenced using the explicit, unsplit MacCormack predictor-corrector scheme [33]. This results in a spatially and temporally discrete, simultaneous system of equations at each grid point. Each simultaneous system is solved, subject to initial and boundary conditions, by using the Householder technique [33]. At the supersonic inflow boundary, all flow quantities are specified as freestream conditions. At the supersonic outflow boundary, non-reflective boundary conditions are used, i.e. all flow quantities are extrapolated from interior grid points. Only the upper half of the flow domain is computed, as the flow is assumed to be symmetric about the centerline of a two-dimensional nozzle. The upper boundary is treated as a solid wall. This implies a non-slip boundary condition (i.e. zero velocities). The wall temperature, species mass fractions and pressure are extrapolated from interior grid points, by assuming an adiabatic, black and non-catalytic wall as well as the boundary layer assumption on the pressure gradient, respectively. Symmetry boundary conditions are imposed at the lower boundary, viz. centerline. Initial conditions are obtained by specifying freestream conditions throughout the flowfield. The resulting set of equations is marched in time, until convergence is achieved. The details of the radiative flux formulation and method of solution are available in [33].

Results and Discussion

Based on the theory and computational procedures described previously, an algorithm has been developed to solve the two-dimensional Navier-Stokes equations for supersonic chemically reacting and radiating flows undergoing vibrational relaxation. The extent of radiative transfer in supersonic flows undergoing thermochemical nonequilibrium, has been investigated. For the temperature range considered in this study, the important radiating species are OH and H_2O. The gray gas formulations are based on the Planck mean absorption coefficient which accounts for the detailed information on different molecular bands. The radiative fluxes have been computed using this 'pseudo-gray' formulation. The justification for using this model is provided in [33].

The specific problem considered is the supersonic flow of premixed hydrogen and air (stoichiometric equivalence ratio ϕ = 0.3) in an expanding nozzle (Fig. 1b). The physical dimension considered for obtaining results is L_X = 2 m. The flow is ignited by the high enthalpy of the flowfield. The inlet conditions which are representative of scramjet combustor exit conditions, are P_∞ = 0.8046 atm, T_∞ = 1890 K and M_∞ = 1.4. This same flow has been computed by other CFD research groups [2, 28, 29].

The first step was to assume chemical nonequilibrium (CNE) in all cases. As a preliminary study, a one-dimensional flow was computed using 101 grid points.

Figure 2 shows the results for the temperature and pressure variations along x. The temperatures exhibit relaxation along the nozzle (Fig. 2a). The vibrational temperature T_V (shown for only one species H_2O that exhibits strongest nonequilibrium effect) deviates significantly from the translational-rotational temperature T. This shows that thermochemical nonequilibrium (TCNE) is still present in the nozzle, and reduces the translational temperature. The pressure profiles (Fig. 2b) do not show any effect of thermal nonequilibrium.

Based on the above understanding of thermochemical nonequilibrium in supersonic hydrogen-air flames, the radiative interactions were examined for two-dimensional flow. A 101 x 31 grid was used for this part of the study. The results were plotted after every four grid points. Three y locations were considered, viz. j = 1, j = jmid, and j = jmax-1, corresponding to the centerline, midway between centerline and wall, and wall boundary layer, respectively. The local thermodynamic equlibrium (LTE) and non-LTE results were obtained by using a value of 0.0 and 5.0 respectively, for the nonequilibrium parameter in Eq. (29).

Figure 3 shows the profiles of the normalized streamwise radiative flux q_{Rx} along the three y locations. It can be seen that the q_{Rx} flux at the j = jmid location is higher than at the other two locations. This is because of the heat release due to chemical reaction. The radiative flux in the wall boundary layer (j = jmax-1) is lower than at the other two locations. This is due to the adiabatic wall boundary condition, which precludes any heat transfer outside the wall. An important effect of thermal nonequilibrium is to reduce the radiative interactions. The q_{Rx} reduces towards the nozzle exit due to cancellation of fluxes in positive and negative directions.

Figure 4 shows the variations of the normal radiative flux q_{Ry} along x, at three y locations. It can be seen that the q_{Ry} flux increases in the positive y direction, reaching a maximum in the wall boundary layer. This is because of the optically thin assumption, which means that there is negligible loss of radiative flux from the wall to neighbouring gas molecules. Also, thermal nonequilibrium reduces the radiative interactions, with the non-LTE fluxes being less than the LTE fluxes. The q_{Ry} profiles exhibit a peak near the nozzle inlet, because of sudden increase in radiating species due to chemical reaction.

Figure 5 shows the temperature profiles along the centerline (j = 1) of the nozzle. It can be seen that vibrational nonequilibrium reduces the translational-rotational temperature. The radiative interactions serve to negate this thermal nonequilibrium effect, with the non-LTE case having more influence than the LTE case. This is because the non-LTE q_{Rx} flux is higher than the LTE q_{Rx} flux (Fig. 3). Figure 6 shows the temperature profiles varying along x, for the three y locations. It can be seen that the temperature at the j = jmid location, is higher than at the other two locations. This is because of the heat release due to chemical reaction. The temperature in the wall boundary layer (j = jmax-1), is lower than the centerline temperature. This is because of the adiabatic wall boundary condition, which prevents heat transfer outside the wall. Consequently, the wall temperature rises towards the nozzle exit.

Figures 7 and 8 show pressure profiles along the x direction. A reduction of pressure due to vibrational nonequilibrium, is observed. This is analogous to the thickening of the boundary layer on a flat plate (i.e. lowering of the pressure) in the presence of thermal nonequilibrium. A trend similar to the temperature profiles (Figs. 5 and 6) can be seen in this case.

Figures 9 and 10 show variations of the vibrational temperature, at the centerline and at three y locations, respectively. An interesting effect of radiative interactions is to reduce the vibrational temperature, thereby negating the thermal nonequilibrium. A similar observation has been made in [49]. This is also in tune with the observations made in Figs. 5 and 6. The reduction in vibrational temperature is due to the q_{Rx} flux which reduces the total energy.

Figure 11 shows profiles of water mass fraction at three y locations. They follow a pattern similar to the temperature and pressure profiles (Figs. 5–8). The peak water production is found to occur at $x / L_X = 0.05$. Thus, it can be seen that the nonequilibrium parameter in Eq. (29) serves to illustrate the relative importance of vibrational relaxation (collision process) over radiative nonequilibrium (emission process). The non-LTE process is emission dominated. On the other hand, the LTE process is collision dominated.

Conclusions

The two-dimensional spatially elliptic Navier-Stokes equations have been used to obtain solutions for supersonic flows undergoing thermochemical nonequilibrium alongwith radiative interactions. The specific problem considered is the premixed flow in a supersonic expanding nozzle. The inlet conditions used in the present study correspond to typical combustor exit conditions of a scramjet engine. Three different nonequilibrium processes were observed, namely chemical, thermal and radiative. It is seen that thermal nonequilibrium is present in the expansion region of the nozzle and lowers the temperature, pressure, species mass fractions as well as the radiative fluxes. The effect of radiative interactions is to reduce the extent of thermal nonequilibrium due to additional mode of energy transfer.

Acknowledgements

The present work was supported by the NASA Langley Research Center through Grant NAG-1-423. The authors are grateful to Dr. J. P. Drummond for providing the basic computer code and valuable suggestions.

References

1. Kumar, A., "Numerical Simulation of Scramjet Inlet Flowfield," NASA TP-25117, May 1986.

2. Drummond, J. P., Hussaini, M. Y. and Zang, T. A., "Spectral Methods for Modelling Supersonic Chemically Reacting Flowfields,"AIAA Journal , Vol. 24, No. 9, September 1986, pp. 1461–1467 ; also Drummond, J. P., "Numerical Simulation of Supersonic Chemically Reacting Mixing Layers," Ph.D. Dissertation, George Washington University, May 1987.

3. Drummond, J. P., Rogers, R. C. and Hussaini, M. Y., "A Detailed Numerical Model of a Supersonic Reacting Mixing Layer," AIAA Paper No. 86–1427, June 1986.

4. Chitsomboon, T., Kumar, A., Drummond, J. P. and Tiwari, S. N., "Numerical Study of Supersonic Combustion Using a Finite-Rate Chemistry Model," AIAA Paper 86–0309, January 1986.

5. Bray, K. N. C., "Atomic Recombination in a Hypersonic Wind Tunnel Nozzle," Journal of Fluid Mechanics, Vol. 6, 1959, p. 1–32.

6. Blythe, P. A., "Nonequilibrium Flow through a Nozzle," Journal of Fluid Mechanics, Vol. 17, 1963, p. 126–140.

7. Sarli V. J., Buswell, W. G. and Zupnik, T. E., NASA–CR–54221, 1964.

8. Blythe, P. A., "Asymptotic Solutions in Nonequilibrium Nozzle Flow," Journal of Fluid Mechanics, Vol. 20, 1964, p. 243

9. Stollery, J. L. and Park, C., "Computer Solutions to the Problem of Vibrational Relaxation in Hypersonic Nozzle Flows," Journal of Fluid Mechanics, Vol. 19, 1964, pp. 113–123.

10. Cheng, H. K. and Lee, R. S., "Freezing of Dissociation in Supersonic Nozzle Flows," AIAA Paper 66–1, 1966.

11. Hall, J. G. and Treanor, C. E., "Nonequilibrium Effects in Supersonic Nozzle Flows," AGARDograph No. 124, December 1967.

12. Anderson, J. D., Jr., "A Time-Dependent Analysis for Vibrational and Chemical Nonequilibrium Nozzle Flows," AIAA Journal, Vol. 8, No.3, March 1970, pp. 545–550.

13. Anderson, J. D., Jr., "Time-Dependent Solutions of Nonequilibrium Nozzle Flows — A Sequel," AIAA Journal, Vol. 8, No. 12, December 1970, pp. 2280–2282.

14. von Rosenberg, C. W., Jr., Bray, K. N. C. and Pratt, N. H., "The Effect of Water Vapor on the Vibrational Relaxation of CO," Proc. 13th Symp. (Intl.) on Combustion, The Combustion Inst., 1971, pp. 89–98.

15. von Rosenberg, C. W., Jr., Bray, K. N. C. and Pratt, N. H., "Shock Tube Vibrational Relaxation Measurements: N_2, Relaxation by H_2O and the CO-N_2 V-V Rate," Journal of Chemical Physics, Vol. 56, No. 7, April 1972, pp. 3230–3237.

16. Kung, R. T. V. and Center, R. E., "High temperature vibrational relaxation of H_2O by H_2O, He, Ar, and N_2," Journal of Chemical Physics, Vol. 62, No. 6, March 1975.

17. Kothari, A. P., Anderson, J. D., Jr. and Jones, E., "Navier-Stokes Solutions for Chemical Laser Flows," AIAA Journal, Vol. 15, No. 1, January 1976, pp. 92–100.

18. Anderson, J. D., Jr., "Gasdynamic Lasers: An Introduction," Academic Press, New York, 1976.

19. Reddy, N. M. and Shanmugasundaram, V., "Theoretical gain-optimization studies in CO_2—N_2 gasdynamic lasers. I — Theory. II — Results of parametric study," Journal of Applied Physics, Vol. 50, April 1979, pp. 2565–2582.

20. Wada, Y., Yamaguchi, M. and Kubota, H., "Numerical Investigation of Nozzle Shape Effects on CO_2 Gas Dynamic Laser Performance," AIAA Paper 87–1452, June 1987.

21. Rakich, J. V., Bailey, H. E. and Park, C., "Computation of Nonequilibrium, Supersonic Three-Dimensional Inviscid Flow over Blunt-Nosed Bodies," AIAA Journal, Vol. 21, 1983, pp. 834–841.

22. Lee, J. H., "Basic Governing Equations for the Flight Regimes of Aeroassisted Orbital Transfer Vehicles," AIAA Progress in Aeronautics and Astronautics, Vol. 96, edited by H. F. Nelson, 1985, pp. 3–53.

23. Gnoffo, P. A., "Application of Program LAURA to Three-Dimensional AOTV Flowfields," AIAA Paper 86–0565, January, 1986.

24. Candler, G. V. and MacCormack, R. W., "The Computation of Hypersonic Ionized Flows in Chemical and Thermal Nonequilibrium," AIAA Paper 88–0511, January, 1988.

25. Gnoffo, P. A., Gupta, R. N., and Shinn, J. L., "Conservation Equations and Physical Models for Hypersonic Air Flows in Thermal and Chemical Nonequilibrium," NASA-TP-2867, February 1989.

26. Finzi, J., Hovis, F. E., Panfilov, V. N., Hess, P. and Moore, C. B., "Vibrational Relaxation of Water Vapor," Journal of Chemical Physics, Vol. 67, No. 9, November 1977, pp. 4053–4061.

27. Center, R. E. and Newton, J. F., "Vibrational relaxation of N_2 by H_2O," Journal of Chemical Physics, Vol. 68, No. 8, April 1978, pp. 3327–3333.

28. Grossmann, B. and Cinella, P., "The Computation of Nonequilibrium , Chemically-Reacting Flows," Computers and Structures, Vol. 30, No. 1/2, 1988, pp. 79–93.

29. Grossmann, B. and Cinella, P., "Flux-Split Al-

gorithms for Flows with Nonequilibrium Chemistry and Vibrational Relaxation," Journal of Computational Physics, Vol. 88, No.1, May 1990, pp. 131–168.
30. Mani, M., Tiwari, S. N., and Drummond, J. P., "Numerical Solution of Chemically Reacting and Radiating Flows," AIAA Paper 87–0324, January 1987.
31. Tiwari, S. N. and Singh, D. J., "Interaction of Transient Radiation in Fully Developed Laminar Flow," AIAA Paper 86–1521, June 1987.
32. Mani, M., Tiwari, S. N., and Drummond, J. P., "Investigation of Two-Dimensional Chemically Reacting and Radiative Supersonic Channel Flows," AIAA Paper 88–0462, January 1988.
33. Mani, M. and Tiwari, S. N., "Investigation of Supersonic Chemically Reacting and Radiating Channel Flow," NASA CR-182726, January 1988 ; also Ph.D. Dissertation by M. Mani, Old Dominion University, May 1988.
34. Chandrasekhar, R., Tiwari, S. N. and Drummond, J. P., "Radiative Interactions in a Hydrogen-Fueled Supersonic Combustor," AIAA Paper 91–0373, January 1991.
35. Tiwari, S. N., Chandrasekhar, R., Thomas, A. M., and Drummond, J. P., "Investigation of Chemically Reacting and Radiating Supersonic Internal Flows," AIAA Paper 91–0572, January 1991.
36. Tiwari, S. N. and Cess, R. D., "The Influence of Vibrational Nonequilibrium upon Infrared Radiative Energy Transfer," Journal of Quantitative Spectroscopy and Radiative Transfer, Vol. 11, 1971, pp. 237–248.
37. Goody, R. M., Atmospheric Radiation, Oxford University Press, London (1964).
38. Gilles, S. E. and Vincenti, W. G., Journal of Quantitative Spectroscopy and Radiative Transfer, vol. 10, 1970, pp. 71–97.
39. Wang, L. S., "The Cooling of a Gas not in Local Thermodynamic Equilibrium by Conduction and Radiation," AIAA Paper 69–638, 1969.
40. Park, C., Nonequilibrium Hypersonic Aerothermodynamics, John Wiley, 1990.
41. Vincenti, W. G. and Kruger, C. H., Jr., Introduction to Physical Gas Dynamics, John Wiley, New York, 1965.
42. Millikan, R. C. and White, D. R., "Systematics of Vibrational Relaxation," Journal of Chemical Physics, Vol. 39, No. 12, 1963.
43. Strehlow, R. A., Combustion Fundamentals, McGraw-Hill, 1984, pp. 23.
44. Hill, T. L., An Introduction to Statistical Thermodynamics, Dover, New York, 1986, p. 186.
45. Herzberg, G., The Spectra and Structures of Simple Free Radicals, Cornell Univ. Press, Ithaca, N. Y., 1971, pp. 65.
46. Sparrow, E. M. and Cess, R. D., Radiation Heat Transfer, Hemisphere Publ. Corp., Washington, D. C., 1978.
47. Tiwari, S. N. and Chandrasekhar, R., "Radiative Interactions in Nonequilibrium Flows," AIAA Paper 92–0122, January 1992.
48. Smith, R. E. and Weigel, B. L., "Analytical and Approximation Boundary Fitted Coordinates System for Fluid Flow Simulation," AIAA Paper 80–0192, January 1980.
49. Gokcen, T. and Park, C.., "The Coupling of Radiative Transfer to Quasi 1–D Flows with Thermochemical Nonequilibrium," AIAA Paper 91–0570, January 1991.

Table 1. Hydrogen-Air Combustion Mechanism (7 species, 7 reactions)

No.	Reaction	A	b	T_a
1	$H_2 + O_2 \rightarrow OH + OH$	1.70E+13	0.0	24233
2	$H + O_2 \rightarrow OH + O$	1.42E+14	0.0	8254
3	$OH + H_2 \rightarrow H_2O + H$	3.16E+07	1.8	1525
4	$O + H_2 \rightarrow OH + H$	2.07E+14	0.0	6920
5	$OH + OH \rightarrow H_2O + O$	5.50E+13	0.0	3523
6	$H + OH + M \rightarrow H_2O + M$	2.21E+22	-2.0	0
7	$H + H + M \rightarrow H_2 + M$	6.53E+17	-1.0	0

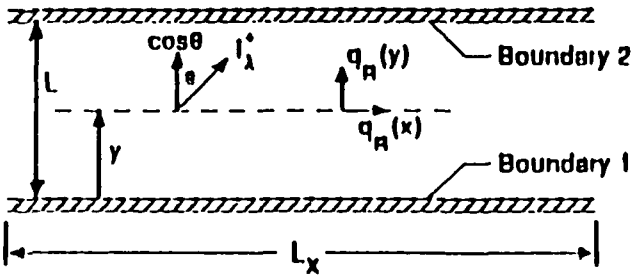

Fig. 1a Plane radiating layer between parallel boundaries

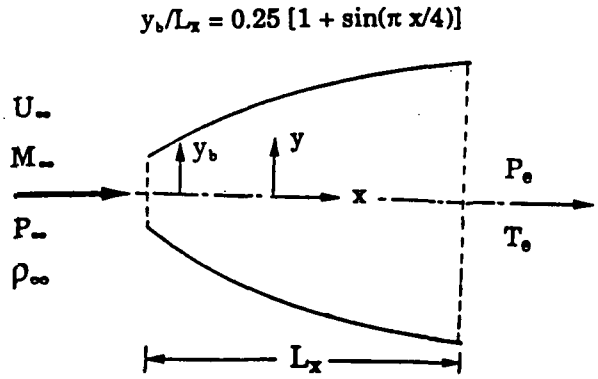

Fig. 1b Schematic diagram of nozzle

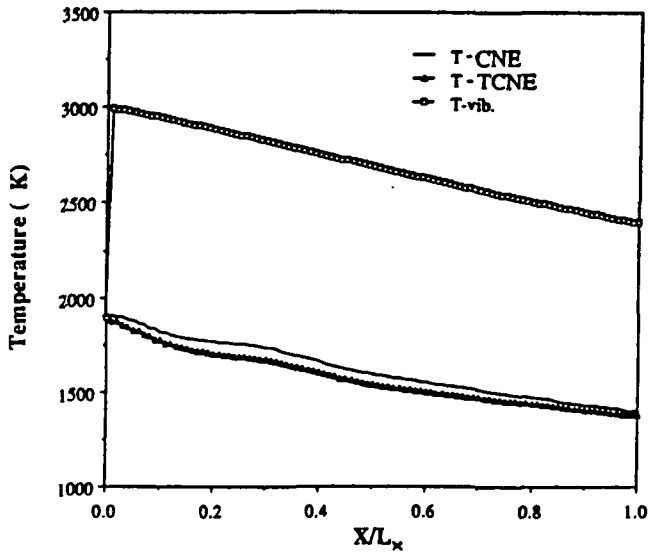

Fig. 2a Temperature profiles (1–D)

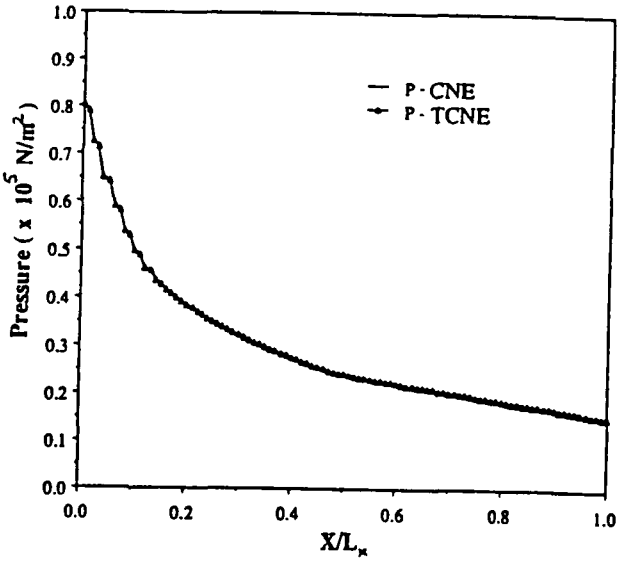

Fig. 2b Pressure profiles (1–D)

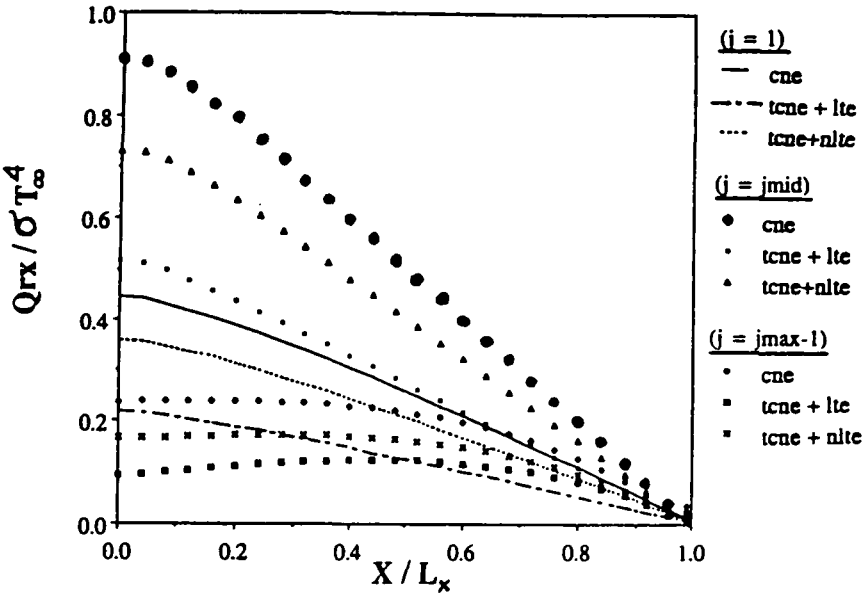

Fig. 3 Streamwise radiative flux profiles

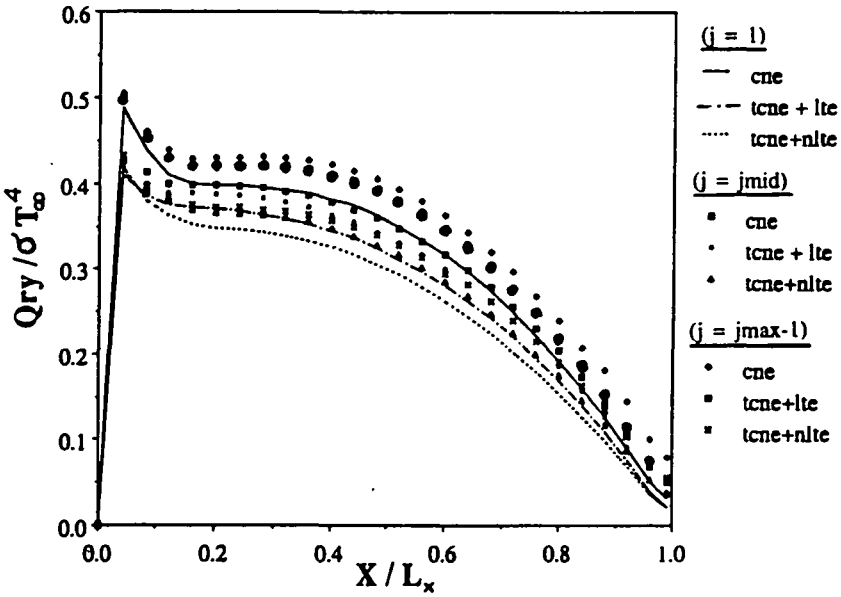

Fig. 4 Normal radiative flux profiles

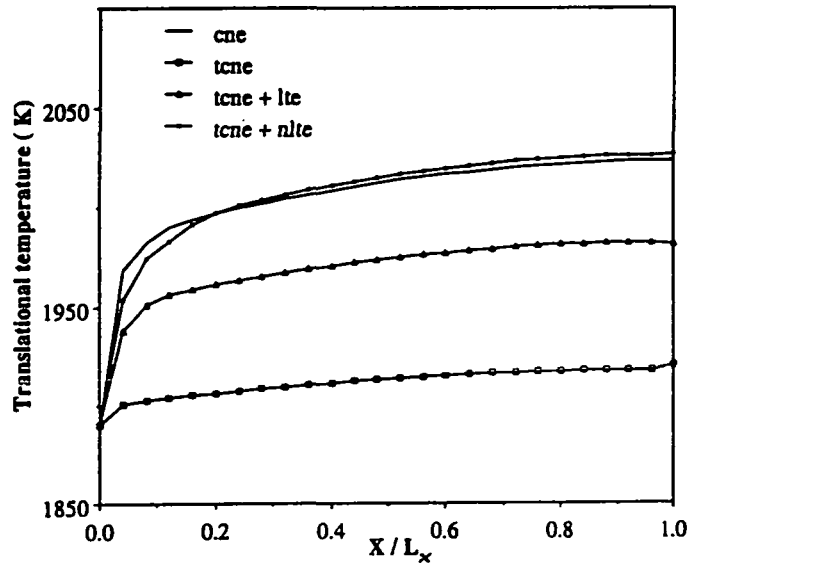

Fig. 5 Centerline temperature profiles (j = 1)

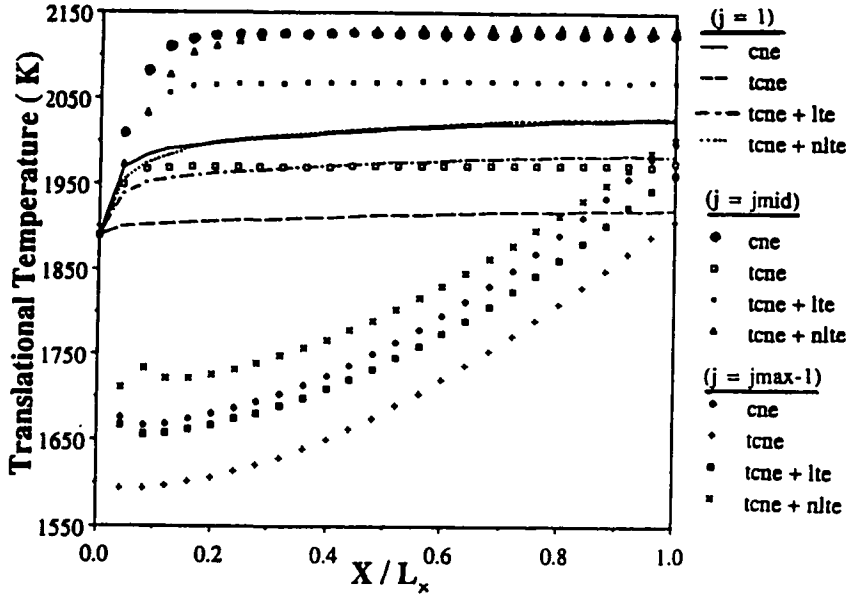

Fig. 6 Temperature profiles

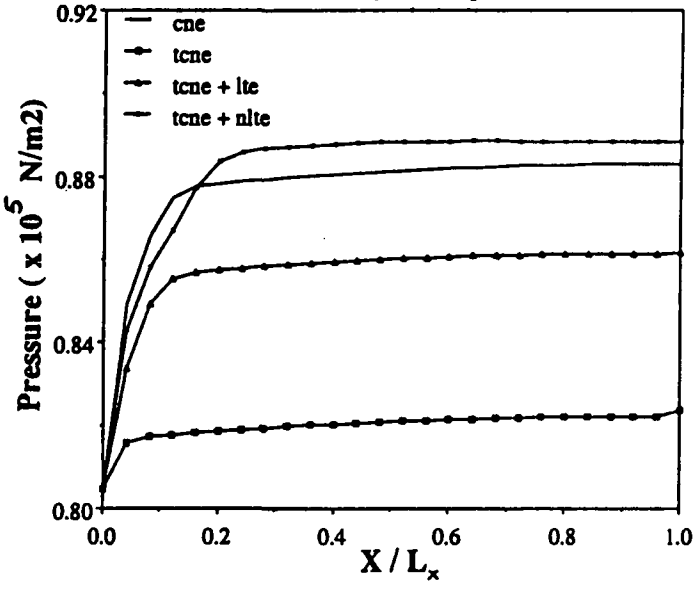

Fig. 7 Centerline pressure profiles (j = 1)

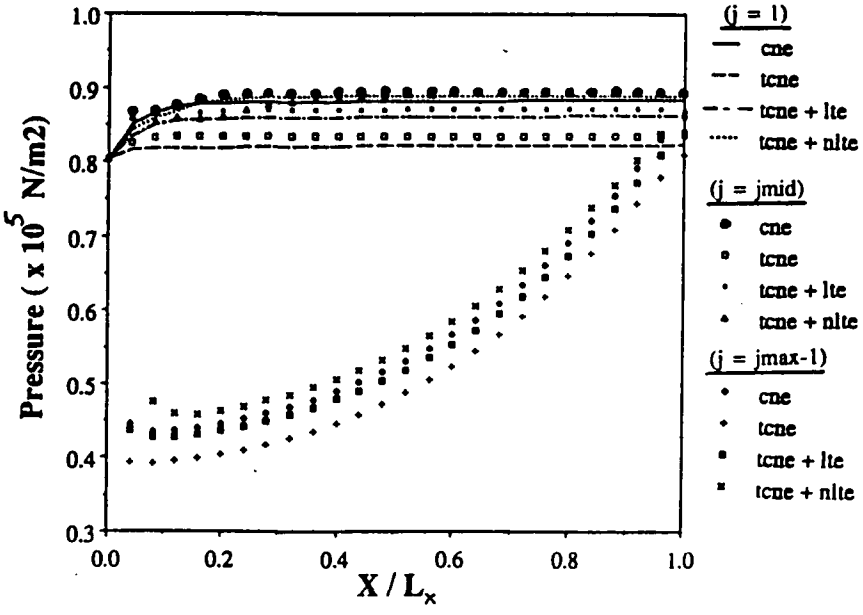

Fig. 8 Pressure profiles

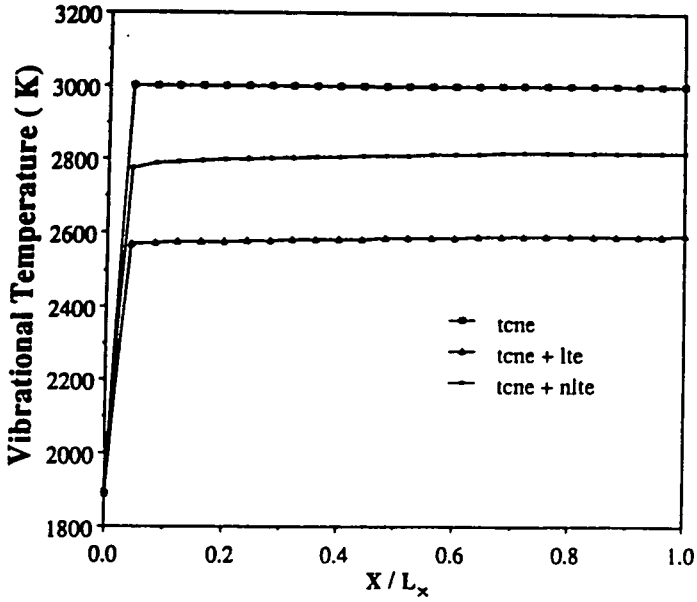

Fig. 9 Centerline vibrational temperature profiles

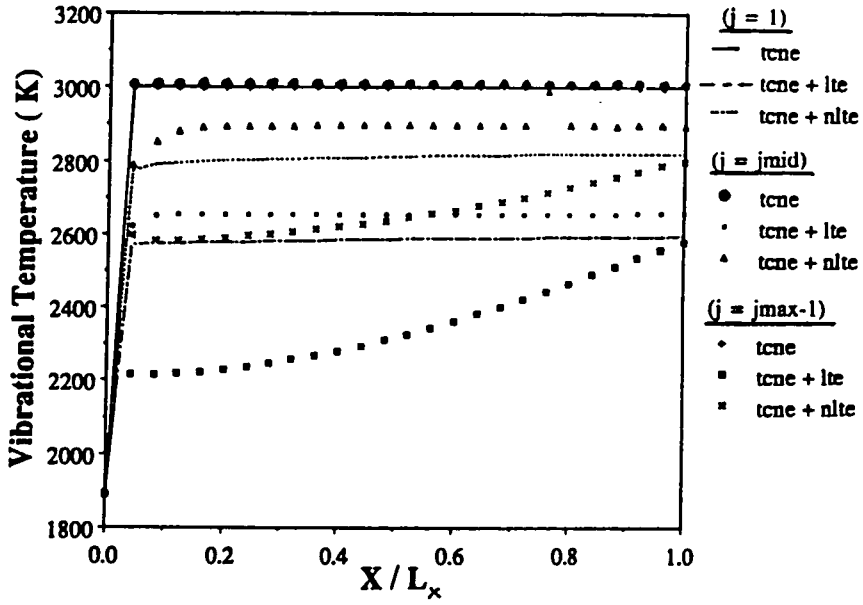

Fig. 10 Vibrational temperature profiles

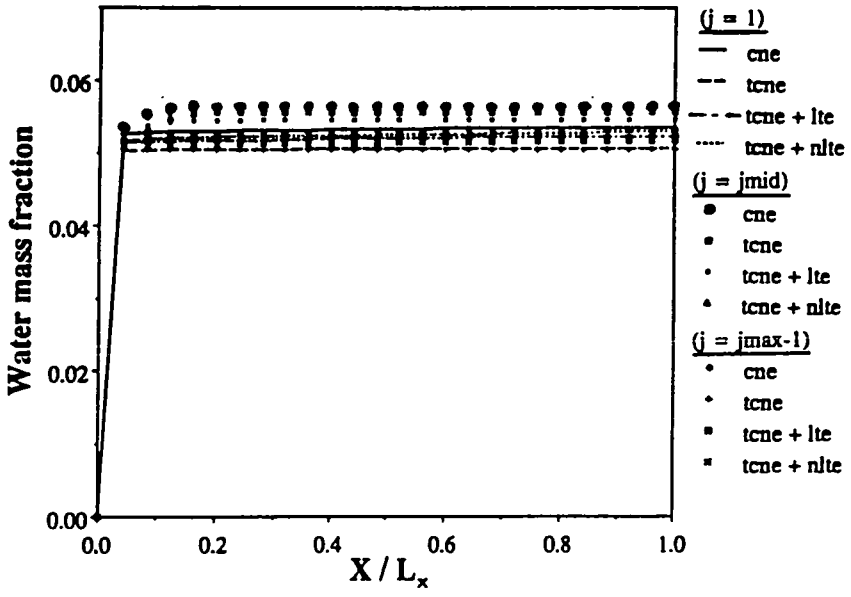

Fig. 11 Water mass fraction profiles